

ISSN 1881-7815 Online ISSN 1881-7823

BST

BioScience Trends

Volume 13, Number 1
February, 2019



www.biosciencetrends.com

BST

BioScience Trends



ISSN: 1881-7815
Online ISSN: 1881-7823

CODEN: BTIRCZ

Issues/Year: 6

Language: English

Publisher: IACMHR Co., Ltd.

BioScience Trends is one of a series of peer-reviewed journals of the International Research and Cooperation Association for Bio & Socio-Sciences Advancement (IRCA-BSSA) Group and is published bimonthly by the International Advancement Center for Medicine & Health Research Co., Ltd. (IACMHR Co., Ltd.) and supported by the IRCA-BSSA and Shandong University China-Japan Cooperation Center for Drug Discovery & Screening (SDU-DDSC).

BioScience Trends devotes to publishing the latest and most exciting advances in scientific research. Articles cover fields of life science such as biochemistry, molecular biology, clinical research, public health, medical care system, and social science in order to encourage cooperation and exchange among scientists and clinical researchers.

BioScience Trends publishes Original Articles, Brief Reports, Reviews, Policy Forum articles, Case Reports, News, and Letters on all aspects of the field of life science. All contributions should seek to promote international collaboration.

Editorial Board

Editor-in-Chief:

Norihiro KOKUDO
National Center for Global Health and Medicine, Tokyo, Japan

Co-Editors-in-Chief:

Xue-Tao CAO
Nankai University, Tianjin, China
Rajendra PRASAD
University of Delhi, Delhi, India
Arthur D. RIGGS
Beckman Research Institute of the City of Hope, Duarte, CA, USA

Chief Director & Executive Editor:

Wei TANG
National Center for Global Health and Medicine, Tokyo, Japan

Senior Editors:

Xunjia CHENG
Fudan University, Shanghai, China
Yoko FUJITA-YAMAGUCHI
Beckman Research Institute of the City of Hope, Duarte, CA, USA
Na HE
Fudan University, Shanghai, China
Kiyoshi KITAMURA
The University of Tokyo, Tokyo, Japan
Misao MATSUSHITA
Tokai University, Hiratsuka, Japan
Munehiro NAKATA
Tokai University, Hiratsuka, Japan
Takashi SEKINE

Toho University, Tokyo, Japan
Fanghua QI
Shandong Provincial Hospital, Ji'nan, China
Ri SHO
Yamagata University, Yamagata, Japan
Yasuhiko SUGAWARA
Kumamoto University, Kumamoto, Japan
Ling WANG
Fudan University, Shanghai, China

Managing Editor:

Jianjun GAO
Qingdao University, Qingdao, China

Web Editor:

Yu CHEN
The University of Tokyo, Tokyo, Japan

Proofreaders:

Curtis BENTLEY
Roswell, GA, USA
Thomas R. LEBON
Los Angeles, CA, USA

Editorial Office

Pearl City Koishikawa 603,
2-4-5 Kasuga, Bunkyo-ku, Tokyo 112-0003, Japan
Tel: +81-3-5840-8764 Fax: +81-3-5840-8765
E-mail: office@biosciencetrends.com

BioScience Trends

Editorial and Head Office

Pearl City Koishikawa 603, 2-4-5 Kasuga, Bunkyo-ku,
Tokyo 112-0003, Japan

Tel: +81-3-5840-8764, Fax: +81-3-5840-8765
E-mail: office@biosciencetrends.com
URL: www.biosciencetrends.com

Editorial Board Members

Girdhar G. AGARWAL <i>(Lucknow, India)</i>	Takahiro HIGASHI <i>(Tokyo, Japan)</i>	Masatoshi MAKUUCHI <i>(Tokyo, Japan)</i>	Shin'ichi TAKEDA <i>(Tokyo, Japan)</i>
Hirotugu AIGA <i>(Geneva, Switzerland)</i>	De-Fei HONG <i>(Hangzhou, China)</i>	Francesco MAROTTA <i>(Milano, Italy)</i>	Sumihito TAMURA <i>(Tokyo, Japan)</i>
Hidechika AKASHI <i>(Tokyo, Japan)</i>	De-Xing HOU <i>(Kagoshima, Japan)</i>	Yutaka MATSUYAMA <i>(Tokyo, Japan)</i>	Puay Hoon TAN <i>(Singapore, Singapore)</i>
Moazzam ALI <i>(Geneva, Switzerland)</i>	Sheng-Tao HOU <i>(Ottawa, Canada)</i>	Qingyue MENG <i>(Beijing, China)</i>	Koji TANAKA <i>(Tsu, Japan)</i>
Ping AO <i>(Shanghai, China)</i>	Yong HUANG <i>(Ji'ning, China)</i>	Mark MEUTH <i>(Sheffi eld, UK)</i>	John TERMINI <i>(Duarte, CA, USA)</i>
Hisao ASAMURA <i>(Tokyo, Japan)</i>	Hirofumi INAGAKI <i>(Tokyo, Japan)</i>	Satoko NAGATA <i>(Tokyo, Japan)</i>	Usa C. THISYAKORN <i>(Bangkok, Thailand)</i>
Michael E. BARISH <i>(Duarte, CA, USA)</i>	Masamine JIMBA <i>(Tokyo, Japan)</i>	Miho OBA <i>(Odawara, Japan)</i>	Toshifumi TSUKAHARA <i>(Nomi, Japan)</i>
Boon-Huat BAY <i>(Singapore, Singapore)</i>	Chunlin JIN <i>(Shanghai, China)</i>	Xianjun QU <i>(Beijing, China)</i>	Kohjiro UEKI <i>(Tokyo, Japan)</i>
Yasumasa BESSHO <i>(Nara, Japan)</i>	Kimitaka KAGA <i>(Tokyo, Japan)</i>	John J. ROSSI <i>(Duarte, CA, USA)</i>	Masahiro UMEZAKI <i>(Tokyo, Japan)</i>
Generoso BEVILACQUA <i>(Pisa, Italy)</i>	Ichiro KAI <i>(Tokyo, Japan)</i>	Carlos SAINZ-FERNANDEZ <i>(Santander, Spain)</i>	Junming WANG <i>(Jackson, MS, USA)</i>
Shiuan CHEN <i>(Duarte, CA, USA)</i>	Kazuhiro KAKIMOTO <i>(Osaka, Japan)</i>	Yoshihiro SAKAMOTO <i>(Tokyo, Japan)</i>	Xiang-Dong Wang <i>(Boston, MA, USA)</i>
Yuan CHEN <i>(Duarte, CA, USA)</i>	Kiyoko KAMIBEPPU <i>(Tokyo, Japan)</i>	Erin SATO <i>(Shizuoka, Japan)</i>	Hisashi WATANABE <i>(Tokyo, Japan)</i>
Naoshi DOHMAE <i>(Wako, Japan)</i>	Haidong KAN <i>(Shanghai, China)</i>	Takehito SATO <i>(Isehara, Japan)</i>	Jufeng XIA <i>(Tokyo, Japan)</i>
Zhen FAN <i>(Houston, TX, USA)</i>	Bok-Luel LEE <i>(Busan, Korea)</i>	Akihito SHIMAZU <i>(Tokyo, Japan)</i>	Lingzhong XU <i>(Ji'nan, China)</i>
Ding-Zhi FANG <i>(Chengdu, China)</i>	Mingjie LI <i>(St. Louis, MO, USA)</i>	Zhifeng SHAO <i>(Shanghai, China)</i>	Masatake YAMAUCHI <i>(Chiba, Japan)</i>
Xiaobin FENG <i>(Beijing, China)</i>	Shixue LI <i>(Ji'nan, China)</i>	Judith SINGER-SAM <i>(Duarte, CA, USA)</i>	Aitian YIN <i>(Ji'nan, China)</i>
Yoshiharu FUKUDA <i>(Ube, Japan)</i>	Ren-Jang LIN <i>(Duarte, CA, USA)</i>	Raj K. SINGH <i>(Dehradun, India)</i>	George W-C. YIP <i>(Singapore, Singapore)</i>
Rajiv GARG <i>(Lucknow, India)</i>	Lianxin LIU <i>(Hefei, China)</i>	Peipei SONG <i>(Tokyo, Japan)</i>	Xue-Jie YU <i>(Galveston, TX, USA)</i>
Ravindra K. GARG <i>(Lucknow, India)</i>	Xinqi LIU <i>(Tianjin, China)</i>	Junko SUGAMA <i>(Kanazawa, Japan)</i>	Benny C-Y ZEE <i>(Hong Kong, China)</i>
Makoto GOTO <i>(Tokyo, Japan)</i>	Daru LU <i>(Shanghai, China)</i>	Hiroshi TACHIBANA <i>(Isehara, Japan)</i>	Yong ZENG <i>(Chengdu, China)</i>
Demin HAN <i>(Beijing, China)</i>	Hongzhou LU <i>(Shanghai, China)</i>	Tomoko TAKAMURA <i>(Tokyo, Japan)</i>	Xiaomei ZHU <i>(Seattle, WA, USA)</i>
David M. HELFMAN <i>(Daejeon, Korea)</i>	Duan MA <i>(Shanghai, China)</i>	Tadatoshi TAKAYAMA <i>(Tokyo, Japan)</i>	<i>(as of February 28, 2019)</i>

Review

- 1 - 9 **Improvement in the diagnosis and treatment of T2 gallbladder carcinoma is pivotal to improvement in the overall prognosis for this disease.**
Di Zhou, Jiandong Wang, Zhiwei Quan, Yong Yang, Fei Ma
- 10 - 22 **Efficacy and safety of external-beam radiation therapy for hepatocellular carcinoma: An overview of current evidence according to the different target population.**
Bing Han, Chuan Li, Hao Meng, Fernando Gomes Romeiro, Andrea Mancuso, Zhirui Zhou, Giovanni Battista Levi Sandri, Ying Xu, Tao Han, Lei Han, Lichun Shao, Xingshun Qi
- 23 - 31 **Anti-inflammatory, anti-oxidative stress and novel therapeutic targets for cholestatic liver injury.**
Yafei Zhang, Yuxuan Lu, Hong Ji, Yiming Li

Original Article

- 32 - 39 **Fibrosis-4 index predicts mortality in HIV/HCV co-infected patients receiving combination antiretroviral therapy in rural China.**
Xiaochen Chen, Xing Liu, Renhai Tang, Runhua Ye, Yuecheng Yang, Shitang Yao, Jibao Wang, Yingying Ding, Song Duan, Na He
- 40 - 48 **Effects of BENC-511, a novel PI3K inhibitor, on the proliferation and apoptosis of A549 human lung adenocarcinoma cells.**
Huiqin Tian, Yu Zhang, Qianyun Zhang, Shuixian Li, Yang Liu, Xiuzhen Han
- 49 - 57 **By regulating miR-182-5p/BCL10/CYCS, sufentanil reduces the apoptosis of umbilical cord mesenchymal stem cells caused by ropivacaine.**
Lisha Li, Yan Sun, Na Zhang, Xuemin Qiu, Ling Wang, Qingyan Luo
- 58 - 69 **Programmed death ligand-1, tumor infiltrating lymphocytes and HLA expression in Chinese extrahepatic cholangiocarcinoma patients: Possible immunotherapy implications.**
Fei Yu, Lei Gong, Zheng Mo, Wenran Wang, Meilong Wu, Jianghui Yang, Qiongqiong Zhang, Li Li, Jingjing Yao, Jiahong Dong
- 70 - 76 **Preoperative evaluation of the degree of liver fibrosis based on matter-element analysis using serological indicators in patients with hepatocellular carcinoma.**
Wei Liu, Xiaosong Li, Weihong Zheng, Rucheng Yao, Jun Zheng
- 77 - 85 **Prognosis for patients with hepatocellular carcinoma (HCC) with bile duct tumor thrombus (BDTT) after surgical treatment.**
Zhichuan Lin, Mingrui Han, Zhi Zhou

Brief Report

- 86 - 90 **Structural analyses of a hemolytic compound found in an extract of *Hypsizygus marmoreus* fruiting bodies at a low pH.**
Yoshiki Oda, Kohsuke Saito, Munehiro Nakata
- 91 - 97 **Novel HDAC6 selective inhibitors with 4-aminopiperidine-1-carboxamide as the core structure enhanced growth inhibitory activity of bortezomib in MCF-7 cells.**
Chenru Zhao, Jianjun Gao, Li Zhang, Li Su, Yepeng Luan
- 98 - 104 **Combined machine learning and functional magnetic resonance imaging allows individualized prediction of high-altitude induced psychomotor impairment: The role of neural functionality in putamen and pallidum.**
Xiaoming Chen, Qian Zhang, Jiye Wang, Zhenlong Xin, Jingyuan Chen, Wenjing Luo

Communication

- 105 - 106 **"History, Tradition, and Progress": The ceremony of 150th Anniversary of the National Center for Global Health and Medicine held in Tokyo, Japan.**
Norihiro Kokudo, Tetsuo Hara

Letter

- 107 - 109 **Prevention of mother-to-child transmission (PMTCT) continues to play a vital role in the response to HIV/AIDS: Current status and future perspectives.**
Qi Tang, Min Liu, Hongzhou Lu

Guide for Authors

Copyright

Improvement in the diagnosis and treatment of T2 gallbladder carcinoma is pivotal to improvement in the overall prognosis for this disease

Di Zhou¹, Jiandong Wang¹, Zhiwei Quan¹, Yong Yang^{1,*}, Fei Ma^{2,*}

¹ Department of General Surgery, XinHua Hospital, Shanghai Jiao Tong University, School of Medicine, Shanghai, China;

² Department of Oncology, XinHua Hospital, Shanghai Jiao Tong University, School of Medicine, Shanghai, China.

Summary Since the American Joint Committee on Cancer (AJCC) subdivided the T2 stage of gallbladder carcinoma (GBC) into T2a and T2b, the diagnosis and treatment of those stages have been a subject of heated discussion and controversy. T2 is a stage of GBC that might be treatable. Based on the extent of lymph node metastasis and distant metastasis, T2 GBC can be classified into various pathological stages such as IIA, IIB, IIIB, and IVB, leading to controversy in clinical settings. This review aims to discuss the effectiveness of and controversies concerning S4b+5 resection, the acceptable extent of lymph node dissection, the timing for treatment of incidental gallbladder cancer, and adjuvant therapy. This review also aims to suggest directions for and recommendations regarding clinical research in the future.

Keywords: Gallbladder carcinoma, adjuvant therapy, chemotherapy, radiotherapy

1. Introduction

Stage T2 gallbladder carcinoma (GBC) is defined as cancer invading the connective tissue around the muscular layer without invasion of the serosa or liver. The TNM staging criteria for GBC (8th edition) of the American Joint Committee on Cancer (AJCC), which was issued on January 1, 2018, subdivided the original T2 stage in the 7th edition into T2a and T2b. T2a is cancer invading the peritoneal side of the gallbladder without invading the serosa while T2b is cancer invading the hepatic side of the gallbladder without invading the liver (1). This change is based on the fact that the location of a lesion may have a significant impact on the treatment regimen and patient outcome. In China, the most updated guidelines for GBC are the "Guidelines for Diagnosis and Treatment of Gallbladder Carcinoma" developed by

the Group of Biliary Surgery of the Chinese Society of Surgery in 2015, but those guidelines did not mention the impact of the location of cancer on the treatment strategy and patient prognosis (2). T2 GBC is a highly unique entity. Based on the extent of lymph node metastasis and distant metastasis, T2 GBC can be classified into various pathological stages such as IIA, IIB, IIIB, and IVB, leading to controversy in clinical settings. For example, when is S4b+5 segmental hepatectomy needed? What is the acceptable extent of lymph node dissection? What is the timing for treatment of incidental GBC? What form of postoperative adjuvant therapy should be used? The data reported in the literature regarding the rate of lymph node metastasis and patient prognosis also vary substantially. While referring to the AJCC's redefinition of T2 GBC, this review will discuss topics that are the subject of heated discussion and controversy. This review will also suggest directions for and recommendations regarding clinical research in the future.

*Address correspondence to:

Dr. Fei Ma, Department of Oncology, XinHua Hospital, Shanghai Jiao Tong University, School of Medicine, No. 1665 Kong Jiang Road, Yang Pu District, Shanghai, China.
E-mail: mafei@xinhua.med.cn

Dr. Yong Yang, Department of General Surgery, XinHua Hospital, Shanghai Jiao Tong University, School of Medicine, No. 1665 Kong Jiang Road, Yang Pu District, Shanghai, China.
E-mail: Ly008344@medmail.com.cn

2. The necessity of S4b+5 liver resection

2.1. Surgical anatomical basis for S4b+5 segmental hepatectomy

The 2015 guidelines refer to a study by Goetze *et al.*

(3) which found that the extent of cystic vein drainage from T2 GBC into the liver was about 2 to 5 cm from the gallbladder bed and was > 4 cm in at least one direction. Wedge resection alone does not guarantee an R0 resection, so an S4b+5 resection is considered essential.

2.2. Current status of S4b+5 resection

According to a statistical study by Sternby *et al.* (4) of 44 articles published between April 2015 and June 2016, S4b+5 segmental hepatectomy improved the prognosis for T2 GBC. However, Sternby *et al.* contended that those studies constituted a low level of evidence because they involved a limited number of cases, they were exclusively retrospective observational studies and case reports, and they did not discuss the impact that lesions on the peritoneal or hepatic side of the gallbladder had on prognosis. In March 2017, Kawahara *et al.* (5) published a retrospective study of 22 patients who underwent surgery for T2 GBC. The authors performed different surgical procedures based on the location of the lesion: full-thickness cholecystectomy (FC) + local lymph node dissection if a lesion of the gallbladder fundus or corpus is on the peritoneal side of the gallbladder (P-type) [author's note: this is T2a]; gallbladder bed resection (GBR) + local lymph node dissection if the lesion is on the hepatic side of the gallbladder (H type) [author's note: this is T2b]; GBR + extrahepatic bile duct resection + local lymph node dissection if the lesion is on the cystic duct (N type). Of 7 patients with the P Type, only one developed bile duct recurrence 5 years after surgery. Of 6 patients with the H Type, one developed bile duct recurrence and another developed lymph node metastasis, but no patients developed liver metastasis; of 9 patients with the N type, 1 developed bile duct recurrence, 1 developed lymph node metastasis, and 2 developed liver metastasis. The 3-year survival rate was 50% for patients with the P Type, 100% for patients with the H Type, and 75% for patients with the N Type compared to patients undergoing S4b+5 liver resection during the same period. Therefore, the authors concluded that FC or GBR could be performed for T2 GBC involving the fundus or corpus of the gallbladder. However, the biggest limitation of that study was the number of cases it included. In 2017, a study with a larger sample size was reported (6). That study involved 6 centers (including 93 patients with T2b GBC and 99 patients with T2a), and it found that S4b+5 resection significantly improved the 5-year survival rate (80.3% vs. 30.0%, $p = 0.032$) for T2b GBC. However, hepatic resection was not associated with prognosis (70.5% vs. 54.8%, $p = 0.111$) for T2a. A couple of recent studies have reached similar conclusions (7-9), but none of them used T2 GBC located in the neck of the gallbladder as a single arm as the study by Kawahara *et al.* did. In addition, a cohort

study of 232 patients with T2 GBC from 2002 to 2012 by the Ontario Cancer Registry in Canada indicated that S4b+5 resection did improve 5-year survival, but the prognosis still remained poor once vessels and lymph ducts were involved (10).

2.3. Discussion

According to most of the large studies cited here, S4b+5 resection improves the prognosis for T2b GBC without liver metastasis. However, there is no strong evidence to support hepatectomy as a way to improve outcomes once liver metastasis has occurred, even if it is S4b or S5 "local metastasis" (M1).

Therefore, the following issues are crucial in clinical practice:

i) Preoperative assessment. ① Preoperative diagnosis and staging: to date, the most commonly used technique for preoperative evaluation of GBC is enhanced CT, which has a diagnostic accuracy of 84-92%, a sensitivity of 73-87%, and a specificity of 88-100%; its sensitivity and accuracy in T2 GBC staging are 73% and 80%, respectively (11-12). In 2014, Bang *et al.* (13) found that high-resolution ultrasound and MRCP may have a higher sensitivity and accuracy than MDCT in the diagnosis of T2 GBC and the differential diagnosis of T2 GBC and gallbladder gland adenoma. A point worth noting is that the definitive diagnosis of T2 GBC among clinicians is only 33.9%, which differs highly from the rate of definitive diagnosis using imaging (8). ② Characterization of the distribution of the cystic veins and involvement of those structures: once the subserosa is invaded, theoretically there is a risk of metastasis through lymph nodes, vessels, or nerve plexus. Metastasis through a cystic vein is the primary method of hematogenous metastasis and liver metastasis. According to anatomical studies, there are two models of drainage of the cystic veins: the first type is from the fundus and corpus of the gallbladder through the liver bed, before merging into branches of the portal vein in S4b, S5 (primary) and S1, S6, and S8 (secondary). This constitutes the anatomical rationale for S4b+5 resection; the second type is the cystic duct draining into the main trunk of the portal vein and somewhere around left and right bifurcation through the triangle of Calot. Alternatively, it may drain, alongside the peribiliary vein, into the portal vein supplying the anterior right lobe of the liver or intra-hepatic branches of the portal vein in S4 and S1. In conclusion, the cystic veins will completely and eventually drain into the portal vein system. However, it may drain into different part of the portal vein in the liver. This may explain the potential cause of recurrence or metastasis in other liver segments even after S4b+5 resection (14). Therefore, preoperative and intraoperative determination of the pattern of cystic vein drainage and the relationship between the lesion and adjacent veins as well as

venous involvement may be helpful in predicting the risk of metastasis and deciding a surgical strategy. In this regard, preoperative hepatic CT angiography, superior mesenteric vein venography CT (CTAP), and intraoperative fluorescein angiography of the cystic artery with indocyanine green (ICG) may provide certain corroboration. A study using ICG has found that about 2/3 of the cystic veins eventually drain into S4 and S5 (15).

ii) Intraoperative evaluation. ① Intraoperative exploration of the liver: Once preoperative imaging has excluded liver metastasis, the liver is often not carefully explored during cholecystectomy, and especially during laparoscopic cholecystectomy. Thus, the risk of micro-metastases of the liver may exist. Like treating liver metastasis of colon cancer (16), intraoperative ultrasound should be used in radical resection for GBC to carefully scan the entire liver, and especially high-risk areas such as S4 and S5. This technique may detect micro-metastatic lesions smaller than 0.5 cm missed before surgery. It is extremely important in terms of assessing the procedure and predicting patient outcome. ② Examination of frozen sections: During cholecystectomy, and especially in the case of incidental gallbladder cancer, frozen sections are usually used to make a "qualitative diagnosis" of the lesion intraoperatively. A gross or microscopic exam tends to ignore the distribution of features of veins and lymphatic ducts, tissue layers infiltrated by a lesion, and most importantly involvement of vessels and nerves in the gallbladder wall adjacent to the lesion.

2.4. Recommendations

i) An S4b+5 liver resection may help to improve the prognosis for T2b GBC, but its long-term effects on T2 cystic duct lesions still need to be studied;

ii) Before surgery for GBC or diseases involving thickening of the gallbladder wall, an accurate differential diagnosis and imaging staging should be performed to the extent possible to reduce the incidence of incidental T2 gallbladder cancer;

iii) Before and during surgery, drainage of the cystic veins into the liver and tumor invasion of the vessel should be thoroughly understood;

iv) The liver should be carefully explored with ultrasound during surgery to avoid overlooking micro-metastases;

v) Frozen sections should be used intraoperatively to determine the exact location of a lesion in gross specimens, the layout of the cystic veins, the extent of invasion by the tumor according to microscopy, and invasion of vessels/nerves in the gallbladder wall around the lesion;

iv) Segmental hepatectomy should be performed for GBC preoperatively staged as T2a based on careful pre/intra-operative evaluation in steps 2 to 5.

3. Determination of the extent of lymphatic dissection

3.1. Anatomical basis for lymph node dissection in stage T2 GBC

Based on pathology, 60% of the patients with T2 GBC are ultimately diagnosed with lymph node metastasis. There are two layers of lymphatic vessels in the gallbladder wall located in the subserosa, mucosa, and muscular layer. The lymphatic metastasis of GBC starts in the gallbladder and pericholecystic lymph nodes located in the triangle of Calot. The lymphatic drainage pathway is mainly: *i) from cystic and choledochal lymph nodes through hepatic artery and portal vein lymph nodes to the abdominal aorta and inferior vena cava lymph nodes; ii) from cystic and hepatoduodenal ligament lymph nodes to the pancreatic head and portal vein lymph nodes; and iii) from portal vein lymph nodes to the superior mesenteric vein lymph nodes.* In the 7th edition of the AJCC's staging criteria, N1 is defined as metastasis in the lymph nodes of the cystic duct, common bile duct, and hepatoduodenal ligament; N2 is defined as metastasis in the post-pancreatic duodenum lymph nodes, lymph nodes around abdominal arteries, superior mesenteric lymph nodes, para-aortic lymph nodes, and para-inferior vein cava lymph nodes. The 5-year survival rate for T2N0M0(II) is 55.56%, that for T2N1M0(IIIB) is 13.89%, and that for T2N2M0(IVB) is 11.11%, while N2 lymph node involvement is equivalent to distant metastasis (M1). Thus, N2 dissection does not improve prognosis (17-18). In the 8th edition of the staging criteria, the number of metastatic lymph nodes is the basis for staging. At least 6 lymph nodes should be sampled, with ≥ 4 positive lymph nodes indicating the N2 stage. This change is mainly based on recognition of the fact that the number of metastatic lymph nodes, instead of affected sites, is a key factor affecting prognosis. However, this is just Level III evidence, which means that there are obvious flaws in the design of the relevant studies and their subject enrollment (19-20).

3.2. Current status of lymph node dissection

Classifications of the extent of lymph node dissection in the West and Japan differ significantly. The classification of the Japanese Society of Hepatobiliary and Pancreatic Surgery is more detailed than the classification of the AJCC. The former includes: D1: bile duct and cystic duct lymph nodes; D2: common hepatic artery lymph nodes anterior and posterior to the hepatic hilum, superior and inferior to the proper hepatic artery, and superior and posterior to the portal vein and pancreatic head; D3: lymph nodes beyond the range of D1 and D2, including lymph nodes of the abdominal cavity and around the aorta. A retrospective study of lymph node dissection pursuant to this classification indicated that: *i) The extent*

of lymph node dissection had no effect on the prognosis for T2 GBC (T2N0M0) confirmed by postoperative pathology and without lymph node metastasis; this finding is consistent with the thinking of the AJCC; *ii*) D2 and even D3 dissection had more of an effect on the 5-year survival rate according to the Japanese Society of Hepatobiliary and Pancreatic Surgery (66.7%) in comparison to that in Europe and the US (53.8%) (9). Two notable issues are: *i*) There is little quality literature on how the location and number of lymph node metastases affect prognosis in D2 and D3 dissection (similar to N2 dissection in the 7th edition of the AJCC's staging criteria). Only one study analyzed pathological data from 9 cases of postoperative lymph node metastasis in patients with a long-term survival longer than 5 years after D2 or D3 dissection (18). In those cases, more than 2 post-pancreatic head and para-common hepatic artery lymph nodes and 9 para-abdominal aorta metastatic lymph nodes were dissected; *ii*) Studies have found that T2b GBC has a higher rate of lymph node metastasis as well as a higher probability of recurrence of distant lymph node metastasis compared to T2a (16% vs. 3%, $p = 0.019$). Thus, T2b GBC has a worse prognosis (20-21). However, few studies have examined the characteristics of lymph node metastasis in T2a and T2b and whether a different extent of dissection needs to be performed, whether it be in Europe, the US, Japan, South Korea, or China.

Another hot topic concerning lymphatic dissection is the need for excision of the extrahepatic bile duct. Theoretically, when dissecting lymph nodes around the extrahepatic bile duct, tissue around the blood vessels needs to be resected as much as possible, but connective tissue of a certain thickness around the extrahepatic bile duct must be preserved, thereby ensuring the blood supply of the biliary tract. If it is completely "skeletonized," this will lead to atrophy, hardening, stenosis, and even necrosis of the extrahepatic bile duct, thereby increasing the risk of bile leakage. Therefore, the hepatoduodenal ligament cannot be "completely dissected" at the histopathological level. In addition, cytological studies have found that there are hidden cancer cell clusters in the submucosal layer of the common bile duct in patients with T2 cancer (22). In a multi-center large-scale retrospective study in Japan, Onoe *et al.* (23) found that patients with T2 GBC with lymph node metastasis (T2N1M0) who underwent extrahepatic bile duct resection had a 5-year survival rate of 45% versus 55% for patients in whom the bile duct was preserved. Patients without lymph node metastasis (T2N0M0) who underwent extrahepatic bile duct resection had a 5-year survival rate of 72% versus 81% for patients in whom the bile duct was preserved; the 5-year survival rate did not differ significantly between the two groups. This indicates that lymph node metastasis is a key factor affecting prognosis, rather than the resection of the extrahepatic bile ducts. Now that T2 has

been further divided into T2a and T2b, relevant studies have not yet been conducted. In addition, relevant studies on the prognosis for extrahepatic bile duct resection for GBC are mere case reports. In Japan, a total of 22 patients with T2 cancer underwent this procedure from 1975 to 2011, and 2 had no. 12 lymph node metastasis (8). Depending on the cut-off point for the date of follow-up in different studies, survival for patients with T2 cancer who underwent extrahepatic bile duct resection ranged from 12-136 months.

3.3. Discussion

The 7th edition of the AJCC's staging criteria focused on site of lymph node metastasis and contended that "extended lymph node dissection" did not improve patient outcomes. The 8th edition focuses on the number of metastatic lymph nodes. This change reflects the idea that "lymph node metastasis means a poor prognosis." However, T2 has now been divided into T2a and T2b, so neither sub-type is in fact sufficient to guide the determination of the extent of lymph node dissection during actual surgery given factors such as the lower level of evidence. Therefore, whether a different extent of lymph node dissection needs to be performed for T2a and T2b warrants more detailed and in-depth study.

3.4. Suggestions

i) The difference in lymph node metastasis between T2a and T2b GBC (T2a and T2b cystic duct carcinoma may be considered separately) probably needs to be studied with preoperative imaging and intraoperative exploration.

ii) Postoperative pathology needs to determine the location of lymph node metastasis and the corresponding number of positive lymph nodes at each site in order to provide a sufficient and persuasive rationale for performing dissection to a different extent with either type.

Controversies in the surgical treatment of stage T2 gallbladder cancer are shown in Figure 1.

4. Timing and precautions for treating incidental T2 GBC

4.1. Current status of diagnosis and treatment of incidental T2 GBC

One problem that cannot be ignored in the diagnosis and treatment of T2 GBC is the diagnosis and treatment of "incidental GBC." "Incidental GBC" refers to GBC as benign disease before cholecystectomy and determined to be GBC by pathology during or after surgery. "Incidental GBC" is found in 0.3-0.9% of all cholecystectomies. The vast majority of incidental GBCs are in the T1b, T2, or T3 stages, with T2 being the most common: up to 47% (24). In general, the rate of resection in incidental

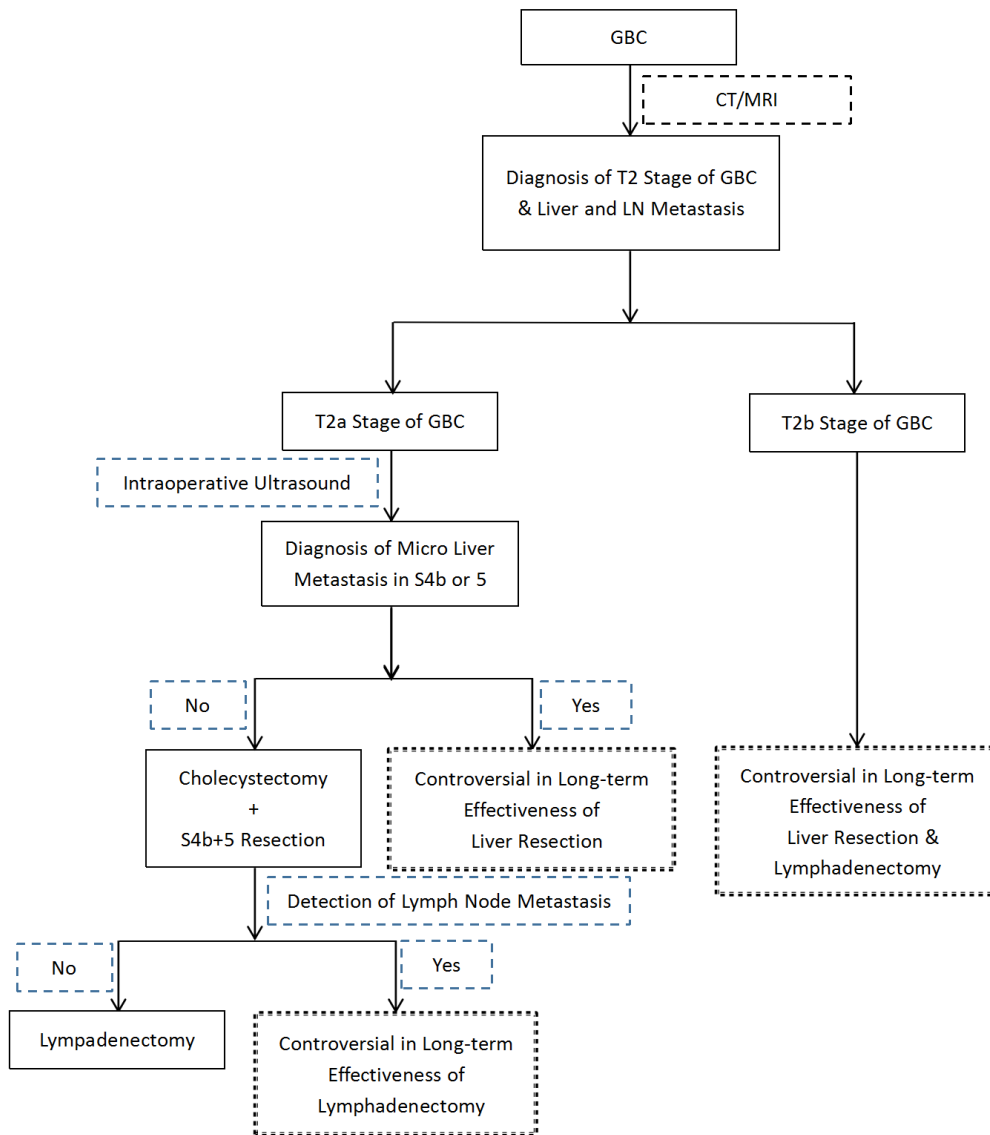


Figure 1. Controversies in the surgical treatment of stage T2 gallbladder cancer.

GBC may be higher than 85%. The rate of lymph node metastasis in T2 GBC is 19-62%, and the residual rate after initial surgery is about 10%. The 5-year survival rate for patients with stage T2 GBC who underwent radical surgery was 78%, which is comparable to that for patients undergoing routine radical surgery for T2 GBC and significantly higher than 38% for patients undergoing simple cholecystectomy (25-26). The rate of lymph node metastasis in patients with incidental T2 GBC and the residual rate of a tumor in primary surgery are significantly lower than those rates in patients with T3 GBC (45-70% and 36%, respectively), and the 5-year survival rate for patients with incidental T2 GBC is significantly higher than that for patients with T3 GBC (8-34%) (24). For patients with stage T3 or more advanced incidental GBC, there may be enough time before surgery and sufficient available resources to assist in diagnosis or early warning, except for a small number of patients who need urgent surgery for "acute severe

cholecystitis, gallbladder perforation, or peritonitis." A question worth considering is whether such cases can be called "incidental gallbladder cancer." In order to reduce the incidence of "incidental gallbladder cancer" and improve the prognosis for those patients, sufficient attention must be paid to preoperative evaluation, primary surgery, and secondary radical surgery.

4.2. *Suggestions*

4.2.1. *Preoperative evaluation: Screening for high-risk patients with "incidental GBC"*

As the concept of laparoscopic cholecystectomy (LC) and day surgery gains traction in hospitals of different levels across the country, preoperative differential diagnosis and treatment for benign gallbladder diseases has become less standardized to some extent. Most surgeons perform LC only after a simple ultrasound and tend to

neglect taking a detailed medical history or performing high-risk screening. Incidental GBC must be kept in mind before the following 13 types of patients undergo a cholecystectomy: (1) elderly patients with gallstones, and especially women. Eight to 10% of patients over 70 years of age with gallstones have associated with gallbladder carcinogenesis; (2) patients with a history of gallstones or cholecystitis for 10 to 15 years or longer; (3) stones larger than 2 cm; (4) fully filled stones; (5) gallbladder wall calcification, porcelain gallbladder, with a malignancy rate as high as 50%; (6) thickening of the gallbladder wall; (7) atrophic gallbladder; (8) gallbladder adenoma or stones with gallbladder polypoid lesions; (9) gallbladder polyps larger than 1 cm; (10) preoperative MRCP suggesting an abnormality in the juncture of the bile and pancreatic ducts; (11) Mirizzi syndrome; (12) previous gallbladder ostomy (27); and (13) in China, patients who have undergone gallbladder-preserving micro-blasting lithotripsy should also be included.

For the above patients, imaging and biochemistry results should be carefully reviewed before surgery, and precancerous lesions such as chronic inflammation, gallbladder mucosal hyperplasia, gallbladder adenomyosis, and yellow granulomatous cholecystitis should be carefully excluded. When the lesion is on the hepatic side of the gallbladder and differential diagnosis is particularly difficult, conventional open surgery should be performed instead of laparoscopic surgery, and pathology of frozen sections should be performed.

4.2.2. Primary surgery: Timely examination of frozen sections

Multi-center studies by Lundgren *et al.* (28) in 2017 and Emmett *et al.* (29) in 2015 indicated that timely examination of frozen gallbladder specimens with gallbladder wall thickening and an abnormal morphology helps to improve the "timely confirmed diagnosis" of incidental GBC and improve prognosis. This is particularly true in elderly patients and patients undergoing emergency cholecystectomy. If laparoscopic exploration reveals a thick gallbladder wall, severe adhesions, or suspected invasion in high-risk patients, then open surgery needs to be performed to avoid cutting through the gallbladder and causing bile to leak. After the resection is complete, frozen sections must be prepared. Even if there is no obvious abnormality, the specimens should be carefully examined after the gallbladder is resected, and the mucosa should be carefully observed for any suspicious lesions before preparing frozen sections. If there is a suspected abnormality, the location should be marked and the pathologist should be informed. Surgery should not conclude until a malignancy-free diagnosis is made. A trocar should be carefully removed to avoid potential implantation.

4.2.3. Secondary cure: Indications and timing

Incidental GBC diagnosed after cholecystectomy should be treated as follows: *i)* TNM staging should be performed as early as possible before the second surgery. ① T staging: to confirm whether the initial surgery is a full-thickness cholecystectomy (FC) and pathological T staging. If the gallbladder is completely resected and the stage is Tis or T1a, no further surgery is needed. If there is residual gallbladder tissue or the pathology is T1b or T2 or more advanced during the first surgery, further surgery may be required. ② N and M staging: to confirm the presence or absence of systemic and lymph node metastasis and to assess the feasibility of further surgery with imaging techniques such as thin-layer dual-source CT or PET-CT. *ii)* The timing of radical surgery is still controversial. The general belief is that immediate radical surgery is necessary when: frozen sections from initial surgery indicate a malignancy; gallbladder inflammation is mild and the anatomical structure of the area to be radically treated is clear; or gallbladder rupture or bile leakage could occur during LC, leading to implantation. Indications for second-stage radical surgery: frozen sections from the primary surgery do not indicate a malignancy; tissue inflammation and adhesions in the area to be radically treated are so severe that its anatomical structure cannot be identified; assessment of tumor resectability and accurate preoperative staging is not feasible in the short term. Currently, there are no prospective, large-sample randomized controlled trials indicating an acceptable interval between primary surgery and secondary radical surgery. In a large-sample retrospective study in 2017, Ethun *et al.* (30) suggested that secondary radical surgery for incidental T1b and T2 GBC should be performed within 4-8 weeks after primary surgery to improve prognosis. Prior to 4 weeks, inflammation, edema, and adhesions caused by the primary surgery will affect radical surgery, while the rate of an R1 or R2 resection increases significantly ($p = 0.05$ and < 0.001). Eight weeks after the primary surgery is long enough to significantly increase the probability of recurrence and metastasis. However, a study has reported that an interval of 3 months is more helpful in eliminating distant metastases, avoiding an unnecessary laparotomy, improving the rate of a radical resection, and improving the long-term survival rate (31) A national multicenter, prospective, randomized, controlled trial should be conducted to determine the optimal timing for radical surgery to treat incidental T2a and T2b GBC in the future.

5. Adjuvant therapy

Postoperative adjuvant therapy is the least valued part of the comprehensive treatment of GBC worldwide. This is explained by the fact that there is no widely accepted or effective adjuvant therapy regimen. Surgeons typically emphasize surgery, the concept of multi-disciplinary treatment (MDT) is seldom adopted, and GBC is

known to be extremely resistant to radiotherapy and chemotherapy. In fact, insightful studies of various agents and new radiotherapy techniques have increasingly reported forms of adjuvant therapy that could improve the prognosis for GBC.

5.1. The significance of adjuvant therapy for T2 GBC

The extent of organ resection and lymphadenectomy in radical surgery for T2 or more advanced GBC has not been determined. Postoperatively, the rate of residual cancer, recurrence, and metastasis is high, so adjuvant therapy is of great significance. In 2017, Mitin *et al.* (32) published statistics on the diagnosis and treatment of 5029 patients with T1-3 N0-1 GBC between 2005 and 2013, and they found that postoperative adjuvant therapy was under-performed for GBC. The proportion of patients receiving adjuvant chemotherapy decreased from 4.2% to 1.7%, the proportion of patients receiving radiotherapy increased from 8.3% to 13.8%, and the proportion of patients receiving a combination of radiotherapy and chemotherapy remained the same at 15.9%. At the same time, adjuvant therapy has been found to significantly improve the 3-year survival rate for patients with GBC except for T1N0. In patients with T2N0 cancer, the 3-year survival rate was 46.8% for surgery alone, 63.0% for adjuvant chemotherapy (AC), and 61.2% for adjuvant chemotherapy and radiation therapy (ACR). The 3-year survival rate differed significantly between surgery alone and AC or ACR, but the results of adjuvant radiotherapy are uncertain. In 2015, Hoehn *et al.* (33) examined clinical data from 6,690 patients with GBC in the National Cancer Database of the American College of Surgeons from 1998 to 2006, and they found that ACR significantly improved the prognosis for patients with T2/3 cancer, and especially lymph node metastasis (T2-3/N1-2) or with an unknown status of lymph node metastasis (T2-3/Nx). Kasumova *et al.* (34) found that patients receiving extended radical + postoperative adjuvant therapy had a significantly longer median survival (23.3 months) than that of patients receiving cholecystectomy + postoperative adjuvant therapy (16.4 months), simple cholecystectomy (12.4 months), or extended GBC surgery (10.7 months). This suggests that adjuvant therapy can benefit patients with T2/3 GBC. Therefore, the short-term effect of cholecystectomy plus postoperative adjuvant therapy is superior to extended resection, which can serve as a potential alternative treatment for high-risk patients who cannot undergo extended radical resection.

5.2. Adjuvant chemotherapy

According to current National Comprehensive Cancer Network (NCCN) guidelines, chemotherapy for GBC involves a 5-fluorouracil (5-FU)-based chemotherapy regimen. Regular options for drugs include 5-FU,

capecitabine, gemcitabine, and oxaliplatin. Most phase II clinical trials support multi-drug combined chemotherapy. To date, numerous clinical trials of adjuvant chemotherapy have been conducted worldwide (Table 1), but only one phase III clinical trial had positive outcomes: gemcitabine plus cisplatin (GP) was superior to gemcitabine alone and significantly prolonged median progression-free survival (PFS) in patients with GBC (35).

5.3. Adjuvant radiotherapy

Adjuvant radiotherapy for GBC includes external, intraoperative, and intra-biliary radiotherapy. Of the three, external radiotherapy is most commonly used. A study has indicated that GBC beyond the T2 stage, and especially that with lymph node metastasis or an R1/2 resection, should be treated with radiotherapy with an intensity of > 40 Gy. The main goal is to reduce the rate of local recurrence (36). However, the preferred dose, timing, and form of radiotherapy have yet to be determined. In addition, new radiotherapy techniques such as stereotactic body radiotherapy (SBRT) are beginning to be used in the clinical treatment of advanced GBC.

5.4. Adjuvant chemo/radiotherapy and neoadjuvant chemo/radiotherapy

Adjuvant chemo-radiation for GBC is mainly a fluorouracil-based regimen combined with external radiotherapy. The main goal is to reduce the rate of local recurrence and thus prolong survival to a certain extent. Recent studies are mostly phase II clinical trials. For example, the SWOG S0809 Phase II trial (37) in 2015 involved patients with T2 or more advanced or lymph node-positive GBC. After the first stage of adjuvant chemotherapy with 4 cycles of gemcitabine (1,000 mg/m² daily, day 1, 8) + capecitabine (1,500 mg/m² daily, day 1-14), the second stage was capecitabine (1,330 mg/m² daily) + concurrent radiotherapy (tumor bed area 54.0-59.4 Gy+ the area of lymphatic drainage 45 Gy). Results indicated that the 2-year overall survival rate was 56% and the 2-year disease-free survival rate was 48%, which are acceptable rates.

Neoadjuvant chemoradiotherapy for GBC is currently in its infancy. That treatment is mainly used to treat patients with unresectable GBC that is beyond the T2 stage. In 2015, Sirohi *et al.* (38) used gemcitabine plus cisplatin as a regimen for the treatment of 37 patients with advanced GBC in India. The treatment achieved a total response rate of 67.5%, and cancer was down-staged in 48.6% of patients. In 17 (46%) the cancer was resectable. In general, the literature indicates that adjuvant chemoradiotherapy and neoadjuvant chemoradiotherapy are indicated for patients with T2 or more advanced GBC, patients with lymph node

Table 1. Clinical trials of adjuvant chemotherapy worldwide

Study Topic	Country
--	China
Efficacy of somatostatin + epirubicin +5-Fu in the treatment of advanced GBC	Australia
The efficacy of postoperative adjuvant chemotherapy for GBC	India
Efficacy of gemcitabine combined with pazopanib in the treatment of GBC	Greece
Selumetinib combined with cisplatin/gemcitabine (CIS/GEM) vs. CIS/GEM alone	Canada
Efficacy of adjuvant chemotherapy followed by adjuvant chemotherapy in patients with GBC	China
Effect of DKN-01 combined with gemcitabine/cisplatin on gallbladder cancer	USA
Efficacy of Acelarin combined with cisplatin in the treatment of locally advanced/metastatic stage Ib GBC	UK
Effect of conservative symptomatic treatment vs. combined with mFOLFOX chemotherapy regimen on locally advanced/metastatic GBC	UK
Efficacy of recombinant EphB4 fusion protein combined with standard chemotherapy regimen in the treatment of advanced/metastatic solid tumors	USA
Genetic analysis of different FOLFIRABRAX doses for the treatment of advanced gastrointestinal tumors	USA
Effect of ADH-1, gemcitabine combined with cisplatin on advanced metastatic GBC	USA
Effect of TAS-102 on advanced biliary tract tumors	USA
Effect of Merestinib (LY2801653) on advanced or advanced GBC in Japanese	Japan
Regorafenib alone for treatment of local progression and metastatic GBC with first-line treatment failure	USA
Effect of T cell-mediated adaptive immune response therapy on Her-2 positive digestive system tumors	China
Regorafenib alone for the treatment of refractory advanced biliary tract tumors	USA
Efficacy of gemcitabine and cisplatin combined with nab- paclitaxel in the treatment of advanced biliary tract tumors	USA
Effect of GEMOX regimen (gemcitabine, cisplatin) vs. XELOX (Xeloda, cisplatin) on advanced biliary tract tumors	South Korea
Ramucirumab for the treatment of advanced GBC	USA

metastasis, patients in whom an R0 resection has not been achieved, or patients with unresectable GBC.

6. Conclusion

Since the AJCC subdivided the T2 stage of GBC into T2a and T2b, the diagnosis and treatment of those stages have been a subject of heated discussion and controversy. T2 is a stage of GBC that might be treatable. Large-scale clinical studies adopting the concepts of comprehensive treatment and multidisciplinary collaboration might make progress in diagnosis, surgery, and adjuvant therapy. Those findings would contribute significantly overall improvement in the prognosis for GBC.

References

- Tang ZH, Tian XD, Wei MY, Wang WM, Quan ZW. Interpretation of the American Cancer Joint Committee's biliary malignant staging system (8th edition). Chinese Journal of Practical Surgery. 2017; 37:248-254. (in Chinese)
- Department of Biliary Surgery, Chinese Medical Association Surgery Branch. Guideline for the diagnosis and treatment of gallbladder cancer (2015 edition). Chinese Journal of Digestive Surgery. 2015; 14:881-890. (in Chinese)
- Goetze TO, Paolucci V. The prognostic impact of positive lymph nodes in stages T1 to T3 incidental gallbladder carcinoma: Results of the German Registry. Surg Endosc. 2012; 26:1382-1389.
- Sternby Eilard M, Lundgren L, Cahlin C, Strandell A, Svanberg T, Sandstrom P. Surgical treatment for gallbladder cancer - A systematic literature review. Scand J Gastroenterol. 2017; 52:505-514.
- Kawahara R, Shirahama T, Arai S, *et al.* Evaluation of surgical procedures for T2 gallbladder cancer in terms of recurrence and prognosis. Kurume Med J. 2017; 63:15-22.
- Lee W, Jeong CY, Jang JY, *et al.* Do hepatic-sided tumors require more extensive resection than peritoneal-sided tumors in patients with T2 gallbladder cancer? Results of a retrospective multicenter study. Surgery. 2017; 162:515-524.
- Ume Y, Miyashita T, Ueda S, Hashida K, Hashimoto Y, Maeda M. Laparoscopic cholecystectomy with full-thickness dissection and laparoscopic resection of the gallbladder bed for polypoid and wall thickening lesions. Nihon Rinsho Geka Gakkai Zasshi. 2014; 75:353-359. (in Japanese)
- Onoe S, Kaneoka Y, Maeda A, Takayama Y, Fukami Y, Isogai M. Hepatectomy of segment 4b and 5 with extrahepatic bile duct resection for pT2 gallbladder carcinoma is valid: a single-institution result. Updates Surg. 2015; 67:265-271.
- Horiguchi A, Miyakawa S, Ishihara S, *et al.* Gallbladder bed resection or hepatectomy of segments 4a and 5 for pT2 gallbladder carcinoma: Analysis of Japanese registration cases by the study group for biliary surgery of the Japanese Society of Hepato-Biliary-Pancreatic Surgery. J Hepatobiliary Pancreat Sci. 2013; 20:518-524.
- Tharmalingam S, Flemming J, Richardson H, Hurlbut D, Nanji S. Surgical practice patterns and outcomes in T2 and T3 gallbladder cancer: Insights from a population based study. HPB. 2017; 19:S34.
- Mitchell CH, Johnson PT, Fishman EK, Hruban RH, Raman SP. Features suggestive of gallbladder malignancy: Analysis of T1, T2, and T3 tumors on cross-sectional imaging. J Comput Assist Tomogr. 2014; 38:235-241.
- Yoshimitsu K, Honda H, Shinozaki K, Aibe H, Kuroiwa T, Irie H, Chijiwa K, Asayama Y, Masuda K. Helical CT of the local spread of carcinoma of the gallbladder: Evaluation according to the TNM system in patients who underwent surgical resection. AJR Am J Roentgenol. 2002; 179:423-428.
- Bang SH, Lee JY, Woo H, Joo I, Lee ES, Han JK, Choi

- BI. Differentiating between adenomyomatosis and gallbladder cancer: Revisiting a comparative study of high-resolution ultrasound, multidetector CT, and MR imaging. *Korean J Radiol.* 2014; 15:226-234.
14. Yoshimitsu K, Honda H, Kaneko K, Kuroiwa T, Irie H, Chijiwa K, Takenaka K, Masuda K. Anatomy and clinical importance of cholecystic venous drainage: Helical CT observations during injection of contrast medium into the cholecystic artery. *AJR Am J Roentgenol.* 1997; 169:505-510.
 15. Kai K, Satoh S, Watanabe T, Endo Y. Evaluation of cholecystic venous flow using indocyanine green fluorescence angiography. *J Hepatobiliary Pancreat Sci.* 2010; 17:147-151.
 16. Lucchese AM, Kalil AN, Schwengber A, Suwa E, Rolim de Moura GG. Usefulness of intraoperative ultrasonography in liver resections due to colon cancer metastasis. *Int J Surg.* 2015; 20:140-144.
 17. Lee SE, Kim KS, Kim WB, Kim IG, Nah YW, Ryu DH, Park JS, Yoon MH, Cho JY, Hong TH, Hwang DW, Choi DW. Practical guidelines for the surgical treatment of gallbladder cancer. *J Korean Med Sci.* 2014; 29:1333-1340.
 18. Shirai Y, Sakata J, Wakai T, Ohashi T, Hatakeyama K. "Extended" radical cholecystectomy for gallbladder cancer: Long-term outcomes, indications and limitations. *World J Gastroenterol.* 2012; 18:4736-4743.
 19. Kondo S, Nimura Y, Hayakawa N, Kamiya J, Nagino M, Uesaka K. Regional and para-aortic lymphadenectomy in radical surgery for advanced gallbladder carcinoma. *Br J Surg.* 2000; 87:418-422.
 20. Shindoh J, de Aretxabala X, Aloia TA, Roa JC, Roa I, Zimmitti G, Javle M, Conrad C, Maru DM, Aoki T, Vigano L, Ribero D, Kokudo N, Capussotti L, Vauthey JN. Tumor location is a strong predictor of tumor progression and survival in T2 gallbladder cancer: An international multicenter study. *Ann Surg.* 2015; 261:733-739.
 21. Sheikh MR, Osman H, Cheek S, Hunter S, Jeyarajah DR. T2 gallbladder cancer-aggressive therapy Is warranted. *Am Surg.* 2016; 82:518-521.
 22. Chikamoto A, Tsuji T, Nakahara O, Sakamoto Y, Ikuta Y, Tanaka H, Takamori H, Hirota M, Kanemitsu K, Baba H. Cancer cells spread through lymph vessels in the submucosal layer of the common bile duct in gallbladder carcinoma. *J Hepatobiliary Pancreat Surg.* 2009; 16:557-561.
 23. Bains L, Kaur D, Kakar AK, Batish A, Rao S. Primary carcinoma of the cystic duct: A case report and review of classifications. *World J Surg Oncol.* 2017; 15:30.
 24. Choi KS, Choi SB, Park P, Kim WB, Choi SY. Clinical characteristics of incidental or unsuspected gallbladder cancers diagnosed during or after cholecystectomy: A systematic review and meta-analysis. *World J Gastroenterol.* 2015; 21:1315-1323.
 25. Duffy A, Capanu M, Abou-Alfa GK, Huitzil D, Jarnagin W, Fong Y, D'Angelica M, Dematteo RP, Blumgart LH, O'Reilly EM. Gallbladder cancer (GBC): 10-year experience at Memorial Sloan-Kettering Cancer Centre (MSKCC). *J Surg Oncol.* 2008; 98:485-489.
 26. Yin XY. Treatment of unexpected gallbladder cancer during and after cholecystectomy. *Chinese Journal of Practical Surgery.* 2015; 35:942-945. (in Chinese)
 27. Contini S, Dalla Valle R, Zinicola R. Unexpected gallbladder cancer after laparoscopic cholecystectomy: An emerging problem? Reflections on four cases. *Surg Endosc.* 1999; 13:264-267.
 28. Lundgren L, Muszynska C, Ros A, Persson G, Gimm O, Valter L, Andersson B, Sandstrom P. Are incidental gallbladder cancers missed with a selective approach of gallbladder histology at cholecystectomy? *World J Surg.* 2018; 42:1092-1099.
 29. Emmett CD, Barrett P, Gilliam AD, Mitchell AI. Routine versus selective histological examination after cholecystectomy to exclude incidental gallbladder carcinoma. *Ann R Coll Surg Engl.* 2015; 97:526-529.
 30. Ethun CG, Postlewait LM, Le N, *et al.* Association of optimal time interval to re-resection for incidental gallbladder cancer with overall survival: A multi-institution analysis from the US Extrahepatic Biliary Malignancy Consortium. *JAMA Surg.* 2017; 152:143-149.
 31. Ausania F, Tsirlis T, White SA, French JJ, Jaques BC, Charnley RM, Manas DM. Incidental pT2-T3 gallbladder cancer after a cholecystectomy: Outcome of staging at 3 months prior to a radical resection. *HPB.* 2013; 15:633-637.
 32. Mitin T, Enestvedt CK, Jemal A, Sineshaw HM. Limited use of adjuvant therapy in patients with resected gallbladder cancer despite a strong association with survival. *J Natl Cancer Inst.* 2017; 109.
 33. Hoehn RS, Wima K, Ertel AE, Meier A, Ahmad SA, Shah SA, Abbott DE. Adjuvant therapy for gallbladder cancer: An analysis of the National Cancer Data Base. *J Gastrointest Surg.* 2015; 19:1794-1801.
 34. Kasumova GG, Tabatabaie O, Najarian RM, Callery MP, Ng SC, Bullock AJ, Fisher RA, Tseng JF. Surgical management of gallbladder cancer: Simple versus extended cholecystectomy and the role of adjuvant therapy. *Ann Surg.* 2017; 266:625-631.
 35. Stein A, Arnold D, Bridgewater J, Goldstein D, Jensen LH, Klumpen HJ, Lohse AW, Nashan B, Primrose J, Schrum S, Shannon J, Vettorazzi E, Wege H. Adjuvant chemotherapy with gemcitabine and cisplatin compared to observation after curative intent resection of cholangiocarcinoma and muscle invasive gallbladder carcinoma (ACTICCA-1 trial) - A randomized, multidisciplinary, multinational phase III trial. *BMC cancer.* 2015; 15:564.
 36. Shui YJ, Wei QC. The role and status of adjuvant chemotherapy and radiotherapy in the comprehensive treatment of gallbladder cancer. *Chinese Journal of Practical Surgery.* 2016; 36:1122-1124. (in Chinese)
 37. Ben-Josef E, Guthrie KA, El-Khoueiry AB, Corless CL, Zalupski MM, Lowy AM, Thomas CR, Jr., Alberts SR, Dawson LA, Micetich KC, Thomas MB, Siegel AB, Blanke CD. SWOG S0809: A phase II intergroup trial of adjuvant capecitabine and gemcitabine followed by radiotherapy and concurrent capecitabine in extrahepatic cholangiocarcinoma and gallbladder carcinoma. *J Clin Oncol.* 2015; 33:2617-2622.
 38. Sirohi B, Mitra A, Jagannath P, Singh A, Ramadvar M, Kulkarni S, Goel M, Shrikhande SV. Neoadjuvant chemotherapy in patients with locally advanced gallbladder cancer. *Future Oncol.* 2015; 11:1501-1509.

(Received January 17, 2019; Revised February 19, 2019; Accepted February 26, 2019)

Efficacy and safety of external-beam radiation therapy for hepatocellular carcinoma: An overview of current evidence according to the different target population

Bing Han^{1,2,3,§}, Chuan Li^{4,§}, Hao Meng^{5,§}, Fernando Gomes Romeiro⁶, Andrea Mancuso^{7,8}, Zhirui Zhou⁹, Giovanni Battista Levi Sandri¹⁰, Ying Xu¹¹, Tao Han¹², Lei Han^{13,*}, Lichun Shao^{3,*}, Xingshun Qi^{1,*}

¹ Department of Gastroenterology, General Hospital of Northern Theater Command (formerly General Hospital of Shenyang Military Area), Shenyang, Liaoning, China;

² Postgraduate College, Jinzhou Medical University, Jinzhou, Liaoning, China;

³ Department of Gastroenterology, No. 463 Hospital of Chinese PLA, Shenyang, Liaoning, China;

⁴ Section of Medical Service, General Hospital of Northern Theater Command (formerly General Hospital of Shenyang Military Area), Shenyang, Liaoning, China;

⁵ Department of Thoracic Surgery, General Hospital of Northern Theater Command (formerly General Hospital of Shenyang Military Area), Shenyang, Liaoning, China;

⁶ Department of Internal Medicine, Botucatu Medical School, Universidade Estadual Paulista (UNESP), Botucatu, SP, Brazil;

⁷ Epatologiae Gastroenterologia, Ospedale Niguarda Ca' Granda, Milano, Italy;

⁸ Medicina Internal, Azienda di Rilievo Nazionale ad Alta Specializzazione Civico - Di Cristina - Benfratelli, Palermo, Italy;

⁹ Department of Radiation Oncology, Fudan University Shanghai Cancer Center, Shanghai, China;

¹⁰ Division of General Surgery and Liver Transplantation, San Camillo Hospital, Rome, Lazio, Italy;

¹¹ Department of Radiotherapy, General Hospital of Northern Theater Command (formerly General Hospital of Shenyang Military Area), Shenyang, Liaoning, China;

¹² Department of Oncology, Cancer Center, General Hospital of Northern Theater Command (formerly General Hospital of Shenyang Military Area), Shenyang, Liaoning, China;

¹³ Department of Hepatobiliary Surgery, General Hospital of Northern Theater Command (formerly General Hospital of Shenyang Military Area), Shenyang, Liaoning, China.

Summary

Hepatocellular carcinoma (HCC) is one of the most common malignant tumors. During the recent years, external-beam radiation therapy (EBRT) has been safely and effectively employed for the management of HCC. We overviewed the current evidence regarding the efficacy and safety of EBRT for HCC according to the different target population. PubMed database was searched for identifying English-language full-text articles regarding EBRT for the treatment of HCC. Search items were "hepatocellular carcinoma AND radiation therapy". Until now, preliminary evidence has suggested the following role of EBRT for HCC. 1) EBRT, especially stereotactic body radiation therapy, is an emerging choice of therapy for small HCC. 2) EBRT combined with non-surgical treatment can achieve an excellent intrahepatic tumor control and a potential survival benefit for huge HCC. 3) Adjunctive EBRT may improve the efficacy of transarterial chemoembolization for HCC with portal vein tumor thrombosis. 4) EBRT can relieve the pain and improve the quality of life for patients with extrahepatic metastases. 5) EBRT may be a bridge to liver transplantation by minimizing the tumor progression. 6) Adjunctive EBRT may reduce the tumor recurrence and improve the survival after resection. In summary, EBRT is a promising choice of treatment of HCC. However, more high-quality evidence is needed to further establish the status of EBRT for the management of HCC.

Keywords: Liver cancer, radiation therapy, evidence, survival

1. Introduction

Hepatocellular carcinoma (HCC) is one of the most common malignancies (1). Treatment selection and prognostic assessment of HCC often depends on the tumor stage, performance status, and severity of liver dysfunction. Currently, there are lots of staging systems for HCC (2-4). Barcelona Clinic Liver Cancer (BCLC) staging system may be the most commonly used system for the management of HCC. According to the BCLC staging system, liver transplantation, surgical resection, and local ablative therapies, such as percutaneous ethanol injection or radiofrequency ablation (RFA), are recommended in the treatment of BCLC stage 0 or A HCC; transarterial chemoembolization (TACE) is recommended in the treatment of BCLC stage B HCC; and sorafenib is recommended in the treatment of BCLC stage C HCC (5). Except for the common therapeutic strategies, lots of novel therapeutic modalities have been widely explored (6,7).

Radiation therapy is a major traditional anticancer modality for solid tumors along with surgery and chemotherapy. In the past, the role of radiation therapy was very limited in the treatment of HCC due to the poor tolerance and low radiosensitivity of liver. Nowadays, internal radiation therapy, such as radioembolization, has been increasingly recognized for the management of HCC (8,9). By comparison, the role of external-beam radiation therapy (EBRT) needs further confirmation in HCC patients. Recently, the 2014 Korean Practice Guideline suggests that EBRT can be considered if patients have preserved liver function (*i.e.*, Child-Pugh class A or superb B), are not eligible for major treatments, have an incomplete response to TACE, or have portal vein invasion when the percentage of irradiated total liver volume receiving ≥ 30 Gy is $\leq 60\%$ there is a demand for alleviating the symptoms caused by primary HCC or its metastases (10).

Modern EBRT has been employed for the management of HCC, which can deliver a higher

radiation dose to the tumor more precisely and produce a lower risk of EBRT-induced liver disease (RILD) (11). More notably, EBRT can result in a high local tumor control rate of 70.0-100.0% in HCC patients (12,13). Considering a promising role of EBRT alone and in combination with other therapies for HCC, this paper aimed to overview the current evidence regarding the efficacy and safety of EBRT for HCC according to the different target population.

2. EBRT approaches

Modern EBRT approaches include 3-dimensional conformal radiation therapy (3D-CRT), intensity-modulated radiation therapy (IMRT), stereotactic ablative body radiation therapy (SBRT), and image-guided radiation therapy. Three major EBRT approaches are reviewed in details as follows.

2.1. 3D-CRT

In contrast to the conventional 2D-RT technique, 3D-CRT uses multiple coplanar or non-coplanar fields in order to reduce the high-dose exposure of normal tissues including the liver and bowels and to increase the tumor dose coverage. With the use of CT images for RT planning and a computerized treatment planning system, the tumor and surrounding normal liver can be accurately delineated, and the delivered dose and irradiated volume of the tumor and normal liver can be precisely evaluated. However, the risk of RILD remains high, especially in patients with Child-Pugh class B or C, prior TACE, portal vein invasion, and hepatitis B carrier status (14,15). Considering that these risk factors are unavoidable in patients undergoing CRT, 3D-CRT is useful to overcome these obstacles and improve the clinical outcomes in terms of tumor control and normal tissue toxicity.

2.2. IMRT

IMRT is an advanced form of conformal RT that facilitates the delivery of a higher radiation dose as compared to 3D-CRT. A computer-aided automated optimization process, known as inverse treatment planning, modulates the intensity of each beam to gain the desired target coverage while minimizing the dose to the normal organs. IMRT has the potential of dose escalation for HCC without an increased risk of RILD as compared to 3D-CRT, which signals the potential for improved survival and quality of life in HCC patients (15,16). However, there is no standard technique for IMRT delivery and the IMRT plan is not always better than the 3D-CRT plan.

2.3. SBRT

SBRT is generally defined as a treatment modality

Released online in J-STAGE as advance publication February 24, 2019.

§These authors contributed equally to this work.

*Address correspondence to:

Dr. Xingshun Qi, Department of Gastroenterology, General Hospital of Northern Theater Command (formerly General Hospital of Shenyang Military Area), No. 83 Wenhua Road, Shenyang 110840, Liaoning Province, China.
E-mail: xingshunqi@126.com

Dr. Lichun Shao, Department of Gastroenterology, No. 463 Hospital of Chinese PLA, No. 46 Xiaoheyan Road, Shenyang 110000, Liaoning Province, China.
E-mail: slc700214@163.com

Dr. Lei Han, Department of Hepatobiliary Surgery, General Hospital of Northern Theater Command (formerly General Hospital of Shenyang Military Area), Shenyang 110840, Liaoning Province, China.
E-mail: hanlei1974@sina.com

for delivering a high dose of radiation to the target in a few fractions (typically 1-5 fractions) with a high degree of precision. SBRT with a common linear accelerator usually utilizes multiple coplanar or non-coplanar static beams or multiple arc beams. To irradiate the tumor more accurately and to increase the sparing of the normal organs, SBRT is performed in combination with at least one kind of image-guided RT technique integrated into the treatment machine. During the last decade, the use of SBRT for HCC has increased substantially and the practice guidelines recommend SBRT as an alternative to the ablation/embolization techniques, or when they have failed or are contraindicated (10). Generally, SBRT was used for the treatment of multiple small HCCs (< 5-6 cm) in patients with Child-Pugh class A or B.

3. Literature search

PubMed database was searched for identifying English-language full-text articles regarding EBRT for the treatment of HCC. Search items were "hepatocellular carcinoma AND radiation therapy".

4. Major findings

Table 1 summarized the survival of HCC patients treated with EBRT. Table 2A summarized the type and incidence of adverse events related to EBRT. Of note, severe EBRT-related adverse event was hardly reported. Additionally, EBRT-related toxicity could develop in all sites of body except cardiotoxicity (17). Only four studies provided the data regarding the grade of adverse events in patients treated with EBRT in Table 2B. Tables 3A and B summarized the study quality.

5. EBRT for small HCC

Surgical resection and LT are the first-line curative treatment options for small HCC (5). However, surgery is often contraindicated in HCC patients with poor liver function. EBRT, especially SBRT, becomes an emerging alternative for small HCC. Studies demonstrated that the tumor control rate of EBRT for small HCC was 89.9-100% and that the 1- and 3-year overall survival rates were 86.0-95.0% and 53.8-70.0%, respectively. Additionally, no RILD was reported, few adverse effects were observed, and the prevalence of grade III toxicity was 0-23.0% (18-20).

5.1. EBRT for patients with poor liver function

In a Canadian prospective study, Culleton *et al.* (21) performed SBRT in patients with Child-Pugh class B or C small HCC. None had any tumor progression at the irradiated site of HCC. Most of adverse effects after SBRT were grade I/II. The median survival time was 7.9

months and the 1-year overall survival rate was 32.3%.

5.2. EBRT vs. resection

In a Chinese comparative study, Su *et al.* (22) found that the local effect of SBRT was similar to that of surgical resection in small HCC patients with 1 or 2 nodules and Child-Pugh A cirrhosis. SBRT was less invasive and had fewer adverse effects than resection. Notably, a propensity score-matching analysis demonstrated that the 1-, 3-, and 5-year overall survival rates were statistically similar between HCC patients undergoing SBRT and those undergoing surgical resection (100%, 91.8%, and 74.3% vs. 96.7%, 89.3%, and 69.2%, respectively).

5.3. EBRT vs. RFA

Two studies compared the outcomes of SBRT vs. RFA for patients with small HCC. Wahl *et al.* (23) found that the time freedom from local progression was not significantly different between patients with HCC \leq 2 cm undergoing SBRT and those undergoing RFA. The patients undergoing SBRT had lower pretreatment Child-Pugh scores and higher pretreatment alpha-fetoprote in levels and were submitted to more liver-directed treatments. No SBRT procedure-related death was reported. The rate of late toxicities was similar between the two groups. Seo *et al.* (24) also conducted a Markov model-based analysis and found a similar median survival time between patients with HCC \leq 3 cm undergoing SBRT and those undergoing RFA (76.5 months vs. 77.4 months). The 5-year overall survival rate was 61.1% and 58.5% in SBRT and RFA groups, respectively.

5.4. EBRT plus TACE vs. TACE alone

In a Japanese study, Honda *et al.* (25) suggested that SBRT in combination with TACE should be effective for the treatment of hypervascular small HCC (\leq 3 cm). No acute toxicities were fatal. No RILD developed. In the combination therapy group, the 1- and 3-year overall survival rates were both 100.0%. By comparison, in the TACE alone group, the 1-, 2-, and 3-year overall survival rates were 88.9%, 73.6%, and 66.1%, respectively.

6. EBRT for huge HCC

In huge HCC (*i.e.*, tumor diameter \geq 10 cm), microvascular invasion is more common and tumor grade is higher (26). Huge HCC often corresponds to the intermediate and advanced stages. Intermediate-stage HCC is treated with TACE, and advanced-stage HCC is treated with sorafenib (27,28). However, the 5-year overall survival rate of huge HCC treated with TACE is less than 10.0% (29). Additionally, the subgroup analysis

Table 1. Survival of HCC patients who underwent EBRT alone or in combination with other interventions: An overview

First author (year)	Country	Treatment	Total dose (Gy)	Fraction (n)	Case (n)	Survival time (months, Median)	1-year OS rate	2-year OS rate	3-year OS rate	5-year OS rate
EBRT for small HCC										
Sanuki (2014)	Japan	SBRT	35 or 40	5	185	NA	95.0%	83.0%	70.0%	NA
Yoon (2013)	Korea	SBRT	30 to 60	3	93	NA	86.0%	NA	53.8%	NA
Kimura (2015)	Japan	SBRT	48	4	65	41.0	92.3%	76.0%	NA	NA
Culleton (2014)	Canada	SBRT	30	6	29	7.9	32.3%	NA	NA	NA
Su (2017)	China	SBRT	NA	NA	117	NA	96.3%	NA	81.8%	70.0%
Wahl (2016)	US	SBRT	27 to 60	3 or 5	224	NA	74.0%	46.0%	NA	NA
Seo (2016)	Korea	SBRT	NA	NA	2,000	78.0	NA	NA	NA	61.1%
Honda (2013)	Japan	SBRT after TACE	48 or 60	4 or 8	365	NA	100%	NA	100%	NA
EBRT for huge HCC										
Que (2014)	Taiwan	SBRT	26 to 40	5	22	11.0	NA	NA	NA	50.0%
Han (2014)	Korea	EBRT plus non-surgical treatment	45 to 62.5	NA	116	14.8	59.5%	NA	19.7%	NA
Guo (2000)	China	EBRT after TACE	25 to 55	NA	107	18.0	59.4%	NA	28.4%	15.8%
Kim (2014)	Korea	EBRT after TACE	37.8 to 58	NA	283	15.3	NA	23.5%	NA	NA
EBRT for HCC with portal vein tumor thrombosis										
Zeng (2005)	China	EBRT	36 to 60	NA	158	8.0	34.8%	NA	NA	NA
Tang (2013)	China	3D-CRT	30 to 52	NA	371	12.3	51.6%	28.4%	19.9%	NA
Yoon (2012)	Korea	3D-CRT after TACE	21 to 60	5	412	10.6	42.5%	22.8%	NA	NA
Yu (2017)	Korea	3D-CRT after TACE	30 to 35	10	69	NA	NA	62.9%	NA	NA
Lu (2015)	China	3D-CRT plus TACE	40 to 52.5	2 to 6	63	13.0	62.4%	20.8%	NA	NA
EBRT for HCC with extrahepatic metastases										
Jiang (2012)	China	EBRT	47 to 60	NA	13	NA	NA	70.7%	NA	NA
Sun (2016)	China	IMRT plus sorafenib	NA	NA	45	21.9 (Mean)	91.1%	78.8%	NA	NA
Casamassima (2012)	Italy	SBRT	36	3	48	NA	39.7%	14.5%	NA	NA
Zhou (2014)	China	EBRT	2	NA	55	13.6	58.7%	32.3%	NA	NA
Park (2015)	Korea	WBRT	30	10	97	3.5	NA	NA	NA	NA
He (2009)	China	EBRT	32 to 66	NA	205	7.4	32.4%	13.2%	NA	NA
Kaizu (1998)	Japan	EBRT	20 to 65	NA	57	6.0	NA	NA	NA	NA
Seong (2005)	Korea	EBRT	12.5 to 50	NA	51	5.0	NA	4.0%	NA	NA
Yamashita (2007)	Japan	EBRT	46 to 60	NA	28	13.0	53.0%	33.0%	NA	NA
Zeng (2005)	China	EBRT	40 to 60	NA	125	9.4	42.1%	3.4%	NA	NA
EBRT as a bridge to LT for HCC										
Katz (2012)	US	SHORT	50	10	18	6.3	NA	NA	NA	NA
Guarneri (2016)	Italy	SBRT	36 to 48	3 to 5	8	3.2	NA	NA	NA	NA
O'Connor (2012)	US	SBRT	33 to 54	3	10	NA	NA	NA	NA	100%
Sapisochin (2017)	Canada	SBRT	8.5 to 54	1 to 6	379	NA	83.0%	NA	61.0%	61.0%
Moore (2017)	Israel	SBRT followed by LT	54	NA	23	NA	NA	NA	NA	NA
Andolino (2011)	US	SBRT followed by LT	44 or 40	3 or 5	60	NA	NA	69.0%	NA	NA
Postoperative adjuvant EBRT										
Yu (2014)	China	Postoperative 3D-CRT	60	NA	119	NA	96.2%	NA	72.6%	48.4%
Wang (2015)	China	Postoperative IMRT	NA	NA	33	NA	NA	NA	67.7%	NA
Bai (2016)	China	Postoperative 3D-CRT	32 to 48	NA	92	14.5	71.1%	NA	NA	NA

Abbreviations: HCC: hepatocellular carcinoma; OS: overall survival; RFA: radiofrequency ablation; TACE: transcatheter arterial chemoembolization; EBRT: external-beam radiation therapy; 3D-CRT: three-dimensional conformal radiation therapy; IMRT: intensity-modulated radiation therapy; SBRT: stereotactic body radiation therapy; WBRT: whole brain radiation therapy; SHORT: stereotactic hypofractionated radiation therapy; NA: not available.

Table 2A. EBRT-related adverse effects in HCC patients

Adverse effects	Incidence (%)	References with data
Systemic symptoms		
Fatigue	4.9-100	Culleton (2014); Su (2017); Que (2014); O'Connor (2012); Sapisochin (2017); Moore (2017); Yu (2014); Wang (2015)
Dizziness	6.7	Lu (2015)
Malaise	20.0	Lu (2015)
Anorexia	8.3-54.5	Yu (2017); Lu (2015); Sun (2016); Zhou (2014); Yamashita (2007); Zeng (2005)
Fever	7.7-20.0	Jiang (2012); Lu (2015); Bai (2016)
Weight loss	4.9	Su (2017)
Pain		
Liver pain	6.7	Lu (2015)
Rib pain	27.3	Que (2014)
Abdominal pain	10.0-100	Culleton (2014); Yu (2017); O'Connor (2012); Wang (2015)
Cutaneous		
Dermatitis	13.6-100	Que (2014); Yamashita (2007); Yu (2014); Wang (2015)
Skin induration	13.6	Que (2014)
Haematological		
Myeloid suppression	10.0-100	Tang (2013); Yu (2014); Bai (2016)
Leukocytopenia	8.3-100	Honda (2013); Lu (2015); Jiang (2012); Sun (2016); Zhou (2014); Yamashita (2007); Zeng (2005); Wang (2015)
Neutropenia	33.3	Yu (2017)
Thrombocytopenia	3.4-100	Culleton (2014); Honda (2013); Que (2014); Yu (2017); Jiang (2012); Sun (2016); Zhou (2014); Yamashita (2007); Zeng (2005)
Low hemoglobin	100	Honda (2013); Wang (2015)
Anemia	4.9-34.8	Su (2017); Yu (2017)
Biochemical		
Creatinine increased	100	Wang (2015)
Bilirubin increased	3.2-100	Culleton (2014); Su (2017); Honda (2013); Que (2014); Han (2014); Yu (2017); Yamashita (2007); Zeng (2005); Andolino (2011); Wang (2015)
ALT increased	3.7-100	Su (2017); Han (2014); Zeng (2005); Tang (2013); Yu (2017); Yamashita (2007); Zeng (2005); Andolino (2011); Wang (2015)
AST increased	20.7-100	Han (2014); Yu (2017); Wang (2015)
High serum transaminases	33.3-100	Honda (2013); Andolino (2011)
GLA increased	100	Wang (2015)
ALP increased	11.7-100	Que (2014); Yu (2017); Andolino (2011); Wang (2015)
Low albumin	28.3-100	Que (2014); Yu (2017); Andolino (2011); Wang (2015)
Gastrointestinal		
Gastrointestinal damage	8.7-27.3	Zhou (2014); Moore (2017)
Nausea	5.8-100	Culleton (2014); Su (2017); Que (2014); Yu (2017); O'Connor (2012); Yu (2014); Wang (2015)
Vomiting	2.9-100	Culleton (2014); Que (2014); Yu (2017); Lu (2015); Zhou (2014); O'Connor (2012); Sapisochin (2017); Yu (2014); Wang (2015); Bai (2016)
Diarrhea	2.9-100	Culleton (2014); Yu (2017); Zhou (2014); Yamashita (2007); Zeng (2005); Yu (2014)
Gastroduodenitis	3.2	Yoon (2012)
Gastroduodenal ulcer	0.9-100	Kim (2013); Yoon (2012); Yamashita (2007); Zeng (2005); Yu (2014)
Gastrointestinal bleeding	1.6-3.2	Wahl (2015); Zeng (2005); Tang (2013)
Abdominal distension	10.0	Culleton (2014)
Esophagitis	25.0	Sun (2016)
Hepatic		
RILD	1.6-100	Culleton (2014); Wahl (2015); Guarneri (2016); Moore (2017); Yu (2014)
Liver injury	20.0-38.9	Zhou (2014); Sapisochin (2017); Bai (2016)
Worsen Child-Pugh score	3.3-10.3	Sanuki (2014); Yoon (2013); Su (2017); Honda (2013); Katz (2011)
Worsen ascite	1.6-36.7	Wahl (2015); Lu (2015)
Infection		
Pneumonia	50.0	Sun (2016)
Kidney injury	5.5	Zhou (2014)

Abbreviations: HCC: hepatocellular carcinoma; EBRT: external-beam radiation therapy; ALT: alanine aminotransferase; AST: aspartate aminotransferase; GLA: glutamy aminotransferase; ALP: alkaline phosphatase; RILD: radiation-induced liver disease. *Note:* Data regarding EBRT-related adverse effects from the studies of Seo (2016), Park (2015), Seong (2005) and He (2009) cannot be obtained.

Table 2B. Grade of EBRT-related adverse effects in HCC patients

Grade of adverse effects	EBRT for small HCC Kimura (2015)	EBRT for huge HCC Guo (2000)	EBRT for HCC with extrahepatic metastases Casamassima (2012)	EBRT for HCC with extrahepatic metastases Kaizu (1998)
	SBRT	EBRT	SBRT	SHORT
I	-	-	-	-
II	-	-	2.1%	22.8%
III	-	9.2%	-	7.0%
IV	1.7%	-	-	-
V	-	-	-	1.8%

Abbreviations: HCC: hepatocellular carcinoma; EBRT: external-beam radiation therapy; SBRT: stereotactic body radiation therapy; SHORT: stereotactic hypofractionated radiation therapy. *Note:* EBRT-related adverse effects were evaluated according to the National Cancer Institute Common Toxicity Criteria version 4.0.

Table 3A. Quality assessment of retrospective studies using Newcastle Ottawa Scale

Author (year)	Representativeness of the exposed cohort	Selection of the non-exposed cohort	Ascertainment of exposure	Demonstration that outcome of interest was not present at start of study	Comparability of cohort on the basis of design or analysis	Assessment of outcomes	Was follow-up long enough for outcomes to occur	Adequacy of follow up of cohorts	Total scale
Samuki (2014)	1 point	1 point	1 point	0 point	0 point	1 point	1 point	1 point	6 points
Yoon (2013)	1 point	1 point	1 point	0 point	0 point	1 point	1 point	1 point	6 points
Kimura (2015)	1 point	1 point	1 point	0 point	0 point	1 point	1 point	1 point	6 points
Su (2017)	1 point	1 point	1 point	0 point	1 point	1 point	1 point	1 point	7 points
Wahl (2016)	1 point	1 point	1 point	0 point	1 point	1 point	1 point	1 point	7 points
Seo (2016)	1 point	0 point	1 point	0 point	1 point	1 point	1 point	1 point	6 points
Honda (2013)	1 point	1 point	1 point	0 point	1 point	1 point	1 point	1 point	7 points
Que (2014)	1 point	1 point	1 point	0 point	0 point	1 point	1 point	1 point	6 points
Han (2014)	1 point	1 point	1 point	0 point	1 point	1 point	1 point	1 point	7 points
Guo (2000)	1 point	1 point	1 point	0 point	1 point	1 point	1 point	1 point	6 points
Kim (2014)	1 point	0 point	1 point	0 point	1 point	1 point	1 point	1 point	7 points
Zeng (2005)	1 point	1 point	1 point	0 point	1 point	1 point	1 point	1 point	6 points
Tang (2013)	1 point	0 point	1 point	0 point	1 point	1 point	1 point	1 point	7 points
Yoon (2012)	1 point	1 point	1 point	0 point	1 point	1 point	1 point	1 point	7 points
Lu (2017)	1 point	1 point	1 point	0 point	1 point	1 point	1 point	1 point	7 points
Jiang (2012)	1 point	1 point	1 point	0 point	0 point	1 point	1 point	1 point	6 points
Sun (2016)	1 point	1 point	1 point	0 point	0 point	1 point	1 point	1 point	6 points
Casamassima (2012)	1 point	1 point	1 point	0 point	0 point	1 point	1 point	1 point	6 points
Zhou (2014)	1 point	1 point	1 point	0 point	0 point	1 point	1 point	1 point	6 points
Park (2015)	1 point	1 point	1 point	0 point	0 point	1 point	1 point	0 point	4 points
He (2009)	1 point	1 point	1 point	0 point	0 point	1 point	1 point	1 point	6 points
Kaizu (1998)	1 point	1 point	1 point	0 point	0 point	1 point	1 point	1 point	6 points
Seong (2005)	1 point	1 point	1 point	0 point	0 point	1 point	1 point	1 point	6 points
Yamashita (2007)	1 point	1 point	1 point	0 point	0 point	1 point	1 point	1 point	6 points
Zeng (2005)	1 point	1 point	1 point	0 point	1 point	1 point	1 point	0 point	6 points
Katz (2012)	1 point	1 point	1 point	0 point	0 point	1 point	1 point	1 point	6 points
Guameri (2016)	1 point	0 point	1 point	0 point	0 point	1 point	1 point	1 point	5 points
O'Connor (2012)	1 point	1 point	1 point	0 point	0 point	1 point	1 point	1 point	6 points
Sapisochin (2017)	1 point	1 point	1 point	0 point	1 point	1 point	1 point	1 point	7 points
Moore (2017)	1 point	1 point	1 point	0 point	1 point	1 point	1 point	1 point	7 points
Andolino (2011)	1 point	1 point	1 point	0 point	1 point	1 point	1 point	1 point	7 points
Wang (2015)	1 point	1 point	1 point	0 point	1 point	1 point	1 point	1 point	7 points
Bai (2015)	1 point	1 point	1 point	0 point	1 point	1 point	1 point	1 point	7 points

Note: Study quality was assessed as follows: low quality = 0-4; high quality = 5-8.

Table 3B. Quality assessment of prospective studies using Newcastle Ottawa Scale

Author (year)	Representativeness of the exposed cohort	Selection of the non-exposed cohort	Ascertainment of exposure	Demonstration that outcome of interest was not present at start of study	Comparability of cohort on the basis of design or analysis	Assessment of outcomes	Was follow-up long enough for outcomes to occur	Adequacy of follow up of cohorts	Total scale
Culleston (2014)	1 point	1 point	1 point	0 point	0 point	1 point	1 point	1 point	6 points
Yu (2017)	1 point	1 point	1 point	0 point	1 point	1 point	1 point	1 point	7 points
Yu (2014)	1 point	1 point	1 point	0 point	1 point	1 point	1 point	1 point	7 points

Note: Study quality was assessed as follows: low quality = 0-4; high quality = 5-8.

of a randomized controlled trial showed little effect of sorafenib in patients with macrovascular invasion and/or extrahepatic spread (30). Recent studies showed that EBRT alone or combined with non-surgical treatment might achieve an excellent intrahepatic tumor control and a potential survival benefit of huge HCC.

6.1. EBRT alone

Between 2009 and 2011, Que *et al.* (31) performed SBRT for 22 patients with huge HCC. The local control rate was 55.5%. The investigators found that 22.7% and 63.6% of patients obtained a complete and partial response, respectively. Acute toxicities related to radiation therapy were tolerable and mild. The median survival time was 11.0 months. The 1-year overall survival rate was 50.0%.

6.2. EBRT plus non-surgical treatment

Between 2001 and 2010, Han *et al.* (32) performed EBRT in combination with TACE, hepatic arterial infusion chemotherapy, or systemic chemotherapy in 116 patients with huge HCC. The local control rate was 81.0%. The median survival time was 14.8 months. The 1- and 3-year overall survival rates were 59.5% and 19.7%, respectively.

6.3. EBRT plus TACE

Between 1989 and 1998, Guo and Yu (33) treated 107 unresectable huge HCC patients with TACE followed by EBRT. Most of side effects occurred after TACE and were transient, and the overall 3-month response rate was 48.6%. The median survival time was 18.0 months. The 1-, 3-, and 5-year overall survival rates were 59.4%, 28.4%, and 15.8%, respectively.

6.4. EBRT plus TACE vs. TACE alone

Kim *et al.* (34) compared the outcomes of patients with EBRT after TACE vs. TACE alone. This combination therapy had significantly superior progression-free survival, intrahepatic control, and overall survival than TACE alone.

7. EBRT for HCC with portal vein tumor thrombosis (PVTT)

Although sorafenib is the first-line treatment option for advanced HCC, its efficacy in HCC patients with PVTT is frequently questioned (35). Additionally, PVTT can lead to the reduction of hepatic blood supply and development of severe portal hypertension related complications, such as gastroesophageal variceal bleeding and ascites (36), which limits the selection of treatment options. Very localized HCC accompanied

by PVTT in patients with preserved hepatic function can be surgically resected (37,38). However, surgical removal of tumor thrombus is rarely performed probably owing to the limited hepatic reserve (39). TACE may be performed safely in HCC patients with PVTT (40), but its efficacy is unsatisfactory (41). Recently, EBRT has been used as an alternative treatment for HCC with PVTT achieving a high response rate.

7.1. EBRT vs. TACE or resection

In 2005, Zeng *et al.* (42) compared the outcomes of EBRT vs. TACE or resection for the treatment of HCC with PVTT. The most common adverse effects of radiation therapy were loss of appetite and nausea. The median survival time was 8.0 and 4.0 months in the EBRT and TACE/resection groups, respectively. The 1-year overall survival rate was 34.8% and 11.4% in EBRT and TACE/resection groups, respectively. In 2013, Tang *et al.* (43) also compared the outcomes of 3D-CRT vs. surgical resection for resectable HCC with PVTT. The median survival time was 12.3 and 10.0 months in 3D-CRT and resection groups, respectively. The 1-, 2-, and 3-year overall survival rates were 51.6%, 28.4%, and 19.9% vs. 40.1%, 17.0%, and 17.0% in 3D-CRT and resection groups, respectively ($P = 0.029$). Both studies suggested a superiority of 3D-CRT over TACE/resection for HCC with PVTT.

7.2. EBRT plus TACE

In 2012, Yoon *et al.* (44) analyzed 412 patients treated with 3D-CRT after TACE for HCC and PVTT. Acute toxicities were mostly mild, such as fatigue, anorexia, and nausea. The objective response rate was 27.9% (complete response rate: 3.6% and partial response rate: 24.3%). The median survival time was 10.6 months. The 1- and 2-year overall survival rates were 42.5% and 22.8%, respectively. Additionally, in 2017, Yu *et al.* (45) reported the safety and efficacy of TACE followed by 3D-CRT in such patients. The median follow-up time was 11.4 months. Liver function status was not significantly worsened after treatment. The 3-month objective response rate at the radiation therapy targeted area was 69.6%. The 2-year overall survival, recurrence-free survival, and progression-free survival rates were 62.9%, 47.6%, and 14.3%, respectively.

7.3. EBRT plus TACE vs. TACE alone

In 2015, Lu *et al.* (46) compared the outcomes of 3D-CRT plus TACE vs. TACE alone. No serious adverse reactions requiring treatment were reported. In the combination treatment group, the median survival time was 13.0 months; and the 1- and 2-year overall survival rates were 62.4% and 20.8%, respectively. By comparison, in the TACE alone group, the

median survival time was 9.0 months; and the 1- and 2-year overall survival rates were 56.5% and 18.8%, respectively. The overall survival was statistically significant between the two groups ($P = 0.047$). Thus, compared with TACE alone, the combination treatment might improve the survival of HCC patients with PVTT.

8. EBRT for HCC with extrahepatic metastases

Currently, extrahepatic metastases can be frequently observed due to the prolonged survival of advanced HCC patients. The most common metastatic organ from HCC was the lung followed by adrenal gland, brain, bone, and lymph node, *etc.* (47-50). Unfortunately, there is no standard treatment for HCC with extrahepatic metastases. Although the resection of isolated metastatic lesions from some malignancies may provide a survival benefit, its role for extrahepatic metastases from HCC is not well-established (51). Recently, EBRT has been used as a palliative treatment to relieve the pain and improve the quality of life in HCC patients with extrahepatic diseases, thereby leading to a satisfactory treatment response.

8.1. Lung metastases

8.1.1. EBRT alone

Jiang *et al.* (52) indicated a pronounced efficacy of EBRT for lung metastases. A total of 13 patients with lung metastases from HCC underwent EBRT. Adverse effects were mild. The median progression-free survival time was 13.4 months. The 2-year survival rate was 70.7%.

8.1.2. EBRT alone vs. EBRT plus sorafenib

Sun *et al.* (53) compared the outcomes of IMRT alone vs. IMRT combined with sorafenib for the treatment of 45 HCC patients with lung metastases. In the IMRT alone group, only one case developed anorexia. In the combination treatment group, most of the toxicities were mild and related to sorafenib. The 1- and 2-year overall survival rates were 66.8% and 30.4% vs. 91.1% and 78.8% in IMRT alone and IMRT plus sorafenib groups, respectively. Thus, EBRT plus sorafenib may be a more promising approach in such patients.

8.2. Adrenal metastases

Casamassima *et al.* (54) treated 48 HCC patients with adrenal metastases by SBRT. The 2-year local control rate was 90.0%. Toxicities were well-tolerated. The median follow-up time was 16.2 months. The 1- and 2-year overall survival rates were 39.7% and 14.5%, respectively. Zhou *et al.* (55) also treated 55 patients with adrenal metastases from HCC by EBRT. Adverse effects

were mild to moderate. All patients experienced the pain relief after the completion of EBRT. The median survival time was 13.6 months. Thus, EBRT may be a good palliative therapy for adrenal metastases from HCC.

8.3. Brain metastases

The prognosis of HCC patients who developed brain metastases is extremely poor, with a reported median survival time of 1.0-3.0 months (56,57). Park *et al.* (58) treated 97 patients with brain metastases from HCC by EBRT alone or after surgery and/or radiosurgery. The median survival time was 3.5 months, which was superior to the previous data (56,57). The whole brain radiation therapy may be a choice of treatment for brain metastases.

8.4. Bone metastases

Bone metastases are a common cause of pain in metastatic HCC. EBRT has been reported to be effective in palliating painful bone metastases with a partial pain relief rate of 80.0-90.0% and a complete pain relief rate of 50.0% (59). The 1- and 2-year overall survival rates were 32.4% and 13.2%, respectively (60). The median survival time of patients treated with EBRT for bone metastases from HCC was 5.0-7.4 months (60-62). A large cohort of HCC patients with bone metastases treated with EBRT suggested that acute EBRT-associated toxicities were mild or absent (60). Therefore, palliative EBRT might be considered for bone metastases from HCC.

8.5. Lymph node metastases

Since HCC invasions are mostly hematogenous, lymph node metastases are uncommon. The incidence of lymph node involvement in HCC patients treated with surgery was reportedly 5.1-7.5% (63), but the incidence from an autopsy series was 25.5-42.0% (64). Yamashita *et al.* (65) performed EBRT on 28 HCC patients with lymph node metastases. Five (18.0%) patients achieved a complete response and 18 (64.0%) patients achieved a partial response. The median survival time was 13.0 months, and the 1- and 2-year overall survival rates were 53.0% and 33.0%, respectively. Zeng *et al.* (66) also suggested that the use of EBRT could improve the survival of patients with lymph node metastases from HCC. The median survival time of patients treated with EBRT was significantly longer than that of patients who did not undergo EBRT (9.4 months vs. 3.3 months, $P < 0.001$). The 1- and 2-year overall survival rates were 42.1% and 19.9% vs. 3.4% and 0% in patients who underwent EBRT and did not undergo EBRT, respectively ($P < 0.001$). Thus, EBRT may be an effective palliative treatment option for lymph node metastases from HCC with a good performance status.

9. EBRT as a bridge to LT for HCC

LT represents the best treatment option for selected HCC (67). However, the use of LT is limited by the shortage of donor organs. Many patients need a long waiting time on the transplant list and may drop out because of tumor progression (68). According to the American Association for the Study of Liver Diseases guidelines regarding the management of HCC, bridging therapies should be applied if the waiting time is longer than 6 months (69). Local treatment as a bridge to LT has been utilized to minimize the tumor progression and reduce the post-transplant recurrence. TACE and RFA are the most common bridging therapies, but generally recommended for only patients with well-compensated cirrhosis (5). Recent studies suggested the potential role of EBRT in such patients. EBRT might be an effective bridging therapy for HCC patients awaiting LT, which may provide an excellent local control with minimal side effects, downsize or stabilize tumors prior to LT, and achieve a good pathological response.

9.1. EBRT as a bridge to LT

At the University of Rochester Medical Center, Katz *et al.* (70) evaluated the bridging role of stereotactic hypofractionated radiation therapy for 18 HCC patients. The most common side effect was fatigue. Neither toxicity grade III nor RILD occurred. All patients were alive without any recurrence. Guarneri *et al.* (71) also investigated the role of SBRT prior to LT in 8 patients with HCC. The complete response rate was 61.5% and the minimal pathological response rate was 15.3%. Two patients developed toxicity grade II, and 1 patient developed a non-classic RILD. During a median follow-up of 9.6 months, 7 patients were alive and free of disease. Besides, at the Baylor Radiosurgery Center, O'Connor *et al.* (72) studied 10 patients treated with LT after SBRT. Four of them experienced acute toxicities, most of which were grade I. During a median follow-up of 62.0 months, all patients were alive without any tumor recurrence. Notably, the 5-year overall survival and disease-free survival rates were both 100%. In a retrospective study, Moore *et al.* included 23 early stage HCC patients who were not eligible for resection or local therapy but underwent SBRT (73). The median overall survival time was 34.2 months without any lethal SBRT-related adverse event. After SBRT, 16 patients became eligible for LT. Among them, 11 patients underwent LT with an excellent 1-year survival rate. Similarly, Andolino *et al.* (12) studied 60 patients with liver-confined HCC treated with SBRT. After SBRT, 23 patients underwent LT, and the progression free survival and overall survival rates at 2 years were 69.0% and 96.0%, respectively. By comparison, 27 patients did not subsequently undergo LT, and the progression free survival and overall survival rates at 2

years were only 33.0% and 47.0%, respectively.

9.2. EBRT vs. TACE or RFA

Sapisochin *et al.* (74) found that SBRT might be as effective as TACE or RFA for maintaining HCC patients on the LT waiting list. The rates of drop-out and postoperative complications were similar between them. The 1-, 3-, and 5-year survival rates from the time of waiting list were similar among them (83.0%, 61.0%, and 61.0% in the SBRT group; 86.0%, 61.0%, and 56.0% in the TACE group; 86.0%, 72.0%, and 61.0% in the RFA group, $P = 0.400$).

10. Postoperative EBRT

Surgical resection is technically difficult for centrally located HCC (75) and HCC located close to the major vessels (76). In such patients, postoperative EBRT might be potentially useful.

10.1. Postoperative EBRT for centrally located HCC

A study by Yu *et al.* (77) evaluated the role of 3D-CRT after narrow-margin resection for centrally located HCC. Fifty-eight of 119 patients were treated with postoperative 3D-CRT. No RILD occurred. Notably, in the subgroup analysis, postoperative 3D-CRT significantly improved the recurrence-free survival of patients with small HCC (≤ 5 cm), but not the overall survival.

10.2. Postoperative EBRT for HCC located close to the major vessels

In an exploratory study, Wang *et al.* (78) treated 116 HCC patients located close to the major vessels by narrow-margin (< 1.0 cm) resection. Among them, 33 patients received postoperative IMRT and 83 did not receive IMRT. During a median follow-up time of 33.0 months, the observed toxicities were mild and no patient developed any RILD. Patients receiving narrow-margin resection plus IMRT had a significantly lower incidence of early recurrence than those receiving narrow-margin resection alone. The 3-year overall survival and disease-free survival rates of narrow-margin resection plus postoperative IMRT were significantly superior to those of narrow-margin resection alone. Additionally, the overall survival and disease-free survival rates of narrow-margin resection plus postoperative IMRT were similar to those of wide-margin resection.

10.3. Postoperative EBRT vs. postoperative TACE

Bai *et al.* (79) evaluated the outcomes of adjuvant 3D-CRT vs. TACE after resection for 92 HCC patients with PVTT. No serious adverse event was observed. The

6- and 12-month overall survival rates were 88.9% and 71.1% in postoperative 3D-CRT group and 80.0% and 53.3% in postoperative TACE group. The median overall survival and disease-free survival were not significantly different between postoperative 3D-CRT and TACE groups.

11. Conclusions

Based on the current evidence, EBRT should be considered in the following conditions. First, EBRT should be a potential alternative choice of therapy for small HCC, especially if the tumor was unresectable. Second, EBRT should be considered for relieving the pain for patients with extrahepatic metastases, especially the bone pain. Third, adjunctive EBRT may be considered in patients with huge HCC, HCC patients with PVTT, HCC patients awaiting LT, and HCC patients treated with resection. However, the role of EBRT remains limited due to the relatively low level of evidence. A majority of studies were retrospective ($n = 33$), and a minority of studies were prospective ($n = 3$). No randomized controlled trial regarding EBRT was performed. Additionally, most of evidence was from Eastern countries. Thus, high-quality clinical trials should be needed to further establish the status of EBRT for the treatment of HCC.

Acknowledgements

All authors have made an intellectual contribution to the manuscript and approved its submission. This study was partially supported by the grant from the National Natural Science Foundation of China (No. 81500474) and China Postdoctoral Science Foundation (2015M582886) for Dr Xingshun Qi.

References

- Torre LA, Bray F, Siegel RL, Ferlay J, Lortet-Tieulent J, Jemal A. Global cancer statistics, 2012. *CA Cancer J Clin.* 2015; 65:87-108.
- Faria SC, Szklaruk J, Kaseb AO, Hassabo HM, Elsayes KM. TNM/Okuda/Barcelona/UNOS/CLIP International Multidisciplinary Classification of Hepatocellular Carcinoma: Concepts, perspectives, and radiologic implications. *Abdom Imaging.* 2014; 39:1070-1087.
- Zhou ZR, Liu M, Lu HR, Li YF, Liang SX, Zhang CY. Validation of different staging systems for hepatocellular carcinoma in a cohort of 249 patients undergoing radiotherapy. *Oncotarget.* 2017; 8:46523-46531.
- Bharadwaj S, Gohel TD. Perspectives of physicians regarding screening patients at risk of hepatocellular carcinoma. *Gastroenterol Rep (Oxf).* 2016; 4:237-240.
- EASL-EORTC clinical practice guidelines: Management of hepatocellular carcinoma. *J Hepatol.* 2012; 56:908-943.
- Mancuso A. Management of hepatocellular carcinoma: Enlightening the gray zones. *World J Hepatol.* 2013; 5:302-310.
- Qi X, Zhao Y, Li H, Guo X, Han G. Management of hepatocellular carcinoma: An overview of major findings from meta-analyses. *Oncotarget.* 2016; 7:34703-34751.
- Ettorre GM, Levi Sandri GB, Laurenzi A, Colasanti M, Meniconi RL, Lionetti R, Santoro R, Lepiane P, Sciuto R, Pizzi G, Cianni R, Golfieri R, D'Offizi G, Pellicelli AM, Antonini M, Vennarecci G. Yttrium-90 radioembolization for hepatocellular carcinoma prior to liver transplantation. *World J Surg.* 2017; 41:241-249.
- Levi Sandri GB, Ettorre GM, Colasanti M, De Werra E1, Mascianà G, Ferraro D, Tortorelli G, Sciuto R, Lucatelli P, Pizzi G, Visco-Comandini U, Vennarecci G. Hepatocellular carcinoma with macrovascular invasion treated with yttrium-90 radioembolization prior to transplantation. *Hepatobiliary Surg Nutr.* 2017; 6:44-48.
- 2014 KLCSSG-NCC Korea practice guideline for the management of hepatocellular carcinoma. *Gut Liver.* 2015; 9:267-317.
- Kalogeridi MA, Zygogianni A, Kyrgias G, Kouvaris J, Chatziioannou S, Kelekis N, Kouloulis V. Role of radiotherapy in the management of hepatocellular carcinoma: A systematic review. *World J Hepatol.* 2015; 7:101-112.
- Andolino DL, Johnson CS, Maluccio M, Kwo P, Tector AJ, Zook J, Johnstone PA, Cardenas HR. Stereotactic body radiotherapy for primary hepatocellular carcinoma. *Int J Radiat Oncol Biol Phys.* 2011; 81:e447-453.
- Huang WY, Jen YM, Lee MS, Chang LP, Chen CM, Ko KH, Lin KT, Lin JC, Chao HL, Lin CS, Su YF, Fan CY, Chang YW. Stereotactic body radiation therapy in recurrent hepatocellular carcinoma. *Int J Radiat Oncol Biol Phys.* 2012; 84:355-361.
- Pan CC, Kavanagh BD, Dawson LA, Li XA, Das SK, Miften M, Ten Haken RK. Radiation-associated liver injury. *Int J Radiat Oncol Biol Phys.* 2010; 76(3 Suppl):S94-100.
- Cheng JC, Wu JK, Huang CM, Liu HS, Huang DY, Tsai SY, Cheng SH, Jian JJ, Huang AT. Dosimetric analysis and comparison of three-dimensional conformal radiotherapy and intensity-modulated radiation therapy for patients with hepatocellular carcinoma and radiation-induced liver disease. *Int J Radiat Oncol Biol Phys.* 2003; 56:229-234.
- Eccles CL, Bissonnette JP, Craig T, Taremi M, Wu X, Dawson LA. Treatment planning study to determine potential benefit of intensity-modulated radiotherapy versus conformal radiotherapy for unresectable hepatic malignancies. *Int J Radiat Oncol Biol Phys.* 2008; 72:582-588.
- Mancuso L, Mancuso A, Scordato F, Pieri M, Eliana Valerio MC. Malignancy and Radiation-Induced Cardiotoxicity. *Cardiovasc Hematol Disord Drug Targets.* 2011; 11:102-108.
- Sanuki N, Takeda A, Oku Y, Mizuno T, Aoki Y, Eriguchi T, Iwabuchi S, Kunieda E. Stereotactic body radiotherapy for small hepatocellular carcinoma: A retrospective outcome analysis in 185 patients. *Acta Oncol.* 2014; 53:399-404.
- Yoon SM, Lim YS, Park MJ, *et al.* Stereotactic body radiation therapy as an alternative treatment for small hepatocellular carcinoma. *PLoS One.* 2013; 8:e79854.
- Kimura T, Aikata H, Takahashi S, Takahashi I, Nishibuchi I, Doi Y, Kenjo M, Murakami Y, Honda Y, Kakizawa H, Awai K, Chayama K, Nagata Y.

- Stereotactic body radiotherapy for patients with small hepatocellular carcinoma ineligible for resection or ablation therapies. *Hepatol Res.* 2015; 45:378-386.
21. Culleton S, Jiang H, Haddad CR, Kim J, Brierley J, Brade A, Ringash J, Dawson LA. Outcomes following definitive stereotactic body radiotherapy for patients with Child-Pugh B or C hepatocellular carcinoma. *Radiother Oncol.* 2014; 111:412-417.
 22. Su TS, Liang P, Liang J, Lu HZ, Jiang HY, Cheng T, Huang Y, Tang Y, Deng X. Long-term survival analysis of stereotactic ablative radiotherapy versus liver resection for small hepatocellular carcinoma. *Int J Radiat Oncol Biol Phys.* 2017; 98:639-646.
 23. Wahl DR, Stenmark MH, Tao Y, Pollom EL, Caoili EM, Lawrence TS, Schipper MJ, Feng M. Outcomes after stereotactic body radiotherapy or radiofrequency ablation for hepatocellular carcinoma. *J Clin Oncol.* 2016; 34:452-459.
 24. Seo YS, Kim MS, Yoo HJ, Jang WI, Paik EK, Han CJ, Lee BH. Radiofrequency ablation versus stereotactic body radiotherapy for small hepatocellular carcinoma: a Markov model-based analysis. *Cancer Med.* 2016; 5:3094-3101.
 25. Honda Y, Kimura T, Aikata H, *et al.* Stereotactic body radiation therapy combined with transcatheter arterial chemoembolization for small hepatocellular carcinoma. *J Gastroenterol Hepatol.* 2013; 28:530-536.
 26. Pawlik TM, Delman KA, Vauthey JN, Nagorney DM, Ng IO, Ikai I, Yamaoka Y, Belghiti J, Lauwers GY, Poon RT, Abdalla EK. Tumor size predicts vascular invasion and histologic grade: Implications for selection of surgical treatment for hepatocellular carcinoma. *Liver Transpl.* 2005; 11:1086-1092.
 27. Forner A, Reig ME, de Lope CR, Bruix J. Current strategy for staging and treatment: The BCLC update and future prospects. *Semin Liver Dis.* 2010; 30:61-74.
 28. Heimbach JK, Kulik LM, Finn RS, Sirlin CB, Abecassis MM, Roberts LR, Zhu AX, Murad MH, Marrero JA. AASLD guidelines for the treatment of hepatocellular carcinoma. *Hepatology.* 2018; 67:358-380.
 29. Poon RT, Ngan H, Lo CM, Liu CL, Fan ST, Wong J. Transarterial chemoembolization for inoperable hepatocellular carcinoma and postresection intrahepatic recurrence. *J Surg Oncol.* 2000; 73:109-114.
 30. Cheng AL, Guan Z, Chen Z, *et al.* Efficacy and safety of sorafenib in patients with advanced hepatocellular carcinoma according to baseline status: Subset analyses of the phase III Sorafenib Asia-Pacific trial. *Eur J Cancer.* 2012; 48:1452-1465.
 31. Que JY, Lin LC, Lin KL, Lin CH, Lin YW, Yang CC. The efficacy of stereotactic body radiation therapy on huge hepatocellular carcinoma unsuitable for other local modalities. *Radiat Oncol.* 2014; 9:120.
 32. Han HJ, Kim MS, Cha J, Choi JS, Han KH, Seong J. Multimodality treatment with radiotherapy for huge hepatocellular carcinoma. *Oncology.* 2014; 87 Suppl 1:82-89.
 33. Guo WJ, Yu EX. Evaluation of combined therapy with chemoembolization and irradiation for large hepatocellular carcinoma. *Br J Radiol.* 2000; 73:1091-1097.
 34. Kim KH, Kim MS, Chang JS, Han KH, Kim DY, Seong J. Therapeutic benefit of radiotherapy in huge (≥ 10 cm) unresectable hepatocellular carcinoma. *Liver Int.* 2014; 34:784-794.
 35. Qi X, Guo X. Sorafenib for the treatment of hepatocellular carcinoma with portal vein tumour thrombosis: A systematic review of comparative studies. *Prz Gastroenterol.* 2015; 10:142-147.
 36. Zhang XB, Wang JH, Yan ZP, Qian S, Du SS, Zeng ZC. Hepatocellular carcinoma with main portal vein tumor thrombus: Treatment with 3-dimensional conformal radiotherapy after portal vein stenting and transarterial chemoembolization. *Cancer.* 2009; 115:1245-1252.
 37. Tanaka A, Morimoto T, Yamaoka Y. Implications of surgical treatment for advanced hepatocellular carcinoma with tumor thrombi in the portal vein. *Hepato-gastroenterology.* 1996; 43:637-643.
 38. Qi X, Wang D, Su C, Li H, Guo X. Hepatic resection versus transarterial chemoembolization for the initial treatment of hepatocellular carcinoma: A systematic review and meta-analysis. *Oncotarget.* 2015; 6:18715-18733.
 39. Le Treut YP, Hardwigsen J, Ananian P, Saisse J, Grégoire E, Richa H, Campan P. Resection of hepatocellular carcinoma with tumor thrombus in the major vasculature. A European case-control series. *J Gastrointest Surg.* 2006; 10:855-862.
 40. Zhao Y, Cai G, Zhou L, Liu L, Qi X, Bai M, Li Y, Fan D, Han G. Transarterial chemoembolization in hepatocellular carcinoma with vascular invasion or extrahepatic metastasis: A systematic review. *Asia Pac J Clin Oncol.* 2013; 9:357-364.
 41. Chern MC, Chuang VP, Cheng T, Lin ZH, Lin YM. Transcatheter arterial chemoembolization for advanced hepatocellular carcinoma with inferior vena cava and right atrial tumors. *Cardiovasc Intervent Radiol.* 2008; 31:735-744.
 42. Zeng ZC, Fan J, Tang ZY, Zhou J, Qin LX, Wang JH, Sun HC, Wang BL, Zhang JY, Jiang GL, Wang YQ. A comparison of treatment combinations with and without radiotherapy for hepatocellular carcinoma with portal vein and/or inferior vena cava tumor thrombus. *Int J Radiat Oncol Biol Phys.* 2005; 61:432-443.
 43. Tang QH, Li AJ, Yang GM, Lai EC, Zhou WP, Jiang ZH, Lau WY, Wu MC. Surgical resection versus conformal radiotherapy combined with TACE for resectable hepatocellular carcinoma with portal vein tumor thrombus: a comparative study. *World J Surg.* 2013; 37:1362-1370.
 44. Yoon SM, Lim YS, Won HJ, Kim JH, Kim KM, Lee HC, Chung YH, Lee YS, Lee SG, Park JH, Suh DJ. Radiotherapy plus transarterial chemoembolization for hepatocellular carcinoma invading the portal vein: long-term patient outcomes. *Int J Radiat Oncol Biol Phys.* 2012; 82:2004-2011.
 45. Yu JI, Park HC, Jung SH, Choi C, Shin SW, Cho SK, Sinn DH, Paik YH, Gwak GY, Choi MS, Lee JH, Koh KC, Yoo BC, Sahinbas H, Paik SW. Combination treatment with transarterial chemoembolization, radiotherapy, and hyperthermia (CERT) for hepatocellular carcinoma with portal vein tumor thrombosis: Final results of a prospective phase II trial. *Oncotarget.* 2017; 8:52651-52664.
 46. Lu DH, Fei ZL, Zhou JP, Hu ZT, Hao WS. A comparison between three-dimensional conformal radiotherapy combined with interventional treatment and interventional treatment alone for hepatocellular carcinoma with portal vein tumour thrombosis. *J Med Imaging Radiat Oncol.* 2015; 59:109-114.
 47. Ikai I, Arii S, Kojiro M, Ichida T, Makuuchi M,

- Matsuyama Y, Nakanuma Y, Okita K, Omata M, Takayasu K, Yamaoka Y. Reevaluation of prognostic factors for survival after liver resection in patients with hepatocellular carcinoma in a Japanese nationwide survey. *Cancer*. 2004; 101:796-802.
48. Momoi H, Shimahara Y, Terajima H, Iimuro Y, Yamamoto N, Yamamoto Y, Ikai I, Yamaoka Y. Management of adrenal metastasis from hepatocellular carcinoma. *Surg Today*. 2002; 32:1035-1041.
 49. Shao YY, Lu LC, Cheng AL, Hsu CH. Increasing incidence of brain metastasis in patients with advanced hepatocellular carcinoma in the era of antiangiogenic targeted therapy. *Oncologist*. 2011; 16:82-86.
 50. Ho CL, Chen S, Yeung DW, Cheng TK. Dual-tracer PET/CT imaging in evaluation of metastatic hepatocellular carcinoma. *J Nucl Med*. 2007; 48:902-909.
 51. Chua TC, Morris DL. Exploring the role of resection of extrahepatic metastases from hepatocellular carcinoma. *Surg Oncol*. 2012; 21:95-101.
 52. Jiang W, Zeng ZC, Zhang JY, Fan J, Zeng MS, Zhou J. Palliative radiation therapy for pulmonary metastases from hepatocellular carcinoma. *Clin Exp Metastasis*. 2012; 29:197-205.
 53. Sun T, He J, Zhang S, Sun J, Zeng M, Zeng Z. Simultaneous multitarget radiotherapy using helical tomotherapy and its combination with sorafenib for pulmonary metastases from hepatocellular carcinoma. *Oncotarget*. 2016; 7:48586-48599.
 54. Casamassima F, Livi L, Masciullo S, Menichelli C, Masi L, Meattini I, Bonucci I, Agresti B, Simontacchi G, Doro R. Stereotactic radiotherapy for adrenal gland metastases: University of Florence experience. *Int J Radiat Oncol Biol Phys*. 2012; 82:919-923.
 55. Zhou LY, Zeng ZC, Fan J, Chen B, Rao SX, He J, Yang P, Hou JZ, Wu ZF, Zhang JY, Hu Y. Radiotherapy treatment of adrenal gland metastases from hepatocellular carcinoma: clinical features and prognostic factors. *BMC cancer*. 2014; 14:878.
 56. Kim M, Na DL, Park SH, Jeon BS, Roh JK. Nervous system involvement by metastatic hepatocellular carcinoma. *J Neurooncol*. 1998; 36:85-90.
 57. Choi HJ, Cho BC, Sohn JH, Shin SJ, Kim SH, Kim JH, Yoo NC. Brain metastases from hepatocellular carcinoma: prognostic factors and outcome: brain metastasis from HCC. *J Neurooncol*. 2009; 91:307-313.
 58. Park JW, Chen M, Colombo M, Roberts LR, Schwartz M, Chen PJ, Kudo M, Johnson P, Wagner S, Orsini LS, Sherman M. Global patterns of hepatocellular carcinoma management from diagnosis to death: the BRIDGE Study. *Liver Int*. 2015; 35:2155-2166.
 59. Ratanatharathorn V, Powers WE, Moss WT, Perez CA. Bone metastasis: Review and critical analysis of random allocation trials of local field treatment. *Int J Radiat Oncol Biol Phys*. 1999; 44:1-18.
 60. He J, Zeng ZC, Tang ZY, Fan J, Zhou J, Zeng MS, Wang JH, Sun J, Chen B, Yang P, Pan BS. Clinical features and prognostic factors in patients with bone metastases from hepatocellular carcinoma receiving external beam radiotherapy. *Cancer*. 2009; 115:2710-2720.
 61. Kaizu T, Karasawa K, Tanaka Y, Matuda T, Kurosaki H, Tanaka S, Kumazaki T. Radiotherapy for osseous metastases from hepatocellular carcinoma: A retrospective study of 57 patients. *Am J Gastroenterol*. 1998; 93:2167-2171.
 62. Seong J, Koom WS, Park HC. Radiotherapy for painful bone metastases from hepatocellular carcinoma. *Liver Int*. 2005; 25:261-265.
 63. Sun HC, Zhuang PY, Qin LX, Ye QH, Wang L, Ren N, Zhang JB, Qian YB, Lu L, Fan J, Tang ZY. Incidence and prognostic values of lymph node metastasis in operable hepatocellular carcinoma and evaluation of routine complete lymphadenectomy. *J Surg Oncol*. 2007; 96:37-45.
 64. Watanabe J, Nakashima O, Kojiro M. Clinicopathologic study on lymph node metastasis of hepatocellular carcinoma: A retrospective study of 660 consecutive autopsy cases. *Jpn J Clin Oncol*. 1994; 24:37-41.
 65. Yamashita H, Nakagawa K, Shiraishi K, Tago M, Igaki H, Nakamura N, Sasano N, Siina S, Omata M, Ohtomo K. Radiotherapy for lymph node metastases in patients with hepatocellular carcinoma: Retrospective study. *J Gastroenterol Hepatol*. 2007; 22:523-527.
 66. Zeng ZC, Tang ZY, Fan J, Qin LX, Ye SL, Zhou J, Sun HC, Wang BL, Wang JH. Consideration of role of radiotherapy for lymph node metastases in patients with HCC: retrospective analysis for prognostic factors from 125 patients. *Int J Radiat Oncol Biol Phys*. 2005; 63:1067-1076.
 67. Mazzaferro V, Regalia E, Doci R, Andreola S, Pulvirenti A, Bozzetti F, Montalto F, Ammatuna M, Morabito A, Gennari L. Liver transplantation for the treatment of small hepatocellular carcinomas in patients with cirrhosis. *N Engl J Med*. 1996; 334:693-699.
 68. Yao FY, Bass NM, Nikolai B, Davern TJ, Kerlan R, Wu V, Ascher NL, Roberts JP. Liver transplantation for hepatocellular carcinoma: Analysis of survival according to the intention-to-treat principle and dropout from the waiting list. *Liver Transpl*. 2002; 8:873-883.
 69. Bruix J, Sherman M. Management of hepatocellular carcinoma: an update. *Hepatology*. 2011; 53:1020-1022.
 70. Katz AW, Chawla S, Qu Z, Kashyap R, Milano MT, Hezel AF. Stereotactic hypofractionated radiation therapy as a bridge to transplantation for hepatocellular carcinoma: clinical outcome and pathologic correlation. *Int J Radiat Oncol Biol Phys*. 2012; 83:895-900.
 71. Guarneri A, Franco P, Trino E, Campion D, Faletti R, Mirabella S, Gaia S, Ragona R, Diotallevi M, Saracco G, Salizzoni M, Ricardi U, Carucci P. Stereotactic ablative radiotherapy in the treatment of hepatocellular carcinoma >3 cm. *Med Oncol*. 2016; 33:104.
 72. O'Connor JK, Trotter J, Davis GL, Dempster J, Klintmalm GB, Goldstein RM. Long-term outcomes of stereotactic body radiation therapy in the treatment of hepatocellular cancer as a bridge to transplantation. *Liver Transpl*. 2012; 18:949-954.
 73. Moore A, Cohen-Naftaly M, Tobar A, Kundel Y, Benjaminov O, Braun M, Issachar A, Mor E, Sarfaty M, Miragilovski D, Hur RB, Gordon N, Stemmer SM, Allen AM. Stereotactic body radiation therapy (SBRT) for definitive treatment and as a bridge to liver transplantation in early stage inoperable Hepatocellular carcinoma. *Radiat Oncol*. 2017; 12:163.
 74. Sapisochin G, Barry A, Doherty M, Fischer S, Goldaracena N, Rosales R, Russo M, Beecroft R, Ghanekar A, Bhat M, Brierley J, Greig PD, Knox JJ, Dawson LA, Grant DR. Stereotactic body radiotherapy vs. TACE or RFA as a bridge to transplant in patients with hepatocellular carcinoma. An intention-to-treat analysis. *J Hepatol*. 2017; 67:92-99.
 75. Cheng CH, Yu MC, Wu TH, Lee CF, Chan KM, Chou

- HS, Lee WC. Surgical resection of centrally located large hepatocellular carcinoma. *Chang Gung Med J.* 2012; 35:178-191.
76. Yoon YS, Han HS, Cho JY, Kim JH, Kwon Y. Laparoscopic liver resection for centrally located tumors close to the hilum, major hepatic veins, or inferior vena cava. *Surgery.* 2013; 153:502-509.
77. Yu W, Wang W, Rong W, Wang L, Xu Q, Wu F, Liu L, Wu J. Adjuvant radiotherapy in centrally located hepatocellular carcinomas after hepatectomy with narrow margin (<1 cm): A prospective randomized study. *J Am Coll Surg.* 2014; 218:381-392.
78. Wang WH, Wang Z, Wu JX, *et al.* Survival benefit with IMRT following narrow-margin hepatectomy in patients with hepatocellular carcinoma close to major vessels. *Liver Int.* 2015; 35:2603-2610.
79. Bai T, Chen J, Xie ZB, Wu FX, Wang SD, Liu JJ, Li LQ. The efficacy and safety of postoperative adjuvant transarterial embolization and radiotherapy in hepatocellular carcinoma patients with portal vein tumor thrombus. *Onco Targets Ther.* 2016; 9:3841-3848.

(Received October 29, 2018; Revised January 15, 2019; Accepted January 26, 2019)

Anti-inflammatory, anti-oxidative stress and novel therapeutic targets for cholestatic liver injury

Yafei Zhang¹, Yuxuan Lu², Hong Ji¹, Yiming Li^{1,*}

¹Department of General Surgery, Second Affiliated Hospital of Xi'an Jiaotong University, Xi'an, Shaanxi, China;

²The High School Affiliated to Xi'an Jiaotong University, Xi'an, Shaanxi, China.

Summary

Cholestasis is a pathological process in which bile drainage is poor for a variety of reasons. Many studies have shown that cholestatic liver injury is a neutrophil-mediated inflammatory response, and oxidative stress induced by neutrophils is the main mechanism of liver cell death. The literature summarizes the bile acid signaling pathway, the neutrophil chemotaxis recruitment process during cholestasis, and the oxidative stress damage produced by neutrophil activation, summarizes the latest research progress. Sphingosine-1-phosphate receptor (S1PR) is a potential therapeutic target for cholestasis that reduces neutrophil aggregation without inhibiting systemic immune status. Early growth response factor 1 (Egr-1) may play a central role in the inflammation induced by cholestasis, and it is also a potential therapeutic target to inhibit the inflammation induced by cholestasis. Strengthening the antioxidant system of hepatocytes to cope with oxidative stress of neutrophils is a feasible treatment for cholestatic liver injury.

Keywords: Cholestatic liver injury, sphingosine-1-phosphate receptor, early growth response factor 1, inflammatory response, oxidative stress

1. Introduction

Cholestasis is a pathophysiological state in which bile duct obstruction or hepatocyte surface bile salt export pump (BSEP) function is inhibited by various reasons. Under normal circumstances, bile acids synthesized in hepatocytes are excreted into the bile duct through the bile duct of hepatocytes, and finally collected into the common bile duct to the duodenum, and only a small amount of bilirubin and bile acid are present in the blood (1). Under pathological conditions, bile drainage causes bile acids and their bound bile salts to accumulate in hepatocytes and serum. Higher levels of bile acids, such as glycochenodeoxycholate (GCDC), have larger toxicity, which induces apoptosis by directly interfering with mitochondrial function or directly causes cell death (2). If pathological obstructive factors are not removed in time, liver fibrosis and cirrhosis will eventually

occur (3). Patients with cholestasis for a long time and severe jaundice will reduce the indication and success rate of operation for primary diseases, and increase the incidence of postoperative complications. With the further development of the disease, the damage of liver function is aggravated, and even multiple organ failure such as liver, kidney, brain and lung occurs after operation (4). However, how cholestasis causes liver damage has always been the focus of researchers' attention (5). At present, there is still a lack of effective treatment for cholestatic liver injury. Therefore, it is of great significance to study the pathogenesis of cholestatic liver disease and find potential therapeutic targets for hepatocyte injury. Many animal models of obstructive cholestasis have confirmed that infiltration of inflammatory cells (mainly neutrophils) at sites of hepatic necrosis is a prominent feature of cholestatic liver injury. Ursodeoxycholic acid (UDCA) has been the first-line treatment for cholestatic hepatitis, but some patients have no response to UDCA treatment or even have increased jaundice after treatment. Inhibiting inflammation, controlling oxidative stress, and searching for specific pathways and therapeutic targets are currently the research hotspots for cholestatic liver injury. At present, the mechanism of cell death caused by cholestasis has

Released online in J-STAGE as advance publication February 27, 2019.

*Address correspondence to:

Dr. Yiming Li, Department of General Surgery, Second Affiliated Hospital of Xi'an Jiaotong University, 157 West 5th Road, Xi'an 710004, People's Republic of China.

E-mail: liyimingdoc@163.com

been studied in depth, summarizing the current research situation and providing a new therapeutic target for the treatment of cholestatic hepatitis.

2. The role of bile acids and bilirubin in cholestasis

2.1. Most bile acids are non-toxic to hepatocytes

Some bile acids or bile salts such as GCDC are highly toxic, but *in vivo* tests in rodents have shown that bile acids are non-toxic even when the bile acid accumulated during cholestasis reaches a micromolar concentration. *In vivo* experiments with cholestasis can be observed that when exposure of individual hepatocytes to serum and bile with bile acids, most bile acids are not toxic unless metabolized to toxic hydrophobic bile acids such as GCDC or Lithocholic acid (LCA) (6).

2.2. Antioxidation of unconjugated bilirubin

Unconjugated bilirubin (UCB) is an antioxidant with physiological antioxidant effects (7). Traditional liver freezing-resuscitation process during liver transplantation can cause damage to liver cells. It has been reported that after liver transplantation with UCB, liver function is significantly improved compared with untreated liver. UCB may be a potential clinical A cell protectant for liver transplantation. This shows that the antioxidant effect of UCB has a certain protective effect on hepatocytes during cholestasis (8).

2.3. Interaction of bile acids with bilirubin

Both bile acids and bilirubin are biomarkers of cholestasis, but their roles are diametrically opposite. Bile acid recruits concentrated granulocytes through the bile acid signaling pathway, causing a large amount of neutrophils to infiltrate in the liver tissue, and damaging the liver tissue through oxidative stress; while UCB is a physiological antioxidant, which can resist bile acid toxicity to a certain extent. In animal models of obstructive cholestasis, hepatic histopathology shows significant oxidative stress damage, which may be related to the toxic effect of bile acids on the liver, which reduces intracellular UCB levels, thereby making hepatocytes susceptible to oxidative stress damage (9).

3. Neutrophil-mediated inflammatory response exists in common animal models of cholestasis

At present, the representative model of extrahepatic cholestasis induction is the bile duct ligation (BDL) model. The representative model of intrahepatic cholestasis induction is alpha-naphthylisothiocyanate (ANTI)-induced cholestasis. Depending on the cause of cholestasis, there are differences between different animal models, but neutrophil-mediated inflammatory

responses are considered to be a common pathogenesis of multiple cholestasis models (10,11).

4. Inflammatory response is the damage mechanism of cholestatic liver injury

4.1. The role of neutrophils in cholestasis

For humans and mice, neutrophils are the most important cellular components of the innate immune system. Liver histopathology showed a large amount of neutrophil infiltration in the necrotic area during cholestasis, suggesting that neutrophils play an important role in liver injury caused by cholestasis.

Experiments showed that after 3 days in the wild-type mouse BDL model, ICAM-1 expression levels increased along the hepatic sinus, portal vein, and hepatocytes, and neutrophils accumulated in large amounts, accompanied by a sharp rise in serum ALT and severe cell necrosis (12). The serum ALT level of ICAM-1 deficient rats was 67% lower than that of wild type mice, the degree of cell necrosis was significantly reduced, and the total amount of neutrophil infiltration in liver tissues was significantly reduced, 85% of which was still in hepatic sinusoids (13). The anti-inflammatory effects of glucocorticoids have protective effects on liver damage in BDL model mice. This indicates that a large amount of neutrophils infiltrate during obstructive cholestasis, and reducing neutrophil aggregation can help reduce liver damage caused by cholestasis.

Neutrophils express myeloperoxidase, which catalyzes the production of large amounts of hypochlorous acid, which kills liver cells by strong oxidation. Immunohistochemistry confirmed that 3-chlorotyrosine-protein complex staining was positive in hepatic necrotic tissue during cholestasis, indicating that neutrophils in the hepatic necrosis area release highly toxic hypochlorous acid, leading to hepatocyte death (14).

Other cells in the innate immune system also play an important role in cholestasis. Kupffer cells are thought to have protective effects against cholestatic liver damage. Experiments showed that the serum transaminase level of Kupffer cells or IL-6 deficient mice was significantly higher than that of normal mice after the BDL model. Histopathology suggested that inflammatory cell infiltration, bile duct proliferation and hepatocyte necrosis were more significant than normal mice. Kupffer cells extracted from the liver of normal BDL model mice were cultured, and IL-6 expression levels were significantly increased (15). This indicates that the protective effect of Kupffer cells on liver during cholestasis is achieved by a IL-6-mediated cytokine-dependent protection mechanism.

4.2. Novel mediators that recruit neutrophil aggregation during cholestasis

Neutrophil-mediated inflammatory response is the main mechanism of liver damage during cholestasis, so the study of specific signaling pathways for concentrated neutrophil aggregation during cholestasis has brought new therapeutic targets for the treatment of cholestatic liver injury. In recent years, studies have found that receptors recognize damage-associated molecular patterns (DAMPs) and thereby activate immune cells, ultimately stimulating a sterile inflammatory response (16).

DAMPs are rapidly released from damaged or necrotic tissue and can also be released by certain activated immune cells, such as mitochondrial DNA, nuclear DNA fragments or ATP (17). DAMPs can be considered as biomarkers for clinical detection of injury. Once DAMPs are released into the blood, the damage can be reflected indirectly by detecting markers in the serum. DAMPs activate cells expressing pattern recognition receptors (PRRs) in the innate immune system, elicit an innate immune response, and initiate an adaptive immune response either directly or indirectly. A variety of DAMPs have been discovered, including high mobility group protein box (HB1), heat shock protein (HSP), uric acid crystals, and hepatomaderived growth factor (HDGF).) *etc.* (18). Among the most important PRRs are Toll-like receptors (TLRs), which are a class of transmembrane receptors with a wide distribution. TLR4 is an important PRR that mediates signal transduction (16).

HMGB1 is a DNA-associated histone deacetylase that is transferred to the cytosol when cells are damaged. Cell necrosis due to cholestasis can cause HMGB1 to be released into serum within 6 hours after liver injury. The acetylated HMGB1 secreted by macrophages acts as a pro-inflammatory signal to promote inflammatory responses and is also an effective chemokine for the recruitment of concentrated neutrophils during cholestasis (19). As a receptor for recognizing DAMPs, TLR expression is significantly up-regulated in patients with chronic cholestasis. Activation of TLR by immune cells in the liver of PBC stimulates local NK cells to attack and kill capillary bile ducts. Experiments have confirmed that blocking the TLR4 signal transduction pathway or blocking HMGB1 with neutralizing antibodies in the ischemia-reperfusion model can effectively inhibit the production of aseptic inflammation (20).

Osteopontin (OPN) is a recently discovered molecule that has chemotactic effects on neutrophils during cholestasis (21). OPN is a pleiotropic protein that can play different roles in different cells (22). Secreted OPN binds to the integrin receptor and acts as a chemokine. Under normal conditions, OPN is expressed in biliary epithelial cells, whereas in chronic liver injury, hepatocytes induce the expression of OPN. Animal experiments show that OPN^{-/-} mice can inhibit neutrophil recruitment and anti-BDL-induced liver injury in the early stage of the experiment, but this

protection is temporary, and the BDL model can show similar liver injury like wild type after 72 hours, which may be related to the production of other chemokines and induction of neutrophil recruitment (23).

Therefore, it is difficult to achieve long-term protection against the liver by inhibiting one of the chemokines. At present, a feasible solution is to inhibit the upstream signaling pathway to activate the immune system or prevent neutrophil-mediated oxidative stress damage, thereby achieving the purpose of alleviating or even eliminating the liver damage caused by the inflammatory reaction.

4.3. Inflammatory stress mediated by the innate immune system during cholestasis

Neutrophils exert cytotoxic effects mainly by producing reactive oxygen species (ROS)(24). Under normal conditions, ROS is produced by mitochondrial respiration and detoxification by intracellular antioxidants. Innate immune cells such as neutrophils produce a large amount of highly toxic ROS to kill hepatocytes during aseptic inflammation. Neutrophils are infiltrated in the liver parenchyma after activation, releasing these toxic mediators to directly kill liver cells. According to reports in the literature, cytokines, chemokines, complement, and even HMGB1, and bile acids can activate neutrophils. Activated neutrophils adhere to target cells *via* CD 18-ICAM-1 interaction, triggering persistent adhesion-dependent oxidative stress damage (25).

Neutrophils produce hypochlorous acid (HClO) through a series of biochemical reactions. As a strong oxidant, hypochlorous acid can bind to various components in cells and kill cells. It is now known that HClO can bind to DNA and proteins, especially to proteins. The combination of sulfhydryl groups further produces toxic chloramines. Exposure of hepatocytes to ROS can impair mitochondrial function, leading to cell death. Experiments have shown that if a cyclosporin analog, such as NIM-811, is used to ablate mitochondrial permeability transition pores, it can counteract early damage to BDL and produce a protective effect (26). In addition, the addition of intracellular antioxidants, such as reduced glutathione, can also produce protection.

Although Kupffer cells can produce oxygen free radicals in the liver ischemia-reperfusion model, oxidative stress is mainly caused by neutrophils during cholestasis. When the number of Kupffer cells is reduced, the damage is aggravated, because the amount of protective cytokine protein produced by Kupffer cells is also decreased.

Based on the above studies, we can find that bile acid can agglomerate neutrophils by increasing ICAM-1 expression level in cholestasis. Neutrophils produce myeloperoxidase, catalyze the production of a large amount of HClO, and kill hepatocytes by strong oxidation. Inflammation-induced cell damage can

produce DAMPs, such as acetylated HMGB1 and TLR4, and then further recruit centralized granulocytes, which can amplify the inflammatory response and further damage the liver cells. Therefore, strengthening the hepatocyte antioxidant system to cope with neutrophil oxidative stress is also a feasible treatment.

In recent years, many scholars have found new drugs and new targets for the treatment of cholestatic liver injury. We searched the existing literature and summarize the new therapeutic drugs and related molecular pathways and therapeutic targets. As shown in Table 1, many drugs and pathways are involved, but the main ways of action are anti-inflammation, anti-oxidation and anti-fibrosis (27-51).

5. Bile acid signaling pathway and its relationship with the innate immune system

5.1. Genetic changes caused by cholestasis

Choles deposition induces many genes in liver cells to change (52). In the BDL model, hepatocytes rapidly up-regulate exporter transporters, such as the multidrug resistance (Mdr) transporter family and BSEP (53), while down-regulating uptake transporters, especially sodium taurocholate cotransporting (sodium taurocholate cotransporting) Polypeptide, Ntcp), aims to reduce the accumulation of bile salts in the liver (54). Post-transcriptional regulation of BSEP results in an overall down-regulation of hepatocyte activity. This series of changes may be an intrinsic regulation process to reduce bile acid emissions into bile after obstruction of bile drainage. In the Mdr-deficient mouse model, it was observed that BSEP mRNA levels increased gradually after birth, but BSEP protein expression levels decreased significantly (55). This compensatory change is to protect the liver cells from the damage caused by the accumulation of bile and to promote the bile acid into the blood and then filter through the urine.

5.2. Endogenous Bile Acid Nuclear Receptor - Farnesol Receptor

The hepatoenteral circulation, bile acid synthesis and metabolic processes of bile acids after cholestasis are automatically regulated by changes in the endogenous bile acid nuclear receptor, Farnesoid X Receptor (FXR). Bile acids act as ligands to activate FXR, up-regulating or down-regulating the expression of these genes by CYP7A1, a rate-limiting enzyme in the classical bile acid synthesis pathway (56). FXR is considered to be an important response element for bile acids during cholestasis. FXR^{-/-} mice are unable to up-regulate BSEP expression and therefore cannot increase bile secretion or tolerate more damage caused by cholestasis (57).

At present, obeticholic acid is an FXR agonist with great potential in the clinical trial of primary biliary

cirrhosis (PBC). Clinically, UDCA is the first-line treatment for patients with PBC, but some patients have poor or no response to UDCA. Alkaline phosphatase, γ -glutamyltransferase and alanine aminotransferase in the serum of these patients were all decreased after treatment with obeticholic acid, indicating that obeticholic acid has a positive effect on protecting liver cells, bile duct epithelial cells and resisting PBC-related liver damage (58).

In the BDL model-induced complete biliary obstruction, the first-line use of cholestasis-induced liver injury, UDCA, may result in more severe liver damage, as the biliary drug UDCA increases biliary pressure and aggravates biliary infarction (59,60). However, patients often do not show an increase in injury when taking the drug. On the one hand, the therapeutic dose is small, and UDCA has a protective effect on mitochondria (61). Therefore, the value of the BDL model in testing the therapeutic effect of cholestatic liver injury remains to be seen.

5.3. Extracellular receptors – G protein coupled receptors

In addition to acting on intracellular receptors, bile acids can also act on extracellular receptors, such as tyrosine kinase receptors and G-protein coupled receptors (GPCRs), or by activation of epidermal growth factor. The epidermal growth factor receptor (EGFR) acts on the downstream mitogen-activated protein kinase. Although these signal cascade amplifications are dependent on the generation of reactive oxygen species and ultimately lead to damage to rat hepatocytes (62).

5.3.1. Sphingosine 1-phosphate receptor family

Sphingosine kinases (SphKs) and its product sphingosine-1-phosphate (S1P) have the effect of regulating hepatocyte apoptosis and survival. The sphingosine-1-phosphate receptor family (S1PR family) is a G protein-coupled receptor with important biological activity (63). In rat hepatocyte experiments, bile acid is a sphingosine-1-phosphate receptor 2 (S1PR2) ligand in the mitogen-activated protein kinase (MAPK) pathway (64). It has been reported in the literature that sphingosine kinase inhibitors can significantly inhibit apoptosis of hepatocytes induced by GCDC and inhibit hepatocyte necrosis. At this time, S1PR1 and S1PR2 are simultaneously inhibited. Exogenous sphingosine kinase also significantly inhibits hepatocyte apoptosis by inhibiting S1PR2 (65). Therefore, S1PR is a potentially valuable therapeutic target for reducing neutrophil aggregation while not inhibiting systemic immune status in cholestasis.

5.3.2. G protein coupled bile acid receptor

G-protein coupled bile acid receptor (GPBAR/TGR5) is

Table 1. Drug therapy for cholestatic liver injury

Drugs	Methods	Signaling Pathway	Targets
Celastrol (27)	ANIT and TAA rat model	SIRT1-FXR signaling pathway	SIRT1, FXR
Andrographolide (28)	ANIT rat model	Anti-inflammatory Anti-oxidative	IL-6, TNF- α , MDA, SOD, GSH, GSH-PX
Rosuvastatin (29)	BDL rat model	HMGB1/TLR4 axis miR-21 signaling	HMGB1, TLR4, miR-21
Shenqi Fuzheng Injection (30)	BDL rat model		PPAR-gamma, COX-2 NF-kappaBp65
Peroxioredoxin 4 (31)	BDL rat model	Anti-inflammatory Anti-oxidative stress Anti-fibrosis	
9-cis-retinoic acid (32)	BDL rat model		MRP3, RXRalpha
Schisandrol B (33)	LCA rat model	PXR pathway	PXR
Glechoma hederacea (34)	BDL rat model	Anti-oxidative Anti-inflammatory Anti-fibrotic HMGB1/TLR4 signaling pathways TGF-beta/Smad signaling	NF-kappaB AP-1 TGF-beta HMGB1 TLR4
Chicken bile powder (35)	ANIT rat model	Restoring bile acid homeostasis Anti-inflammation	FXR NF-kappaB
Auraptene (36)	LCA rat model and <i>in vitro</i>	FXR pathway	FXR
SRT1720 (37)	17alpha-ethinylestradiol rat model	HNF1alpha/FXR signalling pathway Anti-inflammatory	HNF1alpha FXR
Sweroside (38)	ANIT rat model	Regulating bile acids Anti-inflammatory	beta-MCA, CA, TCA
Chlorogenic acid (39)	ANIT rat model	STAT3 and NFkappaB signalling	STAT3, NFkappaB
Vitamin C (40)	LCA rat model	Anti-fibrotic	Gulo
Thymoquinone (41)	BDL rat model	Anti-oxidative	MDA, SOD, GPx
Cilostazol (42)	BDL rat model	Anti-inflammatory Anti-fibrotic	TNF-alpha, TGF-beta PDGF-B
Quercetin (43)	BDL rat model	Anti-inflammatory Anti-oxidative Anti-fibrotic NF-kappaB signaling. TGF-beta/Smad signaling TLR signaling	NF-kappaB TGF-beta TLR
Guava Pulp (44)	BDL rat model and <i>in vitro</i>	Anti-fibrotic Src/MEK/ERK1/2/c-Myc pathway	TGF-beta1, TIMP, COL1alpha1, GP, IL-6 QBC939, p-ERK, c-Myc
Serotonin (45)	BDL rat model		Tph1
Docosahexaenoic acid (46)	BDL rat model	Hepatoprotective Anti-inflammatory Anti-fibrotic NF-kappaB signaling ERK/TGF-beta/Smad pathway	NF-kappaB ERK TGF-beta1
Cyclopamine (47)	BDL rat model	Hedgehog signaling pathway	Sonic Hedgehog, Patched-1 Glioblastoma-1, TNF-alpha IL-1beta, Akt, ERK
Resveratrol (48)	BDL rat model	Hepatoprotective Anti-inflammatory Anti-fibrotic	TNF-alpha, IL-6, collagen Ialpha1, TIMP-1
Caffeic acid phenethyl ester (49)	BDL rat model	Anti-inflammatory Anti-oxidative	MDA, MPO, IL-1alpha IL-6
Tetrathiomolybdate (50)	BDL rat model	Anti-fibrotic	TNF-alpha, TGF-beta1
Aminoguanidine (51)	BDL rat model	Anti-inflammatory Anti-oxidative	IL-1alpha, TNF-alpha

ANIT, alpha-naphthyl isothiocyanate; TAA, thioacetamide; BDL, bile duct ligation; LCA, lithocholic acid.

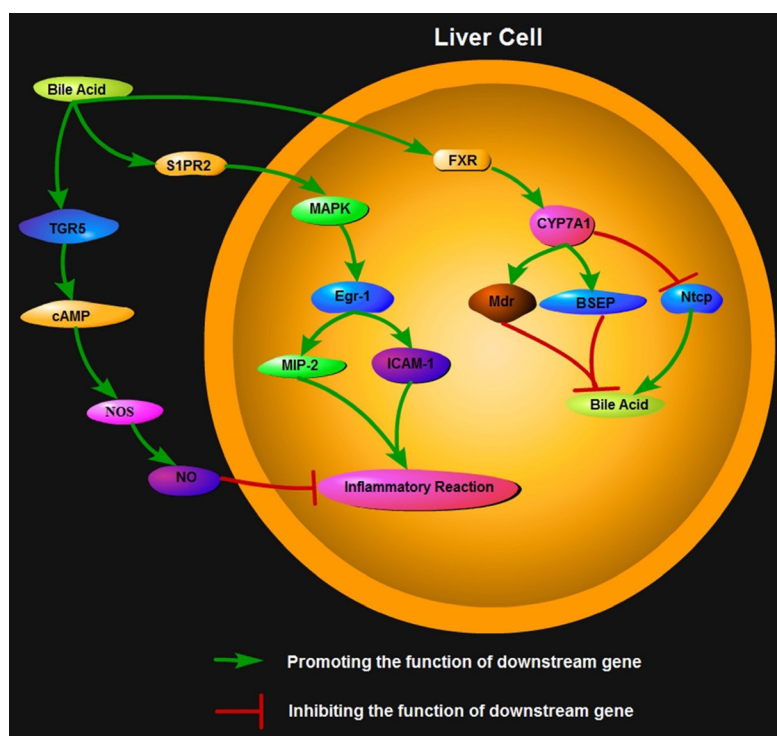


Figure 1. Bile acid signaling pathway and its relationship with the innate immune system. Bile acid acts on intracellular receptors: Bile acid can activate FXR, and then up-regulate Mdr and BSEP genes or down-regulate Ntcp genes through CYP7A1 to reduce intracellular bile acid accumulation. Bile acid acts on extracellular receptors: Bile acid can activate S1PR2 as ligand, up-regulate the level of Egr-1 through the MAPK pathway, and then up-regulate the levels of MIP-2 and ICAM-1 to promote inflammation. In addition, bile acid can also activate TGR5. Activated TGR5 induces NOS synthesis through the cAMP pathway, produces NO and inhibits inflammatory response.

Table 2. The treatment of cholestatic liver injury

Therapeutic method	Bile acid signaling pathway	Therapeutic targets
Anti-inflammatory		OPN, HMGB1, HSP, Uric acid crystal, HDGF
Anti-oxidative stress		GSH, ROS, HClO, Chloramines
Novel therapeutic targets	Intracellular signaling pathway	FXR, CYP7A1, Mdr, BSEP, Ntcp
	Extracellular signaling pathway I	S1PR2, MAPK, Egr-1, MIP-2, ICAM-1
	Extracellular signaling pathway II	TGR5, cAMP, NOS, NO

a novel membrane-bound bile acid receptor expressed in many types of cells, which plays an important role in regulating energy homeostasis and glucose metabolism. *In vitro* experiments showed that TGR5 significantly inhibited macrophage function (66). It is worth noting that the negative regulation of TGR5 on inflammatory responses makes it a potential therapeutic target for immunological liver disease and inflammatory liver disease. It is known that TGR5 is expressed in monocytes, sinusoidal endothelial cells, Kupffer cells, and bile duct epithelial cells, and is also expressed in small amounts in hepatocytes (67).

When cholestasis occurs, Kupffer cells inhibit cytokine synthesis through the TGR5-cAMP pathway, thereby inhibiting inflammatory immune responses (68). The activation of TGR5 on the surface of sinusoidal endothelial cells induces the synthesis of nitric oxide

synthase (NOS) by endothelial cells through the cAMP pathway, thereby producing NO. NO can cause vasodilation to relieve portal hypertension and also play an important role in protecting the liver. In addition, TGR5 stimulates gallbladder filling. Under the action of agonists such as TGR5 agonist and lithocholic acid, the degree of gallbladder filling in TGR5^{-/-} mice is significantly less than that in wild-type mice (69). TGR5 controls bile load during cholestasis and promotes liver regeneration. Animal experiments show that in the BDL model, TGR5 knockout mice have more severe liver damage than normal mice, and there is more inflammatory cell infiltration in the necrotic area (70). This evidence suggests that TGR5 has an important protective effect on the liver during cholestasis, protecting the liver from inflammatory reactions and promoting bile excretion to fill the gallbladder.

INT-767 is a TGR5/FXR dual agonist. Experiments suggest that in the *Mdr2^{-/-}(Abcb4^{-/-})* mouse model, INT-767 can significantly induce bile drainage, cause high gene expression of carbonic anhydrase-14 and increase HCO_3^- release. Carbonic anhydrase-14 increases HCO_3^- transportation, which has a significant effect on improving serum liver enzyme levels, reducing inflammatory infiltration and gallbladder fibrosis (71).

5.4. Early growth response factor 1 (early growth response factor 1, *Egr-1*)

After exposure of primary mouse hepatocytes to chenocholic acid (DCA), chenodeoxycholic acid (CDCA), or taurocholic acid (TCA), the level of intracellular adhesion molecule-1 and macrophage inflammatory protein 2 (MIP-2) increased significantly. Experiments have shown that the upregulation of ICAM-1 and MIP-2 levels is dependent on the transcriptional expression of the *Egr-1* gene (72). *Egr-1* is an important regulator of the expression of many target genes involved in the coupling of external signals to target gene expression. It was reported that normal mouse hepatocytes and FXR knockout mouse liver cells were simultaneously exposed to DCA and CDCA, and there was no difference in *Egr-1* expression level, indicating that *Egr-1* expression was not associated with FXR (73). The expression level of *Egr-1* in hepatocytes using highly-selective MEK inhibitors such as U0126 was significantly decreased, and pretreatment with U0126 prevented *Egr-1* levels in BDL model mice from increasing, indicating the level of *Egr-1* upregulation is dependent on the MAPK pathway during cholestasis (74). *Egr-1* may be central to the inflammatory response caused by cholestasis and a potential therapeutic target for inhibition of inflammatory response during cholestasis (Figure 1).

6. Conclusion

Cholestasis is a complex pathophysiological process with multiple causes, multi-cell involvement. Cholestasis-induced liver injury is mainly a neutrophil-mediated inflammatory response. Therefore, the treatment of cholestatic liver injury is mainly reflected in the inhibition of neutrophil chemotaxis and inhibition of neutrophil-induced oxidative stress. The specific conduction pathway or target can provide new, more specific treatment options to treat cholestatic liver injury (Table 2).

Acknowledgements

This project was supported by the National Natural Science Foundation of China (Nos. 81170454, 30772049 and 30571765).

References

1. Woolbright BL, Jaeschke H. Therapeutic targets for cholestatic liver injury. *Expert Opin Ther Targets*. 2016; 20:463-475.
2. Li Y, Tang R, Leung PSC, Gershwin ME, Ma X. Bile acids and intestinal microbiota in autoimmune cholestatic liver diseases. *Autoimmun Rev*. 2017; 16:885-896.
3. Yang T, Khan GJ, Wu Z, Wang X, Zhang L, Jiang Z. Bile acid homeostasis paradigm and its connotation with cholestatic liver diseases. *Drug Discov Today*. 2019; 24:112-128.
4. Pena Polanco NA, Levy C, Martin EF. Cholestatic Liver Diseases After Liver Transplant. *Clin Liver Dis*. 2017; 21:403-420.
5. Santiago P, Scheinberg AR, Levy C. Cholestatic liver diseases: new targets, new therapies. *Therap Adv Gastroenterol*. 2018; 11:1756284818787400.
6. Woolbright BL, Li F, Xie Y, Farhood A, Fickert P, Trauner M, Jaeschke H. Lithocholic acid feeding results in direct hepato-toxicity independent of neutrophil function in mice. *Toxicol Lett*. 2014; 228:56-66.
7. Galbiati G, Muraca M, Mitry RR, Hughes RD, Lehec SC, Puppi J, Sagias FG, Caruso M, Mieli-Vergani G, Dhawan A. Bilirubin, a physiological antioxidant, can improve cryopreservation of human hepatocytes. *J Pediatr Gastroenterol Nutr*. 2010; 50:691-693.
8. Qaisiya M, Coda Zabetta CD, Bellarosa C, Tiribelli C. Bilirubin mediated oxidative stress involves antioxidant response activation *via* Nrf2 pathway. *Cell Signal*. 2014; 26:512-520.
9. Masubuchi N, Sugihara M, Sugita T, Amano K, Nakano M, Matsuura T. Oxidative stress markers, secondary bile acids and sulfated bile acids classify the clinical liver injury type: Promising diagnostic biomarkers for cholestasis. *Chem Biol Interact*. 2016; 255:83-91.
10. Zhang Y, Hong JY, Rockwell CE, Copple BL, Jaeschke H, Klaassen CD. Effect of bile duct ligation on bile acid composition in mouse serum and liver. *Liver Int*. 2012; 32:58-69.
11. Kodali P, Wu P, Lahiji PA, Brown EJ, Maher JJ. ANIT toxicity toward mouse hepatocytes *in vivo* is mediated primarily by neutrophils *via* CD18. *Am J Physiol Gastrointest Liver Physiol*. 2006; 291:G355-G363.
12. Saito JM, Maher JJ. Bile duct ligation in rats induces biliary expression of cytokine-induced neutrophil chemoattractant. *Gastroenterology*. 2000; 118:1157-1168.
13. Gujral JS, Liu J, Farhood A, Hinson JA, Jaeschke H. Functional importance of ICAM-1 in the mechanism of neutrophil-induced liver injury in bile duct-ligated mice. *Am J Physiol Gastrointest Liver Physiol*. 2004; 286:G499-507.
14. Li M, Cai SY, Boyer JL. Mechanisms of bile acid mediated inflammation in the liver. *Mol Aspects Med*. 2017; 56:45-53.
15. Jones H, Alpini G, Francis H. Bile acid signaling and biliary functions. *Acta Pharm Sin B*. 2015; 5:123-128.
16. Chu M, Zhou M, Jiang C, Chen X, Guo L, Zhang M, Chu Z, Wang Y. *Staphylococcus aureus* Phenol-Soluble Modulins alpha1-alpha3 Act as Novel Toll-Like Receptor (TLR) 4 Antagonists to Inhibit HMGB1/TLR4/NF-kappaB Signaling Pathway. *Front Immunol*. 2018; 9:862.
17. McGill MR, Staggs VS, Sharpe MR, Lee WM, Jaeschke H. Acute Liver Failure Study G. Serum mitochondrial

- biomarkers and damage-associated molecular patterns are higher in acetaminophen overdose patients with poor outcome. *Hepatology*. 2014; 60:1336-1345.
18. McGill MR, Jaeschke H. Mechanistic biomarkers in acetaminophen-induced hepatotoxicity and acute liver failure: from preclinical models to patients. *Expert Opin Drug Metab Toxicol*. 2014; 10:1005-1017.
 19. Toki Y, Takenouchi T, Harada H, Tanuma S, Kitani H, Kojima S, Tsukimoto M. Extracellular ATP induces P2X7 receptor activation in mouse Kupffer cells, leading to release of IL-1 β , HMGB1, and PGE2, decreased MHC class I expression and necrotic cell death. *Biochem Biophys Res Commun*. 2015; 458:771-776.
 20. Yin H, Huang L, Ouyang T, Chen L. Baicalein improves liver inflammation in diabetic db/db mice by regulating HMGB1/TLR4/NF- κ B signaling pathway. *Int Immunopharmacol*. 2018; 55:55-62.
 21. Singh R, Hui T, Matsui A, Allahem Z, Johnston CD, Ruiz-Torruella M, Rittling SR. Modulation of infection-mediated migration of neutrophils and CXCR2 trafficking by osteopontin. *Immunology*. 2017; 150:74-86.
 22. Castello LM, Raineri D, Salmi L, Clemente N, Vaschetto R, Quaglia M, Garzaro M, Gentili S, Navalesi P, Cantaluppi V, Dianzani U, Aspesi A, Chiochetti A. Osteopontin at the Crossroads of Inflammation and Tumor Progression. *Mediators Inflamm*. 2017; 2017:4049098.
 23. Apte UM, Banerjee A, McRee R, Wellberg E, Ramaiah SK. Role of osteopontin in hepatic neutrophil infiltration during alcoholic steatohepatitis. *Toxicol Appl Pharmacol*. 2005; 207:25-38.
 24. Winterbourn CC, Kettle AJ, Hampton MB. Reactive Oxygen Species and Neutrophil Function. *Annu Rev Biochem*. 2016; 85:765-792.
 25. Yang M, Ramachandran A, Yan HM, Woolbright BL, Copple BL, Fickert P, Trauner M, Jaeschke H. Osteopontin is an initial mediator of inflammation and liver injury during obstructive cholestasis after bile duct ligation in mice. *Toxicol Lett*. 2014; 224:186-195.
 26. Okada K, Shoda J, Taguchi K, Maher JM, Ishizaki K, Inoue Y, Ohtsuki M, Goto N, Sugimoto H, Utsunomiya H, Oda K, Warabi E, Ishii T, Yamamoto M. Nrf2 counteracts cholestatic liver injury via stimulation of hepatic defense systems. *Biochem Biophys Res Commun*. 2009; 389:431-436.
 27. Zhao Q, Liu F, Cheng Y, Xiao XR, Hu DD, Tang YM, Bao WM, Yang JH, Jiang T, Hu JP, Gonzalez F, Li F. Celastrol protects from cholestatic liver injury through modulation of SIRT1-FXR signaling. *Mol Cell Proteomics*. 2019; pii: mcp.RA118.000817.
 28. Wang L, Cao F, Zhu LL, Liu P, Shang YR, Liu WH, Dong X, Bao HD, Gong P, Wang ZY. Andrographolide impairs alpha-naphthylisothiocyanate-induced cholestatic liver injury *in vivo*. *J Nat Med*. 2019; 73:388-396.
 29. Nabih ES, El-Kharashi OA. Targeting HMGB1/TLR4 axis and miR-21 by rosuvastatin: role in alleviating cholestatic liver injury in a rat model of bile duct ligation. *Naunyn Schmiedeberg Arch Pharmacol*. 2019; 392:37-43.
 30. Cao F, Liu P, Zhang X, Hu Y, Dong X, Bao H, Kong L, Wang L, Gong P. Shenqi Fuzheng Injection impairs bile duct ligation-induced cholestatic liver injury *in vivo*. *Biosci Rep*. 2019; 39. pii: BSR20180787
 31. Zhang J, Guo X, Hamada T, Yokoyama S, Nakamura Y, Zheng J, Kurose N, Ishigaki Y, Uramoto H, Tanimoto A, Yamada S. Protective effects of peroxiredoxin 4 (PRDX4) on cholestatic liver injury. *Int J Mol Sci*. 2018; 19.
 32. Yuan Z, Wang G, Qu J, Wang X, Li K. 9-cis-retinoic acid elevates MRP3 expression by inhibiting sumoylation of RXR α to alleviate cholestatic liver injury. *Biochem Biophys Res Commun*. 2018; 503:188-194.
 33. Zeng H, Jiang Y, Chen P, Fan X, Li D, Liu A, Ma X, Xie W, Liu P, Gonzalez FJ, Huang M, Bi H. Schisandrol B protects against cholestatic liver injury through pregnane X receptors. *Br J Pharmacol*. 2017; 174:672-688.
 34. Wang YY, Lin SY, Chen WY, Liao SL, Wu CC, Pan PH, Chou ST, Chen CJ. Glechoma hederacea extracts attenuate cholestatic liver injury in a bile duct-ligated rat model. *J Ethnopharmacol*. 2017; 204:58-66.
 35. Li YF, Wu JS, Li YY, Dai Y, Zheng M, Zeng JK, Wang GF, Wang TM, Li WK, Zhang XY, Gu M, Huang C, Yang L, Wang ZT, Ma YM. Chicken bile powder protects against alpha-naphthylisothiocyanate-induced cholestatic liver injury in mice. *Oncotarget*. 2017; 8:97137-97152.
 36. Gao X, Fu T, Wang C, Ning C, Kong Y, Liu Z, Sun H, Ma X, Liu K, Meng Q. Computational discovery and experimental verification of farnesoid X receptor agonist auraptene to protect against cholestatic liver injury. *Biochem Pharmacol*. 2017; 146:127-138.
 37. Yu L, Liu X, Li X, Yuan Z, Yang H, Zhang L, Jiang Z. Protective effects of SRT1720 *via* the HNF1 α /FXR signalling pathway and anti-inflammatory mechanisms in mice with estrogen-induced cholestatic liver injury. *Toxicol Lett*. 2016; 264:1-11.
 38. Yang QL, Yang F, Gong JT, Tang XW, Wang GY, Wang ZT, Yang L. Sweroside ameliorates alpha-naphthylisothiocyanate-induced cholestatic liver injury in mice by regulating bile acids and suppressing pro-inflammatory responses. *Acta Pharmacol Sin*. 2016; 37:1218-1228.
 39. Tan Z, Luo M, Yang J, Cheng Y, Huang J, Lu C, Song D, Ye M, Dai M, Gonzalez FJ, Liu A, Guo B. Chlorogenic acid inhibits cholestatic liver injury induced by alpha-naphthylisothiocyanate: involvement of STAT3 and NF κ B signalling regulation. *J Pharm Pharmacol*. 2016; 68:1203-1213.
 40. Yu SJ, Bae S, Kang JS, Yoon JH, Cho EJ, Lee JH, Kim YJ, Lee WJ, Kim CY, Lee HS. Hepatoprotective effect of vitamin C on lithocholic acid-induced cholestatic liver injury in *Gulo*^{-/-} mice. *Eur J Pharmacol*. 2015; 762:247-255.
 41. Kong LY, Li GP, Yang P, Xi Z. Protective effect of thymoquinone on cholestatic rats with liver injury. *Genet Mol Res*. 2015; 14:12247-12253.
 42. Abdel Kawy HS. Cilostazol attenuates cholestatic liver injury and its complications in common bile duct ligated rats. *Eur J Pharmacol*. 2015; 752:8-17.
 43. Lin SY, Wang YY, Chen WY, Chuang YH, Pan PH, Chen CJ. Beneficial effect of quercetin on cholestatic liver injury. *J Nutr Biochem*. 2014; 25:1183-1195.
 44. Peng J, Yue C, Qiu K, Chen J, Aller MA, Ko KS, Yang H. Protective effects of guava pulp on cholestatic liver injury. *ISRN Hepatol*. 2013; 2013:601071.
 45. Jang JH, Rickenbacher A, Humar B, Weber A, Raptis DA, Lehmann K, Stieger B, Moritz W, Soll C, Georgiev P, Fischer D, Laczko E, Graf R, Clavien PA. Serotonin protects mouse liver from cholestatic injury by decreasing bile salt pool after bile duct ligation. *Hepatology*. 2012; 56:209-218.
 46. Chen WY, Lin SY, Pan HC, Liao SL, Chuang YH, Yen YJ, Lin SY, Chen CJ. Beneficial effect of

- docosahexaenoic acid on cholestatic liver injury in rats. *J Nutr Biochem.* 2012; 23:252-264.
47. Pratap A, Panakanti R, Yang N, Lakshmi R, Modanlou KA, Eason JD, Mahato RI. Cyclopamine attenuates acute warm ischemia reperfusion injury in cholestatic rat liver: hope for marginal livers. *Mol Pharm.* 2011; 8:958-968.
 48. Chan CC, Cheng LY, Lin CL, Huang YH, Lin HC, Lee FY. The protective role of natural phytoalexin resveratrol on inflammation, fibrosis and regeneration in cholestatic liver injury. *Mol Nutr Food Res.* 2011; 55:1841-1849.
 49. Coban S, Yildiz F, Terzi A, Al B, Ozgor D, Ara C, Polat A, Esrefoglu M. The effect of caffeic acid phenethyl ester (CAPE) against cholestatic liver injury in rats. *The J Surg Res.* 2010; 159:674-679.
 50. Song M, Song Z, Barve S, Zhang J, Chen T, Liu M, Arteel GE, Brewer GJ, McClain CJ. Tetrathiomolybdate protects against bile duct ligation-induced cholestatic liver injury and fibrosis. *J Pharmacol Exp Ther.* 2008; 325:409-416.
 51. Yilmaz M, Ara C, Isik B, Karadag N, Yilmaz S, Polat A, Coban S, Duzova H. The effect of aminoguanidine against cholestatic liver injury in rats. *Cell Biochem Funct.* 2007; 25:625-632.
 52. Fani B, Bertani L, Paglianiti I, Fantechi L, De Bortoli N, Costa F, Volterrani D, Marchi S, Bellini M. Pros and Cons of the SeHCAT Test in Bile Acid Diarrhea: A More Appropriate Use of an Old Nuclear Medicine Technique. *Gastroenterol Res Pract.* 2018; 2018:2097359.
 53. Droge C, Bonus M, Baumann U, *et al.* Sequencing of FIC1, BSEP and MDR3 in a large cohort of patients with cholestasis revealed a high number of different genetic variants. *J Hepatol.* 2017; 67:1253-1264.
 54. Jansen PLM. New therapies target the toxic consequences of cholestatic liver disease. *Expert Rev Gastroenterol Hepatol.* 2018; 12:277-285.
 55. Fickert P, Krones E, Pollheimer MJ, *et al.* Bile acids trigger cholemic nephropathy in common bile-duct-ligated mice. *Hepatology.* 2013; 58:2056-2069.
 56. Dempsey JL, Wang D, Siginir G, Fei Q, Raftery D, Gu H, Cui JY. Pharmacological Activation of PXR and CAR Down-regulates Distinct Bile Acid-metabolizing Intestinal Bacteria and Alters Bile Acid Homeostasis. *Toxicol Sci.* 2018. doi: 10.1093/toxsci/kfy271
 57. Hirschfield GM, Mason A, Luketic V, *et al.* Efficacy of obeticholic acid in patients with primary biliary cirrhosis and inadequate response to ursodeoxycholic acid. *Gastroenterology.* 2015; 148:751-761 e758.
 58. Fickert P, Zollner G, Fuchsichler A, Stumptner C, Weiglein AH, Lammert F, Marschall HU, Tsybrovskyy O, Zatloukal K, Denk H, Trauner M. Ursodeoxycholic acid aggravates bile infarcts in bile duct-ligated and Mdr2 knockout mice *via* disruption of cholangioles. *Gastroenterology.* 2002; 123:1238-1251.
 59. Weerachayaphorn J, Luo Y, Mennone A, Soroka CJ, Harry K, Boyer JL. Deleterious effect of oltipraz on extrahepatic cholestasis in bile duct-ligated mice. *J Hepatol.* 2014; 60:160-166.
 60. Fang YW, Han SI, Mitchell C, Gupta S, Studer E, Grant S, Hylemon PB, Dent P. Bile acids induce mitochondrial ROS, which promote activation of receptor tyrosine kinases and signaling pathways in rat hepatocytes. *Hepatology.* 2004; 40:961-971.
 61. Hsiang CY, Lin LJ, Kao ST, Lo HY, Chou ST, Ho TY. Glycyrrhizin, silymarin, and ursodeoxycholic acid regulate a common hepatoprotective pathway in HepG2 cells. *Phytomedicine.* 2015; 22:768-777.
 62. Li S, Qiu M, Kong Y, *et al.* Bile Acid G Protein-Coupled Membrane Receptor TGR5 Modulates Aquaporin 2-Mediated Water Homeostasis. *J Am Soc Nephrol.* 2018; 29:2658-2670.
 63. McMillin M, Frampton G, Grant S, Khan S, Diocares J, Petrescu A, Wyatt A, Kain J, Jefferson B, DeMorrow S. Bile Acid-Mediated Sphingosine-1-Phosphate Receptor 2 Signaling Promotes Neuroinflammation during Hepatic Encephalopathy in Mice. *Front Cell Neurosci.* 2017; 11:191.
 64. Yang Z, Li J, Xiong F, Huang J, Chen C, Liu P, Huang H. Berberine attenuates high glucose-induced fibrosis by activating the G protein-coupled bile acid receptor TGR5 and repressing the S1P2/MAPK signaling pathway in glomerular mesangial cells. *Exp Cell Res.* 2016; 346:241-247.
 65. Kawamata Y, Fujii R, Hosoya M, Harada M, Yoshida H, Miwa M, Fukusumi S, Habata Y, Itoh T, Shintani Y, Hinuma S, Fujisawa Y, Fujino M. A G protein-coupled receptor responsive to bile acids. *J Biol Chem.* 2003; 278:9435-9440.
 66. Keitel V, Donner M, Winandy S, Kubitz R, Haussinger D. Expression and function of the bile acid receptor TGR5 in Kupffer cells. *Biochem Biophys Res Commun.* 2008; 372:78-84.
 67. Li Z, Huang J, Wang F, *et al.* Dual Targeting of Bile Acid Receptor-1 (TGR5) and Farnesoid X Receptor (FXR) Prevents Estrogen-Dependent Bone Loss in Mice. *J Bone Miner Res.* 2018. doi: 10.1002/jbmr.3652.
 68. Lou G, Ma X, Fu X, Meng Z, Zhang W, Wang YD, Van Ness C, Yu D, Xu R, Huang W. GPBAR1/TGR5 mediates bile acid-induced cytokine expression in murine Kupffer cells. *PloS One.* 2014; 9:e93567.
 69. Wang YD, Chen WD, Yu D, Forman BM, Huang W. The G-protein-coupled bile acid receptor, Gpbar1 (TGR5), negatively regulates hepatic inflammatory response through antagonizing nuclear factor kappa light-chain enhancer of activated B cells (NF-kappaB) in mice. *Hepatology.* 2011; 54:1421-1432.
 70. Pean N, Doignon I, Garcin I, Besnard A, Julien B, Liu B, Branchereau S, Spraul A, Guettier C, Humbert L, Schoonjans K, Rainteau D, Tordjmann T. The receptor TGR5 protects the liver from bile acid overload during liver regeneration in mice. *Hepatology.* 2013; 58:1451-1460.
 71. Jadhav K, Xu Y, Xu Y, Li Y, Xu J, Zhu Y, Adorini L, Lee YK, Kasumov T, Yin L, Zhang Y. Reversal of metabolic disorders by pharmacological activation of bile acid receptors TGR5 and FXR. *Mol Metab.* 2018; 9:131-140.
 72. Allen K, Kim ND, Moon JO, Copple BL. Upregulation of early growth response factor-1 by bile acids requires mitogen-activated protein kinase signaling. *Toxicol Appl Pharmacol.* 2010; 243:63-67.
 73. Zhang Y, Xu N, Xu J, Kong B, Copple B, Guo GL, Wang L. E2F1 is a novel fibrogenic gene that regulates cholestatic liver fibrosis through the Egr-1/SHP/EID1 network. *Hepatology.* 2014; 60:919-930.
 74. Koeppel TA, Trauner M, Baas JC, Thies JC, Schlosser SF, Post S, Gebhard MM, Herfarth C, Boyer JL, Otto G. Extrahepatic biliary obstruction impairs microvascular perfusion and increases leukocyte adhesion in rat liver. *Hepatology.* 1997; 26:1085-1091.

(Received October 13, 2018; Revised February 13, 2019; Accepted February 22, 2019)

Fibrosis-4 index predicts mortality in HIV/HCV co-infected patients receiving combination antiretroviral therapy in rural China

Xiaochen Chen^{1,§}, Xing Liu^{1,§}, Renhai Tang², Runhua Ye², Yuecheng Yang², Shitang Yao², Jibao Wang², Yingying Ding¹, Song Duan^{2,*}, Na He^{1,3,*}

¹ Department of Epidemiology, School of Public Health, and the Key Laboratory of Public Health Safety of Ministry of Education, Fudan University, Shanghai, China;

² Dehong Prefecture Center for Disease Control and Prevention, Mangshi, Yunnan, China;

³ Key Laboratory of Health Technology Assessment of Ministry of Health, Fudan University, Shanghai, China.

Summary

End-stage liver disease (ESLD) is among leading causes of death for people living with HIV and HCV. Little is known how liver fibrosis score predicts mortality in HIV/HCV co-infected population under combination antiretroviral therapy (cART). A retrospective cohort study of 691 HIV/HCV co-infected patients receiving cART in Yunnan, China from 2005 to 2016 was carried out to explore the association between Fibrosis-4 index (FIB-4) and all-cause mortality. Cox proportional hazard models were used to estimate the hazard ratios (HRs) for FIB-4 and covariates. After a median follow-up of 4.8 years with a total follow-up time of 3,696 person-years (PY), 131 deaths occurred and the all-cause mortality was 3.5 per 100 PY. The mortality was 2.9 (95% CI: 2.3-3.5)/100 PY for the FIB-4 \leq 3.25 group and 5.8 (4.2-7.4)/100 PY for the FIB-4 > 3.25 group at baseline. People with FIB-4 changed from mild to advanced group showed HR of 1.81 (95% CI: 1.01-3.25) for death, and with FIB-4 sustaining advanced showed HR of 3.11 (1.75-5.54), both compared to those with FIB-4 remained mild, while lower risk of death was observed among married people (HR = 0.63, 95% CI: 0.41-0.99) compared to unmarried, among those with most recent CD4⁺ T cell counts between 200 and 350 cells/ μ L (0.50, 0.30-0.86) and > 350 cells/ μ L (0.25, 0.15-0.41) compared to CD4 under 200 cells/ μ L. Advanced and progressive liver fibrosis is a strong predictor of all-cause mortality in HIV/HCV co-infected patients under cART in China.

Keywords: HIV/HCV co-infection, liver fibrosis, FIB-4, mortality

1. Introduction

With the widespread use of combination antiretroviral therapy (cART), people infected with human immunodeficiency virus (HIV) have a longer lifespan

(1) and non-HIV related diseases are the major burden and causes of death currently. In particular, on the basis of fibrosis, end-stage liver diseases are becoming more prominent in HIV-infected patients (2-4), accounting for 14-18% of deaths (5). Liver fibrosis refers to the excessive deposition of diffuse extracellular matrix and fibrotic lesions in the liver, which is a kind of injury repair responses after chronic hepatic injury. If not treated in time, liver fibrosis may develop into decompensated cirrhosis, and patients would suffer from various consequences including cirrhosis and hepatocellular carcinoma (HCC) (6).

Liver fibrosis can be induced by hepatitis B virus (HBV), hepatitis C virus (HCV), alcohol, long-term use of antiviral drugs, etc, and the process is accelerated by HIV infection (7,8). In China, especially in rural

Released online in J-STAGE as advance publication February 5, 2019.

[§]These authors contributed equally to this work.

*Address correspondence to:

Dr. Song Duan, Dehong Prefecture Center for Disease Control and Prevention, Mangshi, Yunnan 678400, China.
E-mail: dhduansong@sina.com

Dr. Na He, Department of Epidemiology, School of Public Health, Fudan University, Shanghai 20032, China.
E-mail: nhe@fudan.edu.cn, or nhe@shmu.edu.cn

Yunnan, these risk factors are highly prevalent among HIV-infected patients (9,10). The prevalence was 77.7% for HCV infection and 15.5% for HIV/HCV co-infection among injecting drug users (IDU) in Yunnan province (11). And the prevalence of alcohol use was 65% among HIV patients (12). Such high prevalence and co-existence of risk factors bring heavy burden of liver disease to this population. However, how the progression of liver fibrosis affects mortality in HIV-infected people has not been examined.

Severity assessment of liver disease, such as the degree of liver fibrosis, is important for disease progression and treatment guidance for patients with hepatitis C (13). Though liver biopsy is the gold standard, the invasive method may cause some complications, has higher cost, and is difficult to be performed repeatedly for assessing liver fibrosis in community (14,15). In light of these limitations, many noninvasive indicators have been developed to assess the severity of liver fibrosis. FIB-4 is calculated by routinely used biochemical data, *i.e.* alanine transaminase (ALT), aspartate aminotransferase (AST), platelet count and age (16), and is an internationally recognized well-established noninvasive indicator for the degree of liver fibrosis (17-19). Increased FIB-4 has been shown to be associated with increased mortality in general population (20), people with liver diseases (16,21,22) and patients with HIV/HCV coinfection in western countries (23). We conducted this cohort study to examine the utility of liver fibrosis index in predicting mortality among HIV/HCV co-infected patients in the era of cART in Chinese population.

2. Materials and Methods

2.1. Study design and subject

We conducted a retrospective cohort study of HIV/HCV co-infected patients who were under cART in Dehong Prefecture, Yunnan Province, China, a region bordering Myanmar which has high HIV endemic (24,25). The observational study period was from the date of cART initiation (*i.e.* baseline) to 31 March 2016 for all patients. The inclusion criteria for the study participants were as following: *i)* age ≥ 18 years at cART initiation; *ii)* cART initiation no later than 31 March 2015 to ensure that each participants had received cART for at least one year; *iii)* tested positive for serum anti-HCV antibody; *iv)* no evidence of hepatitis B virus infection; *v)* had available biochemical data to calculate FIB-4 (*i.e.* ALT, AST, platelet count); *vi)* had at least one follow-up visit. By March 2016, 1,017 HIV/HCV co-infected patients had been reported (8). Of them, 204 had not initiated cART, 44 were tested positive for hepatitis B surface antigen, 22 did not have biochemical data available at baseline and 56 did not have biochemical data followed-up. Thus, a total of 691 HIV/HCV co-

infected patients under cART were included in the analysis. This study was approved by the Institutional Review Board (IRB) of Chinese National Center for AIDS/STD Control and Prevention and the IRB of Fudan University. Written informed consent was obtained from all study participants.

2.2. Data collection

Epidemiologic data and laboratory measurements were obtained from the Comprehensive Response Information Management System (CRIMS), which is a web-based national database for real-time collection and maintenance of information for HIV infected people in China (26). Demographic characteristics including age, gender, ethnicity, level of education and marital status at initiation of cART were collected. HIV-related data including date of cART initiation, CD4⁺ T cell counts, HIV viral load, ALT, AST, platelet count at both baseline and follow-up were also collected.

FIB-4 score was calculated by the following formula: $\text{AST (IU/L)} \times \text{age (years)} / \text{platelet count (10}^9\text{/L)} \times \text{ALT}^{1/2} \text{ (IU/L)}$ (16). And the FIB-4 score was further categorized into two classes: $\text{FIB-4} \leq 3.25$ indicating no or mild liver fibrosis, and $\text{FIB-4} > 3.25$ indicating advanced liver fibrosis (27). Accordingly, changes in FIB-4 classes were categorized into four groups: G1, sustaining mild fibrosis (FIB-4 remaining ≤ 3.25); G2, change from mild to advanced fibrosis ($\text{FIB-4} \leq 3.25$ at baseline, and > 3.25 in most recent follow-up); G3, change from advanced to mild fibrosis ($\text{FIB-4} > 3.25$ at baseline, and ≤ 3.25 in most recent follow-up); G4, sustaining advanced fibrosis (FIB-4 remaining > 3.25).

2.3. Definition of outcome

The main outcome was all-cause mortality. Dates of death were obtained from CRIMS. All participants were followed until the occurrence of death, loss to follow-up, or end of this observation (March 31, 2016), whichever came first.

2.4. Statistical analysis

Categorical variables were expressed as number and percentage. Continuous variables were presented as median and interquartile range (IQR). χ^2 test was conducted to compare distribution of categorical variables while Mann-Whitney u test or Kruskal Wallis test was conducted to compare continuous variables. The overall mortality, mortalities by FIB-4 classes and by epidemiologic characteristics were calculated as the number of deaths divided by person-years (PY) of follow-up. Univariate Cox proportional hazard models were used to estimate the hazard ratios (HRs) for FIB-4 score and other epidemiologic and clinical variables. In multivariate Cox proportional hazard model, variables

Table 1. Baseline characteristics of HIV/HCV co-infected participants and FIB-4 distributions

Characteristics	Total No. (%) ^a	Fib4 ≤ 3.25 No. (%) ^b	Fib4 > 3.25 No. (%) ^b	P ^c
Age (years)				< 0.001
Median (IQR)	35 (31-40)	35 (31-39)	39 (35-44)	< 0.001
19 - 29	124 (17.9)	111 (89.5)	13 (10.5)	
30 - 39	384 (55.6)	309 (80.5)	75 (19.5)	
40 - 49	168 (24.3)	110 (65.5)	58 (34.5)	
≥ 50	15 (2.2)	5 (33.3)	10 (66.7)	
Gender				0.623
male	674 (97.5)	521 (77.3)	153 (22.7)	
female	17 (2.5)	14 (82.4)	3 (17.6)	
Ethnicity				0.999
Han	311 (45.0)	241 (77.5)	70 (22.5)	
Dai	131 (19.0)	101 (77.1)	30 (22.9)	
Jingpo	223 (32.3)	173 (77.6)	50 (22.4)	
Others	26 (3.8)	20 (76.9)	6 (23.1)	
Education (years)				0.025
0 ~ 6	344 (49.8)	254 (73.8)	90 (26.2)	
7 ~	347 (50.2)	281 (81.0)	66 (19.0)	
Marital status				0.046
unmarried	261 (37.8)	215 (82.4)	46 (17.6)	
married	353 (51.1)	261 (73.9)	92 (26.1)	
Divorced/widowed	77 (11.1)	59 (76.6)	18 (23.4)	
HIV transmission route				0.383
IDU	632 (91.5)	492 (77.8)	140 (22.2)	
Others	59 (8.5)	43 (72.9)	16 (27.1)	
Baseline CD4 ⁺ T cell counts(cells/μL)				0.004
Median(IQR)	269 (181-378)	277 (184-405)	242 (166-321)	0.001
< 200	210 (30.4)	151 (71.9)	128 (28.1)	
200 - 350	283 (41.0)	214 (75.6)	69 (24.4)	
> 350	191 (27.6)	163 (85.3)	28 (14.7)	
ARV regimen type, %				0.001
NVP (vs. EFV/RTV)	302 (44.1)	232 (76.8)	70 (23.2)	
TDF (vs. AZT/d4T/DDI)	251 (36.6)	210 (83.7)	41 (16.3)	
Others	132 (19.3)	88 (66.7)	45 (33.3)	

^aproportion in column; ^bproportion in row; ^cin bold: $p < 0.05$ (Mann-Whitney U test)

of age, gender, ethnicity, level of education, marital status, baseline and most recent CD4⁺ T cell counts in addition to FIB-4 measures were included, either by "forced-entry" or p -value < 0.05 at univariate analysis. Kaplan-Meier survival curves were constructed for each category of changes in FIB-4 class and log-rank test was used for comparisons. Statistical significance was defined as $p < 0.05$. Statistical analyses were performed using SPSS version 22.0 and R version 3.3.2.

3. Results

3.1. Patients characteristics

A total of 691 HIV/HCV co-infected patients were included in the study. The socio-demographic and HIV infection related characteristics were summarized in Table 1. The median age was 35 years old (IQR, 31-40 years). 97.5% were male. 45.0% were Han, the major ethnicity in China, whereas 32.3% were Jingpo and 19.0% were Dai, which are the two major ethnic minority groups in the study area. The majority (91.5%) of the study patients infected with HIV *via* injecting drug use (IDU). The median CD4⁺ T cell counts was 269 cells/μL (IQR, 181-378 cells/μL) at baseline, and

71.1% were less than 200 cells/μL. All patients had initiated cART for HIV, while no one had received treatment for HCV such as ribavirin.

3.2. FIB-4 index and change

At baseline, the median FIB-4 score was 1.78 (IQR, 1.19-3.00). 22.6% of the participants had FIB-4 > 3.25, indicating advanced liver fibrosis. Participants with FIB-4 > 3.25 tended to be older, had lower education, lower baseline CD4⁺ T cell counts, and had ARV regime without NVP or TDF. In contrast, having FIB-4 > 3.25 did not differ significantly by gender, ethnicity or HIV transmission route.

The distribution of FIB-4 and its change by characteristics of HIV/HCV co-infected participants after follow-up were shown in Table 2. 479 (69.3%) had the recent FIB-4 score remained in the mild class, 56 (8.1%) changed from mild to advanced class, 91 (13.2%) changed from advanced to mild class and 65 (9.4%) remained in advanced class. Patients with older age, being male, divorced/widowed, had lower baseline or most recent CD4⁺ T cell counts had higher possibility of sustaining advanced liver fibrosis ($p < 0.05$). While gender, ethnicity, HIV transmission route and most

Table 2. FIB-4 changes by demographic and clinical characteristics of HIV/ HCV co-infected participants

Characteristics	Changes in FIB-4, number and proportion (%)				P ^a
	G1 Sustaining mild	G2 Mild to advanced	G3 Advanced to mild	G4 Sustaining advanced	
Age (years)					< 0.001
Median(IQR)	35 (30-39)	37 (33-41)	38 (34-44)	40 (36-44)	< 0.001
19 - 29	103 (83.1)	8 (6.5)	11 (8.9)	2 (1.6)	
30 - 39	279 (72.7)	30 (7.8)	45 (11.7)	30 (7.8)	
40 - 49	94 (56.0)	16 (9.5)	29 (17.3)	29 (17.3)	
≥ 50	4 (26.7)	1 (6.7)	6 (40.0)	4 (26.7)	
Gender					0.056
male	466 (69.1)	55 (8.2)	89 (13.2)	64 (9.5)	
female	14 (82.4)	0 (0.0)	2 (11.8)	1 (5.9)	
Ethnicity					0.574
Han	213 (68.5)	28 (9.0)	40 (12.9)	30 (9.6)	
Dai	89 (67.9)	12 (9.2)	15 (11.5)	15 (11.5)	
Jingpo	159 (71.3)	14 (6.3)	30 (13.5)	20 (9.0)	
Others	19 (73.1)	1 (3.8)	6 (23.1)	0 (0.0)	
Education (years)					0.028
0 ~ 6	223 (64.8)	31 (9.0)	57 (16.6)	33 (9.6)	
7 ~	257 (74.1)	24 (6.9)	34 (9.8)	32 (9.2)	
Marital status					< 0.001
unmarried	204 (78.2)	11 (4.2)	26 (10.0)	20 (7.7)	
married	225 (63.7)	36 (10.2)	59 (16.7)	33 (9.3)	
Divorced/widowed	51 (66.2)	8 (10.4)	6 (7.8)	12 (15.6)	
HIV transmission route					0.704
IDU	441 (69.8)	51 (8.1)	83 (13.1)	57 (9.0)	
Others	39 (66.1)	4 (6.8)	8 (13.6)	8 (13.6)	
ARV regimen type, %					< 0.001
NVP (vs. EFV/RTV)	202 (66.9)	30 (9.9)	43 (14.2)	27 (8.9)	
TDF (vs. AZT/d4T/DDI)	195 (77.7)	15 (6.0)	29 (11.6)	12 (18.5)	
Others	79 (59.8)	9 (6.8)	18 (13.6)	26 (19.7)	
Baseline CD4 ⁺ T cell counts (cells/μL)					0.009
Median(IQR)	281 (188-416)	239 (159-329)	233 (163-328)	262 (179-303)	0.003
< 200	131 (62.4)	20 (9.5)	39 (18.6)	20 (9.5)	
200 - 350	190 (67.1)	24 (8.5)	35 (12.4)	34 (12.0)	
> 350	153 (80.1)	10 (5.2)	17 (8.9)	11 (5.8)	
Last CD4 ⁺ T cell counts (cells/μL)					0.034
Median (IQR)	523 (347-685)	494 (365-659)	388 (277-556)	409 (257-598)	< 0.001
< 200	40 (61.5)	4 (6.2)	11 (16.9)	10 (15.4)	
200 - 350	78 (61.9)	9 (7.1)	24 (19.0)	15 (11.9)	
> 350	345 (72.5)	42 (8.8)	54 (11.3)	35 (7.4)	
Last HIV RNA (n = 612)					0.146
< 400	353 (68.9)	38 (7.4)	73 (14.3)	48 (9.4)	
≥ 400	71 (71.0)	13 (13.0)	10 (10.0)	6 (6.0)	

^ain bold: $p < 0.05$ (Kruskal - Wallis test).

recent HIV RNA did not show significant association with FIB-4 change.

3.3. Cumulative all-cause mortality based on FIB-4 index

The median follow-up time was 4.8 years (IQR, 3.3-7.6 years), corresponding to 3,696 person-years for the 691 participants. During follow-up, 131 had died and the all-cause mortality was 3.5 per 100 PY (95% CI: 2.9-4.1). The cumulative mortality increased as the FIB-4 score increased both at baseline and at follow-up. The mortality was 2.9/100 PY (95% CI: 2.3-3.5) in the FIB-4 ≤ 3.25 group and 5.8/100 PY (95% CI: 4.2-7.4) in the FIB-4 > 3.25 group at baseline. The cumulative mortality also differed by FIB-4 change: of the four

groups, *i.e.*, G1 (sustaining mild), G2 (changed from mild to advanced), G3 (changed from advanced to mild) and G4 (sustaining advanced), the mortalities were 2.7 (95% CI: 2.1-3.4), 4.3 (2.2-6.4), 4.1 (2.4-5.8) and 8.6 (5.5-11.8) per 100 PY, respectively (Table 3). Log-rank test showed significant difference in survival among the four FIB-4 changing groups (Figure 1).

3.4. Cumulative mortality and associated factors

In simple Cox proportional hazard regression model, the hazard for death was positively associated with older age, baseline FIB-4 >3.25, most recent FIB-4 > 3.25, in sustaining advanced fibrosis group (G4), most recent CD4⁺ T cell counts < 200 cells/μL and most recent HIV RNA > 400 copies/mL. In the multiple regression

Table 3. Cox proportional hazard models for mortality of HIV/HCV co-infected participants

Age (years)	Total No. (%)	No. Deaths	Follow-up in person years	Mortality (/100 PY)	cHR ^a (95% CI)	P	aHR ^b (95% CI)	P
19-29	124 (17.9)	16	744.7	2.1	1.00		1.00	
30-39	384 (55.6)	65	2,107.9	3.1	1.42 (0.81-2.51)	0.259	1.65 (0.90-3.00)	0.104
40-49	168 (24.3)	45	771.2	5.8	2.64 (1.45-4.82)	0.002	2.60 (1.32-5.14)	0.006
≥50	15 (2.2)	5	72.3	6.9	3.33 (1.21-9.17)	0.020	2.32 (0.74-7.26)	0.149
As continuous							1.03 (0.99-1.06)	0.099
Gender								
male	674 (97.5)	130	3,607.8	3.6	1.00		1.00	
female	17 (2.5)	1	88.2	1.1	0.31 (0.04-2.24)	0.248	0.78 (0.10-5.80)	0.805
Ethnicity								
Han	311 (45.0)	62	1,746.0	3.6	1.00		1.00	
Dai	131 (19.0)	22	637.0	3.5	1.01 (0.62-1.65)	0.965	0.99 (0.56-1.77)	0.979
Jingpo	223 (32.3)	41	1,187.0	3.5	0.98 (0.66-1.45)	0.918	0.80 (0.49-1.31)	0.376
Others	26 (3.8)	6	126.0	4.8	1.38 (0.60-3.20)	0.450	1.32 (0.55-3.17)	0.535
Education (years)								
0-6	344 (49.8)	73	1,763.4	4.01	1.00		1.00	
7~	347 (50.2)	58	1,932.6	3.00	0.71 (0.50-1.00)	0.051	0.86 (0.56-1.33)	0.508
Marital status								
unmarried	261 (37.8)	52	1,406.3	3.7	1.00		1.00	
married	353 (51.1)	62	1,899.3	3.3	0.88 (0.61-1.28)	0.504	0.63 (0.41-0.99)	0.043
Divorced/widowed	77 (11.1)	17	390.4	4.4	1.21 (0.70-2.10)	0.489	0.65 (0.34-1.25)	0.202
HIV transmission route								
IDU	632 (91.5)	84	3,410.0	2.5	1.00		1.00 (0.99-1.01)	0.313
Others	59 (8.5)	47	286.0	16.4	0.70 (0.33-1.50)	0.352	0.86 (0.56-1.33)	0.508
Baseline counts CD4 ⁺ T cell(cells/μL)								
<200	210 (30.7)	49	1,269.9	3.9	1.00		1.00	
200-350	283 (41.4)	65	1,712.8	3.8	0.99 (0.68-1.43)	0.935	0.50 (0.30-0.86)	0.012
>350	191 (27.9)	17	684.2	2.5	0.75 (0.42-1.32)	0.318	0.25 (0.15-0.41)	<0.001
As continuous					0.999 (0.998-1.001)	0.312	1.00 (0.99-1.01)	0.313
Last CD4 ⁺ T cell counts (cells/μL)								
<200	65 (9.7)	27	313.0	8.6	1.00		1.00	
200-350	126 (18.9)	32	673.5	4.8	0.54 (0.33-0.91)	0.019	0.50 (0.30-0.86)	0.012
>350	476 (71.4)	57	2,654.0	2.1	0.24 (0.15-0.38)	<0.001	0.25 (0.15-0.41)	<0.001
As continuous					0.998 (0.997-0.999)	<0.001	0.99 (0.96-1.01)	0.354
Baseline FIB-4								
≤3.25	535 (77.4)	84	2,885.3	2.9	1.00		1.00	
>3.25	156 (22.6)	47	810.7	5.8	1.99 (1.39-2.85)	<0.001	1.99 (1.39-2.85)	<0.001
As continuous					1.01 (0.99-1.02)	0.439	0.99 (0.96-1.01)	0.354
Last FIB-4								
≤3.25	571 (82.6)	90	3,055.5	2.9	1.00		1.00	
>3.25	120 (17.4)	41	640.5	6.4	2.15 (1.49-3.11)	<0.001	2.15 (1.49-3.11)	<0.001
FIB-4 change (Baseline - Last)								
G1	480 (69.5)	69	2,545.8	2.7	1.00		1.00	
G2	55 (8.0)	15	356.5	4.2	1.52 (0.87-2.66)	0.144	1.81 (1.01-3.25)	0.047
G3	91 (13.2)	21	509.7	4.1	1.48 (0.91-2.40)	0.112	1.59 (0.92-2.77)	0.097
G4	65 (9.4)	26	301.0	8.6	3.24 (2.06-5.10)	<0.001	3.11 (1.75-5.54)	<0.001
Last HIV RNA (n = 612, copies/mL)								
<400	512 (83.7)	75	2,952.0	2.5	1.00		1.00	
≥400	100 (16.3)	25	537.2	4.7	1.71 (1.07-2.72)	0.024	1.71 (1.07-2.72)	0.024

^acHR, crude hazard ratio; ^baHR, adjusted hazard ratio, adjusted for age, gender, ethnicity, education, marital status, baseline CD4⁺ T cell counts, baseline FIB-4, last CD4⁺ T cell counts, FIB-4 changes. ^cin bold: $p < 0.05$.

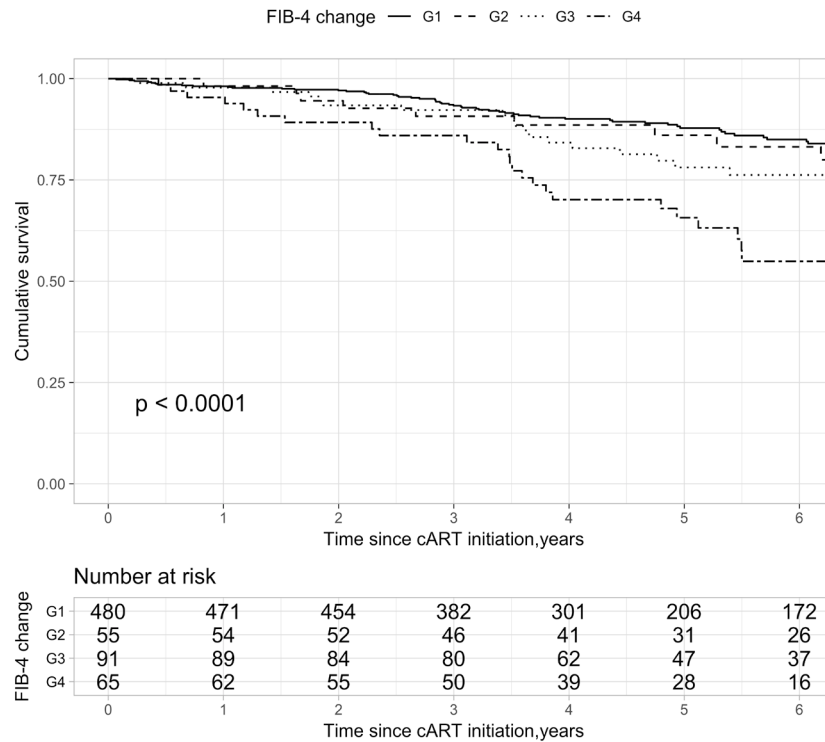


Figure1. Kaplan-Meier survival curves in patients based on the FIB-4 changes. The cumulative mortality differed significantly among the different groups of FIB-4 changes ($p < 0.0001$, log-rank test). G1, solid line, sustaining mild; G2, dashed line, mild- to- advanced; G3, dotted line, advanced-to-mild; G4, two dash line, sustaining advanced.

model, higher risk of death was associated with age at 40-49 years old (adjusted HR: 2.60, 95% CI: 1.32-5.14), FIB-4 changed from mild to advanced group (1.81, 1.01-3.25) and FIB-4 sustaining advanced (3.11, 1.75-5.54) compared to FIB-4 remained mild. While lower risk of death was observed among married people (0.63, 0.41 - 0.99), among those with most recent CD4⁺ T cell counts 200-350 cells/ μ L (0.50, 0.30 - 0.86) and > 350 cells/ μ L (0.25, 0.15-0.41). In particular, baseline FIB-4 > 3.25 remained an independent predictor of increased all-cause mortality when adjusted by age, gender, ethnicity, education, marital status and most recent CD4⁺ T cell counts (1.63, 1.12- 2.38, data not shown in table).

4. Discussion

To the best of our knowledge, the present study is the first to report FIB-4 index as a predictor of all-cause mortality in HIV/HCV co-infected Chinese in the cART era. It suggests with epidemiologic evidence that the index constructed from routinely used laboratory measurements in clinical settings could be applied in prognosis for patients with HIV and HCV.

Noninvasive methods of measuring biomarkers of liver fibrosis alternative to liver biopsy is an important issue in various research fields. Studies found that single biomarker such as serum hyaluronan and biomarkers combined such as Fibro Test had shown

prognostic values in patients with chronic hepatitis C (28,29). Among the combined indexes, FIB-4 score had advantages that it comprises of routinely used biochemical measurements, and shows superiority in accuracy to other markers of fibrosis (30). And FIB-4 was also found to be a successful predictor in distinguishing mild and advanced fibroses in HIV/HCV co-infected patients (31).

In the present study, both baseline FIB-4 higher than 3.25, indicating advanced liver fibrosis, and FIB-4 progressing from mild to advanced fibrosis during follow-up were found to be independent predictors for all-cause mortality among HIV/HCV co-infected participants under cART. This observation is consistent with studies conducted in the western countries (31-33). One large scale cohort conducted in Italy followed up 3,475 HIV patients with or without HCV reported that FIB-4 at cART initiation and its change independently predicted liver related death (34). Our study adds to the knowledge that FIB-4 also has predictive value in Chinese population with high prevalence of HIV/HCV infection, alcohol consumption, at the same time receiving cART.

Meanwhile, the most recent CD4⁺ T cell counts as the marker for immune suppression status predicted mortality in univariate and multiple regression models and the observation was consistent with previous research (35). Although most recent HIV RNA greater than 400 copies/mL was also a risk factor for increased

mortality in univariate model, considering that CD4⁺ T cell counts is highly correlated with HIV viral load, and is more frequently tested for HIV patients, CD4⁺ T cell counts were included in the multiple regression model. The increase in CD4 was shown to be protective against death, and we suggest to include both FIB-4 and CD4 in risk stratification for HIV/HCV patients.

This study has some limitations. First, this study was a retrospective study based on HIV/HCV infection, information on other factors which might had affected the progression of liver fibrosis, such as alcohol consumption, were not collected. Further studies are needed to control potential confounding brought by alcohol consumption and some other important factors. Second, the causes of death cannot be specified and collected in this study. Thus, all analyses were conducted toward all-cause mortality, and the association between liver fibrosis and liver-related deaths had not been explored.

In conclusion, the FIB-4 index as a marker for liver fibrosis is shown to be a predictor for all-cause mortality in HIV/HCV co-infected patients under cART. FIB-4 may help in risk stratification and in estimating risk of death in clinical settings.

Acknowledgements

The authors thank all study participants. This study was supported by the National Science and Technology Major Projects on Infectious Diseases (Grant No. 2018ZX10721102-004), and the National Natural Science Foundation of China (Grant No. 81773485; 81373062).

References

- World Health Organization. Global hepatitis report 2017. <https://apps.who.int/iris/bitstream/handle/10665/255016/9789241565455-eng.pdf?sequence=1>. (accessed April, 2017)
- Weber R, Sabin CA, Friis-Møller N, *et al.* Liver-related deaths in persons infected with the human immunodeficiency virus: The D:A:D study. *Arch Intern Med.* 2006; 166:1632-1641.
- Peters MG. End-stage liver disease in HIV disease. *Top HIV Med.* 2009; 17:124-128.
- Graham CS, Baden LR, Yu E, Mrus JM, Carnie J, Heeren T, Koziel MJ. Influence of human immunodeficiency virus infection on the course of hepatitis C virus infection: A meta-analysis. *Clin Infect Dis.* 2001; 33:562-569.
- Price JC, Thio CL. Liver disease in the HIV-infected individual. *Clin Gastroenterol Hepatol.* 2010; 8:1002-1012.
- Ismail MH, Pinzani M. Reversal of liver fibrosis. *Saudi J Gastroenterol.* 2009; 15:72-79.
- Jain MK, Seremba E, Bhore R, Dao D, Joshi R, Attar N, Yuan HJ, Lee WM. Change in fibrosis score as a predictor of mortality among HIV-infected patients with viral hepatitis. *AIDS Patient Care STDS.* 2012; 26:73-80.
- Ding Y, Duan S, Ye R, Yang Y, Yao S, Wang J, Cao D, Liu X, Lu L, Jia M. More improvement than progression of liver fibrosis following antiretroviral therapy in a longitudinal cohort of HIV-infected patients with or without HBV and HCV co-infections. *J Viral Hepat.* 2017; 24:412-420.
- Zhang F, Zhu H, Wu Y, Dou Z, Zhang Y, Kleinman N, Bulterys M, Wu Z, Ma Y, Zhao D. HIV, hepatitis B virus, and hepatitis C virus co-infection in patients in the China National Free Antiretroviral Treatment Program, 2010-12: A retrospective observational cohort study. *Lancet Infect Dis.* 2014; 14:1065-1072.
- Wei Q, Lin H, Ding Y, Liu X, Wu Q, Shen W, Gao M, He N. Liver fibrosis after antiretroviral therapy in a longitudinal cohort of sexually infected HIV patients in eastern China. *Biosci Trends.* 2017; 11:274-281.
- Zhou YH, Yao ZH, Liu FL, Li H, Jiang L, Zhu JW, Zheng YT. High Prevalence of HIV, HCV, HBV and Co-Infection and Associated Risk Factors among Injecting Drug Users in Yunnan Province, China. *PLoS One.* 2012; 7:e42937.
- Luo XF, Duan S, Duan QX, Pu YC, Yang YC, Ding YY, Gao MY, He N. Alcohol use and subsequent sex among HIV-infected patients in an ethnic minority area of Yunnan province, China. *PLoS One.* 2013; 8:e61660.
- Peters MG, Bacchetti P, Boylan R, French AL, Tien PC, Plankey MW, Glesby MJ, Augenbraun M, Golub ET, Karim R, Parkes J, Rosenberg W. Enhanced liver fibrosis marker as a noninvasive predictor of mortality in HIV/hepatitis C virus-coinfected women from a multicenter study of women with or at risk for HIV. *AIDS.* 2016; 30:723-729.
- Gebo KA, Herlong HF, Torbenson MS, Jenckes MW, Chander G, Ghanem KG, El-Kamary SS, Sulkowski M, Bass EB, Tm JHUEBPC. Role of liver biopsy in management of chronic hepatitis C: A systematic review. *Hepatology.* 2002; 36:S161-S172.
- Bravo AA, Sheth SG, Chopra S. Liver biopsy. *New Engl J Med.* 2001; 344:495-500.
- Tada T, Kumada T, Toyoda H, Kiriya S, Tanikawa M, Hisanaga Y, Kanamori A, Kitabatake S, Yama T, Tanaka J. Long-term prognosis of patients with chronic hepatitis C who did not receive interferon-based therapy: Causes of death and analysis based on the FIB-4 index. *J Gastroenterol.* 2016; 51:380-389.
- Sterling RK, Lissen E, Clumeck N, Sola R, Correa MC, Montaner J, Sulkowski MS, Torriani FJ, Dieterich DT, Thomas DL. Development of a simple noninvasive index to predict significant fibrosis in patients with HIV/HCV coinfection. *Hepatology.* 2006; 43:1317-1325.
- Vallet-Pichard A, Mallet V, Nalpas B, Verkarre V, Nalpas A, Dhalluin-Venier V, Fontaine H, Pol S. FIB-4: An inexpensive and accurate marker of fibrosis in HCV infection. comparison with liver biopsy and fibrotest. *Hepatology.* 2007; 46:32-36.
- Shah AG, Lydecker A, Murray K, Tetri BN, Contos MJ, Sanyal AJ, Nash Clinical Research Network. Comparison of noninvasive markers of fibrosis in patients with nonalcoholic fatty liver disease. *Clin Gastroenterol Hepatol.* 2009; 7:1104-1112.
- Unalp-Arida A, Ruhl CE. Liver fibrosis scores predict liver disease mortality in the United States population. *Hepatology.* 2017; 66:84-95.
- Backus LI, Belperio PS, Shahoumian TA, Mole LA. Impact of sustained virologic response with direct-acting antiviral treatment on mortality in patients with advanced

- liver disease. *Hepatology*. 2017. doi: 10.1002/hep.29408.
22. Vergniol J, Boursier J, Coutzac C, Bertrais S, Foucher J, Angel C, Chermak F, Hubert IF, Merrouche W, Oberti F, de Ledinghen V, Cales P. Evolution of noninvasive tests of liver fibrosis is associated with prognosis in patients with chronic hepatitis C. *Hepatology*. 2014; 60:65-76.
 23. Castellares C, Barreiro P, Martin-Carbonero L, Labarga P, Vispo ME, Casado R, Galindo L, Garcia-Gasco P, Garcia-Samaniego J, Soriano V. Liver cirrhosis in HIV-infected patients: Prevalence, aetiology and clinical outcome. *J Viral Hepat*. 2008; 15:165-172.
 24. He N, Duan S, Ding Y, Rou K, Mcgoogan JM, Jia M, Yang Y, Wang J, Montaner JS, Wu Z. Antiretroviral therapy reduces HIV transmission in discordant couples in rural Yunnan, China. *Plos One*. 2013; 8:e77981.
 25. Jia Y, Sun J, Fan L, Song D, Tian S, Yang Y, Jia M, Lu L, Sun X, Zhang S. Estimates of HIV prevalence in a highly endemic area of China: Dehong Prefecture, Yunnan Province. *Int J Epidemiol*. 2008; 37:1287-1296.
 26. Mao Y, Wu ZY, Poundstone K, Wang CH, Qin QQ, Ma Y, Ma W. Development of a unified web-based national HIV/AIDS information system in China. *Int J Epidemiol*. 2010; 39:ii79-ii89.
 27. Vergniol J, Foucher J, Terrebonne E, Bernard PH, le Bail B, Merrouche W, Couzigou P, de Ledinghen V. Noninvasive tests for fibrosis and liver stiffness predict 5-year outcomes of patients with chronic hepatitis C. *Gastroenterology*. 2011; 140:1970-79, 1979. e1-3.
 28. Guéchet J, Serfaty L, Bonnand AM, Chazouillères O, Poupon RE, Poupon R. Prognostic value of serum hyaluronan in patients with compensated HCV cirrhosis. *J Hepatol*. 2000; 32:447-452.
 29. Ngo Y, Munteanu M, Messous D, Charlotte F, Imbertbismut F, Thabut D, Lebray P, Thibault V, Benhamou Y, Moussalli J. A prospective analysis of the prognostic value of biomarkers (FibroTest) in patients with chronic hepatitis C. *Clin Chem.* 2006; 52:1887-1896.
 30. Poynard T, Ngo Y, Perazzo H, Munteanu M, Lebray P, Moussalli J, Thabut D, Benhamou Y, Ratziu V. Prognostic value of liver fibrosis biomarkers: A meta-analysis. *Gastroenterol Hepatol (N Y)*. 2011; 7:445-454.
 31. Jain MK, Seremba E, Bhore R, Dao D, Joshi R, Attar N, Yuan HJ, Lee WM. Change in fibrosis score as a predictor of mortality among HIV-infected patients with viral hepatitis. *AIDS Patient Care STDS*. 2012; 26:73-80.
 32. Campa A, Martinez SS, Sherman KE, Greer JP, Li Y, Garcia S, Stewart T, Ibrahimou B, Williams OD, Baum MK. Cocaine use and liver disease are associated with all-cause mortality in the miami adult studies in HIV (MASH) Cohort. *J Drug Abuse*. 2016; 2. pii: 27.
 33. Berenguer J, Zamora FX, Aldamiz-Echevarria T, *et al*. Comparison of the prognostic value of liver biopsy and FIB-4 index in patients coinfecting with HIV and hepatitis C virus. *Clin Infect Dis*. 2015; 60:950-958.
 34. Mussini C, Lorenzini P, Puoti M, Lichtner M, Lapadula G, Di Giambenedetto S, Antinori A, Madeddu G, Cozzi-Lepri A, Monforte AD, De Luca A, Grp IFS. Prognostic value of the Fibrosis-4 index in human immunodeficiency virus type-1 infected patients initiating antiretroviral therapy with or without hepatitis C virus. *PloS One*. 2015; 10:e0140877.
 35. Achhra AC, Amin J, Law MG, Emery S, Gerstoft J, Gordin FM, Vjecha MJ, Neaton JD, Cooper DA, Grp IS, Grp ES, Grp SS. Immunodeficiency and the risk of serious clinical endpoints in a well studied cohort of treated HIV-infected patients. *AIDS*. 2010; 24:1877-1886.

(Received December 19, 2018; Revised January 27, 2019; Accepted January 30, 2019)

Effects of BENC-511, a novel PI3K inhibitor, on the proliferation and apoptosis of A549 human lung adenocarcinoma cells

Huiqin Tian^{1,2}, Yu Zhang¹, Qianyun Zhang¹, Shuixian Li¹, Yang Liu¹, Xiuzhen Han^{1,*}

¹Department of Pharmacology, School of Pharmaceutical Sciences, Shandong University, Jinan, Shandong, China;

²Department of Pharmacology, Shandong College of Traditional Chinese Medicine, Yantai, Shandong, China.

Summary

The small chemical compound 8-ethoxy-2-(4-fluorophenyl)-3-nitro-2H-chromene (S14161) was recently identified as an inhibitor of phosphoinositide 3-kinase (PI3K) and reported to inhibit tumor growth. However, its chiral structure and poor solubility prevent its further use. Compound 6-bromo-8-ethoxy-3-nitro-2H-chromene (BENC-511) is an analogue of S14161 produced by structural optimization. A previous study indicated that BENC-511 acted on multiple myeloma and that it had a toxicity by inhibiting the PI3K/protein kinase B (Akt) pathway. However, the effects of BENC-511 on the proliferation and apoptosis of A549 human lung adenocarcinoma cells have not been reported. The current study investigated the effects of BENC-511 on the proliferation and apoptosis of A549 cells *in vitro*. Results indicated that the compound BENC-511 inhibited the viability of A549 cells in a concentration- and time-dependent manner. BENC-511 suppressed proliferation and colony formation *via* S phase arrest. BENC-511 decreased the expression of cyclin A, proliferating cell nuclear antigen (PCNA), B-cell lymphoma-2 (Bcl-2), phospho-mammalian target of rapamycin (p-mTOR), and phospho-Akt (p-Akt) and it increased the expression of p21WAF1CIP1(p21), Caspase-3 and Caspase-9. In conclusion, BENC-511 inhibited the proliferation of A549 human lung adenocarcinoma cells *via* S phase arrest as a result of up-regulation of p21 and reduction of Cyclin A/cyclin-dependent kinase 2 (CDK2)/PCNA complex and it induced apoptosis by reducing the mitochondrial membrane potential *via* the Akt/Bcl-2/Caspase-9 mitochondrial pathway of apoptosis.

Keywords: BENC-511, proliferation, apoptosis, p21, Akt

1. Introduction

Lung cancer is a common malignancy; it is a leading cause of death worldwide and a threat to health and life. The morbidity and mortality of lung cancer have significantly increased over close to 50 years. The incidence of non-small cell lung cancer (NSCLC) has been increasing in recent years, and NSCLC has become the most common type of lung cancer. NSCLC includes squamous cell carcinoma, adenocarcinoma, and large cell carcinoma, and it readily metastasizes, and it readily causes drug resistance compared to small

cell carcinoma. NSCLC cells divide more slowly and spread relatively late. NSCLC accounts for about 80% of all lung cancer, about 75% of cases are identified in the middle-late stages, and its 5-year survival rate is very low (1).

The chemotherapy drugs that are commonly used to treat lung cancer, such as conventional cytotoxic drugs, mainly directly affect cell mitosis and the processes of DNA synthesis and repair. These drugs have a low selectivity and a high toxicity (2). Therefore, several key enzymes associated with tumor cell differentiation and proliferation have been screened as targets. Looking for inhibitors of these key enzyme is an important avenue for development of antitumor drugs today. Moreover, these small molecule inhibitors have better curative effects and cause fewer adverse reactions compared to conventional chemotherapy drugs.

Phosphatidylinositol 3-kinase (PI3K), a lipid

*Address correspondence to:

Dr. Xiuzhen Han, Department of Pharmacology, School of Pharmaceutical Sciences, Shandong University, 44 West Wenhua Road, Jinan 250012, China.

E-mail: xzyhan@sdu.edu.cn

kinase, is a key signaling molecule and is found in all types of cells. Through the recruitment and activation of protein kinase B (Akt), a serine kinase and a main downstream target, PI3K/Akt plays an important role in the processes of cell adhesion, proliferation, survival, differentiation, apoptosis, metabolism, and other many types of cellular processes. Studies have indicated that dysregulation of PI3K/Akt signaling pathway is closely related to tumor development (3). Aberrant activation of PI3K/Akt signaling has been firmly established as a major determinant for cell growth and survival in an array of cancers. Blocking aberrant activation of the PI3K/Akt signaling pathway provides a new strategy for targeted cancer therapy (4). Thus, inhibitors of this signaling pathway would be potential anticancer agents, and particularly for cancer cells surviving and growing largely as a result of aberrant activation of PI3K/Akt signaling.

The small molecule compound S14161, 8-ethoxy-2-(4-fluorinated phenyl)-3-hydrogen nitro-2-benzopyran, has been identified as an inhibitor of PI3K and can inhibit tumor growth. However, its chiral structure and poor solubility prevent its further use (5). In order to obtain better active compounds, a novel analogue of S14161 was designed through structural optimization. This compound, 6-bromo-8-ethoxy-3-nitro-2H-chromene (BENC-511), has potent antiproliferative activity (6). Preliminary experiments indicated that BENC-511 acted on multiple myeloma and prostate cancer and that it had a toxicity by inhibiting the PI3K/Akt pathway (7). However, the effects of BENC-511 on the proliferation and apoptosis of A549 human lung adenocarcinoma cells have not been reported. The current study investigated the effects of BENC-511 on the proliferation and apoptosis of A549 cells *in vitro*. Results indicated that BENC-511 inhibited the proliferation of A549 cells and induced apoptosis by S cell cycle arrest and by reducing the mitochondrial membrane potential. The details of this mechanism still need to be studied further.

2. Materials and Methods

2.1. Materials and Chemicals

S14161 and BENC-511 were synthesized by Zhaopeng Liu (Figure 1) (6). Annexin V-FITC and propidium iodide (PI) were purchased from BD Pharmingen (New Jersey, USA). 3-(4, 5-Dimethylthiazol-2-yl)-2, 5-diphenyltetrazolium bromide (MTT) was purchased from Sigma (Missouri, USA). Fetal bovine serum (FBS) was from Tianjin Biotechnology Development Center (Tianjin, China). Antibodies against Cyclin A, PCNA, p21, Caspase-3, Caspase-9, Bcl-2, Bcl-2 associated X protein (Bax), p-mTOR, mitogen-activated protein kinase (MAPK), and p-Akt (Ser473) were obtained from Cell Signaling Technologies (Danvers, MA, USA). Antibodies against β -actin were purchased from Abgent

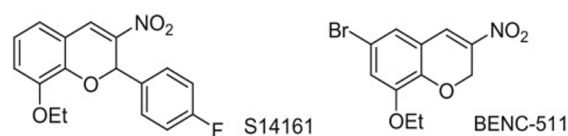


Figure 1. Chemical structure of S14161 and BENC-511.

(Suzhou, China). Horseradish peroxidase-conjugated secondary antibodies and FITC-labeled goat anti-rabbit immunoglobulin G (IgG) were purchased from Beyotime Institute of Biotechnology (Beijing, China). All other chemicals were purchased from Sigma.

2.2. Cell cultures

A549 human lung adenocarcinoma cells were purchased from the American Type Cell Culture (Manassas, Virginia, USA) and were cultured in RPMI-1640 medium supplemented with 10% heat-inactivated FBS, 100 U/mL of penicillin, and 100 μ g/mL of streptomycin at 37°C in a humidified atmosphere containing 5% CO₂. The cells were fed every 2-3 days and detached using 0.05 trypsin/0.02% EDTA once they reached 70-80% confluence. Cells were plated at an appropriate density according to each experimental design.

2.3. Cell proliferation assay

A549 cells were seeded in 96-well plates at a density of 4,000 cells per well. Twenty-four hours later, cells were incubated with S14161 or BENC-511 at concentrations of 5, 10, and 20 μ M for 24, 48, and 72 h respectively, and then cell viability was determined using an MTT assay. Cells were treated with MTT solution (final concentration, 0.5 mg/mL) for 4 h at 37°C. The supernatants were removed carefully, and then 100 μ L DMSO was added to each well to dissolve the precipitate. Absorbance was measured at 570 nm on a microplate reader (Synergy HT).

2.4. Cell morphological analysis

A549 cells were seeded at a density of 2.5×10^5 cells/well in a 6-well plate and grew overnight in a humidified incubator at 37°C with 5% CO₂. The next day, cells were incubated with/without BENC-511 (0.625, 1.25, 2.5, 5, and 10 μ M) for 48 h. After incubation, cell morphology was examined under an inverted microscope ($\times 200$, Olympus, Japan).

2.5. Colony formation

A549 cells were seeded in 6-well plates at a density of 500 cells per well. After cells adhered overnight, cells were left alone or incubated with BENC-511 (0.25, 0.5, 1, and 2 μ M) or S14161 (1 μ M) at 37°C for 24 h.

After incubation, cells were cultured with medium until colonies formed. After growing for 10-14 days, cells were fixed in methanol containing 1% methylene blue, and their morphology was examined under an inverted microscope ($\times 100$).

2.6. Cell cycle analysis

The cell cycle was analyzed *via* flow cytometric analysis after PI staining. A549 cells (5×10^4) were seeded in a dish and then incubated with BENC-511 (2.5, 5, and 10 μM) for 48 h. Cells were harvested, washed, and fixed in cold 70% ethanol overnight and then suspended in a 1 mL PI solution (50 $\mu\text{g}/\text{mL}$ DNase-free RNase A) for 30 min. The cell cycle was analyzed using a FACScan Flow Cytometer (Becton Dickinson, USA). The percentage of cells in the G0/G1, S, and G2/M phases was determined using the software ModFit LT 3.0 (Verity Software House, Topsham, USA).

2.7. Fluorescent staining of nuclei with H33258

A549 cells (5×10^4) were seeded in a dish and then incubated with BENC-511 (1.25, 2.5, 5, and 10 μM) or S14161 (10 μM) for 24 h. Cells were harvested and washed twice with PBS. Cells were then fixed with 3.7% paraformaldehyde for 10 min, washed twice with PBS, and incubated with 10 μM Hoechst 33258 in PBS at room temperature for 30 min. Cells were washed thrice and observed under a fluorescence microscope (IX-7, Olympus, Japan).

2.8. Detection of apoptosis with flow cytometry

FITC-Annexin V/PI double staining was performed as follows. A549 cells (5×10^4) were seeded in a dish and then incubated with BENC-511 (1.25, 2.5, 5, and 10 μM) or S14161 (10 μM) for 24 h. Cells were harvested and washed twice with PBS. Cells (1×10^6) were resuspended in binding buffer (10 mM HEPES/NaOH, pH 7.4, 140 mM NaCl, and 2.5 mM CaCl_2), and FITC-Annexin V and PI, at concentrations of 1 $\mu\text{g}/\text{mL}$, respectively, were added. The mixture was incubated at room temperature for 10 min in the dark, and then cellular fluorescence was measured using flow cytometry analysis performed with the FACScan Flow Cytometer (Becton Dickinson, USA).

2.9. Determination of the mitochondrial transmembrane potential

A JC-1 probe was used to determine the effect of BENC-511 on the mitochondrial transmembrane potential (MTP). Briefly, A549 cells were cultured in 6-well plates at a density of 2.5×10^5 cells /well and incubated with BENC-511 (1.25, 2.5, 5, and 10 μM) or S14161 (10 μM) for 48 h. Then cells were incubated with an equal volume

of JC-1 staining solution (5 $\mu\text{g}/\text{mL}$) at 37°C for 20 min in the dark and rinsed twice with ice-cold JC-1 staining buffer in accordance with the manufacturer's instructions. MTP was monitored by determining the relative amounts of mitochondrial JC-1 monomers (green fluorescence, meaning lower MTP) and aggregates (red fluorescence, meaning higher MTP) using a fluorescence microscope.

2.10. Western blotting

A549 cells were cultured in 6-well plates at a density of 3×10^5 cells/well and incubated with BENC-511 (2.5-20 μM) or S14161 (20 μM) for 48 h. After treatment, cells were collected and lysed with RIPA buffer on ice for 30 min. The suspension was centrifuged at 13,000 g for 15 min at 4°C, and the supernatant was collected. The protein concentration in the total cell lysate was measured using the BCA protein assay kit with bovine serum albumin (BSA) as a standard. Other supernatants were stored at -80°C until Western blotting.

After addition of the sample loading buffer, protein samples were separated using 10% sodium dodecyl sulfate-polyacrylamide gel electrophoresis (SDS-PAGE) and then transferred to polyvinylidene difluoride membranes (PVDF) (Millipore Corporation, Massachusetts, USA) in Tris-glycine buffer. The membranes were blocked with 5% (w/v) non-fat dry milk in 20 mM Tris-buffered saline containing 0.1% (v/v) Tween-20 (TBST) for 2 h. The membranes were incubated with the appropriate primary antibodies at 4°C overnight and then washed three times and exposed to HRP-conjugated secondary antibodies in TBST containing 5% non-fat dry milk for 1 h at room temperature. The primary antibodies included cyclin A, PCNA, p21, Caspase-3, Caspase-9, p-Akt, and β -actin. The membranes were washed again with TBST three times. Antigen-antibody bands were detected using an enhanced chemiluminescence reagent kit (Millipore, Massachusetts, USA) and quantified using densitometry performed with the ChemiDoc XRS+image analyzer (Bio-Rad, California, USA).

2.11. Statistical analyses

Data were analyzed using one-way ANOVA and are presented as the mean \pm S.E.M. A *p* value < 0.05 was considered statistically significant. All experiments were repeated at least three times. Statistical analysis was performed using the software SPSS/Win13.0 (SPSS, Inc., Chicago, IL).

3. Results

3.1. Effects of BENC-511 on the proliferation of A549 cells

To evaluate the effects of BENC-511 on A549 human

lung adenocarcinoma cells, cell proliferation was evaluated using an MTT assay. As shown in Figure 2A, exposure of A549 cells to BENC-511 and S14161 at the concentrations of 5, 10, and 20 μM for 24, 48, and 72 h resulted in decreased cell viability. Compared to S14161, 20 μM BENC-511 had a more potent anti-proliferative effect.

Cell morphology was examined under an inverted microscope after cells were treated with different concentrations of BENC-511 and S14161. As shown in Figure 2B, normal A549 cells had a uniform size and were epithelioid cells with adherent growth. Cells had a smooth cell wall and refracted light. The number of cells decreased gradually as the concentration of BENC-511 increased. Morphological changes in A549 cells were significant at BENC-511 concentrations of 1.25, 2.5, and 5 μM , cell density decreased significantly, cells gradually shrunk, and cells were round in shape; these aspects were concentration-dependent. Some of the cells incubated with 10 μM BENC-511 for 48 h died and floated.

To further confirm the effects of compound BENC-511 on cell proliferation, a colony formation assay was done. It also confirmed that compound BENC-511 inhibited the proliferation of A549 cells (Figure 2C). Compared to compound S14161, BENC-511 had a higher rate of inhibition.

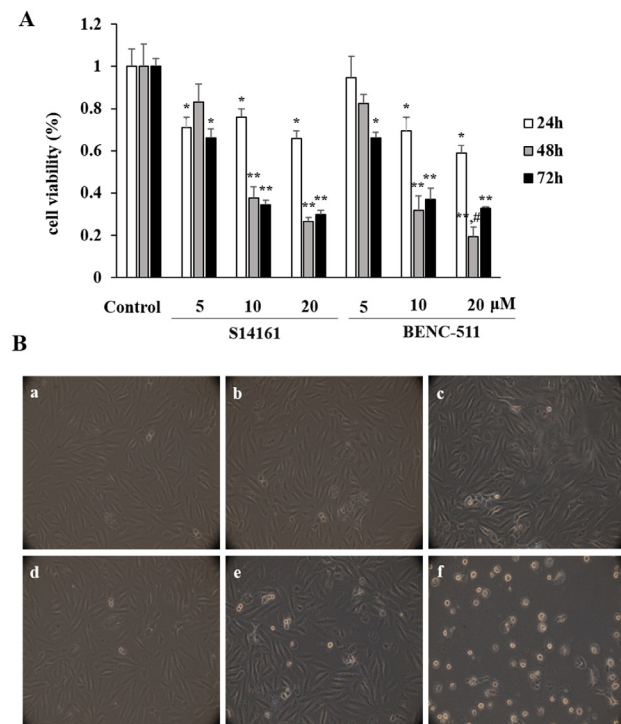


Figure 2. Effects of BENC-511 on cell growth. (A) Detection of cell viability. A549 cells were incubated with S14161 or BENC-511 at concentrations of 5, 10, and 20 μM for 24, 48, and 72 h respectively, and then cell viability was determined using an MTT assay. Three experiments were performed with six samples. Values are expressed as the mean \pm S.D. ($n = 6$). $*p < 0.05$, $**p < 0.01$ compared to the control group. $\#p < 0.05$ compared to S14161. (B) Determination of cell morphology. A549 cells were incubated without (a) or with 0.625 (b), 1.25 (c), 2.5 (d), 5 (e), or 10 μM (f) BENC-511 for 48 h. Cell morphology was assessed using an inverted microscope ($\times 200$) equipped with a quick imaging system. (C) Colony formation assay. A549 cells were seeded in each well and incubated without (a) or with 0.25 (b), 0.5 (c), 1 (d), or 2 μM (e) BENC-511 and with 1 μM S14161 (f) for 24 h. Cells were then transferred to normal medium for two weeks. The colony formation in each well was examined under an inverted microscope ($\times 100$). Values are expressed as the mean \pm S.D. ($n = 6$). $*p < 0.05$, $**p < 0.01$ compared to the control group. $\#p < 0.05$ compared to S14161.

3.2. Effects of BENC-511 on the cell cycle

The proportion of cells in the S phase increased markedly after incubation with BENC-511 (5 and 10 μM) 48 h. BENC-511 arrested the cell cycle in the S phase and prevented progression to the G2/M phase, and it inhibited cell mitosis and proliferation (Figure 3).

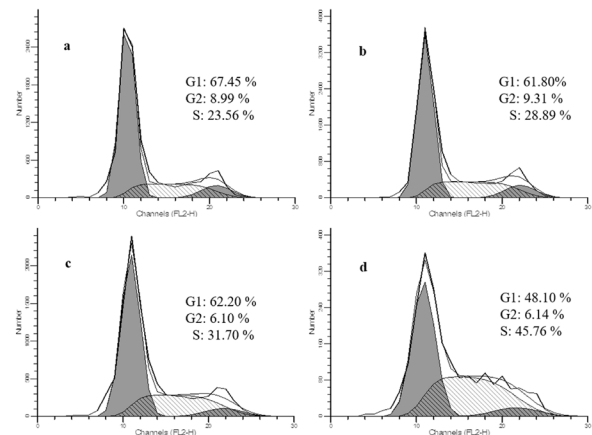


Figure 3. Cell cycle analysis. The cell cycle was analyzed using flow cytometric analysis after PI staining. A549 cells were seeded in a dish and then incubated without (a) or with 2.5 (b), 5 (c), or 10 μM (d) BENC-511 48 h. The cell cycle was analyzed using a FACScan Flow Cytometer.

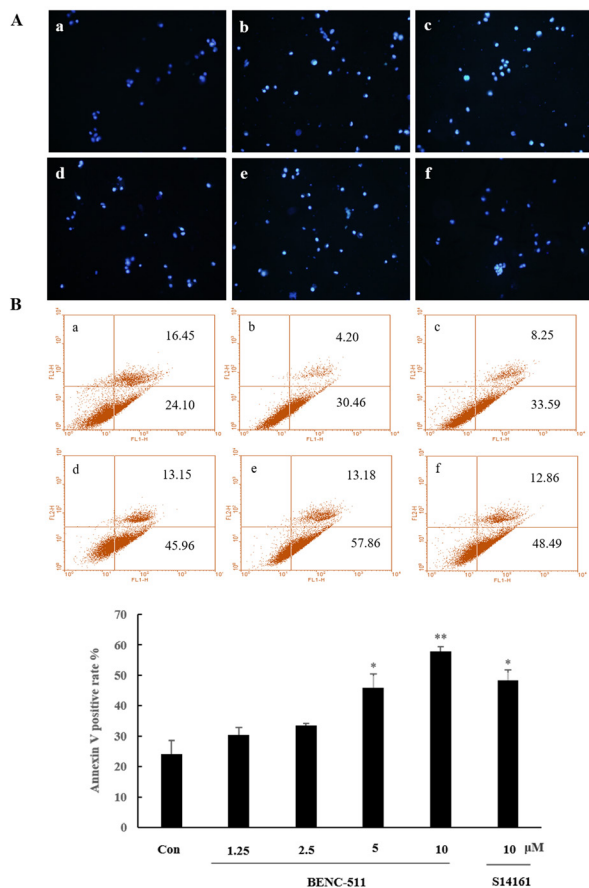


Figure 4. Detection of apoptosis. A549 cells were incubated without (a) or with 1.25 (b), 2.5 (c), 5 (d), or 10 μ M (e) BENC-511 and with 10 μ M S14161 (f) for 24 h. After incubation, the cells were harvested and stained to detect apoptosis. (A) Morphology of apoptotic A549 cells. The cells were then subjected to H33258 staining and viewed under a fluorescence microscope ($\times 200$). (B) FITC-Annexin V/PI double staining. The cells were then stained with FITC-Annexin V/PI and subjected to flow cytometric analysis. Bars represent the mean \pm S.D. (* $p < 0.05$, ** $p < 0.01$ compared to the control group)

3.3. Effects of BENC-511 on apoptosis

To determine the effects of BENC-511 on the apoptosis of A549 cells, cell morphology was examined after Hoechst 33258 staining. As shown in Figure 4A, cell nuclear morphology changed significantly, with heterogeneous intensity and chromatin condensation after cells were incubated with BENC-511. Normal cells had round-shaped nuclei with a homogeneous fluorescence intensity. Cell apoptosis was detected using flow cytometry. Results indicated that Annexin V-positive cells increased with an increase in the concentration of BENC-511 (1.25, 2.5, 5, and 10 μ M). Compared to S14161, 10 μ M BENC-511 induced more marked apoptosis of A549 cells (Figure 4B).

3.4. Effect of BENC-511 on MTP

Mitochondria-dependent apoptosis is related to mitochondrial depolarization. JC-1 is a dual-emission potential-sensitive probe that can be used to measure the mitochondrial membrane potential and assess the apoptosis of A549 cells. Normally, JC-1 accumulates in the mitochondrial matrix to form a polymer that emits intense red fluorescence. However, once cells die, JC-1 can only exist in monomeric form in the cytoplasm due to a decrease in or loss of the membrane potential, resulting in green fluorescence. Therefore, color changes in A549 cells are a very direct reflection of MTP. As shown in Figure 5, results indicated that after A549 cells were incubated with different concentrations of BENC-511 for 48 h, JC-1 fluorescence changed gradually from red to green. BENC-511 induced mitochondrial depolarization. Compared to S14161, BENC-511 induced more marked apoptosis of A549 cells. Results

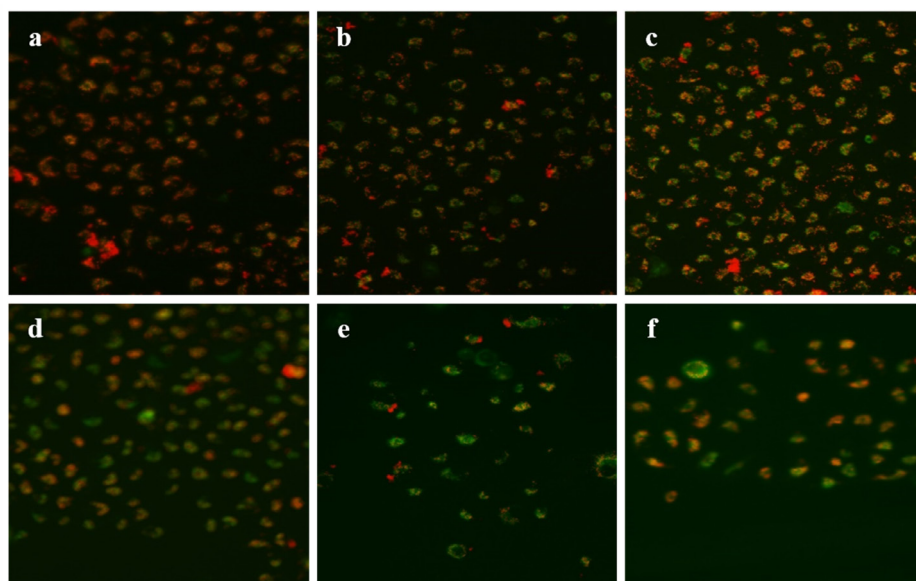


Figure 5. Effects of BENC-511 on MTP in A549 cells. A549 cells were incubated without (a) or with 1.25 (b), 2.5 (c), 5 (d), or 10 μ M (e) BENC-511 and with 10 μ M S14161 (f) for 48 h. MTP was monitored by determining the relative amounts of mitochondrial JC-1 monomers using a fluorescent microscope ($\times 200$).

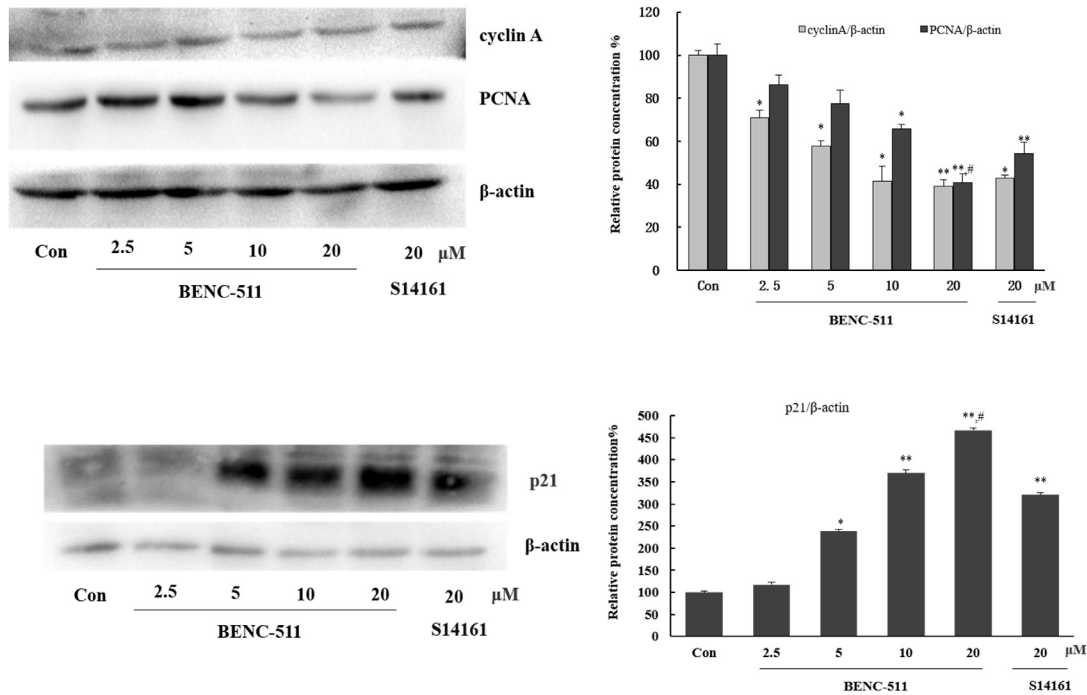


Figure 6. Effect of BENC-511 on expression of cyclin A, PCNA, and p21. A549 cells were incubated with BENC-511 (2.5, 5, 10, and 20 μ M) and S14161 (20 μ M) for 48 h. Cell extracts were subjected to Western blotting with specific antibodies. The expression of β -actin in cell lysates was used as an internal standard. Three experiments were performed. Data presented here are from one representative experiment. Bars represent the mean \pm S.D. (* p < 0.05, ** p < 0.01 compared to the control group, # p < 0.05 compared to S14161).

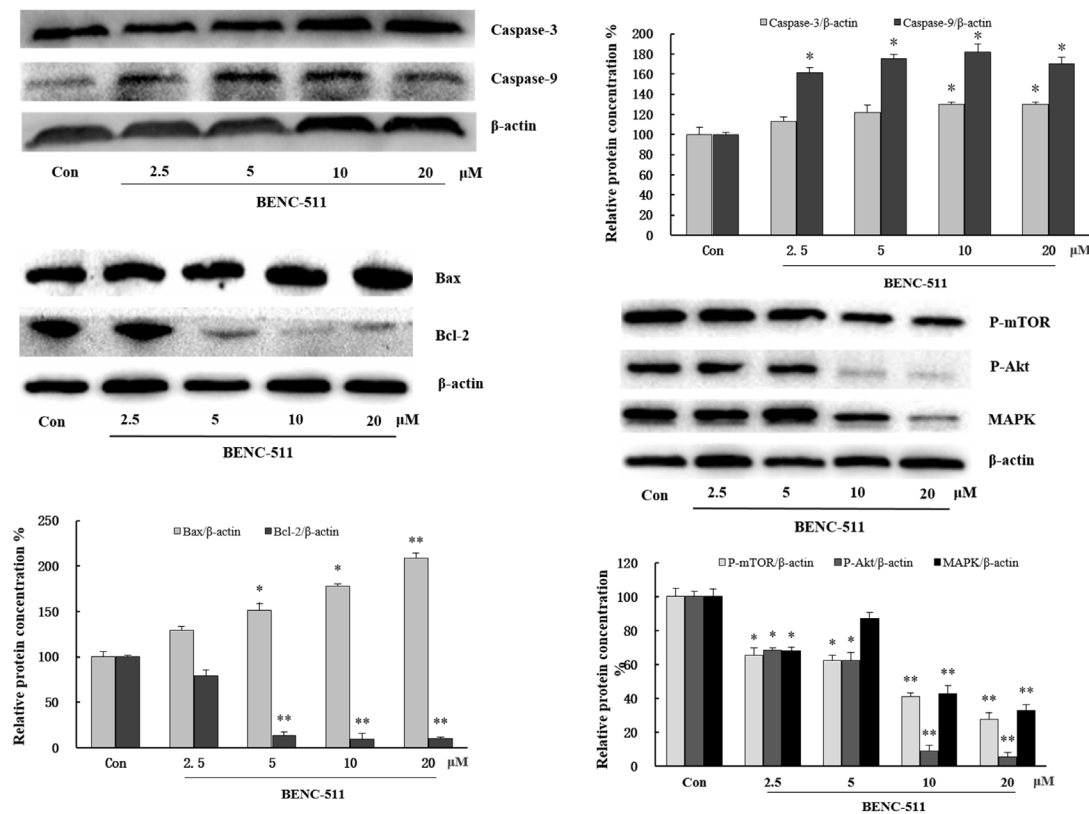


Figure 7. Effect of BENC-511 on expression of caspase-3, Bcl-2, p-mTOR, and P-Akt. A549 cells were incubated with BENC-511 (2.5, 5, 10, and 20 μ M) for 48 h. Cell extracts were subjected to Western blotting with specific antibodies. The expression of β -actin in cell lysates was used as an internal standard. Three experiments were performed. Data presented here are from one representative experiment. Bars represent the mean \pm S.D. (* p < 0.05, ** p < 0.01 compared to the control group, # p < 0.05 compared to S14161).

indicated that BENC-511 induced apoptosis and mitochondrial dysfunction *in vitro*.

3.5. Effects of BENC-511 on the expression of cyclin A, PCNA, p21, caspase-3, Bcl-2, and P-Akt

Western blotting indicated that 2.5-20 μM BENC-511 reduced the expression of cyclin A and PCNA and up-regulated p21 expression in A549 cells (Figure 6). Caspase-3 and Caspase-9 are key members of the Caspase family and are closely related to cell apoptosis. Activated Caspase-3 can split the substrate poly ADP ribose polymerase (PARP), which activates endonuclease and results in DNA degradation, nuclear membrane rupture, and chromatin condensation. The current results indicated that Caspase-3 and Caspase-9 expression increased after cells were incubated with different concentration of BENC-511 (5, 10, and 20 μM). Moreover, BENC-511 (5, 10, and 20 μM) decreased the expression of Bcl-2, p-Akt, p-mTOR, and MAPK and upregulated the expression of Bax (Figure 7). This suggested that BENC-511 may induce the apoptosis of A549 cells by inhibiting Akt *via* the Bcl-2/Caspase-9/Caspase-3 mitochondrial pathway of apoptosis.

4. Discussion

The proliferation and apoptosis of tumor cells are extremely complex processes involving many factors, proteases, and signaling pathways. A previous study indicated that the compound S14161 is a PI3K inhibitor and that it acts on multiple myeloma and other tumors. However, its chiral structure and poor solubility prevent its further use. In order to obtain better active compounds, six S14161 analogues were obtained through structural optimization. BENC-511 plays a more significant role in the inhibition of PI3K/Akt. A previous study indicated that BENC-511 has a certain inhibitory effect on a wide variety of tumor cells, though its mechanism of action differed in different cell lines. The current study has examined the effects of BENC-511 on the proliferation and apoptosis of A549 human lung adenocarcinoma cells *in vitro* and the mechanism of that action.

In vitro experiments indicated that BENC-511 was effective in inhibiting the proliferation of A549 cells. Cell viability decreased in a concentration- and time-dependent manner after cells were incubated with different concentrations of BENC-511. These results were consistent with inhibition of colony formation. BENC-511 significantly increased the proportion of A549 cells in the S phase and arrested the cell cycle in the S phase. Further experiments indicated that BENC-511 induced the apoptosis of A549 cells. Cell morphology changed significantly and cell density decreased significantly after incubation with BENC-511. Changes in the mitochondrial membrane potential were detected, and the gradual change in JC-1 from

red fluorescence to green fluorescence indicated that A549 cells were apoptotic after incubation with BENC-511. After incubation with different concentrations of BENC-511, the number of Annexin V-positive cells increased. Compared to S14161, 10 μM BENC-511 induced more marked cell apoptosis. The current study further explored the potential mechanism by which BENC-511 inhibited proliferation and induced apoptosis. Western blotting indicated that BENC-511 down-regulated the expression of cyclin A, PCNA, and p21 and up-regulated the expression of p21, Caspase-3, and Caspase-9 in A549 cells.

A tumor is a cell cycle disease, and once the cell cycle is dysregulated, the cells proliferate and divide indefinitely. Cyclins control cell cycle progression by regulating the activity of CDKs. Cyclin A is an important regulatory factor for G1/S and G2/M and dual control point for DNA replication and cell mitosis (8). Various cyclins promote the phosphorylation of pRb, Cdc6, and p107 through cyclin-CDK complexes. When Cyclin A is dissociated (not in a complex), the dephosphorylation of CDK substrates can occur, hampering these substrates from governing the processes of DNA synthesis and mitosis (9). PCNA is reported to be a marker of various tumors (10). PCNA can enhance the activity of DNA polymerase and DNA synthesis, and it plays an important role in progression from the G1 phase to the S phase (11).

P21 is located in the nucleus and consists of 164 amino acids. The amino terminus of p21 binds cyclins (amino acids 21-26) and CDK (amino acids 49-72), resulting in inhibition of the activity of cyclin-CDK complexes such as cyclin A-CDK2, cyclin D-CDK4/CDK6, and cyclin E-CDK2 (12). The carboxy terminus binds PCNA, causing DNA polymerase delta not to form a complex with PCNA or leading to a DNA holoenzyme that has trouble sliding along single-stranded DNA, thus affecting the replication of DNA (13,14). An important CDK inhibitor, p21 is undoubtedly a negative regulatory factor for the cell cycle. Several studies have indicated that a high level of p21 expression in tumor tissues can block normal cell cycle progression and suppress tumor development. A high level of p21 can hinder the kinase reaction, thus causing cell cycle arrest in the G1, G2, or S phase (15). The level of a cell cycle regulatory complex (the Cyclin A/CDK2/PCNA complex) plays a decisive role from the S phase to the G2/M phase. The current results indicated that BENC-511 inhibited the proliferation and induced the apoptosis of A549 human lung adenocarcinoma cells. BENC-511 arrested the S phase by down-regulating the expression of cyclin A and PCNA and up-regulating p21 expression. This may be related to a reduction in the level of the Cyclin A/CDK2/PCNA complex and expression of a high level of the cycle regulatory protein p21. Cell apoptosis involves multiple stages including depolarization of

the mitochondrial membrane potential, changes in permeability, the release of cytochrome c into the cytoplasm, condensed chromatin, and the formation of apoptotic bodies (16). There are two main types of pathways by which cell apoptosis occurs: mitochondria-mediated pathways of apoptosis and death receptor-mediated pathways of apoptosis. Stimuli such as ultraviolet radiation, heat stress, and DNA damage trigger mitochondrial apoptosis. Cell components can recognize this stimulus, signal the mitochondria, and increase the permeability of the mitochondrial outer membrane, releasing proteins in the mitochondria into the cytoplasm. The final executor of cell apoptosis are Caspases. Activated Caspase can cleave PARP, which activates endonuclease and results in DNA degradation, nuclear membrane rupture, chromatin condensation, and other typical characteristics of apoptosis. The activation of Caspase-9 is a key step in cell apoptosis that can initiate the Caspase cascade reaction and activate downstream caspase-3 to induce apoptosis. The current results indicated that BENC-511 decreased the mitochondrial membrane potential and the expression of Bcl-2 and it significantly increased the expression of Bax, Caspase-9, and Caspase-3 in the cytoplasm. This suggests that BENC-511 may induce the apoptosis of A549 cells by a mitochondrial pathway of apoptosis.

Studies of the relationship between lung adenocarcinoma and signaling pathways have identified a number of signaling pathways, such as Wnt/beta-catenin (17), Janus kinase/signal transducer and activator of transcription (JAK-STAT) (18) and PI3K/Akt/mTOR (19), and MAPKs (20). In recent years, several studies have reported that p21 and apoptosis are also closely related. p21 inhibits cell apoptosis. Upon DNA damage or other stressors, tumor suppressor p53 is activated, leading to transient expression of p21. This either triggers momentary G1 cell cycle arrest or leads to a chronic state of senescence or apoptosis. However, recent evidence suggests that p21 also acts as an oncogenic factor in a p53-deficient environment (21). The signaling pathways form complex signaling networks and interact with each other to influence the development of lung adenocarcinoma. The current results indicated that BENC-511 decreased the expression of P-Akt, p-mTOR, and MAPK and up-regulated p21 protein expression. This suggests that BENC-511 may induce the apoptosis of A549 cells by inhibiting Akt/mTOR *via* the Bcl-2/Caspase-9/Caspase-3 mitochondrial pathway of apoptosis.

In conclusion, the inhibition of A549 human lung cancer cells by BENC-511 is presumably related to additional signaling pathways and protein targets. Induction of apoptosis is very complex and involves many signaling pathways. Further study needs to be done to fully elucidate the mechanisms by which BENC-511 inhibited the proliferation and induced the apoptosis of A549 cells

Acknowledgements

This work was supported by grants from the Key Research and Development Program of Shandong Province (No. 2016GSF201152) and the Natural Science Foundation of Shandong Province (No. ZR2017MH028) of P. R. China. The authors wish to thank Prof. Zhaopeng Liu for providing the compounds S14161 and BENC-511.

References

- Zhang D, Ma Y, Liu Y, Liu ZP. Synthesis of sulfonylhydrazone- and acylhydrazone-substituted 8-ethoxy-3-nitro-2H-chromenes as potent antiproliferative and apoptosis inducing agents. *Arch Pharm (Weinheim)*. 2014; 347:576-588.
- Hwang KE, Kim HR. Response evaluation of chemotherapy for lung cancer. *Tuberc Respir Dis (Seoul)*. 2017; 80:136-142.
- Davis WJ, Lehmann PZ, Li W. Nuclear PI3K signaling in cell growth and tumorigenesis. *Front Cell Dev Biol*. 2015; 3:24.
- Mayer IA, Arteaga CL. The PI3K/AKT pathway as a target for cancer treatment. *Annu Rev Med*. 2016; 67:11-28.
- Shi M, Zhou X, Zhang Z, Wang M, Chen G, Han K, Cao B, Liu Z, Mao X. A novel PI3K inhibitor displays potent preclinical activity against an androgen-independent and PTEN-deficient prostate cancer model established from the cell line PC3. *Toxicol Lett*. 2014; 228:133-139.
- Han K, Xu X, Chen G, Zeng Y, Zhu J, Du X, Zhang Z, Cao B, Liu Z, Mao X. Identification of a promising PI3K inhibitor for the treatment of multiple myeloma through the structural optimization. *J Hematol Oncol*. 2014; 7:9.
- Yin SQ, Shi M, Kong TT, Zhang CM, Han K, Cao B, Zhang Z, Du X, Tang LQ, Mao X, Liu ZP. Preparation of S14161 and its analogues and the discovery of 6-bromo-8-ethoxy-3-nitro-2H-chromene as a more potent antitumor agent *in vitro*. *Bioorg Med Chem Lett*. 2013; 23:3314-3319.
- Oakes V, Wang W, Harrington B, Lee WJ, Beamish H, Chia KM, Pinder A, Goto H, Inagaki M, Pavey S, Gabrielli B. Cyclin A/Cdk2 regulates Cdh1 and claspin during late S/G2 phase of the cell cycle. *Cell Cycle*. 2014; 13:3302-3311.
- Wheeler LW, Lents NH, Baldassare JJ. Cyclin A-CDK activity during G1 phase impairs MCM chromatin loading and inhibits DNA synthesis in mammalian cells. *Cell Cycle*. 2008; 7:2179-2188.
- Lv Q, Zhang J, Yi Y, Huang Y, Wang Y, Wang Y, Zhang W. Proliferating cell nuclear antigen has an association with prognosis and risks factors of cancer patients: A systematic review. *Mol Neurobiol*. 2016; 53:6209-6217.
- Zhou Y, Hingorani MM. Impact of individual proliferating cell nuclear antigen-DNA contacts on clamp loading and function on DNA. *J Biol Chem*. 2012; 287:35370-35381.
- Kreis NN, Louwen F, Yuan J. Less understood issues: p21 (Cip1) in mitosis and its therapeutic potential. *Oncogene*. 2015; 34:1758-1767.
- Luo Y, Hurwitz J, Massagué J. Cell-cycle inhibition by independent CDK and PCNA binding domains in p21Cip1. *Nature*. 1995; 375:159-161.

14. Waga S, Hannon GJ, Beach D, Stillman B. The p21 inhibitor of cyclin-dependent kinases controls DNA replication by interaction with PCNA. *Nature*. 1994; 369:574-578.
15. Rousseau D, Cannella D, Boulaire J, Fitzgerald P, Fotedar A, Fotedar R. Growth inhibition by CDK-cyclin and PCNA binding domains of p21 occurs by distinct mechanisms and is regulated by ubiquitin-proteasome pathway. *Oncogene*. 1999; 18:4313-4325.
16. Deng J. How to unleash mitochondrial apoptotic blockades to kill cancers? *Acta Pharm Sin B*. 2017; 7:18-26.
17. Gao Y, Liu Z, Zhang X, He J, Pan Y, Hao F, Xie L, Li Q, Qiu X, Wang E. Inhibition of cytoplasmic GSK-3 β increases cisplatin resistance through activation of Wnt/ β -catenin signaling in A549/DDP cells. *Cancer Lett*. 2013; 336:231-239.
18. Liu RY, Zeng Y, Lei Z, Wang L, Yang H, Liu Z, Zhao J, Zhang HT. JAK/STAT3 signaling is required for TGF- β -induced epithelial-mesenchymal transition in lung cancer cells. *Int J Oncol*. 2014; 44:1643-1651.
19. Zhao R, Chen M, Jiang Z, Zhao F, Xi B, Zhang X, Fu H, Zhou K. Platycodin-D induced autophagy in non-small cell lung cancer cells *via* PI3K/Akt/mTOR and MAPK signaling pathways. *J Cancer*. 2015; 6:623-631.
20. Lin CC, Kuo CT, Cheng CY, Wu CY, Lee CW, Hsieh HL, Lee IT, Yang CM. IL-1 beta promotes A549 cell migration *via* MAPKs/AP-1- and NF-kappaB-dependent matrix metalloproteinase-9 expression. *Cell Signal*. 2009; 21:1652-1662.
21. Georgakilas AG, Martin OA, Bonner WM. p21: A two-faced genome guardian. *Trends Mol Med*. 2017; 23:310-319.

(Received January 13, 2019; Revised February 12, 2019; Accepted February 21, 2019)

By regulating miR-182-5p/*BCL10*/*CYCS*, sufentanil reduces the apoptosis of umbilical cord mesenchymal stem cells caused by ropivacaine

Lisha Li^{1,2,3}, Yan Sun^{1,2,3}, Na Zhang^{1,2,3}, Xuemin Qiu^{1,2,3}, Ling Wang^{1,2,3,*}, Qingyan Luo^{1,*}

¹ Obstetrics and Gynecology Hospital of Fudan University, Shanghai, China;

² The Academy of Integrative Medicine of Fudan University, Shanghai, China;

³ Shanghai Key Laboratory of Female Reproductive Endocrine-related Diseases, Shanghai, China.

Summary

Sufentanil is a type of opioid analgesic and is usually used to facilitate painless labor in combination with the local anesthetic ropivacaine. One aim of the current study was to investigate the effects of sufentanil and ropivacaine on umbilical cord mesenchymal stem cells (UCMSCs). A second aim of this study was to determine whether sufentanil attenuated the cytotoxicity of ropivacaine *in vitro*. UCMSCs were divided into 3 groups: one was treated with ropivacaine at a concentration of 50, 100, 200, or 400 µg/mL, another was treated with sufentanil at a concentration of 0.5, 5, 50, or 500 nmol/L, and a third was treated with a combination of ropivacaine at a concentration of 200 µg/mL and sufentanil at a concentration of 0.5, 5, 50, or 500 nmol/L. Results indicated that cell proliferation decreased in cells treated with ropivacaine while it increased in cells treated with sufentanil. In addition, sufentanil limited the inhibitory effect of ropivacaine on UCMSC growth in a dose- and time-dependent manner. Combined treatment with ropivacaine at a concentration of 200 µg/mL and sufentanil at a concentration of 500 nmol/L decreased the proportion of dead and apoptotic UCMSCs, and fewer cells were arrested in the S phase compared to cells treated with ropivacaine. Sufentanil inhibited the apoptosis induced by ropivacaine by increasing miR-182-5p, which regulated the expression of mRNA of the pro-apoptotic genes B-cell lymphoma/leukemia 10 (*BCL10*) and cytochrome c, somatic (*CYCS*). Sufentanil also increased the expression of mRNA of anti-apoptotic genes. In short, ropivacaine inhibits the cell viability and induces the apoptosis of UCMSCs *in vitro* while sufentanil attenuates this apoptosis by regulating miR-182-5p/*BCL10*/*CYCS*.

Keywords: Sufentanil, ropivacaine, umbilical cord mesenchymal stem cells, cell cycle arrest, apoptosis, miR-182-5p, BCL10, CYCS

1. Introduction

The pain of childbirth can cause a series of neuroendocrine

Released online in J-STAGE as advance publication February 17, 2019.

*Address correspondence to:

Dr. Qingyan Luo, Hospital and Institute of Obstetrics and Gynecology, Fudan University, 419 Fangxie Road, Shanghai 200011, China.

E-mail: wsqlyq@126.com

Dr. Ling Wang, Hospital and Institute of Obstetrics and Gynecology, Fudan University, 419 Fangxie Road, Shanghai 200011, China.

E-mail: Dr.wangling@fudan.edu.cn

responses, reduce the placenta blood flow, and cause vasoconstriction and acidosis; these adverse events negatively affect the fetus and mother. Effective labor analgesia can reduce the incidence of these adverse events, shorten the birth process, and reduce energy consumption and labor pains (1,2). Neuraxial anesthesia is considered to be the gold standard for the control of labor pain. Epidural analgesia is considered to be the most effective method of labor analgesia. It is ideal as analgesia and can also be used as anesthesia for a caesarean section in the event that a vaginal delivery is not possible; it also beneficial to the fetus because it increases blood flow through the placenta and it allows a pregnant woman to remain awake so that she can

cooperate with the physician (3,4).

Synergy between opioids and local anesthetics further increases the quality of analgesia and decreases the dose requirement of both local anesthetics and opioids (5). Ropivacaine, as a new local anesthetic, has little cardiac toxicity and no obvious effect on the blood flow of the uterus and placenta. It has a direct role on the nerve roots or spinal cord, it does not cause fetal respiratory inhibition, and it is an effective analgesic (6). Sufentanil is a strong opioid analgesic that is quick-acting, it has a short half-life of elimination, and it has little effect on hemodynamics (7). A combination of ropivacaine and sufentanil is a highly effective form of labor analgesia that can effectively relieve pain, shorten the course of labor, reduce postpartum hemorrhage, and reduce the need to perform a cesarean section (8). However, whether these drugs have an adverse effect on newborn's prognosis is not known.

On the one hand, anesthesia can inhibit the stress reaction caused by surgery and pain, but on the other hand it can also directly or indirectly affect cell function. In clinical settings, studies have found that drugs have no adverse effect on physical and mental development (9,10), but other studies with different concentrations of anesthetics have reported that residual levels of those drugs are detectable in the cord blood and breast milk (11).

Umbilical cord mesenchymal stem cells (UCMSCs) are multi-functional stem cells located in the umbilical cord tissue of the newborn. These cells can differentiate into a variety of tissue cells and they offer promise for their clinical use. In the process of pregnancy and childbirth, the umbilical cord plays an important role in metabolism; substances in the umbilical cord bloodstream play an important role in the function of the umbilical cord (12,13). The effects of sufentanil and ropivacaine on human UCMSCs alone or in combination is still not known.

The current study investigated the cytotoxicity of sufentanil and ropivacaine in UCMSCs alone or in combination, and this study also examined the functions of those drugs. Those findings were analyzed to determine if a combination of sufentanil and ropivacaine could serve as a potential form of anesthesia that reduces cell damage.

2. Materials and Methods

2.1. Cell culture

Human UCMSCs were purchased from the Shanghai Branch of the Chinese Academy of Science and cultured in Dulbecco's modified Eagle's medium (DMEM) containing 10% fetal bovine serum (FBS), 100 U/mL penicillin, and 100 mg/mL streptomycin at 37°C in a 5% CO₂ atmosphere.

2.2. Drug treatments

UCMSCs in the logarithmic growth phase were randomly divided into 4 groups: a blank control group (C), a group of cells treated with ropivacaine (Ro), a group of cells treated with sufentanil (Su), and a group of cells treated with a combination of ropivacaine and sufentanil (Ro + Su). Cells treated with ropivacaine were divided into 4 groups (Ro 50, Ro 100, Ro 200, and Ro 400) depending on the concentration of ropivacaine (50, 100, 200, and 400 µg/mL). Cells treated with sufentanil were divided into 4 groups (Su 0.5, Su 5, Su 50, and Su 500) depending on the concentration of sufentanil (0.5, 5, 50, and 500 nmol/L). Cells treated with a combination of ropivacaine and sufentanil were also divided into 4 groups treated with ropivacaine at a concentration of 200 µg/mL along with different concentrations of sufentanil (0.5, 5, 50, and 500 nmol/L) (Ro 200 + Su 0.5, Ro 200 + Su 5, Ro 200 + Su 50, and Ro 200 + Su 500).

2.3. Cell transfection

UCMSCs were seeded in 6-well plates overnight, treated with different drugs, and then transiently transfected with miR-182-5p inhibitors or mimics with Lipofectamine 2000 (Invitrogen, CA, USA). miR-182-5p mimics (mimics), an miR-182-5p-negative control (miR-NC), an anti-miR-182-5p inhibitor (anti-miR), and a negative control (anti-NC) were synthesized by GenePharma (Shanghai, China). The effects of gene silencing or overexpression were measured using real-time PCR 48 h after transfection.

2.4. Real-time cell analyzer (RTCA) system

The xCELLigence RTCA DP System (ACEA Biosciences, San Diego, California, USA) allows label-free and real-time monitoring of cellular processes, such as cell proliferation, cytotoxicity, adhesion, viability, invasion, and migration using electronic cell sensor array technology. The electrode impedance, displayed as cell index (CI) values, provides quantitative information about the biological status of cells, including their number, viability, and morphology. In brief, 50 µL of cell culture medium at room temperature was added into each well of the E-plate 16 of the xCELLigence RTCA DP System. The E-plate 16 was then connected and checked in the cell culture incubator for proper electrical contacts, and the background impedance was measured for 24 h. The UCMSCs were resuspended in cell culture medium and adjusted to 5,000 cells/well. The cell suspension (100 µL) was added to 50 µL of medium containing wells on the E-plate 16 in order to determine the optimum cell concentration. After incubation at room temperature for 30 min, the E-plate 16 was placed into the cell culture

incubator. Cell adhesion, growth, and proliferation were monitored every h for a period of up to 24 h *via* the incorporated sensor electrode arrays of the E-Plate 16. After 24 h, different concentrations of sufentanil or ropivacaine were added to 200 μ L of cell culture medium, and live cells were monitored every 15 min for a period of up to 96 h. The electrical impedance was measured using the RTCA-integrated software of the xCELLigence System as a dimensionless parameter termed CI.

2.5. RNA extraction and real-time RT-PCR

For PCR analysis, total RNA was isolated with an RNA extraction Kit (Axygen, CA, USA) according to the manufacturer's protocol. RNA purity and concentrations were measured with a NanoDrop 2000c (Thermo, Fisher, MA, USA). RNA (1 μ g) was transcribed into cDNA using reverse transcriptase (Promega, Madison, USA). Normalization controls for mRNA and miRNA were GAPDH and U6 RNA, respectively. Threshold cycle (Ct) values were calculated using the software supplied with the Applied Biosystems 7900 Real-time PCR system. Primer sequences and gene abbreviations are listed in Table 1.

2.6. Measurement of apoptosis

After treatment with ropivacaine at a concentration of 200 μ g/mL, sufentanil at a concentration of 500 nmol/L, or a combination of the two, apoptotic cells were identified using the Annexin V-FITC Apoptosis Detection Kit according to the manufacturer's instructions. UCMSCs were treated with different drugs for 48 h, about 1×10^6 cells from each group were stained with Annexin V-FITC for 30 min at 40C in the dark, cells were stained with propidium iodide for 10 min, and then cells were analyzed with a CyAN ADP flow cytometer (Beckman Coulter, Brea, CA, USA). Each sample was examined twice.

2.7. Cell cycle analysis

Briefly, UCMSCs were treated with ropivacaine at a

concentration of 200 μ g/mL, sufentanil at a concentration of 500 nmol/L, or a combination of the two for 48 h, washed twice with ice-cold PBS, treated with trypsin, and finally fixed in cold 70% ethanol for 30 min at 4°C. The following procedures were carried out in accordance with the manufacturer's instructions for the Cell Cycle and Apoptosis Analysis Kit. Flow cytometry was used to analyze the treated cells.

2.8. Real-time PCR arrays

Each PCR array was a 384-well plate containing gene-specific optimized real-time PCR primer sets for 84 genes related to the induction and inhibition of apoptosis. The PCR array includes primer pairs to quantify RNA18s as a positive control (an invariant highly expressed endogenous control) and genomic DNA as a negative control to detect the presence of genomic DNA contamination. Gene expression profiles were analyzed according to the manufacture's protocol (Wegene Biotech, Shanghai, China), and data was analyzed using software from Wegene Biotech. Genes with fold-changes more than or less than 2.0 were considered to have biological significance.

2.9. Statistical analysis

Each experiment was performed in sextuplicate and repeated at least three times to ensure replicability. Results were analyzed *via* one-way analysis of variance (ANOVA) using the software GraphPad Prism (version 5.0, GraphPad Software, La Jolla, CA, USA), followed by Dunnett's *t*-test. $P < 0.05$ was considered to be significant.

3. Results

3.1. Sufentanil limited the inhibitory effect of ropivacaine on UCMSC growth in a time- and concentration-dependent manner

This study examined the effects of ropivacaine and sufentanil on the growth of UCMSCs. UCMSCs were treated with different concentrations of ropivacaine,

Table 1. The primers used in the study

Gene	Forward Primer	Reverse Primer
<i>miR-182-5p</i>	TGCGGTTTGGCAATGGTAGAAC	CCAGTGCAGGGTCCGAGGT
<i>BCL10</i>	GGAGTGTGAGCCACCTAAG	CTGGGCGATAGAGCAAGAC
<i>CYCS</i>	AAGGCATCACCTGGGGAGAG	ACAGAAACATTCCATCAGCCAT
<i>U6</i>	CTCGCTTCGGCAGCACA	AACGCTTCACGAATTTGCGT
<i>GAPDH</i>	AATCCCATCACCATCTTC	AGGCTGTTGTCATACTTC

Abbreviations: *APAF1*: apoptotic peptidase-activating factor 1; *BAK1*: Bcl-2 homologous antagonist/killer; *BCL2L2*: BCL2-like protein 2; *BCL10*: B-cell CLL/lymphoma 10; *BID*: BH3-interacting domain death agonist; *BIRC3*: Baculoviral IAP repeat-containing protein 3; *BNIP3*: BCL2-interacting protein 3; *CFLAR*: CASP8 and FADD-like apoptosis regulator; *CYCS*: cytochrome c, somatic; *FADD*: Fas-associated protein with a novel death domain; *IGF1R*: insulin-like growth factor 1 receptor; *NOD1*: nucleotide-binding oligomerization domain-containing protein 1; *TNFRSF9*: tumor necrosis factor receptor superfamily member 9; *TNFRSF11B*: TNF receptor superfamily member 11b; *TNFRSF21*: TNF receptor superfamily member 21; *TP53BP2*: tumor protein p53-binding protein 2; *TRAF3*: TNF receptor-associated factor 3

sufentanil, or a combination of the two, and then the xCELLigence RTCA DP System was used to monitor cell proliferation in real time. Ropivacaine was found to inhibit the proliferation of UCMSCs (Figure 1A) while sufentanil promoted the proliferation of UCMSCs (Figure 1B). Sufentanil markedly limited the inhibitory effect of ropivacaine on UCMSC growth in a time- and concentration-dependent manner in the cells treated

with a combination of ropivacaine and sufentanil (Figure 1C).

3.2. Sufentanil inhibited the apoptosis of UCMSCs caused by ropivacaine and it influenced the cell cycle

To determine whether ropivacaine or sufentanil would induce the proliferation of UCMSCs, whether the drugs

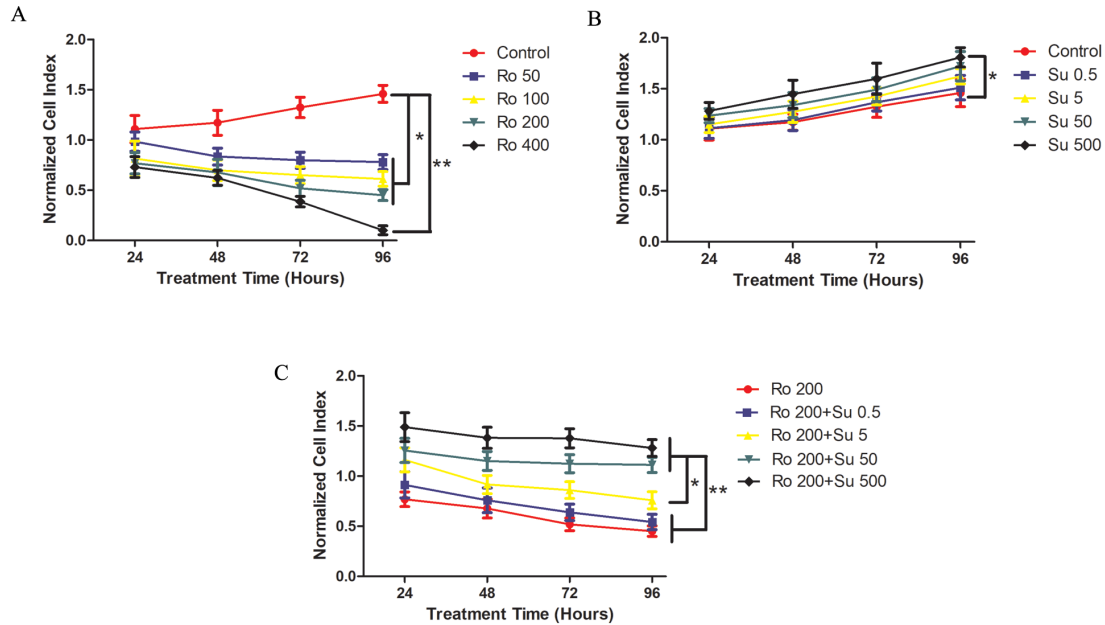


Figure 1. Effect of different concentrations of ropivacaine or sufentanil or a combination of the two on cell proliferation of cultured UCMSCs after treatment for 24, 48, 72, or 96 h. (A) Ropivacaine inhibited the proliferation of UCMSCs in a time- and concentration-dependent manner. (B) Sufentanil promoted the proliferation of UCMSCs in a time- and concentration-dependent manner. (C) Sufentanil limited the inhibitory effect of ropivacaine on UCMSC growth in a time- and concentration-dependent manner. $*p < 0.05$. All results are expressed as the mean \pm SEM, and data are representative of at least three experiments.

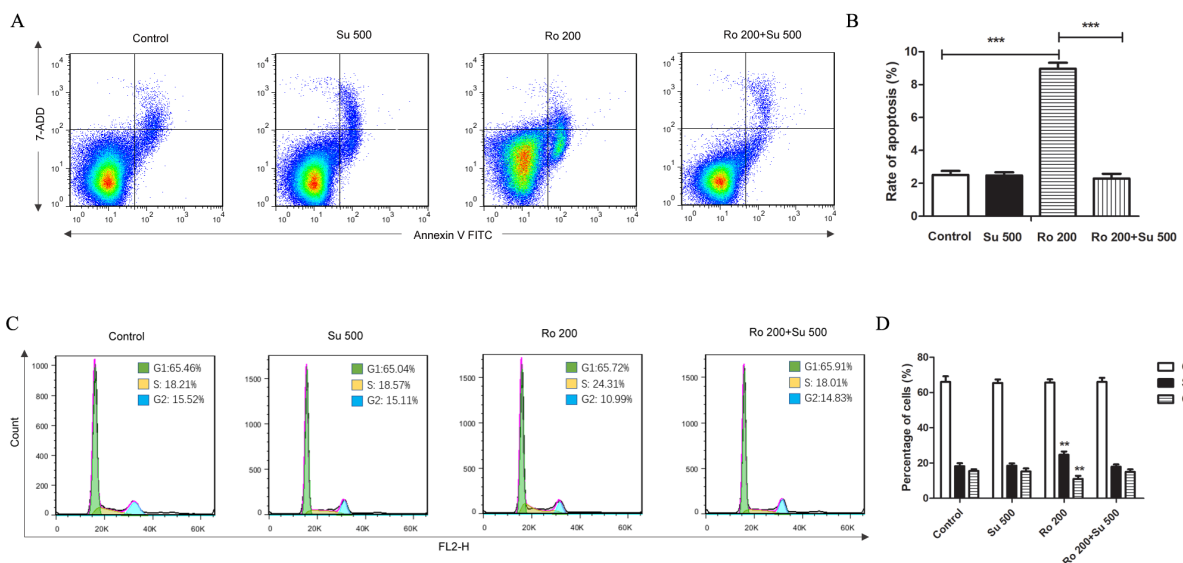


Figure 2. Effect of ropivacaine, sufentanil, or a combination of the two on cell apoptosis and the cell cycle of cultured UCMSCs after treatment for 48 h. (A) Flow cytometry dot plots indicating the binding of Annexin V-FITC (FL-1) and PI uptake (FL-3) of UCMSCs treated with different drugs for 48 h. (B) Rates of apoptotic cells as shown in A. (C) Cell cycle analysis of UCMSCs treated with different drugs for 48 h. The G1, S, and G2 phases are displayed in three different colors in each chart. (D) The percentage of UCMSCs in the G1, S, and G2 phases as shown in (C). $*p < 0.05$. All results are expressed as the mean \pm SEM, and data are representative of at least three experiments.

would affect the apoptosis of those cells was determined. As shown in Figure 2A and 2B, the percentage of apoptotic cells increased in cells treated with ropivacaine at a concentration of 200 µg/mL while treatment with sufentanil at a concentration of 500 nmol/L did not affect apoptosis. A combination of the two drugs decreased the apoptosis of UCMSCs in comparison to cells treated with ropivacaine. Flow cytometry was used to determine whether the promotion of UCMSC proliferation by sufentanil was mediated, at least in part, by affecting cell cycle progression. As shown in Figure 2C and 2D, treatment with ropivacaine at a concentration of 200 µg/mL significantly increased the percentage of UCMSCs in the S phase and decreased the percentage in the G2 phase in comparison to the control group and the cells treated with sufentanil at a concentration of 500 nmol/L. In contrast, treatment with a combination of ropivacaine and sufentanil decreased the number of cells in the S phase and increased the number in the G2 phase compared to cells treated with ropivacaine. These findings indicated that ropivacaine arrested the cell cycle in the S phase and that sufentanil halted that arrest, suggesting that sufentanil modulates the inhibition of cell proliferation by ropivacaine by modulating the S phase of the cell cycle.

3.3. Sufentanil attenuated ropivacaine cytotoxicity by regulating apoptosis-related genes

PCR arrays were used to study the expression of 84 key genes involved in programmed cell death. These 84 genes included those that induced apoptosis, those that inhibited apoptosis, and those that coded for death domain proteins, caspases, and regulators (Figure 3A). Treatment with ropivacaine at a concentration of 200 µg/mL was found to significantly increase the expression of mRNA of most pro-apoptotic genes such as *BCL10*, *CYCS*, *FADD*, and the caspase family (Figure 3B) while treatment with sufentanil at a concentration of 500 nmol/L mainly decreased the expression of mRNA of pro-apoptotic genes and increased the expression of mRNA of anti-apoptotic genes such as *BIRC3*, *BNIP3*, and *BNIP3L* (Figure 3C). Combined treatment with ropivacaine and sufentanil attenuated apoptosis caused by ropivacaine by markedly decreasing the expression of mRNA of pro-apoptotic genes such as *BAK1*, *BCL10*, *CASP1*, *CASP4*, *CYCS*, and *FADD* and by increasing the expression of mRNA of anti-apoptotic genes such as *BIRC3* and *BNIP3* (Figure 3D).

3.4. MiR-182-5p participated in regulating cell proliferation induced by sufentanil and ropivacaine

Based on the apoptosis-regulating genes expressed in cells treated with a combination of ropivacaine and sufentanil, several micro-RNAs that may participate in modulating apoptosis were identified. Results indicated

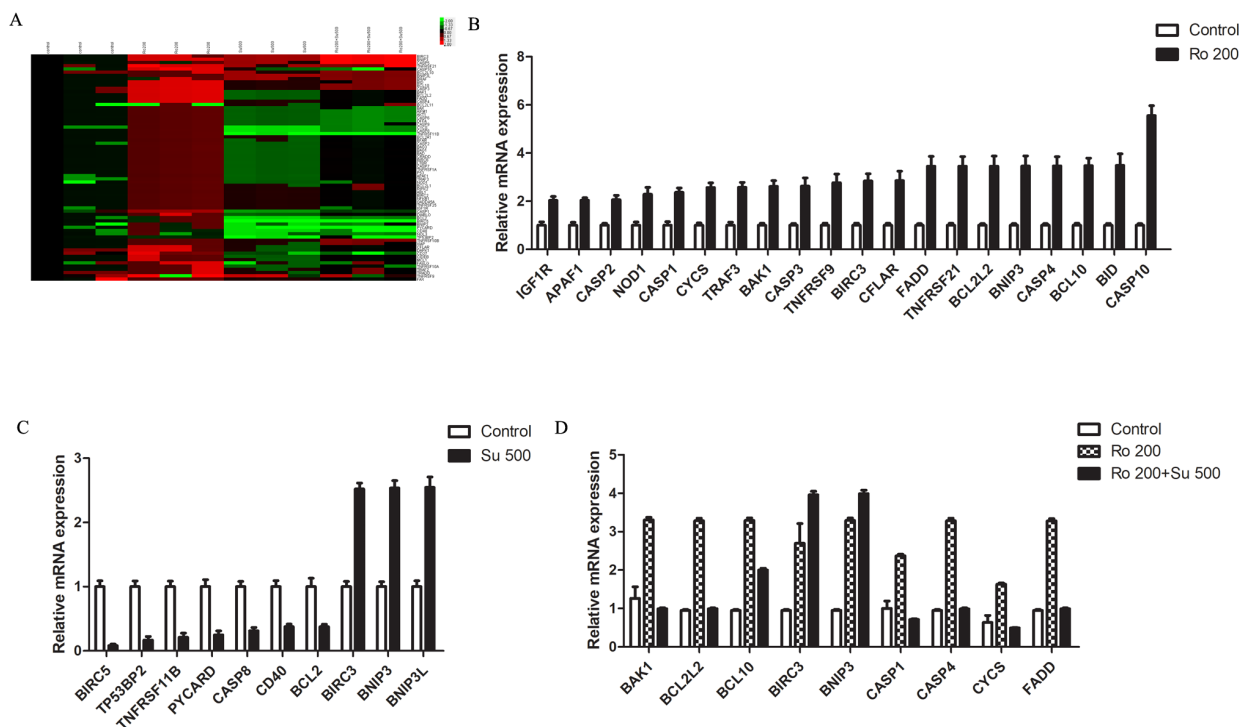


Figure 3. Sufentanil attenuated ropivacaine cytotoxicity by regulating apoptosis-related genes. (A) Eighty-four apoptosis-related genes were analyzed using a PCR array. (B) The levels of expression of mRNA of apoptosis-related genes increased as a result of treatment with ropivacaine at a concentration of 200 µg/mL. (C) The levels of expression of mRNA of apoptosis-related genes were modulated by sufentanil at a concentration of 500 nmol/L. (D) The levels of expression of mRNA of pro-apoptotic and anti-apoptotic genes were modulated by ropivacaine and altered by a combination of ropivacaine and sufentanil. Significance is indicated in all of the bar graphs with **p* < 0.05. All results are expressed as the mean ± SEM, and data are representative of at least three experiments.

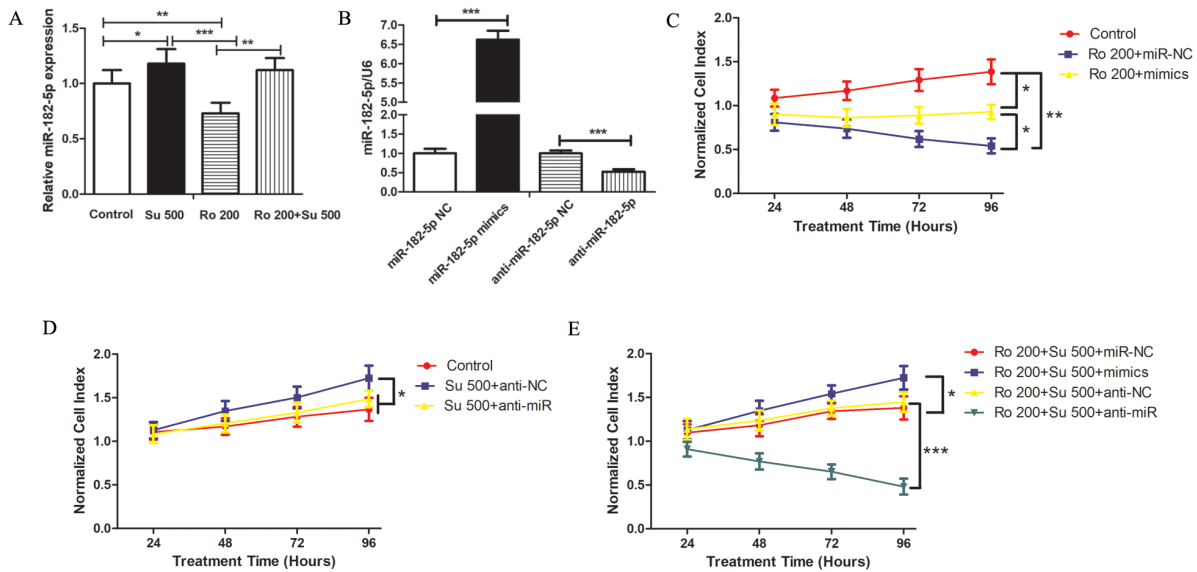


Figure 4. Sufentanil or ropivacaine modulated miR-182-5p expression to regulate cell proliferation (A) The levels of expression of miR-182-5p mRNA in each treatment group after treatment for 48 h. **(B)** The levels of expression of miR-182-5p mRNA in UCMSCs 48 h after transfection with miR-182-5p mimics, inhibitors, or a negative control (NC). **(C)** MiR-182-5p mimics attenuated the inhibition of cell proliferation by ropivacaine. **(D)** MiR-182-5p inhibitors attenuated the promotion of cell proliferation by sufentanil. **(E)** MiR-182-5p mimics improved cell proliferation while inhibitors attenuated cell proliferation in cells treated with a combination of ropivacaine and sufentanil. * $p < 0.05$. All results are expressed as the mean \pm SEM, and data are representative of at least three experiments.

that treatment with sufentanil at a concentration of 500 nmol/L increased the level of miR-182-5p which had decreased as a result of treatment with ropivacaine at a concentration of 200 μ g/mL (Figure 4A). miR-182-5p mimics or miR-182-5p inhibitors (Figure 4B) were used to determine cell proliferation in response to treatment with different drugs. Transfection with miR-182-5p mimics was found to improve cell proliferation in cells treated with ropivacaine at a concentration of 200 μ g/mL (Figure 4C) and cells treated with a combination of ropivacaine and sufentanil (Figure 4E), while transfection with miR-182-5p inhibitors was found to attenuate cell proliferation in cells treated with sufentanil at a concentration of 500 nmol/L (Figure 4D) and cells treated with a combination of ropivacaine and sufentanil (Figure 4E).

3.5. Sufentanil modulated miR-182-5p to inhibit apoptosis caused by ropivacaine by targeting *BCL10* and *CYCS*

To look for the target genes of miR-182-5p in cells rendered apoptotic by drug treatment, online prediction software (TargetScan 7.0 and miRBase) was used to search for the most likely target genes. Results indicated that *BCL2*, *BCL10*, and *CYCS* were the likely target genes of miR-182-5p (Figure 5A). Since *BCL2* is a proven target of miR-182-5p, the current results verified that *BCL2* increased in cells treated with sufentanil at a concentration of 500 nmol/L and transfected with inhibitors (Figure 5C). Expression of *BCL10* and *CYCS* mRNA decreased in cells treated with

ropivacaine at a concentration of 200 μ g/mL (Figure 5B) and cells treated with a combination of ropivacaine and sufentanil (Figure 5D) while it increased in cells treated with sufentanil at a concentration of 500 nmol/L (Figure 5C) and cells treated with a combination of ropivacaine and sufentanil (Figure 5D). miR-182-5p mimics were found to attenuate apoptosis induced by ropivacaine while miR-182-5p inhibitors increased the percentage of apoptotic cells (Figure 5E).

4. Discussion

The current results indicated that treatment with ropivacaine alone induced cytotoxicity in UCMSCs by inhibiting proliferation, impacting the cell cycle, and promoting apoptosis, while treatment with sufentanil had the opposite effect. A combination of ropivacaine and sufentanil attenuated that cytotoxicity by modulating apoptosis-related genes. Several studies on use of a combination of ropivacaine and sufentanil to facilitate painless labor or a cesarean section have found no abnormalities in the clinical assessment of the fetus, liver function, renal function, or routine blood results, but the possible effects of a small amount of the drugs on the newborn over the long-term remain unclear. The current results warrant re-examination of the effects of supplementing narcotics with local anesthetics for labor analgesia.

The current study involved real-time detection of cell proliferation, and results indicated that cell viability decreased markedly as the concentration of ropivacaine increased. However, treatment with

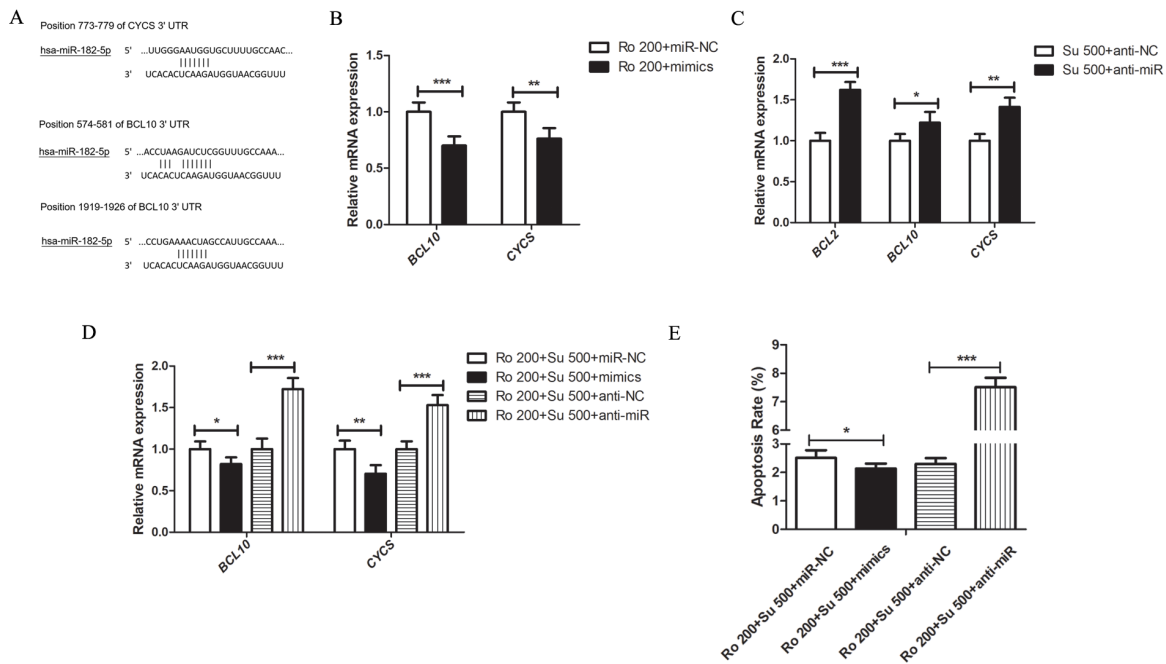


Figure 5. MiR-182-5p improved cell survival and suppressed cell apoptosis by targeting *BCL10* and *CYCS* expression. (A) *BCL10* and *CYCS* were predicted to be target genes of miR-182-5p. (B) The levels of expression of *BCL10* and *CYCS* mRNA decreased in cells treated with ropivacaine after transfection with miR-182-5p mimics (C) The levels of expression of *BCL2*, *BCL10*, and *CYCS* mRNA increased in cells treated with sufentanil after transfection with miR-182-5p inhibitors. (D) MiR-182-5p mimics decreased the levels of expression of *BCL10* and *CYCS* mRNA while inhibitors increased those levels in cells treated with a combination of ropivacaine and sufentanil. (E) MiR-182-5p mimics inhibited apoptosis while inhibitors increased apoptosis in cells treated with a combination of ropivacaine and sufentanil. * $p < 0.05$. All results are expressed as the mean \pm SEM, and data are representative of at least three experiments.

an increasing concentration of sufentanil alone or in combination improved cell viability. In clinical studies, ropivacaine has a low toxicity when administered at a low concentration to provide a motor and sensory nerve block, but adverse reactions to ropivacaine have also been reported (14,15). Many studies have indicated that sufentanil inhibits the growth of cancer cells such as human breast cancer cells or colon and pancreatic cancer cells *in vitro* (16,17). Cord blood contains hematopoietic stem cells that can restore the human hematopoietic and immune systems. Sufentanil may improve cell viability by protecting cell or organ development when a residual amount of the drug enters the bloodstream of a fetus or baby through the umbilical cord or breastfeeding (18).

Apoptosis is an active process of intracellular programmed death that is caused by physiological and pathological changes to remove redundant and damaged cells (19). In the current study, UCMSCs were increasingly arrested in the S phase and displayed more apoptotic characteristics as the concentration of ropivacaine increased. In the tumor microenvironment, sufentanil attenuates cytotoxicity by inhibiting connexin 43-composed gap junction function in the treatment of colorectal cancer (20). Ropivacaine reversibly reduced the permeability of the nerve fiber membrane to sodium ions, it slowed the speed of depolarization, and it alleviated stress (21). Peroxides, DNA damage,

and calcium homeostasis may induce neuron apoptosis, and mitochondrial dysfunction may activate metabolic changes related to apoptosis (22). According to the PCR array of apoptosis-related genes, ropivacaine modulated apoptosis by significantly increasing the expression of mRNA of apoptosis-related genes. This included genes that positively regulate apoptosis such as *BAK1*, *BID*, *BNIP3*, and *CYCS*, the death domain receptors *FADD*, *NOD1*, and *TNFRSF9*, the death domain proteins *TNFRSF21* and *TRAF3*, a gene that negatively regulates apoptosis such as *BCL10*, and the FADD-like apoptosis regulator *CFLAR*. Caspases can be divided into initiators such as *CASP2*, *CASP8*, *CASP9*, and *CASP10*, and effectors such as *CASP3*, *CASP6*, and *CASP7*. *CASP1* and *CASP4* are inflammatory caspases that cleave other proteins, such as the precursors of interleukins, and thus indirectly induce apoptosis (23-25). Ropivacaine modulated caspases such as *CASP2*, *CASP3*, *CASP4* and *CASP10* and caspase activators such as *APAF1* and *CASP1* to induce apoptosis. It also increased anti-apoptotic genes such as *IGF1R*, *BIRC3*, and *BCL2L2*. Sufentanil inhibited apoptosis mainly by decreasing the expression of mRNA of pro-apoptotic genes such as *TP53BP2*, *TNFRSF11B*, and *CD40* and by increasing the expression of mRNA of anti-apoptotic genes such as *BIRC3* and *BNIP3*. In combination, sufentanil may inhibit the expression of mRNA of pro-apoptotic genes and promote the expression of

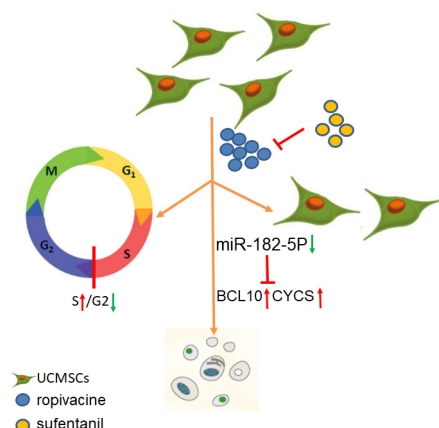


Figure 6. Schematic diagram of sufentanil reducing the apoptosis of UCMSCs caused by ropivacaine. Ropivacaine induced cytotoxicity in UCMSCs by inhibiting their proliferation, impacting the cell cycle, and promoting their apoptosis. Sufentanil improved cell viability and inhibited the apoptotic effects of ropivacaine by increasing miR-182-5p expression, which targeted the pro-apoptotic genes *BCL10* and *CYCS*.

mRNA of anti-apoptotic genes induced by ropivacaine, even though these genes were not affected in cells treated with sufentanil. This may be due to drug interactions that lead to modulation *via* different signaling pathways. Sufentanil may provide protection from myocardial ischemia *via* the PI3K/Akt-GSK-3 β pathway by modulating antiapoptotic proteins (26), and ropivacaine may be a potential treatment for OA by down-regulating the calcineurin/NFAT1 signaling pathway (27). However, the specific mechanism of action of these drugs need to be explored in a future study.

Studies have increasingly indicated that miRNAs play a key role in regulating gene expression during disease progression (28). miR-182-5p has been reported to modulate cell function in many cancers. Inhibiting miR-182-5p by regulating CASP9 expression has a pro-apoptotic and anti-proliferative effect in human breast cancer (29). miR-182-5p promotes cell proliferation and metastasis and it inhibits apoptosis by knocking down RECK and Smad4 in bladder cancer (30), and it promotes the progression of hepatocellular carcinoma by suppressing FOXO3a expression (31). *BCL2* is known to be an anti-apoptotic gene in tumors (32), and miR-182-5p regulates *BCL2L12* and *BCL2* expression in acute myeloid leukemia (33). However, its role as a suppressive miRNA is not clear and needs to be studied. *BCL10* is an apoptotic regulatory molecule that is an antigen receptor-specific regulator of NF- κ B, which is closely associated with the immune response (34). Cytochrome *c* (*Cyt c*), a heme-containing mitochondrial protein, has a critical function in both respiration and apoptosis. During apoptosis, cytochrome is released into the cytosol, where it subsequently participates in the process leading to caspase-9 and caspase-3 activation (35). The current results indicated that miR-182-5p

expression was regulated in UCMSCs by sufentanil or ropivacaine treatment, and that miR-182-5p improved cell survival and suppressed cell apoptosis by targeting *BCL10* and *CYCS* expression. Those drugs may play an anti-apoptotic role by regulating mitochondrial metabolism and the immune response *via* miR-182-5p.

Sufentanil improved cell viability and inhibited the apoptotic effects of ropivacaine by increasing miR-182-5p expression, which targeted the pro-apoptotic genes *BCL10* and *CYCS* in UCMSCs (Figure 6). Further studies are needed to determine the exact mechanisms for those actions. Findings from those studies could lay the foundation for combined use of those drugs in painless labor.

Acknowledgements

This work was supported by grants from the National Natural Science Foundation of China (Nos. 31571196 and 30801502 to Ling Wang), the Shanghai Program for Support of Leading Disciplines-Integrated Chinese and Western Medicine (Nos. 20180101 and 20150407), the Program to Guide Medicine ("Yixueyindao") of the Shanghai Municipal Science and Technology Commission (Nos. 18401902200 and 15401932200 to Ling Wang), the Shanghai Pujiang Program (No. 11PJ1401900 to Ling Wang), the FY2008 JSPS Postdoctoral Fellowship for Foreign Researchers (P08471 to Ling Wang), and the Fund for Young Scientists of the Shanghai Municipal Health and Family Planning Commission (No. 20184Y0218 to Lisha Li).

References

1. Onuoha OC. Epidural analgesia for labor: Continuous infusion versus programmed intermittent bolus. *Anesthesiol Clin*. 2017; 35:1-14.
2. Rooks JP. Labor pain management other than neuraxial: What do we know and where do we go next? *Birth*. 2012; 39:318-322.
3. Simmons SW, Taghizadeh N, Dennis AT, Hughes D, Cyna AM. Combined spinal-epidural versus epidural analgesia in labour. *Cochrane Database Syst Rev*. 2012; 10:CD003401.
4. Deshmukh VL, Ghosh SS, Yelikar KA, Gadappa SN. Effects of epidural labour analgesia in mother and foetus. *J Obstet Gynaecol India*. 2018; 68:111-116.
5. Kinoshita H. Novel insights into the role of anesthetics and opioids in organ or tissue protection. *Curr Pharm Des*. 2014; 20:5671-5672.
6. Ateser RY, Kayacan N. Intrathecal ropivacaine in cesarean delivery. *Niger J Clin Pract*. 2017; 20:1322-1327.
7. Wang Y, Tang H, Guo Q, Liu J, Liu X, Luo J, Yang W. Effects of intravenous patient-controlled sufentanil analgesia and music therapy on pain and hemodynamics after surgery for lung cancer: A randomized parallel study. *J Altern Complement Med*. 2015; 21:667-672.
8. Wang X, Xu S, Qin X, Li X, Feng SW, Liu Y, Wang W, Guo X, Shen R, Shen X, Wang F. Comparison

- between the use of ropivacaine alone and ropivacaine with sufentanil in epidural labor analgesia. *Medicine (Baltimore)*. 2015; 94: e1882.
9. Erasso DM, Chaparro RE, Quiroga Del Rio CE, Karlinski R, Camporesi EM, Saporta S. Quantitative assessment of new cell proliferation in the dentate gyrus and learning after isoflurane or propofol anesthesia in young and aged rats. *Brain Res*. 2015; 1441:38-46.
 10. Hawkins JL. Epidural analgesia for labor and delivery. *N Engl J Med*. 2010; 362:1503-1510.
 11. Bolat E, Bestas A, Bayar MK, Ozcan S, Erhan OL, Ustundag B. Evaluation of levobupivacaine passage to breast milk following epidural anesthesia for cesarean delivery. *Int J Obstet Anesth*. 2014; 23:217-221.
 12. Boroujeni ME, Gardaneh M. Umbilical cord: An unlimited source of cells differentiable towards dopaminergic neurons. *Neural Regen Res*. 2017; 12:1186-1192.
 13. Chao YH, Wu HP, Chan CK, Tsai C, Peng CT, Wu KH. Umbilical cord-derived mesenchymal stem cells for hematopoietic stem cell transplantation. *J Biomed Biotechnol*. 2012; 2012:759503.
 14. Zheng T, Zheng CY, Zheng XC, Zhao RG, Chen YQ. Effect of parthanatos on ropivacaine-induced damage in SH-SY5Y cells. *Clin Exp Pharmacol Physiol*. 2017; 44:586-594.
 15. Li H, Liu T, Zhu Y, Fu Q, Wu W, Deng J, Lan L, Shi S. An in situ-forming phospholipid-based phase transition gel prolongs the duration of local anesthesia for ropivacaine with minimal toxicity. *Acta Biomater*. 2017; 58:136-145.
 16. Gong L, Qin Q, Zhou L, Ouyang W, Li Y, Wu Y, Li Y. Effects of fentanyl anesthesia and sufentanil anesthesia on regulatory T cells frequencies. *Int J Clin Exp Pathol*. 2014; 7:7708-7716.
 17. Bundscherer A, Malsy M, Gebhardt K, Metterlein T, Plank C, Wiese CH, Gruber M, Graf BM. Effects of ropivacaine, bupivacaine and sufentanil in colon and pancreatic cancer cells *in vitro*. *Pharmacol Res*. 2015; 95:126-131.
 18. Bauer C, Pavlakovic I, Mercier C, Maury JM, Koffel C, Roy P, Fellahi JL. Adding sufentanil to ropivacaine in continuous thoracic paravertebral block fails to improve analgesia after video-assisted thoracic surgery: A randomised controlled trial. *Eur J Anaesthesiol*. 2018; 35:766-773.
 19. Chen QL, Gu EW, Zhang L, Cao YY, Zhu Y, Fang WP. Diabetes mellitus abrogates the cardioprotection of sufentanil against ischaemia/reperfusion injury by altering glycogen synthase kinase- β . *Acta Anaesthesiol Scand*. 2013; 57:236-242.
 20. Grosse J, Warnke E, Wehland M, Pietsch J, Pohl F, Wise P, Magnusson NE, Eilles C, Grimm D. Mechanisms of apoptosis in irradiated and sunitinib-treated follicular thyroid cancer cells. *Apoptosis*. 2014; 19:480-490.
 21. Zhang Q, Su M. Sufentanil attenuates oxaliplatin cytotoxicity *via* inhibiting connexin 43-composed gap junction function. *Mol Med Rep*. 2017; 16:943-948.
 22. Gong X, Dan J, Li F, Wang L. Suppression of mitochondrial respiration with local anesthetic ropivacaine targets breast cancer cells. *J Thorac Dis*. 2018; 10:2804-2812.
 23. Dai SH, Chen T, Wang YH, Zhu J, Luo P, Rao W, Yang YF, Fei Z, Jiang XF. Sirt3 protects cortical neurons against oxidative stress *via* regulating mitochondrial Ca^{2+} and mitochondrial biogenesis. *Int J Mol Sci*. 2014; 15:14591-14609.
 24. Song GH, Huang FB, Gao JP, Liu ML, Pang WB, Li WB, Yan XY, Huo MJ, Yang X. Effects of fluoride on DNA damage and caspase-mediated apoptosis in the liver of rats. *Biol Trace Elem Res*. 2015; 166:173-182.
 25. Wan L, Zhang D, Zhang J, Ren L. TT-1, an analog of melittin, triggers apoptosis in human thyroid cancer TT cells *via* regulating caspase, Bcl-2 and Bax. *Oncol Lett*. 2018; 15:1271-1278.
 26. Wu QL, Shen T, Ma H, Wang JK. Sufentanil postconditioning protects the myocardium from ischemia-reperfusion *via* PI3K/Akt-GSK- β pathway. *J Surg Res*. 2012; 178:563-570.
 27. Yao W, Han Q, Wang L, Niu Z. Ropivacaine relieves pain and prevents chondrocyte degradation probably through Calcineurin/NFAT1 signaling pathway in osteoarthritis rats. *Eur J Pharmacol*. 2018; 818:518-524.
 28. Sun Z, Shi K, Yang S, Liu J, Zhou Q, Wang G, Song J, Li Z, Zhang Z, Yuan W. Effect of exosomal miRNA on cancer biology and clinical applications. *Mol Cancer*. 2018; 17:147.
 29. Sharifi M, Moridnia A. Apoptosis-inducing and antiproliferative effect by inhibition of miR-182-5p through the regulation of CASP9 expression in human breast cancer. *Cancer Gene Ther*. 2017; 24:75-82.
 30. Hirata H, Ueno K, Shahryari V, Tanaka Y, Tabatabai ZL, Hinoda Y, Dahiya R. Oncogenic miRNA-182-5p targets Smad4 and RECK in human bladder cancer. *PLoS One*. 2012; 7: e51056.
 31. Cao M, You A, Zhu X, *et al.* miR-182-5p promotes hepatocellular carcinoma progression by repressing FOXO3a. *J Hematol Oncol*. 2018; 11:12.
 32. Delbridge AR, Strasser A. The BCL-2 protein family, BH3-mimetics and cancer therapy. *Cell Death Differ*. 2015; 22:1071-1080.
 33. Zhang S, Zhang Q, Shi G, Yin J. MiR-182-5p regulates BCL2L12 and BCL2 expression in acute myeloid leukemia as a potential therapeutic target. *Biomed Pharmacother*. 2018; 97:1189-1194.
 34. Gehring T, Seeholzer T, Krappmann D. BCL10 - Bridging CARDs to immune activation. *Front Immunol*. 2018; 9:1539.
 35. Wang W, Wu J, Zhang Q, Li X, Zhu X, Wang Q, Cao S, Du L. Mitochondria-mediated apoptosis was induced by oleuropein in H1299 cells involving activation of p38 MAP kinase. *J Cell Biochem*. 2018; doi: 10.1002.

(Received December 6, 2018; Revised February 7, 2019; Accepted February 10, 2019)

Programmed death ligand-1, tumor infiltrating lymphocytes and HLA expression in Chinese extrahepatic cholangiocarcinoma patients: Possible immunotherapy implications

Fei Yu¹, Lei Gong², Zheng Mo³, Wenran Wang^{1,2}, Meilong Wu^{1,2}, Jianghui Yang⁴, Qiongqiong Zhang¹, Li Li⁴, Jingjing Yao⁴, Jiahong Dong^{1,*}

¹ School of Clinical Medicine, Tsinghua University, Beijing, China;

² Department of Hepatopancreatobiliary Surgery, Beijing Tsinghua Changgung Hospital, School of Clinical Medicine, Tsinghua University, Beijing, China;

³ Department of Hematology and Oncology, Beijing Tsinghua Changgung Hospital, School of Clinical Medicine, Tsinghua University, Beijing, China;

⁴ Department of Pathology, Beijing Tsinghua Changgung Hospital, School of Clinical Medicine, Tsinghua University, Beijing, China.

Summary

Immunotherapy might be an effective treatment in extrahepatic cholangiocarcinoma (eCCA), a tumor with extremely limited therapeutic options. Our study is to characterize the programmed death ligand-1 (PD-L1) protein expression and cancer microenvironment profiles in surgically resected eCCA samples. PD-L1 positivity was observed on tumor cells (32.3%) as well as on tumor-associated macrophages (74.2%). PD-L1 expression by eCCA correlated significantly with immune parameters such as intra-tumoral CD3+ tumor infiltrating lymphocytes (TILs) density ($P = 0.002$), intra-tumoral CD8+ TILs density ($P < 0.001$), and the expression pattern of human leukocyte antigen (HLA) class I ($P < 0.001$). Immunofluorescence showed that PD-L1 positive tumor cells were adjacent to PD-1 positive cells and the stroma covered with interferon- γ . Correlation with clinicopathological parameters and survival analyses revealed that PD-L1 positivity in eCCA was related to the absence of venous invasion ($P = 0.030$), improved overall survival ($P = 0.020$) and progression-free survival ($P = 0.011$). HLA class I molecules defect, which is an important mechanism of immune evasion, was frequently observed in eCCA (50.0%) and was associated with a decreased number of intra-tumoral CD8+ TIL density ($P = 0.028$). Additionally, the presence of unusually high numbers of tumor-associated macrophages (TAMs) subsets M2 in most of eCCA (74.2%) was noted. Our study indicated that PD-L1 expression in association with intra-tumoral TILs infiltration and HLA class I expression in 32.3% of the eCCA reflects an active immune microenvironment potentially responsive to PD-1/PD-L1 inhibitors. In addition, the combination of macrophage-targeting agents may provide therapeutic synergy for future immunotherapy.

Keywords: Extrahepatic cholangiocarcinoma, PD-L1, TILs, HLA class I molecules, TAMs

1. Introduction

Cholangiocarcinoma (CCA) is a rare cancer biliary

Released online in J-STAGE as advance publication February 15, 2019.

*Address correspondence to:

Dr. Jiahong Dong, School of Clinical Medicine, Tsinghua University, No.1, Tsinghua Yuan, Haidian District, Beijing, 100084, China.

E-mail: djhtsinghua@163.com

tract malignancy which accounts for less than 3% of all gastrointestinal cancers diagnosed worldwide (1). The incidence of CCA is highest in Thailand, China, and other Asian populations, but is lowest in the western world, presumably reflecting differences in the exposure of genetic and other risk factors (2). Anatomically, CCA can be divided into intrahepatic or extrahepatic subtypes choosing second-order bile ducts as the point of separation (3). The majority of CCA are extrahepatic cholangiocarcinoma (eCCA), whereas

intrahepatic cholangiocarcinoma (iCC) comprise less than 10% of cases (4). eCCA can be classified further into perihilar (pCCA) and distal tumors (eCCA), separated by the cystic duct (5).

Despite advances in development of early detection methodologies, CCA continues to be a challenging malignancy with extremely limited treatment options. A minority of patients at a sufficiently early stage have a chance of curative surgical resection, especially those with localized disease without vascular and/or parenchymal involvement (6). Neoadjuvant chemoradiotherapy followed by liver transplantation offers another therapeutic option that can achieve complete extirpation of locally advanced pCCA in judiciously selected patients (7). For patients beyond the stringent inclusion criteria, no other curative treatment has proved successful (8). Locally advanced or metastatic CCA can be treated with chemotherapeutic regimens but is of limited effectiveness, unlike the improvement in survival achieved in colorectal and gastric cancers (9). Recent genomic sequencing technologies have facilitated the identification of therapeutic targets in various solid tumors, implicating a promising strategy for CCA (10). However, success rate from bench to bedside has so far remained significantly low due to lack of objective clinical response (11).

Monoclonal antibodies directed at the programmed cell death protein 1 (PD-1) immune checkpoint and one of its ligands, PD-L1, has demonstrated impressive antitumor responses (12). By activating T cell-mediated immunity, some meaningful anti-tumor responses were observed in late-stage melanoma – a type of cancer largely resistant to standard chemotherapy (13). Subsequently, the clinical value of the PD-1/PD-L1 axis has been extended in non-small cell lung cancer and other solid tumors (14). However, to date there is scarce data regarding the expression of PD-L1 and its role in tumor microenvironment of eCCA (15). Recently, Dirk Walter *et al* reported a relatively low frequency of PD-L1 positivity (8/69, 11.6%) in eCCA arising in the European population (16). However, this positive rate cannot be generalized to other regions due to ethnic disparities of molecular patterns among eCCA patients (17). Therefore, further analysis of PD-L1 expression in eCCA in populations with different ethnic backgrounds was necessary, as it might personalize the treatment for this ethnic-heterogeneous disease.

The overexpression of PD-L1 in a tumor site may predict the response to PD-1/PD-L1 antibodies (18,19). However, the determinants of reliable response or primary resistance to immune checkpoint inhibition are clearly multi-faceted (20). For example, Tumor-infiltrating lymphocytes (TILs) are the main executioners of antitumor immunity, but reduced expression of major histocompatibility complex (MHC; also known as human leukocyte antigen (HLA) in

humans) can render the malignant cells "invisible" to the immune system (21). TILs as well as HLA antigens have been reported to be predictive markers for PD-1/PD-L1 checkpoint blockades in many cancers, but no study has, to our knowledge, evaluated these important prerequisites in a clinicopathologic study of eCCA, so far (16,22).

This study was performed to characterize the expression of PD-L1 in a Chinese cohort of eCCA patients, and to correlate the results with the clinicopathological findings including the outcome. Furthermore, to support a rationale regarding the application of PD-1/PD-L1 blockades, we assessed some important immune modulators in the tumor microenvironment such as TILs, tumor-associated macrophages (TAMs) and HLA-I expression.

2. Materials and Methods

2.1. Patient material

The current study evaluated formalin-fixed paraffin-embedded (FFPE) tumor sections from eCCA patients who underwent curative-intent surgery from January 2015 to September 2017, in Beijing Tsinghua Changgung Hospital affiliated with Tsinghua University, one of the leading Chinese medical centers for hepatobiliary surgery. None of the patients had received any neoadjuvant treatment followed by curative resection. Pathologic diagnoses were confirmed by a pathologist (H. F. Yin) according to the 7th American Joint Committee on Cancer (AJCC) and the histologic types were determined by the WHO classification. Patients with other primary tumors of hepatobiliary system such as Gallbladder and/or ampullary carcinoma, were excluded from the current study.

For the patients enrolled, clinicopathologic information available included demographic information (age and sex), AJCC stage, grading (G), presence of venous invasion (V), presence of perineural invasion (P), and tumor infiltration of resection margins (R). Progression-free survival (PFS) is defined by the interval from surgery to recurrence deadline date of the study (October 2018). Overall survival (OFS) is defined as the duration from surgery to date of death or deadline date of the study. Informed consent for the use of samples was obtained individually from each patient. This retrospective study was approved with the agreement of ethics committee of the Beijing Tsinghua Changgung Hospital affiliated to Tsinghua University.

Tumor samples from a cohort of 62 surgically resected eCCA (45 pCCA and 17 dCCA) were analyzed. The group included 41 males (66.1%) and 21 females (33.9%), aged between 22 and 81 years (mean age, 60.8 years). The perioperative mortality was 6.5% (4 patients) and thus those patients were not included

in further survival analysis. Kaplan-Meier survival analysis according to clinicopathological characteristics indicated that our cases are representative of an average eCCA population and thus provide a better baseline for the retrospective analysis (Figure S1, <http://www.biosciencetrends.com/action/getSupplementalData.php?ID=37>).

2.2. Immunohistochemistry and scoring

After review of all surgically resected specimens stained with hematoxylin and eosin (H&E), a representative slide with a sufficient eCCA fraction was chosen for research. 4- μ m paraffin embedded tissues were deparaffinized, cleared and rehydrated through decreasing concentration of ethanol (100%, 95%, 85%, and 75%). Heat-induced epitope retrieval was performed in a solution of EDTA, pH 8.0. Monoclonal primary antibodies against (PD-L1, 1/200, E1L3N, Cell Signaling Technology, Danvers, MA, USA; CD3, 1/150, ab16669, Abcam, Cambridge, UK; CD4, 1/400, ab133616, Abcam, Cambridge, UK; CD8, 1/200, ab17147, Abcam, Cambridge, UK; CD163, 1/500, EPR19518, Abcam, Cambridge, UK; HLA Class one, 1/300, EMR8-5, Abcam, Cambridge, UK) were incubated overnight at 4°C. Detection of immunolabeling was performed by incubation with biotinylated secondary antibodies (SignalStain® Boost IHC Detection Reagent; Cell Signaling Technology, Danvers, MA, USA). To verify antibody specificity, positive controls consisted of human placental tissue for PD-L1 and human tonsil tissues for the marker of TILs. Endothelial cells or T cells were included to serve as a positive internal control for HLA class I antibody. The stained slides were scanned with a high throughput digital slide scanner (Pannoramic 250 Flash III and Viewer, 3DHISTECH) to obtain a whole slide image. All sections were examined and scored independently by two pathologists (J.J.Y. and L.L) blinded to the clinical data. When coming to a point of discrepancies, re-evaluation and discussion were conducted to reach a consensus opinion.

The expression of PD-L1 was assessed on tumor cells, lymphocytes as well as on macrophages. Cells expressing PD-L1 on membranes were regarded as positive, while cytoplasmic staining only was termed as negative. For tumor cells positivity, the intensity (0, no staining; 1, weak; 2, moderate; 3, intense) and the percentage of membranous positivity (0 – 100%) were considered collectively. Total immunostaining score (TIS) was calculated by multiplying the percentage of the positive cells by the staining intensity. TIS score (0 – 300), with a score ≥ 3 being defined as PD-L1 positivity according to recent studies with the same antibody (16,23).

Instead of measuring TILs dichotomically, we quantified the density of TILs by averaging the number

of positive cells (CD3, CD4 and CD8) within at least five HPF areas (Perimeter: 1960.0 μ m, Area: 0.305 mm^2). To reduce heterogeneity, both inside the tumor and surrounding the cancer nest were scored separately when possible. TAMs were classified into low or high groups based upon the cut-off value of $> 20\%$ CD163+ cells as previously described (24).

HLA class I expression was divided into three criteria for membrane expression as previously described: negative ($< 25\%$ HLA positive tumor cells), heterogeneous (between 25% and 75% HLA positive tumor cells) or positive ($> 75\%$ HLA positive tumor cells) (25,26). Positive or heterogeneous HLA class I expression were assigned to the "high HLA-I expression" group while negative expression was defined as the "low HLA-I expression" group.

2.3. Immunofluorescent staining and scoring

After deparaffinization, rehydration and heat-induced antigen retrieval, tissue samples were incubated overnight with the primary anti-human PD-L1 (Rabbit mAb, 1/200, E1L3N, Cell Signaling Technology, Danvers, MA, USA) combined with anti-human PD-1 (Mouse mAb, 1/100, ab52587, Abcam, Cambridge, UK), or anti-human PD-L1 (Mouse mAb, 1/100, EMR8-5, Abcam, Cambridge, UK) combined with anti-human interferon γ (IFN- γ) (Rabbit mAb, 1/200, ab9657, Abcam, Cambridge, UK). Slides were then incubated with secondary antibodies: goat anti-rabbit-FITC (ab6717, Abcam, Cambridge, UK) and goat anti-mouse-TRITC (ab6786, Abcam, Cambridge, UK). Nuclei were stained with 4,6-diamidino-2-phenylindole (#4083, Cell Signaling Technology, Danvers, MA, USA). Fluorescent images were analyzed with a fluorescence microscope (BX53, Olympus).

In humans, macrophages polarize into two extremes from the classically activated M1 macrophages (CD14+ CD163-) to the alternatively activated M2 macrophages (CD14+ CD163+) (27). To define macrophage polarization, CD14 (Mouse mAb, 1/300, ab182032, Abcam, Cambridge, UK) was used as macrophage surface marker, and polarized macrophage was identified by expression of the CD163 (Rabbit mAb, 1/500, ab182422, Abcam, Cambridge, UK): CD14+CD163+ cells indicated the immunosuppressive M2 subset while CD14+CD163- cells were considered as the immunostimulatory M1 subset. The numbers of CD14 positive cells and CD163 positive cells were counted respectively in five representative visual fields with high-power fields (HPF \times 400).

2.4. Statistical analysis

The associations of PD-L1 expression with each clinicopathological characteristic were analyzed with the χ^2 test or Fisher's exact test, as appropriate. Mann-

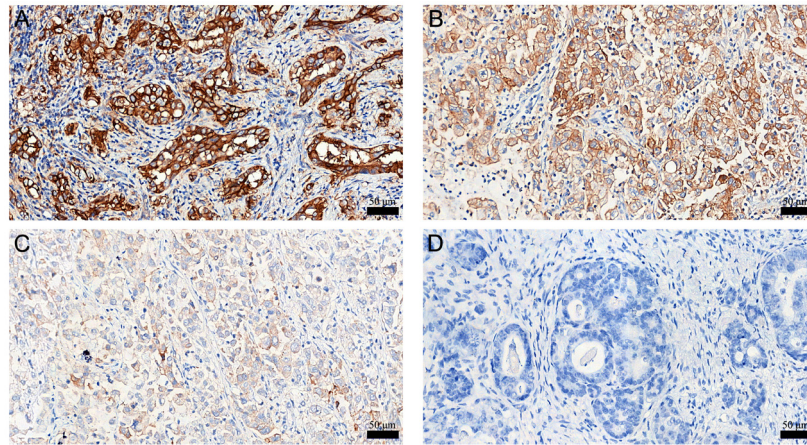


Figure 1. Representative immunohistochemical images for PD-L1 in eCCA with strong (A), moderate (B), weak (C) and no (D) PD-L1 expression. In these tissues, PD-L1 showed membrane-accentuated expression, also often accompanied by cytoplasmic expression. Cells with PD-L1 expression on the membrane were assessed as PD-L1 positive, whereas only cytoplasmic PD-L1 expression were assessed as PD-L1 negative.

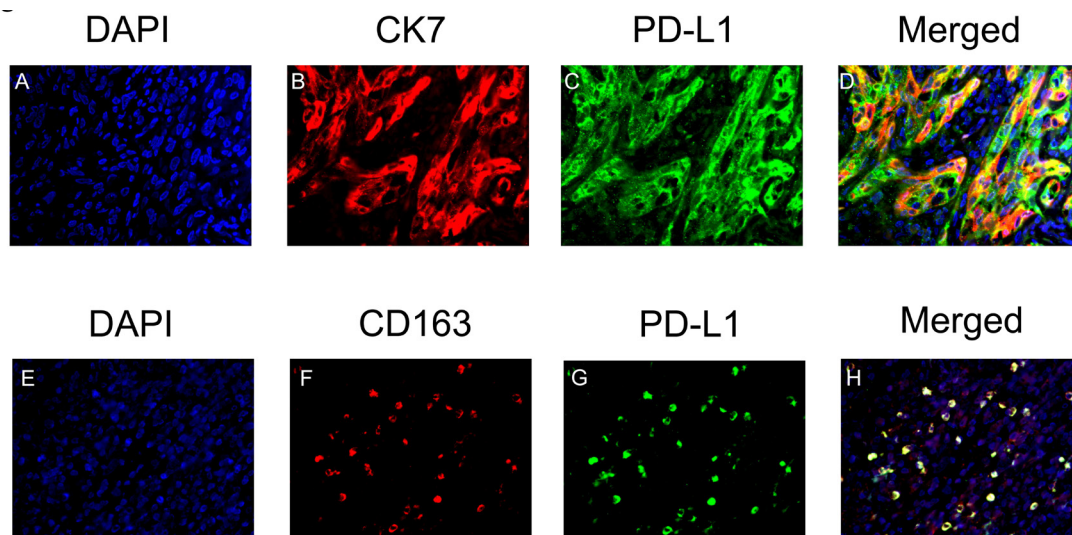


Figure 2. Identification of PD-L1-positive tumor cells (A–D) and tumor-infiltrating macrophages (TAMs) (E–H) in eCCA. Representative double immunofluorescence staining shows monochromatic PD-L1 (in green), CK7 (in red), CD163 (in red) images, and colocalized PD-L1/CK7, PD-L1/CD163, and DAPI (4',6-diamidino-2-phenylindole) (in blue).

Whitney *U*-test was used to detect differences in density of the TILs between groups of patients. Kaplan-Meier survival curves were generated and log-rank test was used for assessing PD-L1 in relation to overall and progression-free survival. *P*-values were two-sided, and *P*-values of < 0.05 were considered statistically significant. The statistical analyses were performed using SPSS version 20.0 software (Chicago, IL).

3. Results

3.1. PD-L1 expression in eCCA and its association with eCCA clinicopathological features

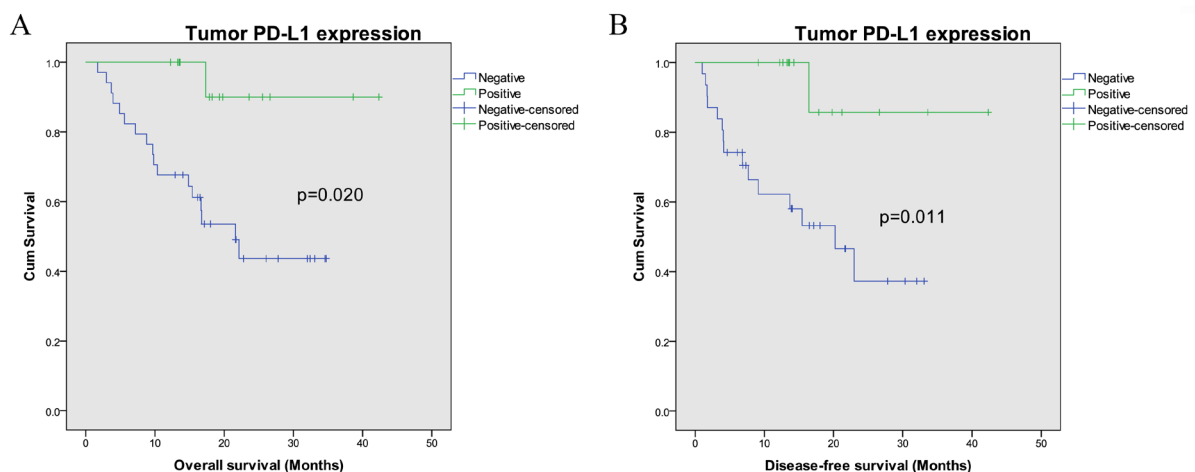
PD-L1 positive cells were identified in 46 patients analyzed (46/62, 74.2%); however, in only 20 patients (20/62, 32.3%) PD-L1 positivity was expressed on

tumor cells (Figure 1A-D). In these 20 PD-L1 positive eCCA, PD-L1 was co-expressed by tumor cells as well as a few macrophages. For the remaining 26 eCCA, PD-L1 positivity was merely expressed by macrophages. Expression of PD-L1 by both tumor cells and macrophages was confirmed by PD-L1 and CK7, and PD-L1 and CD163 double-immunofluorescence staining (Figure 2A-D, E-H). Tumor cell staining for PD-L1 occurred in two patterns: focal (17/20, 85.0%) or diffuse (3/20, 15.0%) (Figure S2, <http://www.biosciencetrends.com/action/getSupplementalData.php?ID=37>). On investigation of clinicopathological features, significant correlations between tumoral PD-L1 expression and absence of venous invasion was observed ($P = 0.030$) (Table 1).

To evaluate the correlation between PD-L1 in eCCA specimens ($n = 58$) and the prognosis of eCCA patients,

Table 1. Correlation between PD-L1 expression and variable clinicopathologic parameters in 62 eCCA

Variable	Patients (total)	%	PD-L1 positive tumor	%	PD-L1 negative tumor	%	P-value
Age (years)							
≥ 60	37	59.7	7	63.6	30	58.8	0.971
< 60	25	40.3	4	36.4	21	59.7	
Gender							
Male	41	66.1	13	65.0	28	66.7	0.897
Female	21	33.9	7	35.0	14	33.3	
Localization							
pCCA	45	72.6	13	65.0	32	76.2	0.356
dCCA	17	27.4	7	35.0	10	23.8	
Grading							
G1-G2	46	74.2	9	81.8	33	78.6	0.353
G3	16	25.8	2	18.2	9	21.4	
Tumour size (mm)							
≥ 30	18	29.0	8	40.0	10	23.8	0.236
< 30	44	71.0	12	60.0	32	76.2	
Venous invasion							
V0	31	50.0	14	70.0	25	59.5	0.030*
V1	31	50.0	6	30.0	17	40.5	
Perineural invasion							
PN0	11	17.7	5	25.0	6	14.3	0.311
PN1	51	82.3	15	75.0	36	85.7	
Lymph node metastasis							
N0	34	54.8	12	60.0	22	52.4	0.598
N1	28	45.2	8	40.0	20	47.6	
Resection margin							
R0	48	77.4	18	81.8	30	76.5	0.192
R1	14	22.6	2	18.2	12	23.5	
AJCC classification							
I-II	23	37.1	10	50.0	13	31.0	0.169
III-IV	39	62.9	10	50.0	29	69.0	
CD163 infiltrate							
High	42	67.7	18	90.0	33	78.6	0.478
Low	20	32.3	2	10.0	9	21.4	
HLA expression							
High	44	71.0	20	100.0	0	0.0	< 0.001*
Low	18	29.0	24	57.1	18	42.9	

**Figure 3. Association of PD-L1 expression and post-treatment outcome (A and B) of eCCA.** PD-L1 positivity in tumor cells is associated with better overall and progression-free survival. P value obtained by log-rank test.

Kaplan-Meier survival curves were generated. Patients with PD-L1 expression at the tumor site showed better overall and progression-free survival (log rank test; $P = 0.020$ and 0.011 respectively) compared to those with negative PD-L1 expression (Figure 3A-B).

3.2. Correlation between TIL subtype densities and PD-L1 expression in eCCA

To reveal the correlation between PD-L1 expression and immune infiltration in eCCA, staining of TIL

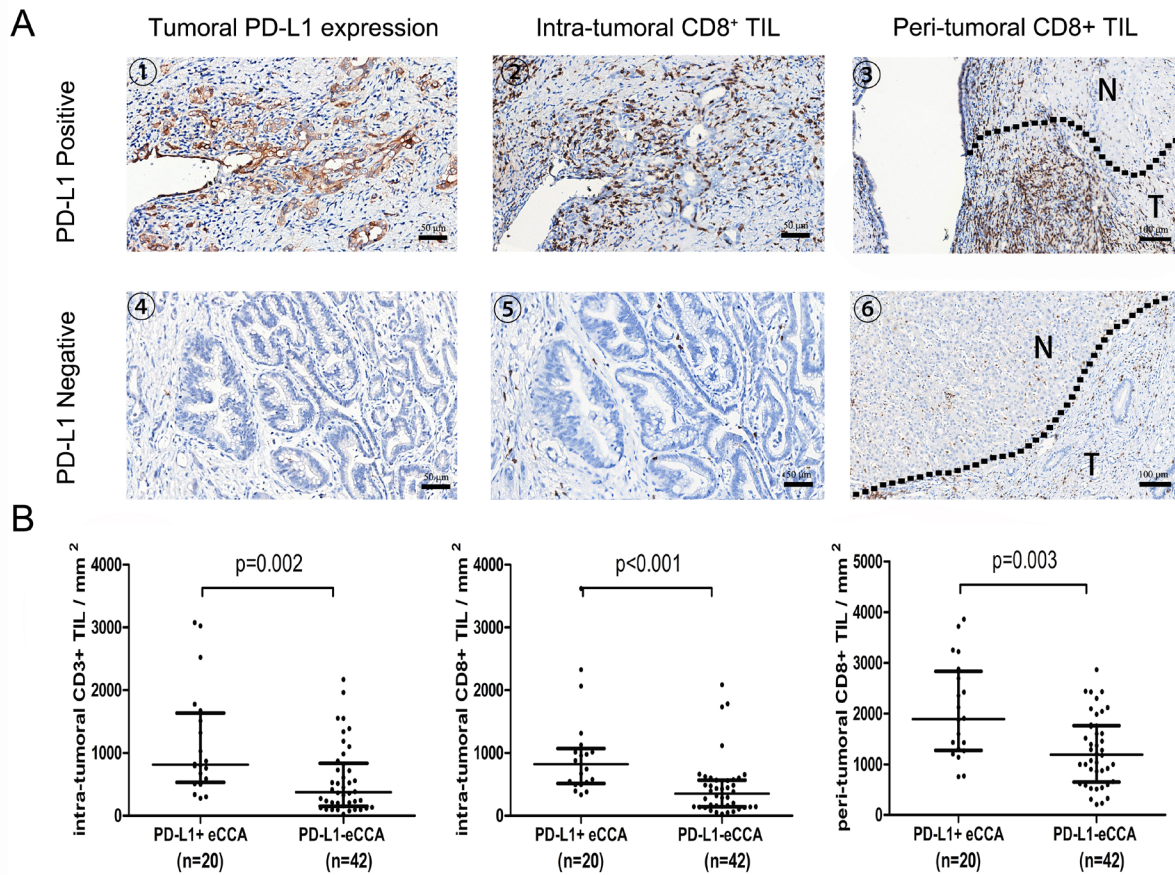


Figure 4. Expression of PD-L1 correlated with TIL density (CD8+). Representative immunohistochemical images of PD-L1 and CD8 show that peri/intra – tumoral CD8⁺ TIL density was higher in tumors with positive expression of PD-L1 than in the tumors with negative expression of PD-L1 (A). Figures were taken from the same areas in serial sections (A① and A②, A④ and A⑤), respectively. The area marked 'T' represents eCCA area, and the area marked 'N' represents normal extrahepatic bile duct (A③) or normal hepatic tissue (A⑥). Mann-Whitney *U*-test reveals that intra-tumoral CD3⁺ and peri/intra – tumoral CD8⁺ TIL density was higher in eCCA cases showing positive expression of PD-L1 (B).

subpopulations with CD3, CD4 or CD8 antibodies was performed separately. In 62 eCCA cases, patients with positive expression of PD-L1 had higher density of intra-tumor CD3⁺ and CD8⁺ TIL (Mann-Whitney *U*-test; $P = 0.002$ and $P < 0.001$ respectively), and higher peri-tumor CD8⁺ TIL (Mann-Whitney *U*-test; $P = 0.003$) (Figure 4B). However, there was no significant difference of CD4⁺ TIL density between positive and negative PD-L1 expressions. When serial sections from eCCA were stained with the anti-PD-L1 antibodies, tumoral PD-L1 staining and accumulated stromal CD8⁺ immune cells were present in the same region of each tissue. (Figure 4A).

As PD-L1 attenuates antitumor immune system depending on PD-1/PD-L1 protein-protein interaction, we performed double immunofluorescence staining for PD-L1/PD-1 for the sample with PD-L1 positive expression ($n = 20$). In all PD-L1 positive tumors, a positive membranous PD-1 expression was found on cells in the PD-L1 positive tumor site (Figure 5A). The relative proximity of PD-1 to PD-L1 provides evidence of a direct contact between PD-1-positive and PD-L1-positive cells. It is known that in vitro, PD-L1 can be strongly induced on the surface of cancer cells by

adding IFN- γ (28). Using double immunofluorescence staining, we observed that IFN- γ was concentrated between PD-L1 positive tumors and the TILs (Figure 5B). PD-L1 expression on cancer cells in eCCA may therefore be caused by IFN- γ

3.3. eCCA exhibits different patterns of HLA Class I expression in the tumor microenvironment

As HLA class I molecules are involved in cytotoxic T cell recognition of malignant cells, we determined its expression profile in eCCA by immunohistochemistry, using antibodies against classical HLA class I molecules (monoclonal anti-pan HLA class I antibody, EMR8-5, which recognizes HLA class I -A, -B, and -C). Staining patterns on normal biliary epithelial cells from extrahepatic bile duct were also evaluated (Figure 6). Interestingly, HLA class I was positive on the cell membrane of normal biliary epithelial cells and the same expression pattern was detected in only 31 (50%) of tumor lesions. HLA class I molecule defect was observed in 31 (50%) of lesions, heterogeneous in 13 (21.0%) and negative in 18 (29.0%). Based on the basal level of PD-L1 expression in normal tissue,

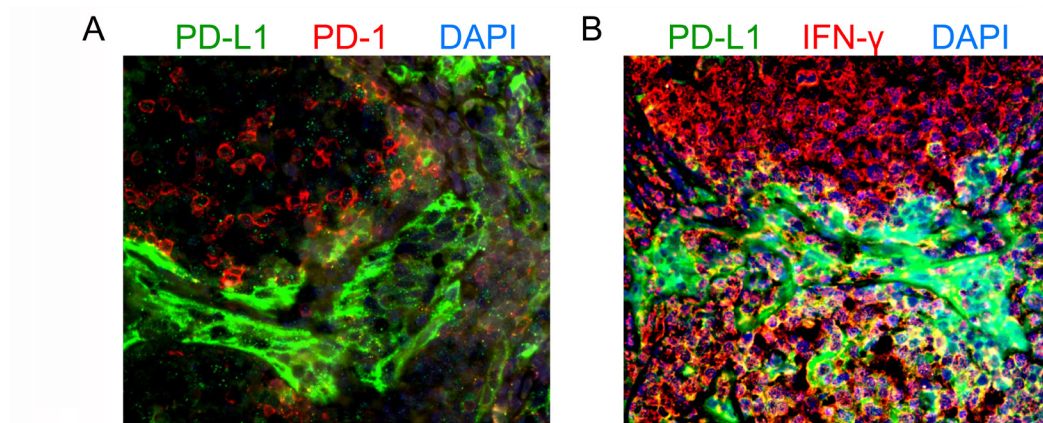


Figure 5. Representative double immunofluorescence staining of PD-L1 (green) and PD-1 (red) (A), and PD-L1 (green) and IFN- γ (red) (B).

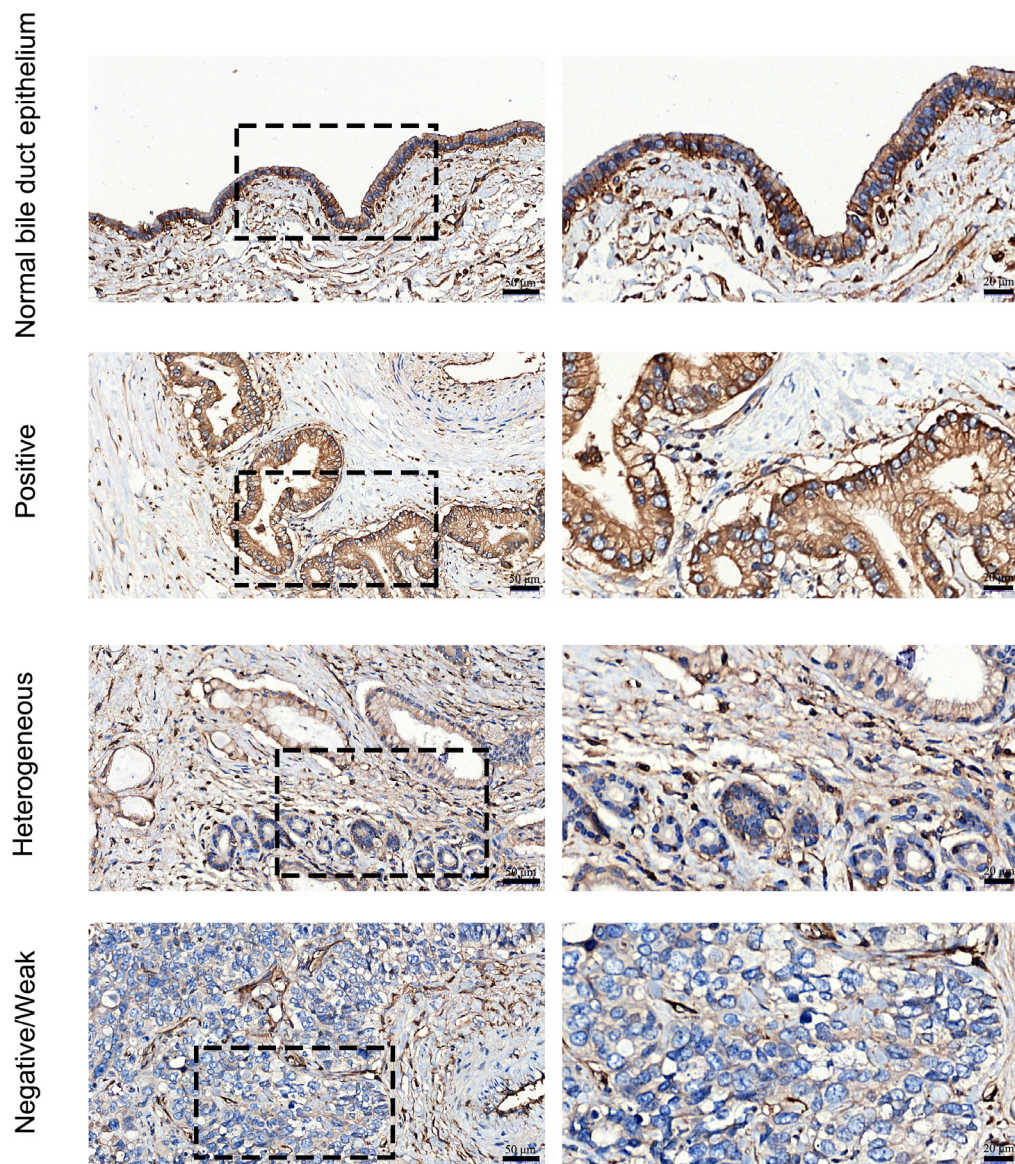


Figure 6. HLA class I expression in eCCA. Representative staining patterns of HLA class I expression in normal biliary epithelial cells and eCCA using immunohistochemistry. In general, basal level of positive HLA class I expression was found on normal biliary epithelial cells.

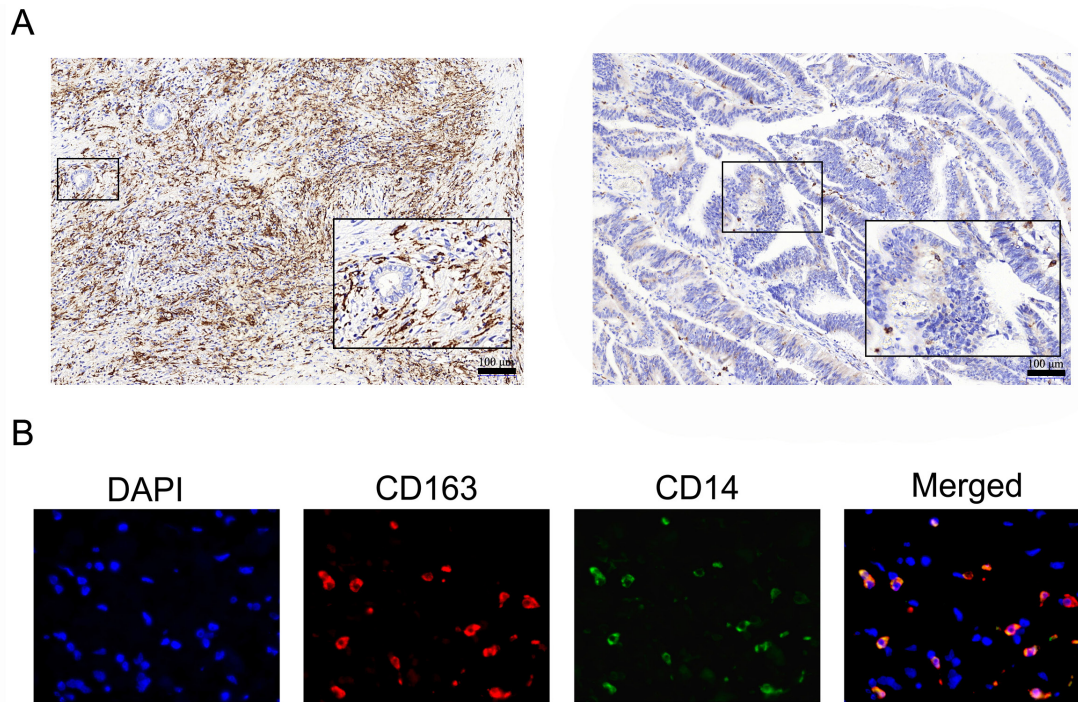


Figure 7. CD163 infiltrate in eCCA. eCCA with low CD163 infiltrate (< 20%) and high CD163 infiltrate (> 20%) (A). Characterization of tumor-associated macrophages in eCCA (B). Antibodies against CD14 (green) and CD163 (red) were used to detect macrophages and characterize their polarization as CD14+CD163- represented M1 type, while M2CD14+CD163+ represented M2.

our data demonstrated that HLA class I molecule downregulation is a frequent phenomenon observed in eCCA.

In 62 eCCA cases evaluated, CD8+ TIL density was higher in the high HLA-I expression group (positive and heterogeneous expression, $n = 43$) than that in the low HLA-I expression group (absolutely negative expression, $n = 18$) (Mann-Whitney U -test; $P = 0.028$,) (Figure S3, <http://www.biosciencetrends.com/action/getSupplementalData.php?ID=37>). Additionally, high HLA-I expression was significantly associated with upregulated PD-L1 expression of tumor cells ($P < 0.001$). However, no other associations were found between other clinicopathological parameters and HLA-I expression (Table S1, <http://www.biosciencetrends.com/action/getSupplementalData.php?ID=37>).

3.4. eCCA-infiltrating macrophages mainly exhibit M2-phenotype

TAM have often been classified into two subtypes: M1 (tumor killing macrophages) and M2 (tumor promoting macrophages) (29). The M2 macrophages in the tumor microenvironment highly associated with tumor-promoting properties and thus evaluation of M2 macrophages in eCCA is important. On 62 tumors evaluated, 46 were highly infiltrated by M2 macrophages in relation to the expression of CD163 (74.2%) (Figure 7A). By using a combination of immunofluorescent staining, M2 macrophages

represented the predominant macrophage population in eCCA as nearly all CD14 positive cells also expressed CD163, which acted as a M2-like surface profile (Figure 7B). However, no impact of M2 macrophage infiltration on PD-L1 expression or clinicopathological characteristics was observed (Table S2, <http://www.biosciencetrends.com/action/getSupplementalData.php?ID=37>).

4. Discussion

The past decade of cancer research has generated encouraging results for cancer prevention by directly targeting the immune system using immune modulating agents (30). PD-1/PD-L1 checkpoint blockade is of considerable interest, being capable of eliciting durable responses in several different malignancies including, but not limited to, melanoma, lung and renal cancers (31). Whereas PD-L1/PD-1 inhibitor therapy is an active field of clinical research, few studies have attempted to evaluate the feasibility of targeting PD-L1/PD-1 pathway in CCA, because of its rarity (32). Furthermore, immune response in tumor microenvironment is complex, and PD-L1 expression alone may not represent the whole predictive value. Infiltrating lymphocytes and immune-modulatory molecules in tumor sites, such as MHC, have been noticed to associate with treatment effects of anti-PD-1/PD-L1 therapy (20). Thus, a better understanding of the eCCA immune microenvironment may be essential

to optimize and to personalize immunotherapies, as well as to precisely predict their efficacies in current immunotherapies.

A limited number of papers have assessed PD-L1 expression in eCCA on particular demographic groups, suggesting an East-West difference in expression pattern of PD-L1. Takashi Ueno *et al.*, using two different monoclonal antibodies against PD-L1, described its expression in Japanese patients being 36% and 45%, respectively (33). MA *et al.* found similar PD-L1 expression in Chinese cases (30/70, 42.86%) (22). In contrast, the work by Dirk Walter *et al.*, focused on Caucasian cohorts and reported a low frequency of PD-L1 expression (8/69, 11.6%) in their patients (16). Our screening of PD-L1 expression by immunohistochemistry in Chinese eCCA revealed that the rate of PD-L1-positive tumors was 32.3% (20/62), which was consistent with the Asian cohorts, and again found to be higher than the Caucasian group. Considering we used clone anti-PD-L1 antibodies and the method to assess cell surface PD-L1 expression following Dirk Walter's protocol used in Caucasian samples, the discrepancy might be race/ethnicity-related. Interestingly, an integrated genomic and transcriptomic analysis of 582 Asian and 256 Caucasian primary liver cancers (hepatocellular carcinoma and cholangiocarcinoma) has identified vast race/ethnicity-related heterogeneity suggesting Asian CCA were more likely to be infiltrated by T cells (17). Since tumor-T cell interaction is an important prerequisite for tumor PD-L1 expression, this finding may explain in part the higher levels of PD-L1 expression in Asian eCCA compared with Caucasian eCCA.

To date, two regulator mechanisms of PD-L1 induction have been proposed: intrinsic and extrinsic mechanisms (28). Intrinsic induction of PD-L1 is due to oncogenic-driven pathways, demonstrating no correlation with innate immune status (34). In contrast to the intrinsic mechanism, extrinsic induction of PD-L1 in tumor site is an adaptation to an on-going anti-tumor immunity, a process termed adaptive resistance (28). Specifically, the released pro-inflammatory cytokines, particularly IFN- γ from activated T cells trigger the expression of PD-L1 on cancer cells (35). PD-L1 binding to PD-1 on T cells that on the one hand leads to T cell exhaustion can also be targeted by PD-L1/PD-1 blockades to reactivate an anti-tumor response (35). Additionally, accumulating evidence suggested that tumor microenvironment characterized by inflammatory infiltration act as a precondition for PD-1/PD-L1 checkpoint blockades (36). In our eCCA study, the PD-L1 positivity was associated with significantly increased intra-tumoral CD3+ and CD8+ TILs infiltrate, indicating an immune-active microenvironment in PD-L1 positive eCCA. Additionally, PD-L1 expression was predominantly restricted to the regions where accumulated stromal

CD8+ TILs are present, reaffirming the colocalization of inflammatory response with PD-L1 expression in eCCA. Expectedly, the current study showed that PD-L1 positive eCCA cells were adjacent to PD-1-positive cells and surrounded by IFN- γ . Taken together, our findings suggest that upregulation of PD-L1 in eCCA is due to an adaptive immune response based on the association of PD-L1 and tumor-infiltrating lymphocytes including CD8-positive TILs and on the finding of colocalization of proinflammatory cytokines. Furthermore, our finding that PD-L1 positive eCCA cells were adjacent to PD-1 positive TILs predicted a greater chance of response to PD-L1/PD-1 checkpoint blockade therapy.

Considering the immune evasion mechanism by PD-1/PD-L1 pathway, PD-L1 overexpression was generally expected to be linked with progression and poor prognosis (37). While others claimed conflicting results, colorectal cancer for example, PD-L1 positive was reported to be associated with low malignant features and a longer disease-free survival or overall survival (38). Similarly, the clinical association of PD-L1 expression remained controversial in eCCA studies, especially survival. MA *et al.* showed in a series of 70 eCCA patients that PD-L1 expression was associated with advanced TNM stage, lymphatic metastasis and an unfavorable outcome (22). However, Dirk Walter reported no prognosis difference between PD-L1 positive and PD-L1 negative expression in 69 eCCA patients (16). In this study, we assess the prognostic role of PD-L1 expression in 62 patients with eCCA and observed that PD-L1 expression was associated with absence of vascular invasion and better outcome. These inconsistencies may be explained by a restricted number of cases in the current eCCA studies, thereby resulting in an inadequate statistical efficacy. More recently, a large scale comprehensive genomic study involving nearly 500 CCAs showed an improved survival in patients with specific upregulation of immune checkpoint genes (39). Considering the complex dynamics from initiate anti-tumor immune responses to adaptive immune resistance, we prefer the view of PD-L1 as a positive marker for prognosis. In contrast to CTLA-4, which attenuates the initial T cell activation stage, PD-L1 is induced as a protective response to pre-existing successful anti-tumor immunity (40). On theoretical grounds, despite that PD-L1 positive tumor cells have become protected from cellular immune attack, activated TILs in tumor microenvironment may still have a positive impact on survival by recognition and destruction of other PD-L1 negative cells. Moreover, our study found that the PD-L1 expression was significantly associated with absence of vascular invasion, which reinforces the notion that on-going antitumor immunity to prevent the spread of malignant cells remained in PD-L1 positive eCCA, thereby improving the clinical outcome of patients in

our study.

HLA class I molecules, composed of a polymorphic heavy chain encoded by HLA-A, -B, and -C genes, are expressed by most cell types and present peptides derived from cellular proteins to CD8⁺ T cells (41). As a prerequisite for recognition of malignant cells, normal expression of HLA class I molecules on tumor cell surface is crucial to evoke anti-tumor immune responses (42). Moreover, the preexisting HLA class I level in the tumor region has a vital role in determining the efficiency of cancer immunotherapy (43). Unfortunately, current evidence indicated that loss or selective downregulation of HLA expression is not random but a frequent finding in various types of cancer, which has been described from 16% for cutaneous melanoma to 50% for prostate cancer (44). However, no data of HLA expression in eCCA had been published so far. We report herein for the first time that a significant percentage of eCCA are heterogeneous (21.0%) or total loss (29.0%). Generation of MHC-I deficient tumor cells is believed to be a consequence of continuous exposure to the host's immune response (44). Conversely, established HLA-I expression pattern may also rearrange the anti-tumor response via affecting tumor infiltration, which has been well described in non-small cell lung cancer (25). At early stages, tumors are HLA-I positive/ heterogeneous and are highly infiltrated with lymphocytes; while at later stages, tumor nests are mostly HLA-I negative, which forms an immunosuppressive microenvironment that prevents intra-tumor immune cell infiltration (39). In this regard, it can be theoretically proposed that TILs tend to infiltrate into high HLA-I expression (positive/ heterogeneous) tumors, which undergo long-time interactions with cancer cells, thereby triggering the induction of inhibitory molecule genes. This may explain in our eCCA study why tumor HLA-I expression was strongly correlated with TILs infiltration as well as tumor PD-L1 expression. Interestingly, recent integrative clustering of gene expression in 489 CCA samples has uncovered concordant results that a distinct subtype demonstrating upregulation of immune checkpoint genes also displayed a high level of infiltrating immune cells as well as pathways involved in antigen presentation (39). All together, we deduced that PD-L1 positive eCCA may be susceptible to treatment with immune checkpoint inhibitors for elevated antigen exposure as well as the local pro-inflammatory state in patients.

Among antigen presenting cells recruited to the tumor site, macrophages are often most abundant although their population is highly heterogeneous (29). Newly recruited macrophages adopt a pro-inflammatory phenotype designated as M1 macrophages, which have roles in mounting anti-cancer responses. However, once the tumor microenvironment is established, the M1 macrophages are educated into a pro-tumor

phenotype, M2 macrophages (29). The antitumor mechanisms of M2 macrophages include extracellular matrix remodeling, stimulation of tumor angiogenesis and more importantly inhibition of cytotoxic T-cell responses (45). Indeed, M2 macrophages in tumors are emerging as a key player for the efficacy of PD-1/PD-L1 checkpoint blockades and are frequently evaluated in clinical studies (46). In this study, we found that M2 macrophages highly infiltrate into eCCA and are present at either PD-L1 positive tumors or negative tumors. The presence of unusually high numbers of M2 macrophages in eCCA is still uncertain and, further, this recruitment is likely to be more common in hypoxic tumor tissue than normoxic tumor tissues (47). Concerning the dual role of TAMs in tumor sites, therapeutic protocol included the promotion of anti-cancer functions of M1 macrophages, the reduction of M2 macrophages, and the re-programming of M2 into M1 phenotype (48). Kidney and ovarian cancer are excellent examples of tumors with a distinguishable hybrid phenotype of TAMs that share both M1 and M2 properties, implicating ideal candidates for M1-targeted therapy (49,50). While in eCCA, we found that most macrophages display an M2 phenotype as almost all of the CD14⁺ cells also co-expressed CD163 protein. Therefore, rather than boosting local protective M1 macrophage responses, ablation or repolarization of M2 macrophages might contribute efficiently to eCCA treatments.

eCCA is a highly malignant carcinoma and so far, the role of chemotherapy or radiotherapy is uncertain (6). In our study, the PD-L1-positive eCCA with characteristics of markedly increased TILs density, notably CD8⁺ TILs, together with high HLA class I expression represented a group of patients who would benefit from PD-1/PD-L1-targeted therapies. For the other patients, combinations of therapies were likely required to recover HLA class I expression or to active suppression of inflammatory infiltration (34). Of note, the majority of eCCA in our series preferentially accumulated M2 macrophages, which have been proven to confer PD-1/PD-L1 blockade resistance (46). In view of our study and previous literature, we can speculate that the targeting macrophages in various ways within TME may lead to potent efficacy of PD-1/PD-L1 blockade.

Given that eCCA remains a rare disease in the world, the major limitation of our study is the relatively small number of cases and we attempted to assess different available correlations between immune features, clinicopathologic data and outcome. Other limitations include the retrospective design of this study and the lack of data available for response to PD-1/PD-L1 inhibitors. Future prospective studies with large cohorts of Chinese eCCA patients treated with PD-1/PD-L1 blockades are required to determine whether our findings are clinically meaningful.

Acknowledgements

This study was supported by Beijing Municipal Administration of Hospital's Mission Plan (Code: SML20152201) and Beijing Municipal Administration of Hospital's Clinical Medicine Development of Special Funding Support (Code: ZYLX201712)

References

- Razumilava N, Gores GJ. Cholangiocarcinoma. *Lancet*. 2014; 383:2168-2179.
- Khan SA, Toledano MB, Taylor-Robinson SD. Epidemiology, risk factors, and pathogenesis of cholangiocarcinoma. *HPB (Oxford)*. 2008; 10:77-82.
- Khan SA, Emadossadaty S, Ladep NG, Thomas HC, Elliott P, Taylor-Robinson SD, Toledano MB. Rising trends in cholangiocarcinoma: Is the ICD classification system misleading us? *J Hepatol*. 2012; 56:848-854.
- DeOliveira ML, Cunningham SC, Cameron JL, Kamangar F, Winter JM, Lillemoe KD, Choti MA, Yeo CJ, Schulick RD. Cholangiocarcinoma: Thirty-one-year experience with 564 patients at a single institution. *Ann Surg*. 2007; 245:755-762.
- Esnaola NF, Meyer JE, Karachristos A, Maranki JL, Camp ER, Denlinger CS. Evaluation and management of intrahepatic and extrahepatic cholangiocarcinoma. *Cancer*. 2016; 122:1349-1369.
- Khan SA, Davidson BR, Goldin RD, Heaton N, Karani J, Pereira SP, Rosenberg WM, Tait P, Taylor-Robinson SD, Thillainayagam AV, Thomas HC, Wasan H; British Society of Gastroenterology. Guidelines for the diagnosis and treatment of cholangiocarcinoma: An update. *Gut*. 2012; 61:1657-1669.
- Darwish Murad S, Kim WR, Harnois DM, *et al*. Efficacy of neoadjuvant chemoradiation, followed by liver transplantation, for perihilar cholangiocarcinoma at 12 US centers. *Gastroenterology*. 2012; 143:88-98.e83; quiz e14.
- Schweitzer N, Vogel A. Systemic therapy of cholangiocarcinoma: From chemotherapy to targeted therapies. *Best Pract Res Clin Gastroenterol*. 2015; 29:345-353.
- Massani M, Nistri C, Ruffolo C, Bonariol R, Pauletti B, Bonariol L, Caratozzolo E, Morana G, Bassi N. Intrahepatic chemotherapy for unresectable cholangiocarcinoma: review of literature and personal experience. *Updates Surg*. 2015; 67:389-400.
- Jiao Y, Pawlik TM, Anders RA, *et al*. Exome sequencing identifies frequent inactivating mutations in BAP1, ARID1A and PBRM1 in intrahepatic cholangiocarcinomas. *Nat Genet*. 2013; 45:1470-1473.
- Hay M, Thomas DW, Craighead JL, Economides C, Rosenthal J. Clinical development success rates for investigational drugs. *Nat Biotechnol*. 2014; 32:40-51.
- Topalian SL, Drake CG, Pardoll DM. Immune checkpoint blockade: A common denominator approach to cancer therapy. *Cancer cell*. 2015; 27:450-461.
- Mahoney KM, Freeman GJ, McDermott DF. The next immune-checkpoint inhibitors: PD-1/PD-L1 blockade in melanoma. *Clin Ther*. 2015; 37:764-782.
- Menon S, Shin S, Dy G. Advances in Cancer Immunotherapy in Solid Tumors. *Cancers (Basel)*. 2016; 8. pii: E106.
- Rizvi S, Khan SA, Hallemeier CL, Kelley RK, Gores GJ. Cholangiocarcinoma – evolving concepts and therapeutic strategies. *Nat Rev Clin Oncol*. 2018; 15:95-111.
- Walter D, Herrmann E, Schnitzbauer AA, Zeuzem S, Hansmann ML, Peveling-Oberhag J, Hartmann S. PD-L1 expression in extrahepatic cholangiocarcinoma. *Histopathology*. 2017; 71:383-392.
- Chaisaingmongkol J, Budhu A, Dang H, *et al*. Common Molecular Subtypes Among Asian Hepatocellular Carcinoma and Cholangiocarcinoma. *Cancer cell*. 2017; 32:57-70. e53.
- Enwere EK, Kornaga EN, Dean M, Koulis TA, Phan T, Kalantarian M, Kobel M, Ghatage P, Magliocco AM, Lees-Miller SP, Doll CM. Expression of PD-L1 and presence of CD8-positive T cells in pre-treatment specimens of locally advanced cervical cancer. *Mod Pathol*. 2017; 30:577-586.
- Maruse Y, Kawano S, Jinno T, Matsubara R, Goto Y, Kaneko N, Sakamoto T, Hashiguchi Y, Moriyama M, Toyoshima T, Kitamura R, Tanaka H, Oobu K, Kiyoshima T, Nakamura S. Significant association of increased PD-L1 and PD-1 expression with nodal metastasis and a poor prognosis in oral squamous cell carcinoma. *Int J Oral Maxillofac Surg*. 2018; 47:836-845.
- Zhao X, Subramanian S. Intrinsic resistance of solid tumors to immune checkpoint blockade therapy. *Cancer Res*. 2017; 77:817-822.
- Garrido F, Ruiz-Cabello F, Aptsiauri N. Rejection versus escape: The tumor MHC dilemma. *Cancer Immunol Immunother*. 2017; 66:259-271.
- Ma K, Wei X, Dong D, Wu Y, Geng Q, Li E. PD-L1 and PD-1 expression correlate with prognosis in extrahepatic cholangiocarcinoma. *Oncol Lett*. 2017; 14:250-256.
- Katsuya Y, Fujita Y, Horinouchi H, Ohe Y, Watanabe S, Tsuta K. Immunohistochemical status of PD-L1 in thymoma and thymic carcinoma. *Lung Cancer*. 2015; 88:154-159.
- Zhang QW, Liu L, Gong CY, Shi HS, Zeng YH, Wang XZ, Zhao YW, Wei YQ. Prognostic significance of tumor-associated macrophages in solid tumor: A meta-analysis of the literature. *PloS One*. 2012; 7:e50946.
- Kostine M, Briaire-de Bruijn IH, Cleven AHG, Vervat C, Corver WE, Schilham MW, Van Beelen E, van Boven H, Haas RL, Italiano A, Cleton-Jansen AM, Bovée JVMG. Increased infiltration of M2-macrophages, T-cells and PD-L1 expression in high grade leiomyosarcomas supports immunotherapeutic strategies. *Oncoimmunology*. 2018; 7:e1386828.
- Garrido F, Perea F, Bernal M, Sanchez-Palencia A, Aptsiauri N, Ruiz-Cabello F. The Escape of Cancer from T Cell-Mediated Immune Surveillance: HLA Class I Loss and Tumor Tissue Architecture. *Vaccines (Basel)*. 2017; 5. pii: E7.
- Quero L, Hanser E, Manigold T, Tiaden AN, Kyburz D. TLR2 stimulation impairs anti-inflammatory activity of M2-like macrophages, generating a chimeric M1/M2 phenotype. *Arthritis Res Ther*. 2017; 19:245.
- Sanmamed MF, Chen L. Inducible expression of B7-H1 (PD-L1) and its selective role in tumor site immune modulation. *Cancer J*. 2014; 20:256-261.
- Lee HW, Choi HJ, Ha SJ, Lee KT, Kwon YG. Recruitment of monocytes/macrophages in different tumor microenvironments. *Biochim Biophys Acta*. 2013;

- 1835:170-179.
30. Kyi C, Postow MA. Checkpoint blocking antibodies in cancer immunotherapy. *FEBS Lett.* 2014; 588:368-376.
 31. Drake CG, Lipson EJ, Brahmer JR. Breathing new life into immunotherapy: Review of melanoma, lung and kidney cancer. *Nat Rev Clin Oncol.* 2014; 11:24-37.
 32. Abou-Alfa GK, Andersen JB, Chapman W, *et al.* Advances in cholangiocarcinoma research: report from the third Cholangiocarcinoma Foundation Annual Conference. *J Gastrointest Oncol.* 2016; 7:819-827.
 33. Ueno T, Tsuchikawa T, Hatanaka KC, Hatanaka Y, Mitsuhashi T, Nakanishi Y, Noji T, Nakamura T, Okamura K, Matsuno Y, Hirano S. Prognostic impact of programmed cell death ligand 1 (PD-L1) expression and its association with epithelial-mesenchymal transition in extrahepatic cholangiocarcinoma. *Oncotarget.* 2018; 9:20034-20047.
 34. Zhang Y, Chen L. Classification of advanced human cancers based on tumor immunity in the MicroEnvironment (TIME) for cancer immunotherapy. *JAMA Oncol.* 2016; 2:1403-1404.
 35. Zou W, Chen L. Inhibitory B7-family molecules in the tumour microenvironment. *Nat Rev Immunol.* 2008; 8:467-477.
 36. Day D, Monjazeb AM, Sharon E, Ivy SP, Rubin EH, Rosner GL, Butler MO. From famine to feast: Developing early-phase combination immunotherapy trials wisely. *Clin Cancer Res.* 2017; 23:4980-4991.
 37. Wu P, Wu D, Li L, Chai Y, Huang J. PD-L1 and survival in Ssolid tumors: A meta-analysis. *PloS One.* 2015; 10:e0131403.
 38. Wei XL, Wu QN, Chen DL, Zeng ZL, Lu JB, Liu ZX, Ju HQ, Ren C, Pan ZZ, Wang FH, Xu RH. The clinical and biomarker association of programmed death ligand 1 and its spatial heterogeneous expression in colorectal cancer. *J Cancer.* 2018; 9:4325-4333.
 39. Jusakul A, Cutcutache I, Yong CH, *et al.* Whole-Genome and Epigenomic Landscapes of Etiologically Distinct Subtypes of Cholangiocarcinoma. *Cancer Discov.* 2017; 7:1116-1135.
 40. Parry RV, Chemnitz JM, Frauwirth KA, Lanfranco AR, Braunstein I, Kobayashi SV, Linsley PS, Thompson CB, Riley JL. CTLA-4 and PD-1 receptors inhibit T-cell activation by distinct mechanisms. *Mol Cell Biol.* 2005; 25:9543-9553.
 41. Tang Q, Nie F, Kang J, Ding H, Zhou P, Huang J. NIEluter: Predicting peptides eluted from HLA class I molecules. *J Immunol Methods.* 2015; 422:22-27.
 42. del Campo AB, Carretero J, Aptsiauri N, Garrido F. Targeting HLA class I expression to increase tumor immunogenicity. *Tissue Antigens.* 2012; 79:147-154.
 43. Aptsiauri N, Carretero R, Garcia-Lora A, Real LM, Cabrera T, Garrido F. Regressing and progressing metastatic lesions: resistance to immunotherapy is predetermined by irreversible HLA class I antigen alterations. *Cancer Immunol Immunother.* 2008; 57:1727-1733.
 44. Chang CC, Campoli M, Ferrone S. HLA class I defects in malignant lesions: what have we learned? *Keio J Med.* 2003; 52:220-229.
 45. Qian BZ, Pollard JW. Macrophage diversity enhances tumor progression and metastasis. *Cell.* 2010; 141:39-51.
 46. Santoni M, Romagnoli E, Saladino T, Foghini L, Guarino S, Capponi M, Giannini M, Cognigni PD, Ferrara G, Battelli N. Triple negative breast cancer: Key role of Tumor-Associated Macrophages in regulating the activity of anti-PD-1/PD-L1 agents. *Biochim Biophys Acta Rev Cancer.* 2018; 1869:78-84.
 47. Raggi F, Pelassa S, Pierobon D, Penco F, Gattorno M, Novelli F, Eva A, Varesio L, Giovarelli M, Bosco MC. Regulation of Human Macrophage M1-M2 Polarization Balance by Hypoxia and the Triggering Receptor Expressed on Myeloid Cells-1. *Front Immunol.* 2017; 8:1097.
 48. Noy R, Pollard JW. Tumor-associated macrophages: from mechanisms to therapy. *Immunity.* 2014; 41:49-61.
 49. Kovaleva OV, SamoiloVA DV, Shitova MS, Gratchev A. Tumor Associated Macrophages in Kidney Cancer. *Anal Cell Pathol (Amst).* 2016; 2016:9307549.
 50. Zhang M, He Y, Sun X, Li Q, Wang W, Zhao A, Di W. A high M1/M2 ratio of tumor-associated macrophages is associated with extended survival in ovarian cancer patients. *J Ovarian Res.* 2014; 7:19.

(Received January 11, 2019; Revised January 29, 2019; Accepted February 9, 2019)

Preoperative evaluation of the degree of liver fibrosis based on matter-element analysis using serological indicators in patients with hepatocellular carcinoma

Wei Liu^{1,§}, Xiaosong Li^{1,§}, Weihong Zheng², Rucheng Yao¹, Jun Zheng^{1,*}

¹ Department of Hepatopancreatobiliary Surgery, The First College of Clinical Medical Sciences, Three Gorges University, Yichang, Hubei, China;

² Department of Pharmacology, Medical Science College, Three Gorges University, Yichang, Hubei, China.

Summary

Evaluation of the degree of liver fibrosis is an important basis for the clinical diagnosis and treatment of patients with hepatocellular carcinoma (HCC). It is meaningful to make a preoperative evaluation with non-invasive methods. In the current study, 12 commonly used preoperative serological indicators from 161 HCC patients with different degree of liver fibrosis were collected retrospectively, and 8 of the indicators (ALB, PA, TBil, INR, AST, GGT, ALP, and PT) were ultimately used in matter-element analysis to create a formula. The relationship between those results and the histological sub-classification of the Laennec liver fibrosis scoring system was analyzed. The calculated value of R from this formula will indicate the differing degree of liver fibrosis in a patient: *i*) the value of $0.802 \leq R < 1$ indicates the early stage of liver cirrhosis, which corresponds to Laennec stages 0-3; *ii*) the value of $0.752 \leq R < 0.802$ indicates the mild stage of liver cirrhosis, which corresponds to Laennec stage 4A; *iii*) the value of $0.698 \leq R < 0.752$ indicates the moderate stage of liver cirrhosis, which corresponds to Laennec stage 4B; and *iv*) the value of $0.444 \leq R < 0.698$ indicates the severe stage of liver cirrhosis, which corresponds to Laennec stage 4C. The hope is that this formula for preoperative evaluation of the degree of liver fibrosis using non-invasive methods would be useful in the clinical diagnosis and treatment of patients with HCC in the future.

Keywords: Liver cirrhosis, Laennec system, matter-element analysis

1. Introduction

Cirrhosis is defined as regenerative nodules surrounded by extensive fibrosis (1). Liver fibrosis is a pathological process of abnormal proliferation of connective tissues caused by various pathogenic factors, in which excessive extracellular matrix proteins accumulate in the liver. Among the various causes of liver fibrosis, viral hepatitis, alcoholic liver, fatty liver, and autoimmune diseases are the most common in clinical settings (2-4). Without proper treatment, liver fibrosis

can eventually develop into cirrhosis and hepatocellular carcinoma (HCC) with the progression of the disease (5-7). Therefore, evaluation of the degree of liver fibrosis is an important basis for the clinical diagnosis and treatment of patients with the disease.

For semi-quantitative estimation of fibrosis, the Laennec system (Table 1) that is based on histological parameters of fibrous septa according to their width and number has been proposed. The Laennec system subdivides the most severe stage of fibrosis (F4) into 4A, 4B, and 4C in order to acknowledge the varying severity of cirrhosis (8-10). However, the Laennec system is based on histological parameters of fibrous septa. Preoperative evaluation of the degree of liver fibrosis based on a simple and effective non-invasive method would prove beneficial.

The search for disease-related biomarkers in plasma has made rapid progress over the past few years, and the

[§]These authors contributed equally to this work.

*Address correspondence to:

Dr. Jun Zheng, Department of Hepatopancreatobiliary Surgery, The First College of Clinical Medical Sciences, Three Gorges University, No. 183 Yiling Road, Yichang, Hubei 443003., China.

E-mail: zhengjun1995@163.com

significance of biomarkers in diagnosis of disease has been widely demonstrated (11). Determining a useful method of evaluating the degree of liver fibrosis with serological biomarkers would be of great significance.

Various scoring formulae have been devised to evaluate HCC with serological biomarkers (12). A previous study by the current authors found that a scoring formula for liver injury (SFLI) was useful in the assessment of liver damage (13). SFLI was based on matter-element analysis. In the current study, matter-element analysis was used to create a formula based on serological indicators to facilitate preoperative evaluation of the degree of liver fibrosis in patients with HCC. The relationship between those results and the histological sub-classification of the Laennec system was analyzed.

2. Materials and Methods

2.1. Study population

From June 2010 to June 2015, 362 patients with HCC were treated in the Department of Liver Surgery of Yichang Central People's Hospital; 300 of those patients were diagnosed with different degrees of liver fibrosis. Patients under 30 years of age or over 70 years of age were excluded, patients with active hepatitis, patients using immunosuppressive or antiviral drugs, and patients with HIV, HCV, decompensation of the liver, alcoholic hepatitis, or an autoimmune disease were also excluded. Ultimately, 161 patients were enrolled in this study.

Data such as the patient's medical history, results of physical examinations, results of B-mode ultrasound, computed tomography (CT) scans, magnetic resonance imaging (MRI) scans, biochemistry, and results of post-operative pathology were retrospectively collected for all 161 patients. Paraffin-embedded specimens were obtained from Yichang Central People's Hospital for research purposes. This study was approved by the Ethics Committee of the First Clinical Medicine College Hospital of China Three Gorges University.

2.2. Collection of data on serological indicators

Data on the following 12 commonly used serological indicators were collected in this study: serum albumin (ALB), prealbumin (PA), serum total bilirubin (TbIL), the international normalized ratio (INR), aspartate aminotransferase (AST), gamma-glutamyl transpeptidase (GGT), alkaline phosphatase (ALP), prothrombin time (PT), serum creatinine (SCr), alanine aminotransferase (ALT), activated partial thromboplastin time (APTT), and thrombin time (TT). The serological indicators were collected in the first morning when the patients visited the doctors.

The normal values for these indicators were: ALB,

35-55 g/L; PA, 100-400 mg/L; TBiL, 2.04-20.4 μmol/L; INR, 0.8-1.5; AST, 0-40 U/L; GGT, 0-54 U/L; ALP, 39-117 U/L; PT, 11-13s; SCr, 70-106 μmol/L; ALT, 0-40 U/L; APTT, 28-41s; TT, 13-18s.

In order to comply with the statistical principles of matter-element analysis, the 161 patients were divided into 8 groups by age: 30-34, 35-39, 40-44, 45-49, 50-54, 55-59, 60-64, and 65-69.

2.3. Pathological grading according to the Laennec system

After they were embedded in paraffin, 161 liver tissue specimens were cut into sections. Masson trichrome staining was performed as usual. All pathological sections were graded independently by two pathologists in this Hospital, the samples with the same result were selected and graded according to the Laennec liver fibrosis scoring system (9,14).

In accordance with the histological sub-classification of the Laennec system (Table 1), liver fibrosis in 161 patients was divided into 7 degrees from mild to severe. Liver fibrosis was grades 0-3 (the early stage of liver cirrhosis) in 15 patients, grade 4A (the mild stage of liver cirrhosis) in 42, grade 4B (the moderate stage of liver cirrhosis) in 55, and grade 4C (the severe stage of liver cirrhosis) in 49.

2.4. Creation of a scoring formula using matter-element analysis

In the process of creating a mathematical formula to score liver fibrosis, matter-element analysis was mainly used to solve for the weight of each detection index. The R value was calculated according to the fibrosis scoring formula. The method used was as follows:

(1) The age range of patients in the experiment was considered to be T_m , each measurement indicator was considered to be C_n , and the obtained data were considered to be X_{ji} ($j=1,2,\dots,m; i=1,2,\dots, n$). The following matter elements were successfully constructed:

		T_1	T_2	...	T_m
$R_{nm} =$	C_1	X_{11}	X_{21}	...	X_{m1}
	C_2	X_{12}	X_{22}	...	X_{m2}

	C_n	X_{1n}	X_{2n}	...	X_{mn}

(2) Determination of the membership degree (U): in order to obtain the weight of each measurement indicator in the fibrosis scoring formula, a measurement standard should be determined. This standard was determined using membership degree (U), which was

determined using the following method:

smaller measurement values indicated better results:

$$U_{ji} = \frac{\max X_{ji} - X_{ji}}{\max X_{ji} - \min X_{ji}}$$

greater measurement values indicated better results:

$$U_{ji} = \frac{X_{ji} - \min X_{ji}}{\max X_{ji} - \min X_{ji}}$$

where $\max X_{ji}$ and $\min X_{ji}$, represent the corresponding maximum and minimum values of X_{ji} in each age group respectively.

(3) Conversion of the membership degree into relevance: the relevance conversion is the conversion between the degree of membership and the correlation coefficient. Since the correlation coefficient (ξ) is equivalent to the membership function, the correlation coefficient ξ_{ji} can be determined from the membership coefficient U_{ji} , namely: $\xi_{ji} = U_{ji}$ ($j=1,2,\dots,m; i=1,2,\dots,n$).

(4) Establishment of the fuzzy matter element:

		P_1	P_2	...	P_m
$R_\xi =$	C_1	ξ_{11}	ξ_{21}	...	ξ_{m1}
	C_2	ξ_{12}	ξ_{22}	...	ξ_{m2}

	C_n	ξ_{1n}	ξ_{2n}	...	ξ_{mn}

(5) Solving the weight for each indicator in the fibrosis scoring formula

W_j represents the weight for each indicator:

$$W_j = \frac{m}{\sum_{j=1}^m \xi_{ji}} / \frac{n}{\sum_{i=1}^n \xi_{ji}}$$

And

		C_1	C_2	...	C_n
$R_w =$	W_j	W_1	W_2	...	W_n

2.5. Statistical analysis

All of the determined indicators were used to construct

a table, and Excel and the statistical software SPSS 18.0 were used to perform statistical analysis. The results are expressed as the mean + SD ($\pm S$). LSD and SNK were used when homogeneity of variance was present in group pair-wise comparisons, or Tamhane's T2 was more appropriate. ALB, PA, TBI, L, SCr, INR, ALT, AST, gamma-GT, ALP, PT, and APTT were compared with their corresponding normal values. An Excel function was used to perform a *t*-test and the software SPSS18.0 was used to perform a *t*-test and analysis of variance. $p < 0.05$ served as the level of significance, and $p < 0.01$ indicated a significant difference.

The one-way analysis of variance was performed if the obtained data followed a normal distribution. Otherwise, the Kruskal Wallis test was used instead to analyze the correlation. In addition, Spearman rank correlation analysis was used in the correlation of all indexes and pathological diagnosis of the stage of liver fibrosis.

3. Results

3.1. Screening on preoperative serological indicators

Serological indicators and the stage of fibrosis were analyzed in the 161 patients according to the Laennec liver fibrosis scoring system (Table 1). Correlation analysis indicated that 11 of the 12 indicators were correlated with the Laennec liver fibrosis scoring system (Table 2), although some of the correlations were relatively weak ($r_s < 0.4$). To optimize indicator selection, APTT and TT were excluded from analysis since these two indicators had a very low correlation. SCr was also excluded because its *p* value was greater than 0.05. Moreover, ALT was excluded since it belongs to the same system as AST, and AST is reported to be more strongly correlated with liver fibrosis than ALT (15).

Ultimately, 8 indicators – ALB, PA, TBI, L, INR, AST, GGT, ALP, and PT – were selected for use in creating a formula using matter-element analysis.

3.2. Creation of the liver fibrosis formula

A database of the 8 preoperative serological indicators was created, and statistical analysis was performed using the statistical software SPSS18.0. Patients were divided into 8 age groups in increments of 5 years. Comparison between groups was performed with the range of reference values and the overall mean according to the *t*-test. A result greater than the upper limit or less than the lower limit was considered significant, with a test level (α) of 0.05. Indicators resulting in significant differences were incorporated into the element of matter-element analysis, and the liver fibrosis formula was then created.

Liver fibrosis in the 161 patients was classified as grades 0, 1, 2, 3, 4A, 4B, and 4C. The 8 preoperative

Table 1. The Laennec liver fibrosis scoring system in liver biopsies*

Stage	Name	Septa (thickness and number)	Criteria	Score
0	No definite fibrosis	+/-	No definite fibrosis.	0
1	Minimal fibrosis	+	No septa or rare thin septum; may have portal expansion or mild sinusoidal fibrosis.	1
2	Mild fibrosis	++	Occasional thin septa; may have portal expansion or mild sinusoidal fibrosis.	2
3	Moderate fibrosis	+++	Moderate thin septa; up to incomplete cirrhosis.	3
4A	Cirrhosis, mild, definite, or probable	++++	Marked septation with rounded contours or visible nodules; Most septa are thin (one broad septum allowed).	4
4B	Moderate cirrhosis	+++++	At least two broad septa, but no very broad septa and less than half of biopsy length composed of minute nodules	5
4C	Severe cirrhosis	+++++	At least one very broad septum or more than half of biopsy length composed of minute nodules (micronodular cirrhosis)	6

*Histological sub-classification according to the Laennec system based on references (9,14).

Table 2. Spearman correlation analysis between serum markers and the Laennec liver fibrosis scoring system

Serum markers	r _s	p value
ALB (g/L)	- 0.213	0.003
PA (mg/L)	- 0.344	0.000
TBiL (µmol/L)	0.232	0.041
INR	0.128	0.000
AST (U/L)	0.357	0.000
GGT (U/L)	0.311	0.002
ALP (g/L)	0.212	0.004
PT (s)	0.198	0.048
SCr (µmol/L)	0.358	0.435
ALT (U/L)	0.214	0.000
APTT (s)	0.111	0.025
TT (s)	0.125	0.032

ALB, albumin; PA, prealbumin; TBiL, total bilirubin; INR, international normalized ratio; AST, aspartate aminotransferase; GGT, gamma-glutamyl transpeptidase; ALP, alkaline phosphatase; PT, prothrombin time; SCr, serum creatinine; ALT, alanine aminotransferase; APTT, activated partial thromboplastin time; TT, thrombin time.

*p < 0.05 or **p < 0.01 vs. normal value.

serological indicators from those 161 patients were substituted into the liver fibrosis scoring formula to calculate the R value. The R value was then compared to the Laennec liver fibrosis scoring system, and a grading standard for the liver fibrosis scoring formula was obtained.

Using matter-element analysis, the following liver fibrosis formula was created with the 8 preoperative serological indicators:

$$R = a \times \frac{ALB - 22.17}{49.56} + b \times \frac{PA - 4.7}{202.6} + c \times \frac{117.9 - TBiL}{113.98} + d \times \frac{2.36 - INR}{1.56} + e \times \frac{304 - AST}{289} + f \times \frac{774 - GGT}{759} + g \times \frac{646 - ALP}{594} + h \times \frac{28.5 - PT}{17.7}$$

In this formula, ALB, PA, TBiL, INR, AST, GGT, ALP, and PT represent the clinical levels of these 8 indicators. The weights are represented by a-h, and they were determined using matter-element analysis. From a-h, the determined values were 0.0739, 0.1694, 0.0519, 0.0029, 0.1467, 0.1663, 0.3527, and 0.0362. The pre-set data are from the 161 patients; 22.17 and 4.7 are the minimum detected values for ALB and PA, respectively, whereas 117.9, 2.36, 304, 774, 646, and 28.5 represent the maximum clinical values for TBiL, INR, AST, GGT, ALP, and PT, respectively (Table 3). The values of the denominators in the formula were equal to the maximum values minus the minimum values. The value of R calculated using this formula will indicate the patient's stage of liver fibrosis.

3.3. Degree of liver fibrosis according to the R value

Based on the R value according to the above formula, different degrees of liver fibrosis were identified: *i*) the value of $0.802 \leq R < 1$ indicates the early stage of liver cirrhosis, which corresponds to Laennec stages 0-3; *ii*) the value of $0.752 \leq R < 0.802$ indicates the mild stage of liver cirrhosis, which corresponds to Laennec stage 4A; *iii*) the value of $0.698 \leq R < 0.752$ indicates the moderate stage of liver cirrhosis, which corresponds to Laennec stage 4B; and *iv*) the value of $0.444 \leq R < 0.698$ indicates the severe stage of liver cirrhosis, which corresponds to Laennec stage 4C. In addition, $R = 1$ indicates normal liver tissue, representing well liver function.

4. Discussion

Liver cirrhosis is a disease that affects a massive number

Table 3. Test results of liver fibrosis indicators for different age groups

Age (years)	n	ALB (g/L)	PA (mg/L)	Tbil (μ mol/L)	INR	AST (U/L)	GGT (U/L)	ALP (g/L)	PT (s)
Normal values	161	35 - 55	100 - 400	2.04 - 20.4	0.8 - 1.5	0 - 40	0 - 54	39 - 117	11 - 13
30 - 34	6	34.82 \pm 6.41	124.61 \pm 72.01	38.69 \pm 17.57	1.28 \pm 0.19**	70.83 \pm 71.39**	94.28 \pm 115.83*	122.43 \pm 91.34	14.12 \pm 2.45**
35 - 39	23	35.24 \pm 5.61	133.48 \pm 67.32*	35.82 \pm 72.29**	1.23 \pm 0.17**	71.06 \pm 64.01**	96.78 \pm 112.45**	121.43 \pm 67.69	13.65 \pm 2.17**
40 - 44	27	35.16 \pm 5.69	132.50 \pm 71.65**	31.73 \pm 42.65**	1.17 \pm 0.16**	70.21 \pm 71.44**	134.32 \pm 120.35**	132.56 \pm 98.87**	13.17 \pm 2.63
45 - 49	38	35.89 \pm 5.42*	129.37 \pm 68.51*	28.32 \pm 62.21**	1.16 \pm 0.15**	71.81 \pm 67.79**	125.44 \pm 134.39**	137.23 \pm 89.19	13.10 \pm 2.82
50 - 54	26	33.96 \pm 5.59**	119.54 \pm 81.20**	26.89 \pm 56.43*	1.19 \pm 0.14**	69.36 \pm 81.33**	125.21 \pm 113.64**	121.34 \pm 86.23	13.86 \pm 2.21**
55 - 59	21	33.51 \pm 7.07**	121.46 \pm 59.26**	27.05 \pm 82.26*	1.15 \pm 0.16**	67.60 \pm 43.12*	123.89 \pm 132.24**	128.54 \pm 101.37	14.02 \pm 2.14
60 - 64	11	34.21 \pm 6.37**	114.59 \pm 87.31**	32.49 \pm 55.73	1.12 \pm 0.19**	72.97 \pm 69.45**	116.14 \pm 125.38*	129.32 \pm 83.46	13.11 \pm 2.76
65 - 69	9	33.42 \pm 5.81	125.48 \pm 68.24*	38.45 \pm 72.29**	1.10 \pm 0.13**	68.38 \pm 75.24**	114.54 \pm 115.04**	135.12 \pm 99.87	12.48 \pm 2.38

ALB, albumin; PA, prealbumin; Tbil, total bilirubin; INR, international normalized ratio; AST, aspartate aminotransferase; GGT, gamma-glutamyl transpeptidase; ALP, alkaline phosphatase; PT, prothrombin time. * $p < 0.05$ or ** $p < 0.01$ vs. normal value.

of patients worldwide. As this disease progresses, it is more difficult to cure clinically. Many cases of liver fibrosis develop into liver cirrhosis and even liver cancer due to delayed diagnosis. Therefore, liver cirrhosis needs to be properly diagnosed and staged.

A liver biopsy is still considered to be the "gold standard" for evaluating the severity of liver cirrhosis (16,17). For example, the pathological grading of fibrosis in China is divided into four stages according to the prevention and treatment of viral hepatitis, and liver cirrhosis is the highest level. Nonetheless, long-term clinical practice has revealed that conditions differ in different patients with liver cirrhosis, challenging classification based on a liver biopsy. The traumatic consequences of liver biopsy are discouraging to most patients and could result in accidental deaths in extreme cases.

To overcome the aforementioned problems with liver biopsy, some studies have developed mathematical methods to evaluate liver function. The semi-quantitative Child-Pugh score is widely used to evaluate liver function, and it takes into account both clinical and biochemical parameters in patients with liver cirrhosis (18). Recent studies have also found that the MELD score was better at assessing the severity and prognosis of end-stage liver diseases than the Child-Pugh score (19-21).

Another important factor for evaluating the clinical treatment of liver cirrhosis is the stage. The Laennec liver fibrosis scoring system is widely used in clinical settings, and it divides liver cirrhosis into several levels according to the thickness of the fibrous septa and regenerative nodules. However, the Laennec system is not flawless. In some cases, stage 4C liver fibrosis was expected to improve to stage 4A after anti-fibrosis therapy, but the grading system could not accurately identify that improvement, which could lead to false conclusions. Therefore, more accurate grading methods need to be devised to classify liver cirrhosis in more detail (22-25).

The liver has a variety of metabolic functions, and it also has a strong capacity for storage, compensation, and regeneration. When the liver is damaged to a certain extent, the amount of some substances synthesized and secreted by the liver or the activity of some enzymes in serum will be abnormal. Detection of these indicators can indicate liver damage and pathological changes. SFLI was obtained using matter-element analysis, and studies have indicated that its results agree with the Child-Pugh classification and also provide a more objective basis for early diagnosis, grading of liver function, and determination of the development of liver cirrhosis and its prognosis (12,13). Liver fibrosis is a process of abnormal proliferation of connective tissue in the liver caused by various pathogenic factors. All liver injury and repair and healing processes cause fibrosis, which is accompanied by the expression or

inhibition of fibrosis-related proteins. Therefore, the current study used matter-element analysis to create a formula based on serological indicators in order to facilitate preoperative evaluation of the degree of liver fibrosis in patients with HCC. This study also analyzed the relationship between the results of that formula and histological sub-classification of the Laennec system. The hope is to devise a simple and universally acceptable method that can indicate the degree of liver fibrosis in patients with HCC in a short of time following a clinical examination.

In conclusion, 8 preoperative serological indicators (ALB, PA, TBil, INR, AST, GGT, ALP, and PT) were retrospectively determined in 161 patients with HCC and different degrees of liver fibrosis to establish a formula using matter-element analysis. The hope is that such a formula for preoperative evaluation of the degree of liver fibrosis using non-invasive methods would be useful in the clinical diagnosis and treatment of patients with HCC in the future.

Acknowledgements

The authors wish to thank Dr. Xiao Tan and Professor Sen Liu (China Three Gorges University) for helpful discussions and thank the members of the Department of Pathology of Yichang Central Hospital for their outstanding technical assistance. This work was financially supported by China Three Gorges University (2015KZL14).

References

- Schuppan D, Afdhal NH. Liver cirrhosis. *Lancet*. 2008; 371:838-851.
- Schiff ER, Sorrell MF, Maddrey EC, editors. *Schiff's Diseases of the Liver*. 9th Edition Lippincott, Williams & Wilkins; Philadelphia: 2003.
- Sherlock S, Dooley J, editors. *Diseases of the Liver and Biliary System*. 11th Edition Blackwell Science; Oxford, UK; Malden, MA: 2002.
- Bircher J, Benhamou JP, McIntyre N, Rizzetto M, Rodes J, editors. *Oxford Textbook of Clinical Hepatology*. 2nd Edition Oxford University Press; 1999.
- Bravo AA, Sheth SG, Chopra S. Liver biopsy. *N Engl J Med*. 2001; 344:495-500.
- Baranova A, Lal P, Biredinc A, Younossi ZM. Non-invasive markers for hepatic fibrosis. *BMC Gastroenterol*. 2011; 11:91.
- Wanless IR, Nakashima E, Sherman M. Regression of human cirrhosis. Morphologic features and the genesis of incomplete septal cirrhosis. *Arch Pathol Lab Med*. 2000; 124:1599-1607.
- Wang W, Li J, Pan R, A S, Liao C. Association of the Laennec staging system with degree of cirrhosis, clinical stage and liver function. *Hepatol Int*. 2015; 9:621-626.
- Kim SU, Oh HJ, Wanless IR, Lee S, Han KH, Park YN. The Laennec staging system for histological sub-classification of cirrhosis is useful for stratification of prognosis in patients with liver cirrhosis. *J Hepatol*. 2012;57:556-563.
- Almpanis Z, Demonakou M, Tiniakos D. Evaluation of liver fibrosis: "Something old, something new...". *Ann Gastroenterol*. 2016; 29:445-453.
- Smith JO, Sterling RK. Systematic review: Non-invasive methods of fibrosis analysis in chronic hepatitis C. *Aliment Pharmacol Ther*. 2009; 30:557-576.
- Zheng J, Xing RC, Zheng WH, Liu W, Yao RC, Li XS, Du JP, Li L. A comparative study on postoperative mortality prediction of SFLI scoring system and Child-Pugh classification in patients with hepatocellular carcinoma. *J BUON*. 2017; 22:709-713.
- Liu W, Zheng J, Xing R. Clinical significance of a scoring formula of liver injury for the preoperative evaluation of patients with liver cirrhosis. *Eur J Gastroenterol Hepatol*. 2014; 26:95-100.
- Kim MY, Cho MY, Baik SK, Park HJ, Jeon HK, Im CK, Won CS, Kim JW, Kim HS, Kwon SO, Eom MS, Cha SH, Kim YJ, Chang SJ, Lee SS. Histological subclassification of cirrhosis using the Laennec fibrosis scoring system correlates with clinical stage and grade of portal hypertension. *J Hepatol*. 2011; 55:1004-1009.
- Ding XJ, Li SB, Li SZ, Liu HS, Liu B, Xu FM, Gu RW. A quantitative of the relationship between levels of liver fibrosis markers in sera and fibrosis stages of liver tissues of patients with of chronic hepatic diseases. *Zhonghua Gan Zang Bing Za Zhi*. 2005; 13:911-914. (in Chinese)
- Sebastiani G, Alberti A. Non-invasive fibrosis biomarkers reduce but not substitute the need for liver biopsy. *World J Gastroenterol*. 2006; 12:3682-3694.
- Sebastiani G. Non-invasive assessment of liver fibrosis in chronic liver diseases: Implementation in clinical practice and decisional algorithms. *World J Gastroenterol*. 2009; 15:2190-2203.
- Manley BJ, Tennenbaum DM, Vertosick EA, Hsieh JJ, Sjoberg DD, Assel M, Benfante NE, Strobe SA, Kim E, Casuscelli J, Becerra MF, Coleman JA, Hakimi AA, Russo P. The difficulty in selecting patients for cytoreductive nephrectomy: An evaluation of previously described predictive models. *Urol Oncol*. 2017; 35(:35.e1-35.e5.
- Nishikawa H, Osaki Y. Liver cirrhosis: Evaluation, nutritional status, and prognosis. *Mediators Inflamm*. 2015; 2015:872152.
- Gallegos-Orozco JF, Vargas HE. Liver transplantation: From Child to MELD. *Med Clin North Am*. 2009; 93:931-950.
- Kamath PS, Wiesner RH, Malinchoc M, Kremers W, Therneau TM, Kosberg CL, D'Amico G, Dickson ER, Kim WR. A model to predict survival in patients with end-stage liver disease. *Hepatology*. 2001; 33:464-470.
- Davis GL, Esteban-Mur R, Rustgi V, Hoefs J, Gordon SC, Trepo C, Shiffman ML, Zeuzem S, Craxi A, Ling MH, Albrecht J. Interferon alfa-2b alone or in combination with ribavirin for the treatment of relapse of chronic hepatitis C. International Hepatitis Interventional Therapy Group. *N Engl J Med*. 1998; 339:1493-1499.
- Lai CL, Chien RN, Leung NW, Chang TT, Guan R, Tai DI, Ng KY, Wu PC, Dent JC, Barber J, Stephenson SL, Gray DF. A one-year trial of lamivudine for chronic hepatitis B. Asia Hepatitis Lamivudine Study Group. *N Engl J Med*. 1998; 339:61-68.
- McHutchison JG, Gordon SC, Schiff ER, Shiffman ML, Lee WM, Rustgi VK, Goodman ZD, Ling MH, Cort S, Albrecht JK. Interferon alfa-2b alone or in combination

- with ribavirin as initial treatment for chronic hepatitis C: Hepatitis Interventional Therapy Group. *N Engl J Med.* 1998; 339:1485-1492.
25. Shiratori Y, Imazeki F, Moriyama M, Yano M, Arakawa Y, Yokosuka O, Kuroki T, Nishiguchi S, Sata M, Yamada G, Fujiyama S, Yoshida H, Omata M. Histologic improvement of fibrosis in patients with hepatitis C who have sustained response to interferon therapy. *Ann Intern Med.* 2000; 132:517-524.

(Received November 30, 2018; Revised February 15, 2019; Accepted February 26, 2019)

Prognosis for patients with hepatocellular carcinoma (HCC) with bile duct tumor thrombus (BDTT) after surgical treatment

Zhichuan Lin*, Mingrui Han, Zhi Zhou

Department of Hepatobiliary Surgery, Zhangzhou Affiliated Hospital, Fujian Medical University, Zhangzhou, Fujian, China.

Summary

Hepatocellular carcinoma (HCC) with bile duct tumor thrombus (BDTT) is rarely seen in clinical practice, and its treatment strategies and prognosis are still a subject of debate. To ascertain the characteristics of and prognosis for HCC with BDTT, 49 patients with HCC with BDTT were studied out of 763 consecutive patients with HCC who underwent surgical treatment from July 2004 to May 2018. The clinical characteristics of and prognosis for those 49 patients were reviewed and analyzed retrospectively. Of the 49 patients, 25 underwent radical resection, 7 underwent thrombectomy through a choledochotomy, and 17 underwent palliative internal and external bile duct drainage. Results indicated that patients who underwent a radical resection had a better prognosis than patients in the other two groups, with a median survival of 19 months vs. 8 months and 3 months ($p < 0.001$). Moreover, the preoperative bilirubin level ($p = 0.025$), intraoperative blood loss ($p = 0.006$), tumor size ($p = 0.005$), and the presence of portal and hepatic vein tumor thrombi ($p = 0.021$) were significant prognostic factors associated with long-term survival for patients who underwent radical resection in this study. Radical resection should be performed with adequate preoperative preparation for patients with HCC with BDTT in whom surgery is not contraindicated.

Keywords: Hepatocellular carcinoma (HCC), bile duct tumor thrombus (BDTT), surgical treatment

1. Introduction

Hepatocellular carcinoma (HCC) is the fifth most common malignancy worldwide, with > 500,000 new cases annually, and it is the second leading cause of cancer-related mortality worldwide (1,2). The incidence of HCC is increasing worldwide and especially in Asian-Pacific countries, and half of all cases occur in China (3). HCC with bile duct tumor thrombus (BDTT) is rarely seen in clinical practice, and its incidence has been reported to be 1.2-12.9% (4-9). Due to a lack of awareness of HCC with BDTT, some patients fail to receive effective treatment. This is especially true for those with obstructive jaundice who are considered to be in the late stage of tumor progression.

The principle for surgical treatment of HCC with BDTT is the removal of primary HCC and BDTT, and active surgical resection may benefit patients (10-12). Patients with HCC and BDTT may undergo radical resection, thrombectomy through a choledochotomy, palliative internal and external bile duct drainage, or transarterial chemoembolization (TACE) depending on the type of BDTT. However, the treatment strategies and prognosis for patients with HCC with BDTT are still a subject of debate (13,14).

To ascertain the characteristics of and prognosis for HCC with BDTT, clinical features of and surgical outcomes for patients who underwent different surgical treatments were retrospectively analyzed. The prognostic factors associated with long-term survival for patients with HCC with BDTT who underwent radical resection were also analyzed in this study.

2. Patients and Methods

2.1. Patients

From July 2004 to May 2018, a total of 763 consecutive

Released online in J-STAGE as advance publication February 27, 2019.

*Address correspondence to:

Dr. Zhichuan Lin, Department of Hepatobiliary Surgery, Zhangzhou Affiliated Hospital, Fujian Medical University, No. 59 Shengli West Road, Xiangcheng District, Zhangzhou, Fujian, China.

E-mail: linzhichuan1976@163.com

patients with HCC underwent surgical treatment out of 4,693 patients with primary HCC who were treated at Zhangzhou Hospital affiliated with Fujian Medical University. Of these patients, 49 were identified as having HCC with BDTT (Figure 1), accounting for 1.04% (49/4693) of all patients with primary HCC and 6.42% (49/763) of patients who underwent HCC resection.

The medical records of those 49 patients, including the characteristics of their underlying liver disease, tumor characteristics, and prognosis were retrospectively reviewed.

2.2. Diagnosis and classification

The workup before surgical treatment included

liver function tests, viral screening, and imaging studies. Laboratory results were obtained upon admission before surgical treatment. Tumors were evaluated using abdominal ultrasonography (US), computed tomography (CT), hepatic angiography, and magnetic resonance imaging (MRI). If necessary, direct cholangiography [percutaneous transhepatic cholangiography and drainage (PTCD) or endoscopic retrograde cholangiography (RECP)] or magnetic resonance cholangiopancreatography (MRCP) was performed before surgery to evaluate the extent of biliary invasion. Bile duct invasion by HCC was suspected when peripheral bile duct dilatation or tumor thrombus was detected on US or CT, and bile duct invasion was confirmed with direct cholangiography or MRCP as

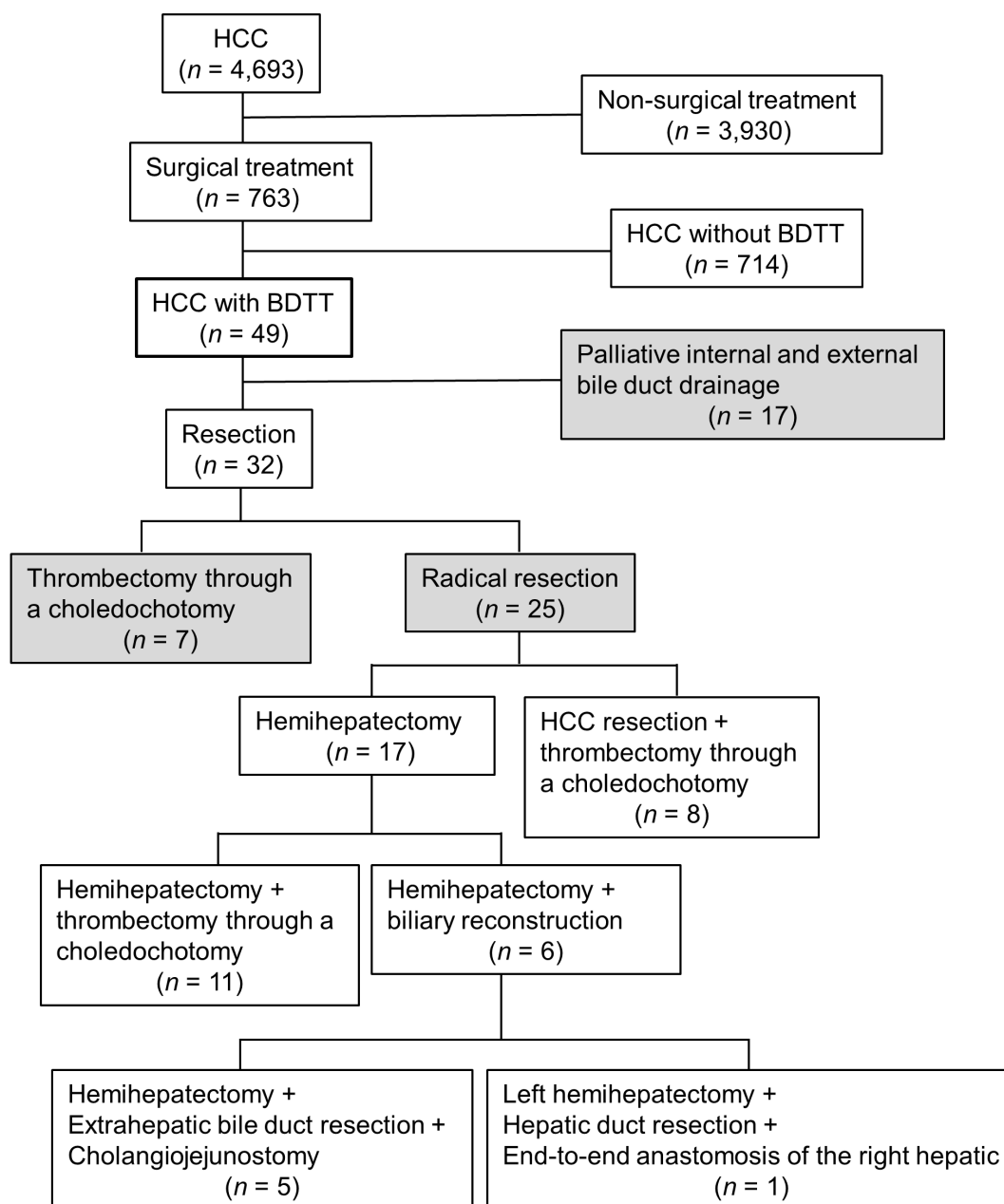


Figure 1. Flow chart for patients included in this study. BDTT, bile duct tumor thrombus; HCC, hepatocellular carcinoma.

obstruction or stenosis of the biliary trees.

The tumor thrombus was histopathologically examined in patients with HCC with BDTT who underwent surgical treatment.

The Ueda (6) classification of HCC with BDTT was used in this study: *i*) type I: BDTT located in the secondary branch of the bile duct tree; *ii*) type II: BDTT extending to the first branch of the bile duct tree; *iii*) type IIIa: BDTT extending to the common hepatic duct; type III: an implanted tumor growing in the CBD, and *iv*) type IV: floating tumor debris from the ruptured tumor in CBD (15).

2.3. Treatment strategies

Resectability was determined based on the patient's general condition, tumor status, pre-operative liver function tests, preoperative diagnosis of the location of the primary tumors, extension of BDTT, and the future remnant liver parenchyma.

Patients with HCC with BDTT who had an unresectable tumor or in whom a lesion could not be found underwent thrombectomy through a choledochotomy.

Patients with advanced disease or disease complicated by chronic diseases and without surgical indications underwent palliative internal and external bile duct drainage (PTCD, ERCP, or intraductal stent drainage) or TACE.

2.4. Follow-up

During the first 3 months after surgical treatment, patients were re-examined every month. Afterwards, patients were re-examined every 3 months. Clinical, laboratory, and radiological data were collected during each follow-up visit.

All patients were followed until October 2018. Survival was measured from the time of surgical treatment, and death was the endpoint.

2.6. Statistical analysis

The statistical software SPSS 19.0 was used for statistical analysis. The life table method was used to estimate the survival rate, and the survival analysis was based on the log-rank (Mantel-Cox) method. Quantitative data are expressed as the mean \pm standard deviation (mean \pm S.D.). Qualitative data were tested using the Chi-square test. Statistical significance was defined as a *p* value $<$ 0.05.

3. Results

3.1. Clinicopathological data

Forty-nine patients with HCC and BDTT were enrolled

in this study, including 43 males and 6 females with an average age of 55.51 ± 13.09 years. Out of 49 patients, 33 (67.35%) had different degrees of yellowing of the whites of the eyes and the skin as well as dark urine with elevated bilirubin levels ranging from 34.6 to 505.0 $\mu\text{mol/L}$. Some patients had a fever, abdominal pain, bloating, pruritus, and paler stool. Thirty-two patients (65.31%) had an elevated alpha-fetoprotein (AFP) level, and 41 patients (83.67%) tested positive for hepatitis B virus surface antigen (HBsAg).

Out of 49 patients, 35 (71.43%) were diagnosed with HCC with BDTT before surgical treatment. Of the 14 remaining patients (14/49, 28.57%), 11 were misdiagnosed as having hilar cholangiocarcinoma, 1 was misdiagnosed as having ampullary carcinoma, 1 was misdiagnosed as having pancreatic head cancer, and 1 was misdiagnosed as having bile duct stones.

Results of diagnostic ultrasonography were positive in 14.29% of patients (7/49), CT results were positive in 35.00% (14/40), and MRCP results were positive in 59.18% (29/49). A biliary tumor thrombus was diagnosed with ERCP at a rate of 100% (8/8).

The tumor thrombus was histopathologically examined in patients with HCC with BDTT who underwent surgical treatment (Figure 2). HCC with BDTT was divided into the following categories: a simple tumor thrombus and a blood clot mixed with a tumor thrombus. The BDTT was yellowish, brownish, or purplish-black in color and had a pathological type identical to that of a hepatic primary tumor.

According to the Ueda classification of HCC with BDTT, 2 patients had type I tumors, 2 had type II, 42 had type III, and 3 had type IV.

3.2. Surgical treatment

Twenty-five patients underwent radical resection, 7 underwent thrombectomy through a choledochotomy, and 17 underwent palliative internal and external bile duct drainage (Figure 1).

Out of 25 patients who underwent radical resection, 2 had type I tumors, 2 had type II, and 21 had type III according to the Ueda classification. Seventeen patients underwent hemihepatectomy, including 11 who underwent hemihepatectomy plus thrombectomy through a choledochotomy (Figure 3A) and 6 who underwent biliary reconstruction (Figure 3B and 3C). Of the 6 patients who underwent biliary reconstruction, 5 underwent hemihepatectomy plus extrahepatic bile duct resection plus cholangiojejunostomy and 1 underwent left hemihepatectomy plus common hepatic duct resection plus end-to-end anastomosis of the right hepatic duct to the common bile duct. In addition, 8 patients in this group underwent HCC resection plus thrombectomy through a choledochotomy due to severe cirrhosis (Figure 3D), and the surgical margin was greater than 1 cm.

Seven patients underwent thrombectomy through a

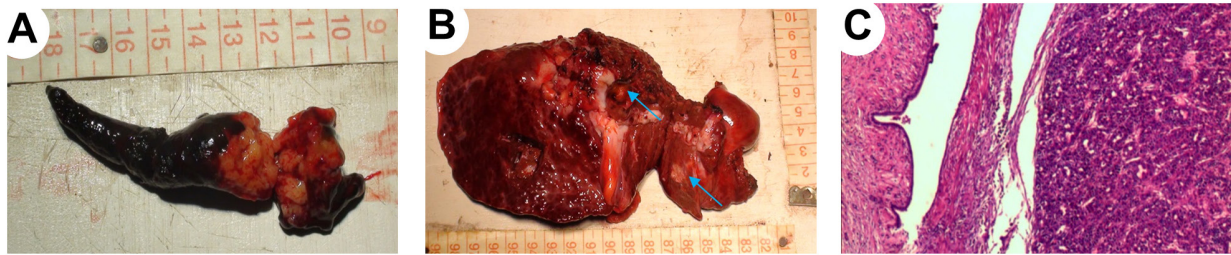


Figure 2. Histopathological examination of the tumor thrombus in patients with HCC with BDTT who underwent surgical treatment. (A) BDTT; (B) HCC with BDTT; (C) Postoperative pathology: HCC with BDTT. BDTT, bile duct tumor thrombus; HCC, hepatocellular carcinoma.

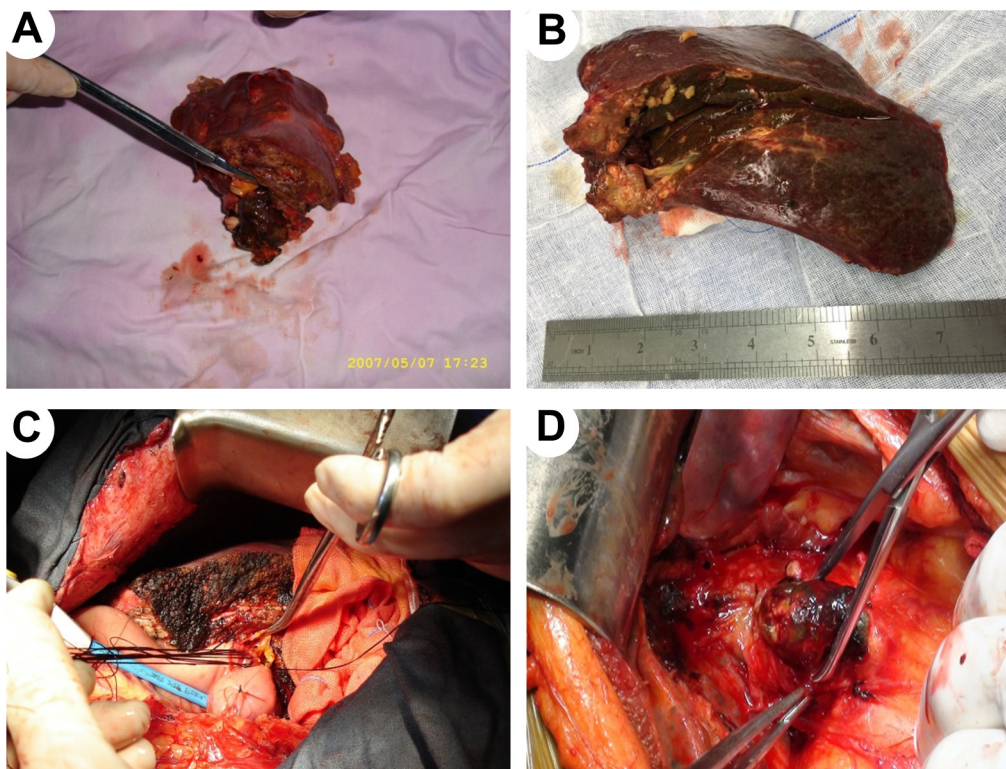


Figure 3. Surgical treatment of patients with HCC with BDTT. (A), Hemi hepatectomy plus thrombectomy through a choledochotomy; (B), Left lateral hepatic lobectomy plus thrombectomy through a choledochotomy; (C), Hemi hepatectomy plus right Roux-en-Y hepaticojejunostomy; (D), Thrombectomy through a choledochotomy. BDTT, bile duct tumor thrombus; HCC, hepatocellular carcinoma.

choledochotomy, including 4 with type III tumors and 3 with type IV according to the Ueda classification.

A total of 17 patients underwent palliative internal and external bile duct drainage, including 5 who underwent ERCP plus biliary stenting, 4 who underwent TACE, 3 who underwent PTCD, 2 who underwent ERCP plus TACE, 2 who underwent PTCD plus TACE, and 1 who underwent PTCD plus ERCP. All 17 patients had type III tumors according to the Ueda classification.

3.3. Perioperative outcome

The operating time, intraoperative blood loss, rate

of blood transfusion, duration of postoperative hospitalization, surgical complications, and mortality for the 25 patients who underwent radical resection and 7 patients who underwent thrombectomy through a choledochotomy are shown in Table 1.

Two of these patients died of liver failure after surgery. Both of the 2 patients had intraoperative blood loss of greater than 1,500 mL, liver failure occurred 1 week after surgery, and they died within 2 months after surgery although they received supportive treatment including artificial liver support.

Eight patients developed surgical complications, including 2 who had gastric bleeding due to a stress

Table 1. Perioperative outcome for patients with HCC with BDTT who underwent radical resection or thrombectomy through a choledochotomy

Items	Patients who underwent radical resection (n = 25)	Patients who underwent thrombectomy through a choledochotomy (n = 7)
Operating time (mean ± S.D.) (min)	333.00 ± 260.00	194.28 ± 15.39
Intraoperative blood loss (mean ± S.D.) (mL)	962.00 ± 856.26	175.57 ± 69.86
Rate of blood transfusion (%)	60	0
Duration of postoperative hospitalization (days)	19.68 ± 10.21	10.71 ± 4.98
Rate of surgical complications (%)	32.00	14.86
Surgical mortality rate	8.00	0

BDTT, bile duct tumor thrombus; HCC, hepatocellular carcinoma.

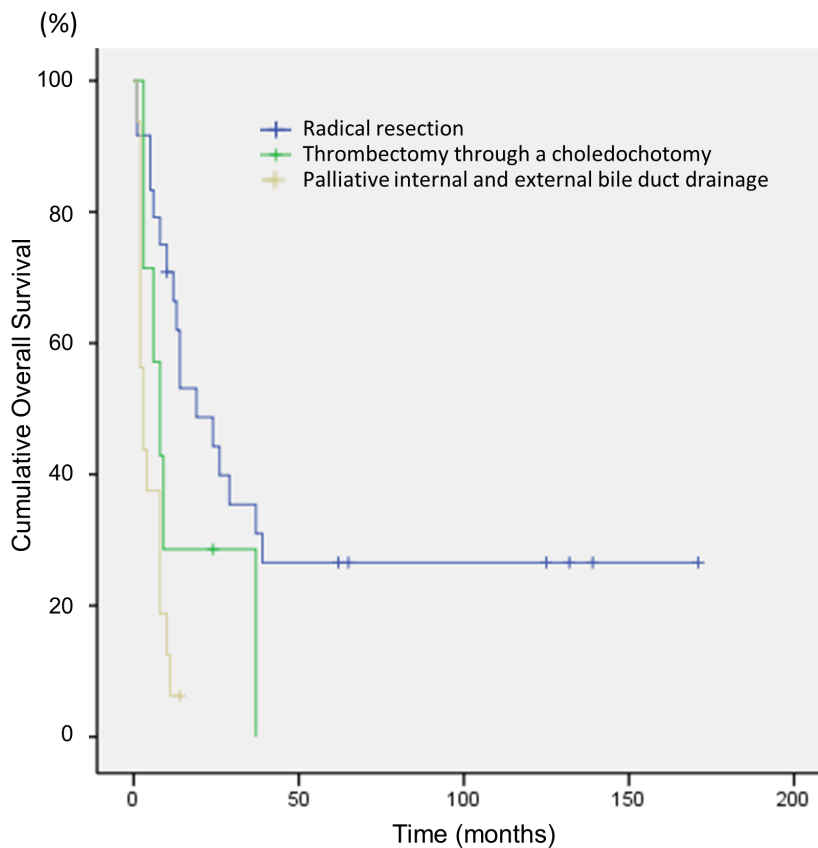


Figure 4. Survival curve for patients with HCC with BDTT receiving different treatments. BDTT, bile duct tumor thrombus; HCC, hepatocellular carcinoma.

ulcer and were cured after treatment, 3 who had subphrenic effusion, and 3 who had a pulmonary infection. All 8 patients recovered with treatment.

3.4. Prognosis: Survival

The 49 patients with HCC with BDTT had a 1-year survival rate of 42.86% (21/49), a 3-year survival rate of 18.37% (9/49), and a 5-year survival rate of 12.24% (6/49).

The 25 patients who underwent radical resection had a median survival of 19 months and a 1-year survival rate of 68.00% (17/25), a 3-year survival rate of 32.00% (8/25), and a 5-year survival rate of 24.00% (6/25).

The 7 patients who underwent thrombectomy through a choledochotomy had a median survival of 8 months and a 1-year survival rate of 28.57% (2/7), a 3-year survival rate of 14.29% (1/7), and a 5-year survival rate of 0% (0/7).

The 17 patients who underwent palliative internal and external bile duct drainage had a median survival of 3 months and a 1-year survival rate of 5.89% (1/17), a 3-year survival rate of 0% (0/17) (1/7), and a 5-year survival rate of 0% (0/17).

The survival curves for patients who received above different treatments are shown in Figure 4 ($p < 0.001$).

3.5. Prognostic factors for long-time survival of patients who underwent radical resection

Table 2. Data from 6 patients with HCC with BDTT who underwent radical resection

Patient No.	Age	TBIL	DBIL	Tumor location	Size	Intraoperative blood loss	Vascular tumor thrombus	Surgical approach	Postoperative relapse	Treatment after relapse	Survival (months)
1	58	198	117	III, IV	3.0 × 3.0	600	-	Left hepatocellular carcinoma resection with thrombectomy through a choledochotomy	6	Left hemi hepatectomy plus right Roux-en-Y hepaticojejunostomy	172
2	54	176	114	I	4.0 × 3.0	500	-	Left hemi hepatectomy with thrombectomy through a choledochotomy	-	-	140
3	50	169	100	II, III, IV	4.0 × 3.0	500	-	Left hemi hepatectomy plus right Roux-en-Y hepaticojejunostomy	-	-	133
4	42	16	10	V	4.0 × 4.0	800	-	Right hemi hepatectomy with thrombectomy through a choledochotomy	65	TACE	126
5	39	11	6	IVb	3.0 × 2.5	100	-	Resection of liver segment IVb	-	-	66
6	15	61	32	II, III	2.5 × 1.0	150	-	Left hemi hepatectomy plus end-to-end anastomosis of the right hepatic duct to the common bile duct	-	-	63

BDTT, bile duct tumor thrombus; HCC, hepatocellular carcinoma, TACE, transarterial chemoembolization.

Out of 25 patients who underwent radical resection, 6 without portal vein and hepatic vein tumor thrombus are still alive with a long-term survival of more than 60 months (Table 2). Of the 6 patients, 4 lived for 120 months, and the longest survival was 172 months to date. No portal or hepatic vein tumor thrombi were found in these patients.

Of these patients, patient 1 underwent HCC resection (junction of segments III and IV) plus thrombectomy through a choledochotomy. Recurrence of a thrombus in the left hepatic duct 6 months after surgery resulted in multiple tumors in the residual left lobe of the liver. Left hemihepatectomy plus liver hilar bile duct resection with right Roux-en-Y hepaticojejunostomy was performed. The patient has survived 172 months after surgery. Patient 4 was diagnosed with HCC of right hepatic segment VII 65 months after surgery and underwent TACE. No new lesions were detected during the 61 months of follow-up. The patient has survived 126 months after surgery. Patient 5 was the only patient with a type II tumor who recovered considerably after surgery and who has survived 66 months after surgery. Patient 6 was a 15-year-old patient who underwent left hemihepatectomy plus common hepatic duct resection with end-to-end anastomosis of the right hepatic duct to the common bile duct. The biliary tract

was reconstructed during surgery, and the patient has survived for 63 months.

Analysis with the Mantel-Cox model indicated that the preoperative bilirubin level ($p = 0.025$), intraoperative blood loss ($p = 0.006$), tumor size ($p = 0.005$), and presence of portal and hepatic vein tumor thrombi ($p = 0.021$) were significant prognostic factors associated with long-term survival for patients who underwent radical resection in this study (Table 3).

4. Discussion

Of 49 patients with HCC with BDTT, 25 underwent radical resection, 7 underwent thrombectomy through a choledochotomy, and 17 underwent palliative internal and external bile duct drainage. Patients who underwent a radical resection had a better prognosis than patients in the other two groups ($p < 0.001$). Moreover, the preoperative bilirubin level, intraoperative blood loss, tumor size, and presence of portal and hepatic vein tumor thrombi were identified as prognostic factors associated with long-term survival for patients who underwent a radical resection

The principle for surgical treatment of HCC with BDTT is the removal of primary HCC and BDTT. Active surgical resection may benefit patients (10-12).

Table 3. Log-rank (Mantel-Cox) tumor-free survival data for 25 patients with HCC with BDTT who underwent radical resection

Variable	Number of patients	Survival (months)	Log-rank (Mantel-Cox), <i>p</i> value
Sex			
Male	21	4 7.750 ± 25.041	0.906
Female	4	56.951 ± 16.068	
Age			
≥ 50 years	16	31.603 ± 10.102	0.772
< 50 years	9	34.000 ± 12.905	
HbsAg test			
Positive	20	65.386 ± 16.819	0.244
Negative	5	16.750 ± 7.609	
Degree of liver cirrhosis			0.209
Mild	5	61.286 ± 16.403	
Moderate-severe	20	19.000 ± 10.350	
Number of masses			
Single	23	61.664 ± 15.454	0.096
Multiple	2	7.500 ± 6.500	
AFP level			
≥ 400 ng/mL	10	37.500 ± 15.312	0.379
< 400 ng/mL	15	65.579 ± 19.986	
Type of liver resection			0.937
Liver lobectomy	8	28.333 ± 9.081	
Hemi hepatectomy	17	58.111 ± 16.674	
Preoperative total bilirubin level			
≤ 200 μmol/L	16	75.240 ± 18.864	0.025
> 200 μmol/L	9	14.286 ± 5.153	
Intraoperative blood loss			0.006
≤ 200 mL	5	90.250 ± 22.493	
200-1000 mL	13	36.400 ± 20.009	
> 1000 mL	7	10.857 ± 4.748	
Size of HCC			0.005
≥ 5 cm	12	15.833 ± 2.828	
< 5 cm	13	102.958 ± 23.080	
Portal vein and hepatic vein tumor thrombus			0.021
No	20	70.012 ± 17.260	
Yes	5	10.400 ± 2.015	

BDTT, bile duct tumor thrombus; HCC, hepatocellular carcinoma.

A higher rate of resection is associated with significantly prolonged survival for some patients (16,17). At the current authors' facility, the surgical procedure and scope of resection depend on the patient's liver reserve function, residual liver volume, and Ueda classification. Depending on the patient's condition, routine PTCO or endoscopic nasobiliary drainage (ENBD) was performed before surgery to reduce the degree of jaundice, and different types of liver resection were performed during surgery. Most cases of HCC with BDTT were classified as category Ueda type III. The formation of a tumor thrombus in the ipsilateral bile duct with contralateral compensatory enlargement of the liver (*i.e.*, atrophic-hypertrophic syndrome) makes tumor resection easier.

The surgical plan should be individually based on the degree of the close relationship between the tumor thrombus and extrahepatic biliary duct. Depending on the location of the HCC and BDTT, HCC resection or hemihepatectomy plus thrombectomy through choledochotomy is chosen. In cases where the BDTT is firmly attached to or even invades the extrahepatic bile duct wall, extrahepatic bile duct resection should be

considered (15,18,19). In the current study, 2 patients who underwent HCC resection and thrombectomy through a choledochotomy had recurrence of the tumor thrombus in the left hepatic duct within 6 months after surgery, which resulted in multiple tumors in the residual left lobe of the liver. Further surgery, such as hemi hepatectomy, hilar biliary duct resection, or Roux-en-Y hepaticojejunostomy, was performed. Intraoperative cholangioscopy was used to rule out the presence of a tumor thrombus in the intrahepatic distal bile duct and as an important examination to prevent recurrence. At present, the 2 patients who underwent further surgery are in satisfactory condition. This finding indicates that surgery remains an effective treatment for tumor recurrence. Liver hilar lymph node dissection was performed in 7 patients, but metastatic lymph nodes were not noted. Thus, additional studies with larger samples need to be performed to decide whether to routinely perform hilar lymph node dissection in patients with HCC with BDTT.

Two patients of the current patients (intraoperative blood loss > 1,500 mL) had liver failure and died within

2 months after surgery after the failure of artificial liver support and other treatments. Preoperative preparation should be sufficient, with particular attention devoted to reducing the preoperative bilirubin level (and especially the direct bilirubin level), retention of an adequate residual liver volume, and reduction of intraoperative blood loss. These key factors affect patients perioperatively.

Patients with HCC with BDTT for which radical surgery is not indicated should have external and internal hepatobiliary drainage tubes placed *via* PTCO or ENBD and undergo bile duct stenting to reduce the degree of jaundice and alleviate pruritis. Transarterial embolization may be another option in this case (16,20).

A comparative analysis of HCC with BDTT versus HCC without BDTT by Rammohan *et al.* (21) indicated that the degree of preoperative jaundice and tumor size were important factors affecting prognosis. This result was consistent with the current finding that the degree of preoperative jaundice was the main factor influencing long-term survival ($p < 0.05$). Analysis of the 25 patients in the current study indicated that intraoperative blood loss and portal vein and hepatic vein tumor thrombi were the main factors influencing long-term survival ($p < 0.05$). A vascular tumor thrombus was not noted in the 6 patients surviving long term (more than 60 months).

5. Conclusion

Surgical radical resection is the key to a favorable prognosis for patients with HCC with BDTT. In the current study, the preoperative bilirubin level, intraoperative blood loss, tumor size, and presence of portal and hepatic vein tumor thrombi were significant prognostic factors associated with long-term survival for patients who underwent radical resection. However, this study was retrospective, it had a small sample size, and it was conducted at a single center. Multicenter, prospective studies with a larger sample need to be conducted to verify the effectiveness of radical resection.

Radical resection should be performed with adequate preoperative preparation for patients with HCC with BDTT in whom surgery is not contraindicated. If radical resection is not indicated, then thrombectomy through a choledochotomy or internal and external drainage of the biliary duct and TACE should be performed to alleviate symptoms, improve quality of life, and promote longer survival.

References

- Forner A, Llovet JM, Bruix J. Hepatocellular carcinoma. *Lancet*. 2012; 379:1245-1255;
- Song P, Cai Y, Tang H, Li C, Huang J. The clinical management of hepatocellular carcinoma worldwide: A concise review and comparison of current guidelines from 2001 to 2017. *Biosci Trends*. 2017; 11:389-398.
- Torre LA, Bray F, Siegel RL, Ferlay J, Lortet-Tieulent J, Jemal A. Global cancer statistics, 2012. *CA Cancer J Clin*. 2015; 65:87-108.
- Navadgi S, Chang CC, Bartlett A, McCall J, Pandanaboyana S. Systematic review and meta-analysis of outcomes after liver resection in patients with hepatocellular carcinoma (HCC) with and without bile duct thrombus. *HPB (Oxford)*. 2016; 18: 312-316.
- Gao J, Zhang Q, Zhang J, Kong J, Wang S, Ding X, Ke S, Sun W. Radiofrequency ablation of the main lesion of hepatocellular carcinoma and bile duct tumor thrombus as a radical therapeutic alternative: Two case reports. *Medicine (Baltimore)*. 2015; 94:e1122.
- Ueda M, Takeuchi T, Takayasu T, Takahashi K, Okamoto S, Tanaka A, Morimoto T, Mori K, Yamaoka Y. Classification and surgical treatment of hepatocellular carcinoma (HCC) with bile duct thrombi. *Hepatogastroenterology*. 1994; 41:349-354.
- Zeng H, Xu LB, Wen JM, Zhang R, Zhu MS, Shi XD, Liu C. Hepatocellular carcinoma with bile duct tumor thrombus: A clinicopathological analysis of factors predictive of recurrence and outcome after surgery. *Medicine (Baltimore)*. 2015; 94:e364.
- Pang YB, Zhong JH, Luo XL, Ou C, Guo Z, Xiang BD, Peng NF, Li LQ. Clinicopathological characteristics and liver stem cell marker expression in hepatocellular carcinoma involving bile duct tumor thrombi. *Tumour Biol*. 2016; 37:5879-5884.
- Huang JF, Wang LY, Lin ZY, Chen SC, Hsieh MY, Chuang WL, Yu MY, Lu SN, Wang JH, Yeung KW, Chang WY. Incidence and clinical outcome of icteric type hepatocellular carcinoma. *J Gastroenterol Hepatol*. 2002; 17:190-195.
- Kasai Y, Hatano E, Seo S, Taura K, Yasuchika K, Uemoto S. Hepatocellular carcinoma with bile duct tumor thrombus: Surgical outcomes and the prognostic impact of concomitant major vascular invasion. *World J Surg*. 2015; 39:1485-1493.
- Oba A, Takahashi S, Kato Y, Gotohda N, Kinoshita T, Shibasaki H, Ikeda M, Konishi M. Usefulness of resection for hepatocellular carcinoma with macroscopic bile duct tumor thrombus. *Anticancer Res*. 2014; 34:4367-4372.
- Wong TC, Cheung TT, Chok KS, Chan AC, Dai WC, Chan SC, Poon RT, Fan ST, Lo CM. Outcomes of hepatectomy for hepatocellular carcinoma with bile duct tumour thrombus. *HPB (Oxford)*. 2015; 17:401-408.
- Wang C, Yang Y, Sun D, Jiang Y. Prognosis of hepatocellular carcinoma patients with bile duct tumor thrombus after hepatic resection or liver transplantation in Asian populations: A meta-analysis. *PLoS One*. 2017; 12:e0176827.
- Chotiromniramit A, Liwattanakun A, Lapisatepun W, Kolum W, Sandhu T, Junrungsee S. A single institution report of 19 hepatocellular carcinoma patients with bile duct tumor thrombus. *J Hepatocell Carcinoma*. 2017; 4:41-47.
- Hu XG, Mao W, Hong SY, Kim BW, Xu WG, Wang HJ. Surgical treatment for hepatocellular carcinoma with bile duct invasion. *Ann Surg Treat Res*. 2016; 90: 139-146.
- Moon DB, Hwang S, Wang HJ, *et al.* Surgical outcomes of hepatocellular carcinoma with bile duct tumor thrombus: A Korean multicenter study. *World J Surg*. 2013; 37:443-451.
- Yeh CN, Jan YY, Lee WC, Chen MF. Hepatic resection

- for hepatocellular carcinoma with obstructive jaundice due to biliary tumor thrombi. *World J Surg.* 2004; 28:471-475.
18. Clavien PA, Petrowsky H, DeOliveira ML, Graf R. Strategies for safer liver surgery and partial liver transplantation. *N Engl J Med.* 2007; 356:1545-1559.
 19. Peng BG, Liang LJ, Li SQ, Zhou F, Hua YP, Luo SM. Surgical treatment of hepatocellular carcinoma with bile duct tumor thrombi. *World J Gastroenterol.* 2005; 11:3966-3969.
 20. Park S, Park JY, Chung MJ, Chung JB, Park SW, Han KH, Song SY, Bang S. The efficacy of endoscopic palliation of obstructive jaundice in hepatocellular carcinoma. *Yonsei Med J.* 2014; 55:1267-1272.
 21. Rammohan A, Sathyanesan J, Rajendran K, Pitchaimuthu A, Perumal SK, Balaraman K, Ramasamy R, Palaniappan R, Govindan M. Bile duct thrombi in hepatocellular carcinoma: is aggressive surgery worthwhile? *HPB (Oxford).* 2015; 17:508-513.

(Received September 27, 2019; Revised February 17, 2019; Accepted February 22, 2019)

Structural analyses of a hemolytic compound found in an extract of *Hypsizygus marmoreus* fruiting bodies at a low pH

Yoshiki Oda^{1,§}, Kohsuke Saito^{2,§}, Munehiro Nakata^{2,*}

¹Technology Joint Management Office, Research Promotion Division, Tokai University, Hiratsuka, Kanagawa, Japan;

²Department of Applied Biochemistry, Tokai University, Hiratsuka, Kanagawa, Japan.

Summary The current study determined the structure of a hemolytic compound found in an extract from the fruiting bodies of the edible mushroom *Hypsizygus marmoreus* when its pH was lowered. The hemolytic compound was purified using the modified Bligh and Dyer method followed by chromatography using reversed phase and silica gel columns. Structural analyses of the purified hemolytic compound were performed using NMR and ESI-MS. The deduced structure indicated a *trans,trans*-5,8-docosadienoic acid calcium salt. Although numerous proteinous hemolysins from various mushrooms have been described, the current study is the first to report on a low-molecular-weight hemolytic compound derived from an *H. marmoreus* extract.

Keywords: Docosadienoic acid, hemolysis, *Hypsizygus marmoreus*, mushroom

1. Introduction

Hemolytic proteins (hemolysins) have been identified in various mushroom fruiting bodies (1) such as aegerolysin in *Agrocybe aegerita* (2), *flammutoxin* in *Flammulina velutipes* (3), pleurotolysin and ostreolysin in *Pleurotus ostreatus* (4,5), erylysins in *P. eryngii* (6), nebrodeolysin in *P. nebrodensis* (7), schizolysin in *Schizophyllum commune* (8), and volvatoxin in *Volvarilla volvacea* (9). Although some mushroom hemolysins have been reported to recognize particular lipids comprising target cell membranes (4,5,10,11) and/or to form pores on those membranes (10,12,13), the physiological significance of hemolysins or cell membrane disruption in the life cycle of mushrooms has yet to be determined.

Hypsizygus marmoreus (buna-shimeji, or brown beech mushroom) is an edible mushroom. Proteinous hemolysins from other mushrooms have been identified, but a proteinous hemolysin from *H. marmoreus* has not been described thus far. A previous study by the

current authors indicated that an extract of *H. marmoreus* fruiting bodies exhibited hemolytic activity against sheep red blood cells (RBCs) when the extract was incubated at a pH of 5.5 (14). The same study reported that the hemolytic compound exhibited lipid-like characteristics since the compound was water-insoluble and it was fractionated in a chloroform layer by the Bligh and Dyer method (14). The current study purified that hemolytic compound and it determined the structure of that compound.

2. Materials and Methods

2.1. Fruiting bodies and reagents

Fruiting bodies of *H. marmoreus* were purchased from a local market. Excised fruiting bodies were freeze-dried and stored at -30°C until use. Sheep blood was obtained from Nippon Bio-Supp Center, Tokyo, Japan. All chemicals used were of analytical grade.

2.2. Hemolysis assay

Hemolytic activity was determined as described previously (14). Briefly, sheep RBCs were washed with phosphate-buffered saline (PBS) three times. A suspension of sheep RBCs (0.1 mL) was mixed with 1.9 mL of distilled water in order to cause osmotic lysis, and absorbance was measured at 541 nm using a

Released online in J-STAGE as advance publication January 30, 2019.

[§]These authors contributed equally to this work.

*Address correspondence to:

Dr. Munehiro Nakata, Department of Applied Biochemistry, Tokai University, Hiratsuka, Kanagawa 259-1292, Japan.

E-mail: nak@tsc.u-tokai.ac.jp

UV-Vis spectrophotometer (UVmini 1240; Shimadzu, Kyoto, Japan). PBS was added to the suspension so that the absorbance at 541 nm would be 0.500.

A reaction mixture (2 mL) containing 0.1 mL of suspended sheep RBCs prepared as described above, PBS, and a sample was incubated at 37°C for 10 min. A positive control was prepared by mixing 0.1 mL of suspended sheep RBCs with 1.9 mL of distilled water, and a negative control was prepared by similarly mixing the sheep RBCs with PBS. After centrifugation at 2,200 rpm for 5 min at 4°C, the absorbance of the supernatant was measured at 541 nm. One hundred percent lysis was defined as the absorbance of the supernatant obtained from osmotically lysed cells (the positive control) (5).

2.3. Generation and preparation of a crude hemolytic compound

Pieces of freeze-dried fruiting bodies of *H. marmoreus* (54 g) were ground and sonicated 10 times for 2 sec in 10 mM phosphate buffer (pH 7.3). The homogenate was centrifuged at 12,000 rpm for 30 min. In order to generate the hemolytic compound, the extract was mixed with an equal volume of a 0.1 M acetate buffer (pH 5.5) and incubated at 37°C for 30 min. The mixture was then centrifuged at 12,000 rpm for 20 min at 4°C. The precipitate was dissolved in ethanol and subjected to a modified Bligh and Dyer method with ethanol instead of methanol as described previously (14,15). The resulting fat-soluble fraction was dried *in vacuo* and dissolved in 50% ethanol.

2.4. Purification of a hemolytic compound via column chromatography

The sample dissolved in 50% ethanol was loaded onto a Strata C18-E cartridge column (500 mg/6 mL; Phenomenex, Torrance, CA, USA) equilibrated with the same solvent. The column was washed with 50% ethanol, and then stepwise elution was performed with 75 and 100% ethanol. Elution was monitored at 210 nm. Fraction size was 4 mL. Fractions with hemolytic activity were pooled and dried *in vacuo*.

The sample was subsequently dissolved in *n*-hexane/diethyl ether/acetic acid (80: 30: 1, v/v) and passed through a Wakogel C-200 column (ϕ 1.2 × 46 cm; Wako Pure Chemical Industries, Osaka, Japan) equilibrated with the same solvent system at a flow rate of 0.6 mL/min. The fractions (1 mL each) were collected, and the absorbance at 210 nm was measured. The hemolytic active fractions were pooled and subjected to rechromatography under the same conditions.

2.5. Thin layer chromatography (TLC)

TLC was performed with high-performance TLC

silica gel 60 plates (Merck, Kenilworth, NJ, USA) and chloroform/methanol/water (60: 35: 6, v/v) or *n*-hexane/diethyl ether/acetic acid (80: 30: 1, v/v) as a development solvent. Lipids were detected with primulin staining, phosphomolybdic acid staining, and iodine vapor (16-19). TLC plates were also subjected to a hemolysis assay to detect hemolytic compounds as described previously (20).

2.6. Structural analyses of the hemolytic compound

Mass spectrometry analysis of the hemolytic compound was performed with a JMN-T100LP electrospray ionization mass spectrometer (JEOL, Tokyo, Japan). Electron probe microanalysis (EPMA) to detect carbon and calcium was performed on a silicon wafer using an EPMA-1610 electron probe microanalyzer (Shimadzu, Kyoto, Japan). Samples were dissolved in 0.1-0.2 mL of ethanol and subjected to the analyses.

Nuclear magnetic resonance (NMR) was analyzed using a 500 MHz Avance III HD NMR Spectrometer (Bruker, Bremen, Germany) at 300 K. Spectra were obtained from 6 mg of the purified hemolytic compound in 5-mm tubes (Kusanokagaku, Tokyo, Japan). The sample was dissolved in 0.45 mL of deuterated methanol (99.8%, Acros Organics, Geel, Belgium) containing tetramethylsilane (δ H = 0.00) as an internal reference. Data from one-dimensional (proton, carbon, DEPT135; distortionless enhancement by polarization transfer) and two-dimensional homonuclear (correlation spectroscopy (COSY); nuclear Overhauser effect spectroscopy (NOESY)) and H-detected heteronuclear (heteronuclear multiple-quantum coherence (HMQC); heteronuclear multiple bond coherence (HMBC)) experiments were recorded and processed using the software TopSpin 3.5 pl 5 (Bruker).

3. Results and Discussion

A hemolytic fat-soluble fraction was prepared from an extract of *H. marmoreus* fruiting bodies by lowering its pH and subjecting the extract to a modified Bligh and Dyer method as described in the Materials and Methods. To purify the hemolytic compound from the fraction, C18 cartridge column chromatography was performed as described in the Materials and Methods. As shown in Figure 1A, substances detected at 210 nm were eluted with 50% ethanol, and strong hemolytic activity was evident with 75% ethanol. Weak activity was also noted in the eluent with 100% ethanol.

The major active fraction was then subjected to silica gel column chromatography as described in the Materials and Methods. As shown in Figure 1B, hemolytic activity was detected as a single peak. The active fraction was subjected to rechromatography for further purification. TLC analysis indicated that the final active fraction produced a single spot detected

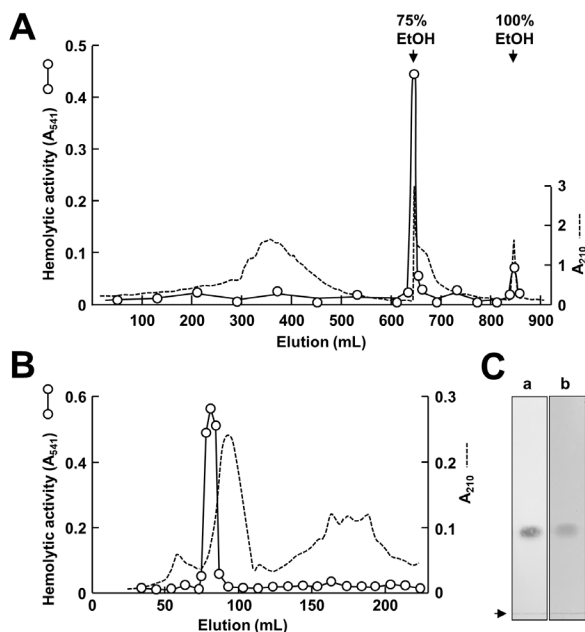


Figure 1. Purification of a hemolytic compound via reversed phase and silica column chromatography. (A) Chromatogram when using the Strata C18-E cartridge column. (B) Chromatogram when using the Wakogel C-200 column. Chromatography was performed as described in the Materials and Methods. (C) TLC analysis of a hemolytic compound purified via rechromatography with a silica gel column. *n*-hexane/diethyl ether/acetic acid (80: 30: 1, v/v) was used as a development solvent. Detection was performed using phosphomolybdic acid staining (lane a) and iodine vapor (lane b). An arrow indicates the origin.

with phosphomolybdic acid staining and iodine vapor (Figure 1C). During this purification, 8.8 mg of the purified hemolytic compound was obtained from 1,360 mg of the fat-soluble substance (data not shown).

EPMA qualitatively detected calcium in the purified hemolytic sample by EPMA (data not shown). ESI-MS indicated an *m/z* of 710.5. The hemolytic compound was subjected to NMR analyses to determine its structure. ^1H and ^{13}C NMR data are summarized in Figure 2 and Table 1.

The relative configuration of the hemolytic compound was determined using NOESY NMR. Long-range NOE interactions between H-4 and H-6, H-8 and H-10, H-7 and H-9, H-5 and H-7 were observed (Figure 3). The deduced structure of the hemolytic compound indicated a calcium salt of *trans,trans*-5,8-docosadienoic acid (Figure 4).

The current study revealed that the hemolytic compound found in a low pH extract of the fruiting bodies of *H. marmoreus* was a *trans,trans*-5,8-docosadienoic acid. Proteinous hemolysins have been identified from various mushrooms, and these proteinous hemolysins are active in the first extract with buffers at a neutral pH (1-9). In contrast, the hemolytic compound from *H. marmoreus* was a type of fatty acid identified when the mushroom extract had a low pH (14). This may be the first low-molecular-weight

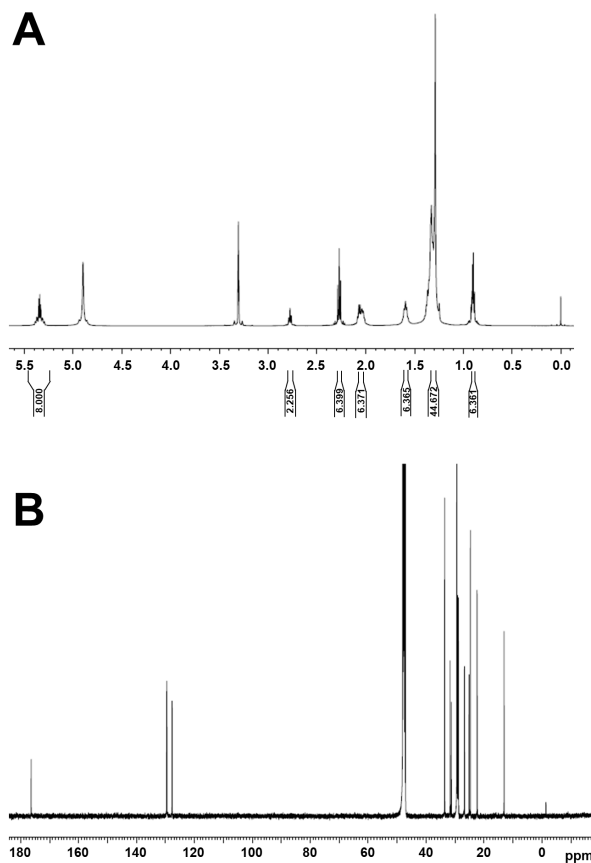


Figure 2. NMR spectra. (A) ^1H NMR (500 MHz), (B) ^{13}C NMR (125 MHz).

Table 1. ^1H NMR and ^{13}C NMR data

Position	^1H NMR (integration of protons)	^{13}C NMR
1 (COOH)		176.2, 176.3
2	1.59 (2H), 2.27 (2H)	33.3, 33.5
3	1.59 (2H), 2.27 (2H)	24.6, 24.6
4	1.34 (2H), 1.59 (2H)	28.9, 28.9
5	5.34 (2H)	129.4, 129.4
6	5.33 (2H)	129.5, 129.5
7	2.27 (2H), 2.76 (2H)	25.1, 25.1
8	5.35 (2H)	127.6, 127.6
9	5.36 (2H)	127.7, 127.7
10	2.03 (4H)	26.7, 26.7
11	1.31 (2H), 2.06 (2H)	29.1, 29.1
12	1.29 (4H)	29.4, 29.4
13	1.29 (4H)	29.3, 29.3
14-16	1.29-1.37 (12H)	28.7, 28.8, 28.8, 28.9, 28.9, 29.2
17	1.34 (4H)	29.0, 29.1
18	1.29 (4H)	26.7, 26.7
19	1.29 (4H)	29.4, 29.4
20	1.29 (4H)	31.2, 31.6
21	1.32 (4H)	22.2, 22.3
22 (CH ₃)	0.90 (6H)	13.0, 13.1

compound found by means of assaying the hemolytic activity of mushroom components.

Although fatty acids are known to potentially cause hemolysis by disrupting the cell membrane structure, the hemolytic fatty acid from *H. marmoreus* was

uniquely found in a fruiting body extract. In a previous study by the current authors, hemolytic activity was not detected when an extract was heated before its pH was lowered, but activity was evident when the extract was heat-stable after its pH was lowered (14). Therefore, some precursor substances may exist in fruiting bodies and some enzymes may release hemolytic fatty acids from those precursors. A previous study by the current authors indicated that hemolytic activity was Ca^{2+} -

dependent and effectively inhibited in the presence of PMSF (which is a serine protease inhibitor) when the pH of an extract was lowered (14). Since the hemolytic compound examined in the current study was a fatty acid, some serine esterases/lipases possessing a catalytically active serine residue in the active site (21) might cleave the hemolytic fatty acid from a precursor.

Numerous types of fatty acids, including a small amount of docosadienoic acid ($\text{C}_{22:2}$), have been found in various mushrooms (22-25). Curiously, only *trans,trans*-5,8-docosadienoic acid was identified as a major hemolytic compound in the current study. Although other hemolytic substances were detected in the fat-soluble fraction according to TLC analysis and reversed-phase column chromatography, the docosadienoic acid was a major component purified as a hemolytic compound. One possibility is that the fruiting bodies of *H. marmoreus* might contain this type of fatty acid in abundance. Although 5,8-docosadienoic acid is a unique fatty acid in terms of the positions of double bonds, Δ^5 - and Δ^8 -fatty acid desaturases have been found in *H. marmoreus* (26,27). Another possibility is that enzymes acting to release hemolytic fatty acids might be specific to this type of fatty acid. Why the fatty acid calcium salt was obtained as a hemolytic compound in this study is still not known. Hydrogen ions in the fatty acid might be exchanged for calcium ions in the extract when its pH is lowered. Further study of the precursors and the enzymes such as esterases/lipases in fruiting bodies of *H. marmoreus* may be needed.

Mushroom hemolysins are thought to protect a fungus from outside factors or to participate in fusion of mycelia in the life cycle of basidiomycetes (1). The hemolytic compound found in the current study is not thought to exist as a free active substance. If its appearance is regulated in the life cycle of *H. marmoreus*, the current findings might represent a new step in determining the physiological role of hemolytic components in basidiomycetes.

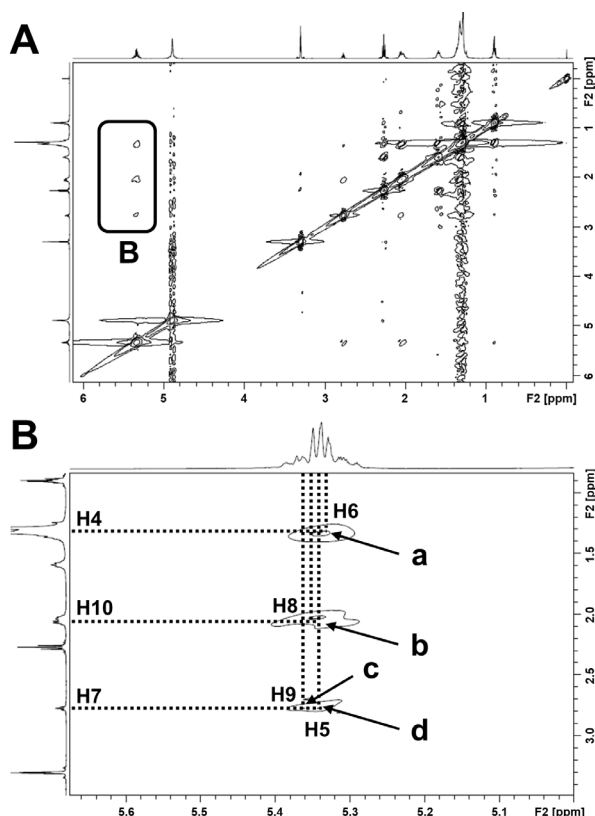


Figure 3. NOESY Spectra. Panel A shows the whole spectrum, and the indicated area is expanded in panel B. Arrows a-d indicate the long-range NOE interactions between H-4 and H-6, H-8 and H-10, H-7 and H-9, and H-5 and H-7, respectively.

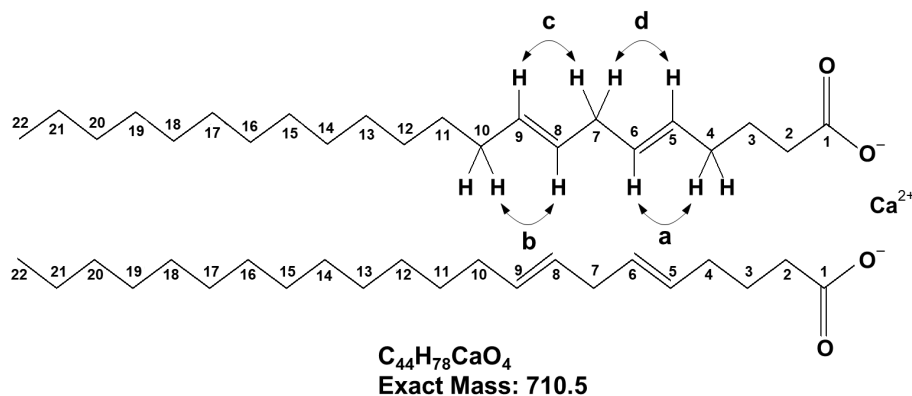


Figure 4. Deduced structure of the hemolytic compound purified from a low pH-treated extract of *H. marmoreus* fruiting bodies. NOE interaction; a (H-4 and H-6), b (H-8 and H-10), c (H-7 and H-9), d (H-5 and H-7).

References

1. Nayak AP, Green BJ, Beezhold DH. Fungal hemolysins. *Med Mycol.* 2013; 51:1-16.
2. Berne S, Krizaj I, Pohleven F, Turk T, Macek P, Sepčić K. Pleurotus and Agrocybe hemolysins, new proteins hypothetically involved in fungal fruiting. *Biochim Biophys Acta.* 2002; 1570:153-159.
3. Bernheimer AW, Oppenheim JD. Some properties of flammutoxin from the edible mushroom *Flammulina velutipes*. *Toxicon.* 1987; 25:1145-1152.
4. Sepčić K, Berne S, Potrich C, Turk T, Macek P, Menestrina G. Interaction of ostreolysin, a cytolytic protein from the edible mushroom *Pleurotus ostreatus*, with lipid membranes and modulation by lysophospholipids. *Eur J Biochem.* 2003; 270:1199-1210.
5. Tomita T, Noguchi K, Mimuro H, Ukaji F, Ito K, Sugawara-Tomita N, Hashimoto Y. Pleurotolysin, a novel sphingomyelin-specific two-component cytotoxic protein from the edible mushroom *Pleurotus ostreatus*, assembles into a transmembrane pore complex. *J Biol Chem.* 2004; 279:26975-26982.
6. Shibata T, Kudou M, Hoshi Y, Kudo A, Nanashima N, Miyairi K. Isolation and characterization of a novel two-component hemolysin, erylysin A and B, from an edible mushroom, *Pleurotus eryngii*. *Toxicon.* 2010; 56:1436-1442.
7. Lv H, Kong Y, Yao Q, Zhang B, Leng FW, Bian HJ, Balzarini J, Van Damme E, Bao JK. Nebrodeolysin, a novel hemolytic protein from mushroom *Pleurotus nebroidensis* with apoptosis-inducing and anti-HIV-1 effects. *Phytomedicine.* 2009; 16:198-205.
8. Han CH, Zhang GQ, Wang HX, Ng TB. Schizolysin, a hemolysin from the split gill mushroom *Schizophyllum commune*. *FEMS Microbiol Lett.* 2010; 309:115-121.
9. Weng YP, Lin YP, Hsu CI, Lin JY. Functional domains of a pore-forming cardiotoxic protein, volvatoxin A2. *J Biol Chem.* 2004; 279:6805-6814.
10. Sepčić K, Berne S, Rebolj K, Batista U, Plemenitas A, Sentjurc M, Macek P. Ostreolysin, a pore-forming protein from the oyster mushroom, interacts specifically with membrane cholesterol-rich lipid domains. *FEBS Lett.* 2004; 575:81-85.
11. Bhat HB, Kishimoto T, Abe M, Makino A, Inaba T, Murate M, Dohmae N, Kurahashi A, Nishibori K, Fujimori F, Greimel P, Ishitsuka R, Kobayashi T. Binding of a pleurotolysin ortholog from *Pleurotus eryngii* to sphingomyelin and cholesterol-rich membrane domains. *J Lipid Res.* 2013; 54:2933-2943.
12. Schlumberger S, Kristan-Črnigoj K, Ota K, Frangež R, Molgó J, Sepčić K, Benoit E, Maček P. Permeability characteristics of cell-membrane pores induced by ostreolysin A/pleurotolysin B, binary pore-forming proteins from the oyster mushroom. *FEBS Lett.* 2013; 588:35-40.
13. Tomita T, Ishikawa D, Noguchi T, Katayama E, Hashimoto Y. Assembly of flammutoxin, a cytolytic protein from the edible mushroom *Flammulina velutipes*, into a pore-forming ring-shaped oligomer on the target cell. *Biochem J.* 1998; 333:129-137.
14. Saito K, Hazama S, Oda Y, Nakata M. pH-dependent exhibition of hemolytic activity by an extract of *Hypsizygus marmoreus* fruiting bodies. *Biosci Trends.* 2018; 12:325-329.
15. Bligh EG, Dyer WJ. A rapid method of total lipid extraction and purification. *Can J Biochem Physiol.* 1959; 37:911-917.
16. Vioque E, Holman RT. Characterization of the ketodienes formed in the oxidation of linoleate by lipoxidase. *Arch Biochem Biophys.* 1962; 99:522-528.
17. Feizi T, Stoll MS, Yuen CT, Chai W, Lawson AM. Neoglycolipids: Probes of oligosaccharide structure, antigenicity, and function. *Methods Enzymol.* 1994; 230:484-519.
18. Zarzycki PK, Bartoszek MA, Radziwon AI. Optimization of TLC detection by phosphomolybdic acid staining for robust quantification of cholesterol and bile acids. *J Planar Chromatogr.* 2006; 19:52-57.
19. Fuchs B, Süß R, Teuber K, Eibisch M, Schiller J. Lipid analysis by thin-layer chromatography--A review of the current state. *J Chromatogr A.* 2011; 1218:2754-2774.
20. Sharma OP, Kumar N, Singh B, Bhat TK. An improved method for thin layer chromatographic analysis of saponins. *Food Chem.* 2012; 132:671-674.
21. Akoh CC, Lee GC, Liaw YC, Huang TH, Shaw JF. GDSL family of serine esterases/lipases. *Prog Lipid Res.* 2004; 43:534-552.
22. Pedneault K, Angers P, Gosselin A, Tweddell RJ. Fatty acid composition of lipids from mushrooms belonging to the family Boletaceae. *Mycol Res.* 2006; 110:1179-1183.
23. Pedneault K, Angers P, Avis TJ, Gosselin A, Tweddell RJ. Fatty acid profiles of polar and non-polar lipids of *Pleurotus ostreatus* and *P. cornucopiae* var. 'citrinopileatus' grown at different temperatures. *Mycol Res.* 2007; 111:1228-1234.
24. Günç Ergönül P, Akata I, Kalyoncu F, Ergönül B. Fatty acid compositions of six wild edible mushroom species. *Scientific World Journal.* 2013; 2013:163964.
25. Doğan HH, Akbaş G. Biological activity and fatty acid composition of Caesar's mushroom. *Pharm Biol.* 2013; 51:863-871.
26. UniProtKB - A0A151W9W9 (<http://www.uniprot.org/uniprot/A0A151W9W9>) (accessed January 10, 2019).
27. UniProtKB - A0A151WBS4 (<http://www.uniprot.org/uniprot/A0A151WBS4>) (accessed January 10, 2019)

(Received January 14, 2019; Revised January 26, 2019; Accepted January 28, 2019)

Novel HDAC6 selective inhibitors with 4-aminopiperidine-1-carboxamide as the core structure enhanced growth inhibitory activity of bortezomib in MCF-7 cells

Chenru Zhao^{1,2,§}, Jianjun Gao^{1,§,*}, Li Zhang², Li Su², Yepeng Luan^{2,*}

¹ Department of Pharmacology, School of Pharmacy, Qingdao University, Qingdao, Shandong, China;

² Department of Medicinal Chemistry, School of Pharmacy, Qingdao University, Qingdao, Shandong, China.

Summary

In epigenetics, histone deacetylases (HDACs) are well validated targets for the development of anticancer drugs. In this work, we reported the design and synthesis of a series of twenty-two novel (*E*)-*N*-hydroxycinnamamide-based HDAC inhibitors with 4-aminopiperidine-1-carboxamide as the core structure. Most newly synthesized compounds displayed high inhibition rates toward HDAC at the concentration of 1 μ M. Among them, the inhibition rates of compounds LYP-2, LYP-3, LYP-6, and LYP-15 were more than 75%. Furthermore, compounds LYP-2, LYP-3, and LYP-6 potently inhibited the activity of HDAC6 with selectivity over HDAC1. We chose LYP-2 and LYP-6 to test its antiproliferative effect on breast cancer cells MCF-7. Either LYP-2 or LYP-6 alone moderately suppressed the cell growth, but could synergistically enhance the inhibitory effect of bortezomib. These results suggested that combined HDAC6 inhibitor and bortezomib regimen might be an option for breast cancer treatment.

Keywords: HDAC, HDAC6, selective, inhibitors, cancer

1. Introduction

In the field of epigenetics, acetylation is the most common covalent modification, playing important roles in the regulation of normal cellular processes such as cell differentiation, proliferation, angiogenesis, and apoptosis (1). Dysregulation of acetylation has been associated with diverse human diseases including cancers (2). The level of acetylation of histones and non-histone proteins is governed by two antagonistic families of enzymes: histone deacetylases (HDACs) and histone acetyl transferases (HATs) (3). HDACs are a family of eraser enzymes that are responsible for removing an acetyl group from the ϵ -amino groups

of lysine residues present within core histones and many non-histone proteins. Silencing or inhibiting HDACs can impair cell cycle, cell growth, chromatin decondensation, cell differentiation, apoptosis, and angiogenesis in several cancer cell types. Therefore, HDACs have emerged as important therapeutic targets for cancers (4).

The known HDACs are divided into four classes based on their sequence homology: Class I HDACs including HDAC1, 2, 3, and 8; Class II HDACs including Classes IIa (HDAC4, 5, 7, and 9) and IIb (HDAC6 and 10); Class III HDACs, known as sirtuins (sirt1-7); and Class IV HDAC (HDAC11). Class I, II, and IV are all Zn²⁺ dependent while Class III is NAD⁺-dependent (5). HDAC6 belonging to class IIb has recently emerged as an attractive drug target for the treatment of several human diseases including Alzheimer's disease, autoimmune disorders, and cancers (6). As a cytoplasmic enzyme, HDAC6 uniquely features two deacetylase domains, a dynein motor binding domain to enable HDAC6 to shuttle cargo along the microtubule and a zinc finger ubiquitin-binding domain at the C-terminus. Functionally, HDAC6 is able to remove the acetyl group from lysine residues

[§]These authors contributed equally to this work.

*Address correspondence to:

Dr. Jianjun Gao, Department of Pharmacology, School of Pharmacy, Qingdao University, 38 Dengzhou Road, Qingdao 266021, Shandong, China.

E-mail: gaojj@qdu.edu.cn

Dr. Yepeng Luan, Department of Medicinal Chemistry, School of Pharmacy, Qingdao University, 38 Dengzhou Road, Qingdao 266021, Shandong, China.

E-mail: yluan@qdu.edu.cn

mainly in non-histone substrates, including α -tubulin (7), Hsp90 (8), cortactin (9), and peroxiredoxin (10), and plays important roles in microtubule dynamics and chaperone activities. In contrast to the lethal effect of HDAC1-3 suppression, it has been reported that mice with HDAC6 knocked out are effectively normal (11). Indeed, HDAC6 inhibitors do not seem to be cytotoxic toward normal cells and have fewer side effects than pan-HDACis.

Considering the value to develop HDAC6 selective inhibitors, here, we report the design, synthesis and activity studies of 22 novel HDAC inhibitors with the 4-aminopiperidine-1-carboxamide as the core structure, some of them were identified as potent HDAC6 selective inhibitors. Antiproliferative activities and drug combination effect of representative compounds were also evaluated.

2. Materials and Methods

2.1. Chemistry

All of the chemical solvents and reagents, which were analytically pure without further purification, were commercially available. Thin-layer chromatography was performed on 0.20 mm Silica Gel 60 F254 plates (Qingdao Haiyang Chemical, China). ^1H NMR and ^{13}C NMR spectra were recorded on a Bruker Avance 400 spectrometer (Bruker Company, Germany) or a Varian spectrometer (Varian, Palo Alto, CA, USA), using tetramethylsilane as an internal standard. Chemical shifts were given in parts per million. Mass spectra were recorded on a Q-TOF Premier mass spectrometer (Micromass, Manchester, U.K.).

2.2. Cell line and cell culture

Breast carcinoma cell MCF-7 was employed in the present study. The cell line was obtained from China Cell Bank (Shanghai, China) and maintained in Iscove's Modified Dulbecco's Medium (IMDM; Thermo Fisher Scientific) supplemented with 10% fetal bovine serum (FBS; PAN Biotech) at 37°C in a humid atmosphere (5% CO_2 -95% air).

2.3. In vitro HDAC inhibition fluorescence assay

In brief, 10 μL of enzyme solution (HeLa cell nuclear extract, HDAC1, or HDAC6) was mixed with different concentrations of tested compounds (50 μL). The mixture was incubated at 37°C for 5 min, followed by adding 40 μL fluorogenic substrate (Boc-Lys(acetyl)-AMC). After incubation at 37°C for 30 min, the mixture was quenched by addition of 100 μL of developer containing trypsin and trichostatin A (TSA). Over another incubation at 37°C for 20 min, fluorescence intensity was measured using a microplate reader at excitation and emission

wavelengths of 390 and 460 nm, respectively. The inhibition ratios were calculated from the fluorescence intensity readings of tested wells relative to those of control wells, and the IC_{50} values were calculated using a regression analysis of the concentration/inhibition data.

2.4. Cell proliferation assay

Cells (5×10^3 per well) seeded in 96-well plates were exposed to HDACis, bortezomib, or their combination for 72 h. Then the medium was removed and the wells were washed with phosphate-buffered saline (PBS). The 3-(4,5-dimethylthiazol-2-yl)-2,5-diphenyltetrazolium bromide (MTT) assay was performed by adding 20 μL of MTT (5 mg/mL, Sigma-Aldrich) for 4 h. Light absorbance of the solution was measured at 490 nm on a microplate reader (TECON, Swiss) (12,13).

2.5. Statistical analyses

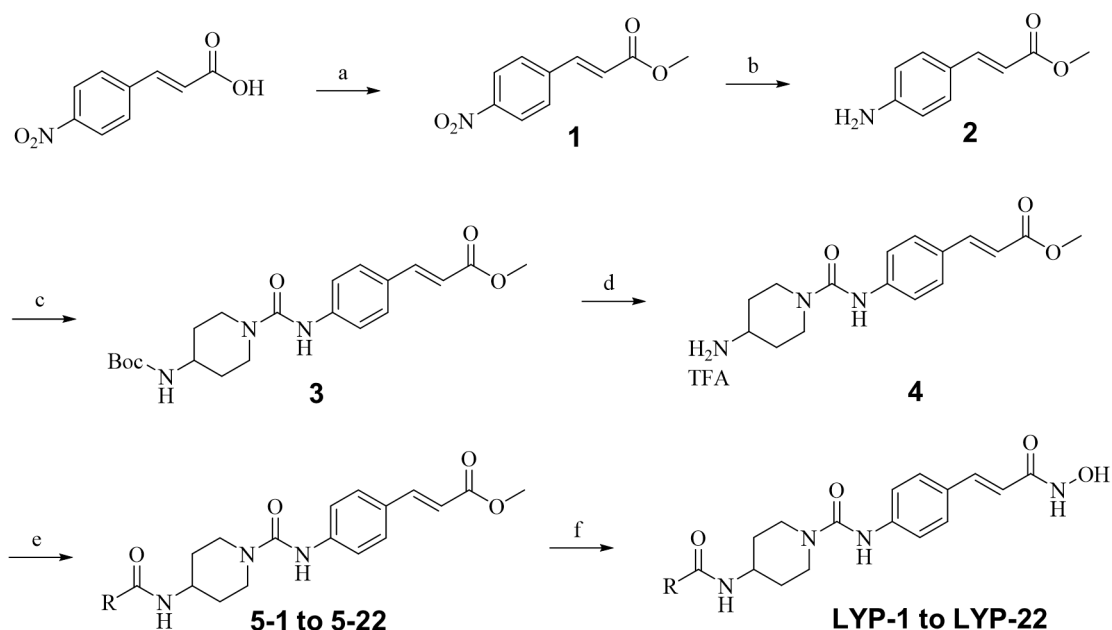
Data were expressed as mean \pm S.D. for three different determinations. Statistical significance was analyzed by one-way analysis of variance (ANOVA) followed by Dunnett's multiple range tests. The value of $p < 0.05$ was considered as statistically significant. Statistical analysis was performed using the SPSS/Win 16.0 software (SPSS, Inc, Chicago, IL, USA).

3. Results and Discussion

3.1. Synthesis of compounds

The general procedure to synthesize the target molecules was depicted in Scheme 1. Commercially available starting material 4-nitrocinnamic acid was refluxed with drops of concentrated sulfuric acid in methanol to give methyl 4-nitrocinnamic acid (**1**). The nitro group of compound **1** was then reduced to amino group to give compound **2**. Under nitrogen atmosphere protection, compound **2** was mixed with triphosgene and 4-(*N*-tert-butoxycarbonylamino)piperidine sequentially to give the compound **3**. The tert-butoxycarbonyl (Boc) protecting group was removed by treating with 20% (v/v) DCM solution of trifluoroacetic acid (TFA) to give the key intermediate **4**. Then, different aryl groups were introduced by treatment with the mixture of corresponding aromatic acid, HATU and DIPEA in anhydrous DMF to get the compounds **5-1** to **5-22** which were directly converted into target molecules **LYP-1** to **LYP-22** by condensed with NH_2OH in anhydrous methanol. Specific synthesized methods and spectroscopy data of the above compounds see supplementary data (<http://www.biosciencetrends.com/action/getSupplementalData.php?ID=38>).

3.2. Inhibitory effect of target compounds on HDAC activity



Scheme 1. Reagents and conditions. a. conc. H_2SO_4 , MeOH; b. Fe powder, NH_4Cl , EtOH and H_2O , reflux, 4 h; c. triphosgene, 4-(*N*-tert-butoxycarbonylamino)piperidine, anhydrous DCM; d. TFA:DCM = 1:4, r.t.; e. aromatic acid, HATU, DIPEA, dry DMF, r.t.; f. NH_2OH , KOH, MeOH.

All the synthesized compounds were first screened for their inhibitory activity against Hela cell nucleus extracts (HDACs). The data are summarized in Table 1. Vorinostat (SAHA) was tested as a pan-HDAC reference inhibitor. Among all 22 compounds, four of them, LYP-2, 3, 6 and 15 displayed stronger activities to HDACs with the inhibition rate more than 75%, and the inhibition rate of SAHA was 96.8%.

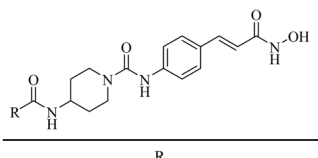
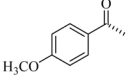
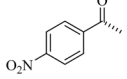
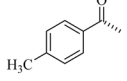
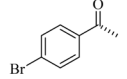
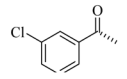
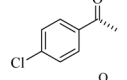
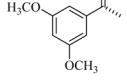
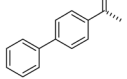
With four potent HDACs inhibitors in hand, we go further to evaluate their selectivity toward different HDAC isoforms belonging to different classes. Majority of HDACs share a common pharmacophore model consisting of three parts: a hydrophobic cap structure that can interact with the rim at the entrance of the active pocket of HDACs; a zinc ion binding group (ZBG); and a linker responsible for the connection between the cap and the ZBG and for interaction with the hydrophobic tunnel of the active site (14). By analyzing the structure features, it was found that our compounds possessed a bigger "cap" part than the pan-HDACi SAHA. So, we envisioned that our compounds may have selective inhibitory activities toward the HDAC6, because HDAC6 has a relative wider surface of the active pocket than other HDAC isoforms which can accommodate huge cap groups and this makes it possible to design highly selective HDAC6 inhibitors such as tubastatin-A (15). So, these four representative compounds were evaluated for their inhibitory activity against HDAC1 and HDAC6. Results in Table 2 showed that compared with SAHA, compounds LYP-2, -3, and -6 exhibited different degrees of selectivity for HDAC6 over HDAC1 isoform except for LYP-15.

Among these four compounds, LYP-2 displayed the most potent HDAC6 inhibitory activity ($\text{IC}_{50} = 12.3$ nM) and LYP-6 possessed best selectivity over HDAC1 even better than that of ACY-1215, a well-known HDAC6 inhibitor currently under clinical trials, which validate our compound design strategy.

3.3. Cell proliferation inhibition

The effect of LYP-2 and LYP-6 on cell viability was determined using MTT assay. Breast cancer cell MCF-7 was treated with different concentrations of LYP-2 or LYP-6 for 72 h. As shown in Figure 1A, either LYP-2 or LYP-6 dose-dependently suppressed the growth of MCF-7 cells. However, both the compounds demonstrated moderate growth inhibitory effect on this cell line, with IC_{50} values more than $30 \mu\text{M}$. Previously studies showed that selective inhibition of HDAC6 increases α -tubulin acetylation and accumulation of ubiquitinated proteins in cancer cells, with synergistic cytotoxicity in combination with proteasome inhibitor bortezomib (16). We therefore examined the effect of LYP-2 or LYP-6 plus bortezomib on the proliferation of MCF-7 cells. Cells were treated with different concentrations of bortezomib in presence or absence of LYP-2 or LYP-6 for 72 hours. As shown in Figures 1C and 1D, LYP-2 and LYP-6 dose-dependently enhanced the growth inhibitory effect of bortezomib. To explore the interactive effect between the compounds with bortezomib, we calculated the combination index (CI) values of bortezomib plus LYP (10 μM) using the CompuSyn software and determined interaction

Table 1. Structures of all 22 compounds and their inhibition rates against HDACs (Hela cell nucleus extracts) at 1 μ M concentration

Compound		Inhibition rate
LYP-1		69.5%
LYP-2		83.1%
LYP-3		78.4%
LYP-4		68.6%
LYP-5		58.3%
LYP-6		75.5%
LYP-7		69.5%
LYP-8		72.9%
LYP-9		72.9%
LYP-10		73.8%
LYP-11		37.0%

types according to the Chou-Talalay Method (17). The analysis revealed that combining LYP-2 or LYP-6 and bortezomib gave rise to an additive or synergistic effect when bortezomib was used at relatively low concentrations (< 100 nM) (Figures 1E and 1F). These results implied that HDAC6 inhibition may improve the efficacy of proteasome inhibitor bortezomib in breast cancer.

HDACs as an important anti-cancer drug targets have attracted many attentions. Till now, four HDACis, vorinostat, romidepsin, belinostat, and panobinostat, have been approved by the FDA for treatment of cancers including cutaneous T-cell lymphoma, peripheral T-cell lymphoma (PTCL), and multiple myeloma (18). The benzamide-based Class I HDAC-selective inhibitor chidamide has been approved in

Table 1. Structures of all 22 compounds and their inhibition rates against HDACs (Hela cell nucleus extracts) at 1 μ M concentration (continued)

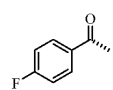
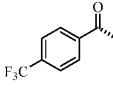
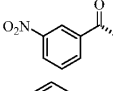
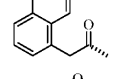
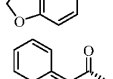
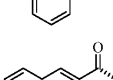
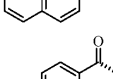
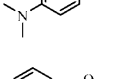
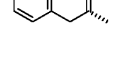
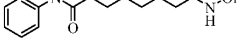
LYP-12		66.5%
LYP-13		67.6%
LYP-14		65.3%
LYP-15		78.9%
LYP-16		63.1%
LYP-17		66.1%
LYP-18		67.8%
LYP-19		61.6%
LYP-20		25.8%
LYP-21		71.1%
LYP-22		68.5%
SAHA		96.8%

Table 2. Inhibitory activity of four representative compounds toward HDAC1 and 6

Compound	IC ₅₀ ^a , nM		SF(6/1) ^b
	HDAC1 (class I)	HDAC6 (class IIb)	
LYP-2	177.3	12.3	14.41
LYP-3	408.1	31.7	12.87
LYP-6	775.8	21.0	36.94
LYP-15	107.0	49.9	2.14
SAHA	44.6	21.6	2.06
ACY1215	66.8	5.3	12.6

^aThe IC₅₀ values are the means of two experiments, with intra- and inter-assay variations of < 10%. ^bSF(6/1): selectivity factor for HDAC6 over HDAC1 (SF6/1 = IC₅₀(HDAC1)/IC₅₀(HDAC6)).

China for the treatment of relapsed or refractory PTCL (19). Apart from these five approved, there are several other HDACis at different stages of clinical trials against cancers. That said, shortcomings of HDACis

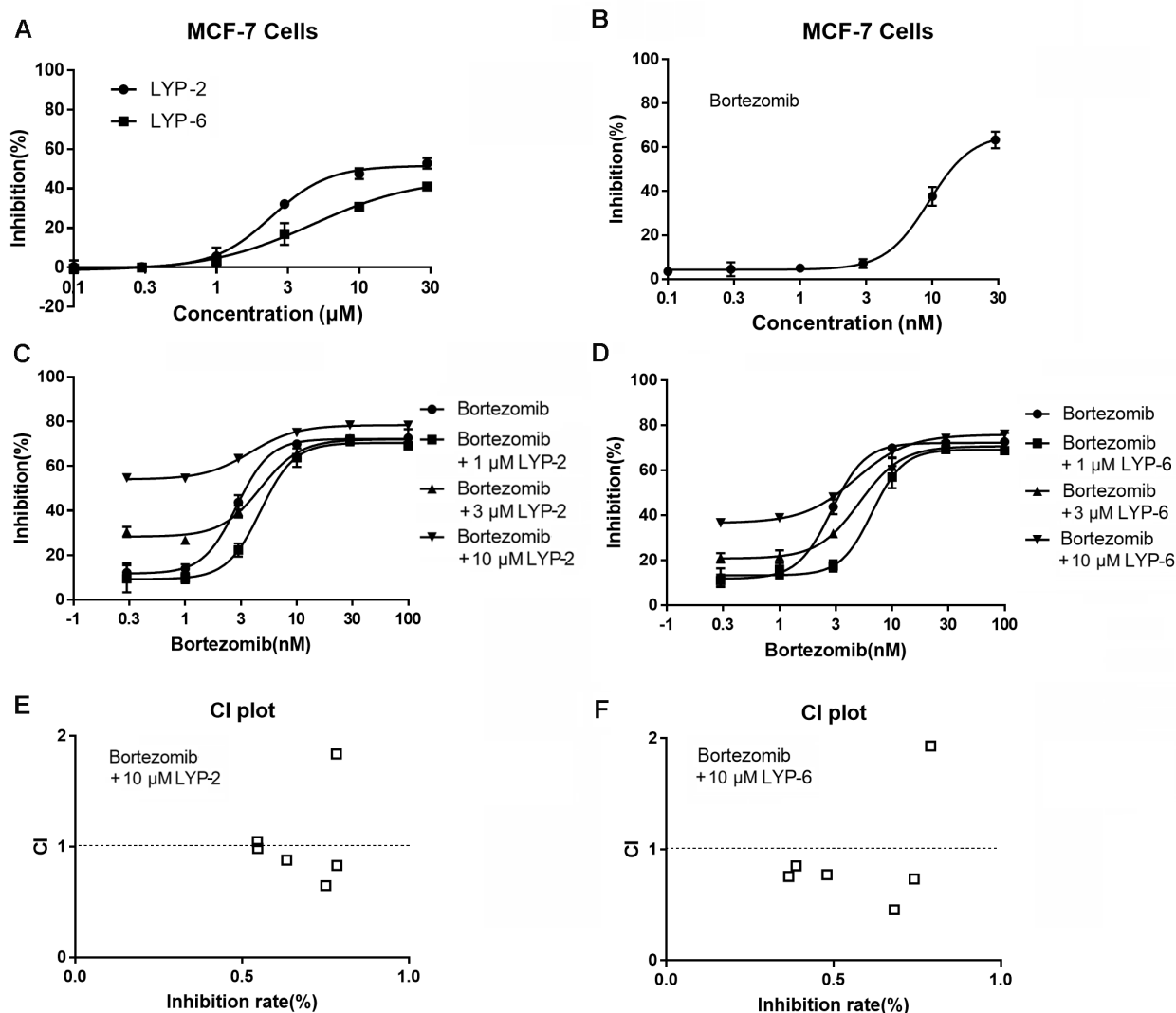


Figure 1. Inhibition of breast cancer cell MCF-7 proliferation. (A and B) Cells were incubated with different concentrations of LYP-2, LYP-6, or bortezomib for 72 hours and then subjected to MTT assay. (C and D) Cells were exposed to bortezomib alone or in combination with LYP-2 or LYP-6 at a fixed concentration (1, 3, and 10 μM , respectively) for 72 h before subjected to MTT assay. (E and F) Combination indexes (CI) of bortezomib plus LYP-2 or LYP-6 (10 μM) were calculated using the CompuSyn software and were plotted against cell inhibition rates.

still exist, one of which is the toxicity (18). In order to avoid unwanted toxicities, isoform selective HDACis are developed, especially the HDAC6 selective inhibitors, many of which have exhibited promising application values.

A number of HDAC6-selective inhibitors with diverse structural skeletons have been reported. The first HDAC6-selective inhibitor, tubacin, achieved selectivity through a bulky, relatively complex capping group (20). Unfortunately, the poor pharmacokinetic properties limited its application. In contrast, another well-known HDAC6 selective inhibitor ACY-1215 has a rigid and less cumbersome capping group contributing to its HDAC6 selectivity; nevertheless, it exhibited a selectivity index of only about 10 against HDAC1-3 (21). We designed and synthesized a series of novel HDACis with the N-phenylpiperidine-1-carboxamide as the skeleton in this work. Most of them displayed

potent HDAC inhibitory activity and three of them were HDAC6 selective inhibitors. The selective index of compound LYP-6 was 36.94, much higher than the reference compound ACY-1215 which validates our design strategy.

Previous studies suggested that HDAC6 expression could be upregulated by estrogen, suggesting that there might be a link between the levels of HDAC6 expression and progression of breast cancer (22). We tested whether our newly discovered HDAC6 inhibitors have growth inhibitory ability on breast cancer cells. We found that although LYP-2 and LYP-6 dose-dependently inhibited the proliferation of MCF-7, their efficacy is moderate with IC_{50} values more than 30 μM . This result is consistent with a previous study in which HDAC6 selective inhibitor 4-hydroxybenzoic acid failed to induce significant cell death in MCF-7 cells at concentrations below 20 μM (23). On the other hand,

several studies demonstrated that HDAC6 inhibition sensitized the antitumor efficacy of chemotherapeutic drugs such as adriamycin and 5-fluorouracil (23,24). In the present study, we found that LYP-2 and LYP-6 enhanced the antiproliferative effect of bortezomib in MCF-7 cells and this combined treatment demonstrated an additive or synergistic effect. The safety and efficacy of bortezomib plus other chemotherapeutic drugs against breast cancer is currently under clinical trials. Our results suggested HDAC6 inhibitor might be an option in bortezomib based combined regimen in treatment of breast cancer in the future.

4. Conclusion

We designed and synthesized 22 novel HDAC inhibitors with the 4-aminopiperidine-1-carboxamide as the core structure. Within these compounds, LYP-2, LYP-3, and LYP-6 were identified as potent HDAC6 selective inhibitors. LYP-2 and LYP-6 showed moderate efficacy in suppressing the proliferation of breast cancer cells MCF-7, however, both compounds additively or synergistically enhanced the growth inhibitory effect of bortezomib. Combined HDAC6 inhibitor and bortezomib for treatment of breast cancer warrants further study in the future.

Acknowledgements

We gratefully acknowledge the financial support from the National Science Foundation for Young Scientists of China to Y. L. (NSFC no. 81602947) and J. G. (NSFC no. 81503094), China Postdoctoral Science Foundation (no. 2016M600524), and Qingdao Postdoctoral Applied Research Project (no. 2016072; Jianjun Gao, Qingdao University).

References

- Di Gennaro E, Bruzzese F, Caraglia M, Abruzzese A, Budillon A. Acetylation of proteins as novel target for antitumor therapy: Review article. *Amino Acids*. 2004; 26:435-441.
- Secrist JP, Zhou X, Richon VM. HDAC inhibitors for the treatment of cancer. *Curr Opin Investig Drugs*. 2003; 4:1422-1427.
- Zhang Y, Fang H, Jiao J, Xu W. The structure and function of histone deacetylases: The target for anti-cancer therapy. *Curr Med Chem*. 2008; 15:2840-2849.
- West AC, Johnstone RW. New and emerging HDAC inhibitors for cancer treatment. *J Clin Invest*. 2014; 124:30-39.
- Zhang L, Han Y, Jiang Q, Wang C, Chen X, Li X, Xu F, Jiang Y, Wang Q, Xu W. Trend of histone deacetylase inhibitors in cancer therapy: Isoform selectivity or multitargeted strategy. *Med Res Rev*. 2015; 35:63-84.
- Kalin JH, Bergman JA. Development and therapeutic implications of selective histone deacetylase 6 inhibitors. *J Med Chem*. 2013; 56:6297-6313.
- Hubbert C, Guardiola A, Shao R, Kawaguchi Y, Ito A, Nixon A, Yoshida M, Wang XF, Yao TP. HDAC6 is a microtubule-associated deacetylase. *Nature*. 2002; 417:455-458.
- Kovacs JJ, Murphy PJ, Gaillard S, Zhao X, Wu JT, Nicchitta CV, Yoshida M, Toft DO, Pratt WB, Yao TP. HDAC6 regulates Hsp90 acetylation and chaperone-dependent activation of glucocorticoid receptor. *Mol Cell*. 2005; 18:601-607.
- Zhang X, Yuan Z, Zhang Y, Yong S, Salas-Burgos A, Koomen J, Olashaw N, Parsons JT, Yang XJ, Dent SR, Yao TP, Lane WS, Seto E. HDAC6 modulates cell motility by altering the acetylation level of cortactin. *Mol Cell*. 2007; 27:197-213.
- Leng Y, Wu Y, Lei S, Zhou B, Qiu Z, Wang K, Xia Z. Inhibition of HDAC6 Activity Alleviates Myocardial Ischemia/Reperfusion Injury in Diabetic Rats: Potential Role of Peroxiredoxin 1 Acetylation and Redox Regulation. *Oxid Med Cell Longev*. 2018; 2018:9494052.
- Song Y, Lim J, Seo YH. A novel class of anthraquinone-based HDAC6 inhibitors. *Eur J Med Chem*. 2019; 164:263-272.
- Sun Z, Zhu Y, Aminbuhe, Fan Q, Peng J, Zhang N. Differential expression of APE1 in hepatocellular carcinoma and the effects on proliferation and apoptosis of cancer cells. *Biosci Trends*. 2018; 12:456-462.
- Yao H, Zhou L, Tang L, Guan Y, Chen S, Zhang Y, Han X. Protective effects of luteolin-7-O-glucoside against starvation-induced injury through upregulation of autophagy in H9c2 Cells. *Biosci Trends*. 2017; 11:557-564.
- Bian J, Luan Y, Wang C, Zhang L. Discovery of N-hydroxy-4-(¹H-indol-3-yl)butanamide as a histone deacetylase inhibitor. *Drug Discov Ther*. 2016; 10:163-166.
- Butler KV, Kalin J, Brochier C, Vistoli G, Langley B, Kozikowski AP. Rational design and simple chemistry yield a superior, neuroprotective HDAC6 inhibitor, tubastatin A. *J Am Chem Soc*. 2010; 132:10842-10846.
- Amengual JE, Johannet P, Lombardo M, et al. Dual Targeting of Protein Degradation Pathways with the Selective HDAC6 Inhibitor ACY-1215 and Bortezomib Is Synergistic in Lymphoma. *Clin Cancer Res*. 2015; 21:4663-4675.
- Zhang SS, Ni YH, Zhao CR, Qiao Z, Yu HX, Wang LY, Sun JY, Du C, Zhang JH, Dong LY, Wang K, Gao JJ. Capsaicin enhances the antitumor activity of sorafenib in hepatocellular carcinoma cells and mouse xenograft tumors through increased ERK signaling. *Acta Pharmacol Sin*. 2018; 39:438-448.
- Lakshmaiah KC, Jacob LA, Aparna S, Lokanatha D, Saldanha SC. Epigenetic therapy of cancer with histone deacetylase inhibitors. *J Cancer Res Ther*. 2014; 10:469-478.
- Lu X, Ning Z, Li Z, Cao H, Wang X. Development of chidamide for peripheral T-cell lymphoma, the first orphan drug approved in China. *Intractable Rare Dis Res*. 2016; 5:185-191.
- Lernoux M, Schnekenburger M, Dicato M, Diederich M. Anti-cancer effects of naturally derived compounds targeting histone deacetylase 6-related pathways. *Pharmacol Res*. 2018; 129:337-356.
- Cao J, Lv W, Wang L, Xu J, Yuan P, Huang S, He Z, Hu J. Ricolinostat (ACY-1215) suppresses proliferation

- and promotes apoptosis in esophageal squamous cell carcinoma *via* miR-30d/PI3K/AKT/mTOR and ERK pathways. *Cell Death Dis.* 2018; 9:817.
22. Inoue A, Yoshida N, Omoto Y, Oguchi S, Yamori T, Kiyama R, Hayashi S. Development of cDNA microarray for expression profiling of estrogen-responsive genes. *J Mol Endocrinol.* 2002; 29:175-192.
 23. Wang XN, Wang KY, Zhang XS, Yang C, Li XY. 4-Hydroxybenzoic acid (4-HBA) enhances the sensitivity of human breast cancer cells to adriamycin as a specific HDAC6 inhibitor by promoting HIPK2/p53 pathway. *Biochem Biophys Res Commun.* 2018; 504:812-819.
 24. Tan Y, Zhang S, Zhu H, Chu Y, Zhou H, Liu D, Huo J. Histone deacetylase 6 selective inhibitor ACY1215 inhibits cell proliferation and enhances the chemotherapeutic effect of 5-fluorouracil in HCT116 cells. *Ann Transl Med.* 2019; 7:2.

(Received February 1, 2019; Revised February 27, 2019; Accepted February 28, 2019)

Combined machine learning and functional magnetic resonance imaging allows individualized prediction of high-altitude induced psychomotor impairment: The role of neural functionality in putamen and pallidum

Xiaoming Chen[§], Qian Zhang[§], Jiye Wang[§], Zhenlong Xin, Jingyuan Chen^{*}, Wenjing Luo^{*}

Department of Occupational and Environmental Health, the Ministry of Education Key Lab of Hazard Assessment and Control in Special Operational Environment, School of Public Health, Air Force Medical University, Xi'an, Shaanxi Province, China.

Summary

Hypoxia exposure during high-altitude expedition cause psychomotor impairment. Neuroimaging studies indicated that the impairment may be significantly associated with neuron loss and decreased regional homogeneity (ReHo) in several brain regions, suggesting the neural functionality in these regions may be utilized to predict psychomotor impairment under exposure. In this study, 69 subjects come from Shaanxi-Tibet immigrant cohort. Reaction time (RT) tasks were performed to measure the subject's psychomotor function before and after 2-year high-altitude exposure. For each individual, the RT differences between pre-exposure and post-exposure were calculated, which were referred to as "targets" in model establishment. Rs-fMRI data were acquired at the same time with RT tasks. For each individual, the map of ReHo alteration was generated, from which the patterns would be recognized. A pattern recognition procedure was utilized to train and test the predictive models. Two different cross-validation strategies were utilized to evaluate the model performance: leave-one-out cross-validation and four-fold cross-validation. For the models displaying significant R^2 and MSE, weight maps were built. As a result, the predictive models were able to decode the changes of simple and recognition reaction time from the alterations of brain activation under the exposure. The regions with highest contributions to the predictions were bilateral putamen and bilateral pallidum, suggesting that predictions were mainly based on the patterns concentrated in these regions. This study was a proof of concept study designed to examine whether individual-level psychomotor impairment under high-altitude exposure could be predicted by a combination of pattern recognition approach and neuroimaging data.

Keywords: High altitude, psychomotor impairment, pattern recognition, regional homogeneity

Released online in J-STAGE as advance publication February 27, 2019.

[§]These authors contributed equally to this work.

^{*}Address correspondence to:

Prof. Wenjing Luo and Prof. Jingyuan Chen, Department of Occupational and Environmental Health, the Ministry of Education Key Lab of Hazard Assessment and Control in Special Operational Environment, School of Public Health, Air Force Medical University, 169 Changlexi Road, Xi'an, Shaanxi 710032 China.

E-mail: luowenj@fmmu.edu.cn (Luo WJ)
jy_chen@fmmu.edu.cn (Chen JY)

1. Introduction

At high-altitude, hypoxia together with other physiological stressors, including low temperature, ultraviolet rays and dehydration, may lead to a decline in cognitive function (1). Previous studies have proved that acute and chronic hypoxia exposure during high-altitude expedition cause impairment in working memory, learning ability, attention and concentration. Recently, according to a previous study based on Tibet immigration population in China, two-year hypoxia

exposure may lead to a significant impairment in psychomotor function, *i.e.*, prolonged simple and recognition reaction time (2). Psychomotor function is related to daily affairs like driving a car, attending to conversation, tracking and responding to a set of simple instructions, whose impairment may cast a negative influence upon the life quality and work efficiency of high-altitude immigrants.

Neuroimaging approaches including high resolution 3D anatomical imaging and resting-state functional magnetic resonance imaging (rs-fMRI) have been employed to reveal the structural and functional basis of the hypoxia induced psychomotor impairment. Our previous work indicated the neuron loss and decreased regional homogeneity (ReHo) in several brain regions, *i.e.*, putamen, superior temporal gyrus and anterior cingulate gyrus, may greatly contribute to the psychomotor impairment (2). ReHo was designed to reflect the similarity of the time series of a given voxel to those of its neighboring voxels, which may function as a potential sign of local neural functionality (3). Thus, we inferred that the alteration of regional neural activity may serve as a biomarker predicting the potential psychomotor impairment under high-altitude exposure and reflecting the individual's vulnerability to hypoxia stress. In clinical practice, the potential biomarker may be referred by physicians when they gave advices to voluntary high-altitude immigrants. In parallel, it also helps to understand the pathophysiological processes associated with these neurobehavioral alterations and provide biologically-relevant targets that can guide high-altitude impairment prevention and novel treatment development (4,5).

Machine learning (ML) techniques can help to discover the potential biomarkers within the neuroimaging data. Compared with conventional univariate analyses, ML techniques are able to make regionally specific inferences about abnormalities in brain function associated with the impairment at the individual level (6). As a subfield of ML, pattern recognition approach uses computer-based techniques to automatically discover patterns in the data, which be utilized to identify relationships between patterns of brain activity and continuous measures of neurobehavior. In our case, ReHo data can be analyzed by pattern recognition approach to decode individual-level psychomotor measures (4).

The aim of this study was thus to use functional neuroimaging and pattern recognition approach to determine whether the change of psychomotor measures before and after high-altitude exposure could be decoded from patterns of ReHo alteration. This study has the potential to identify important biomarkers not only to help determine vulnerability to high-altitude hypoxia stress at the individual level, but also to pave the way forward for future studies using ML technique to predict other clinical outcomes in high-altitude immigrants.

2. Materials and Methods

2.1. Subjects

The protocol was approved by the Ethics Committee of the Medical Faculty of Fourth Military Medical University (registry no. KY20143344-1). All the studies were conducted in accordance with the ethical principles for medical research involving human subjects as defined in the Declaration of Helsinki.

All the subjects in this study come from Shaanxi-Tibet immigrant cohort (STI cohort). The details about this cohort have been described previously (2). The STI cohort study was launched in 2014, included 69 young healthy high school graduates in Shaanxi who were admitted into Tibet University for four-year higher education. Baseline investigation, neurobehavioral and MRI measures were performed on July, 2014 in Xi'an (altitude 466 m), China. The information about high-altitude exposure history, medical history and sociodemographic status (parental education, vocation, socioeconomic status, *etc.*) were collected at baseline. The follow-up investigation and measures were performed on May 2016 in Lhasa (altitude 3,658 m).

Reaction time (RT) tasks were performed to measure the subject's psychomotor function before and after exposure, which consisted of visual simple reaction time (VSRT), audial simple reaction time (ASRT), visual recognition reaction time (VRRT) and audial recognition reaction time (ARRT). All the procedures were performed in the pattern of CNS Vital Signs (<http://www.cnsvs.com/>).

2.2. Rs-fMRI data acquisition and analysis

Rs-fMRI data were acquired with General Electric Discovery MR750 3.0T (General Electric Co. Ltd., Connecticut, USA) in Xijing Hospital of Air Force Medical University and the General Hospital of Tibet Military Region, respectively. The details about MRI scanning have been described previously (2). Data preprocessing was performed with the SPM8 and Data Processing Assistant for Resting-state fMRI Advanced (DPARSFA) tools as previously described (2,7). The KCC (Kendall's coefficient concordance) value between the time series of a given voxel and those of its nearest 26 neighboring voxels was calculated in a voxel-wise method. Then, ReHo map for each individual was transformed to MNI coordinates and spatially smoothed (full width at half maximum [FWHM] = 8 mm). Finally, the ReHo map of each individual was divided by its own mean ReHo for standardization purposes.

2.3. Predictive models establishment

For each individual, the RT alteration during the exposure (RT post-exposure – RT pre-exposure)

was calculated, which was referred to as "target" in the process of model establishment. Then, the ReHo difference between pre-exposure and post-exposure (ReHo post-exposure – ReHo pre-exposure) was calculated in the similar method used for calculating the RT alteration. For each individual, the map of ReHo differences was referred to as "input", from which the patterns would be recognized in the process of model establishment (2,8).

A standard procedure in Pattern Recognition for Neuroimaging Toolbox (PRoNTTo) (<http://www.mnl.cs.ucl.ac.uk/pronto/>) was utilized to train and test the predictive models. The models were trained to learn the association between the ReHo and RT alterations using the examples in training sets. Three Pattern recognition algorithms currently available in PRoNTTo: Relevance Vector Regression (RVR), Gaussian Process Regression (GPR) and Kernel Ridge Regression (KRR) were utilized to extract predictive patterns within the data of ReHo alterations (9). In the preliminary research, we found there were no significant differences in the performance of the three different algorithms. Herein, we only present the results of RVR for the sake of brevity. RVR is a probabilistic kernel-based pattern recognition method using Bayesian inference to obtain sparse regression models, and allows the extraction of patterns within a high-dimensional feature space, which was widely used in previous studies (10).

Two different cross-validation strategies were utilized to evaluate the model performance: leave-one-out cross-validation and 4-fold cross-validation. Leave-one-out cross validation is a frequently used validation method, involving leaving one subject out as the validation data, training the model on other N-1 subjects, and doing so N times so that each subject is left out once. In 4-fold cross-validation, the original sample is randomly partitioned into 4 equal sized subsamples. Of the 4 subsamples, a single subsample is retained as the validation data, and the remaining 3 subsamples are used as training data (4).

In both cross-validation strategies, the RT alteration(s) left out for test was/were decoded from the corresponding data of ReHo alterations using the model trained on the remaining data. Agreement between predicted and actual RT alterations was assessed using two different metrics: coefficient of determination (R^2) and mean squared error (MSE). Statistical significance for both metrics was determined by permutation tests with 1000 times. Results were considered significant if the $p < 0.05$ (4,9).

2.4. Weight map

For pattern recognition models showing significant R^2 and MSE, weight maps were built at both voxel and region level. For each brain region defined by the Anatomical Automatic Labeling (AAL) atlas, the

mean of all voxel weights (absolute values) within this region were computed. Then, all the labelled regions were ranked according to the percentage of the total normalized weights they contributed in the pattern recognition modelling (4,9).

3. Results and Discussion

3.1. Subjects' characteristics

The average age of the subjects (M: 48; F: 21) was 18.2 ± 0.3 (range: 17.5 – 19.1) at baseline. In the 1st year of follow-up, the cumulative high-altitude exposure time of the subjects was 270.0 ± 7.4 d (range: 257 – 299 d), while in the second year, the exposure time increased to 280.8 ± 7.3 d (range: 268 – 314 d). No major health problems occurred during the follow-up. The detailed demographic and socioeconomic information of subjects were reported in our previous study (2).

3.2. Performance of the predictive model

The correlations between the predicted RT alterations and the actual values were displayed in Figure 1. Coefficient of determination (R^2) and mean squared error (MSE) were calculated for each prediction to assess the goodness-of-fit. As a result, the R^2 and MSE between the predicted and actual VSRT alteration were 0.33 ($p = 0.003$) and 0.01 ($p = 0.001$), respectively; Similar results were obtained in the prediction of ASRT alteration, the R^2 and MSE were 0.46 ($p = 0.001$) and 0.01 ($p = 0.001$). The R^2 and MSE between the predicted and actual VRRRT alteration were 0.14 ($p = 0.045$) and 0.04 ($p = 0.013$), respectively; while the R^2 and MSE between the predicted and actual ARRT alteration were 0.25 ($p = 0.014$) and 0.02 ($p = 0.001$). In summary, the predictive models were able to decode high-altitude induced psychomotor impairments from the changes of brain activation during the exposure.

3.3. Regions contributed to prediction

The weight maps of patterns contributed to predictions were displayed in Figure 2. The voxel-based weight maps were located on the left, while the region-based weight maps (computed from the voxel based predictive pattern) were located on the right. The color of each region corresponds to the normalized average of voxels weights within the regions (in absolute value). The top 10 ranked regions according to normalized weights per region were displayed in Table 1, which represent over 15% of the total weights in the decision functions. Generally, the regions with highest contributions to the predictions were bilateral putamen and bilateral pallidum, while Heschl's gyrus and cuneus gyrus also contributed to the predictions, suggesting that predictions were mainly based on the patterns

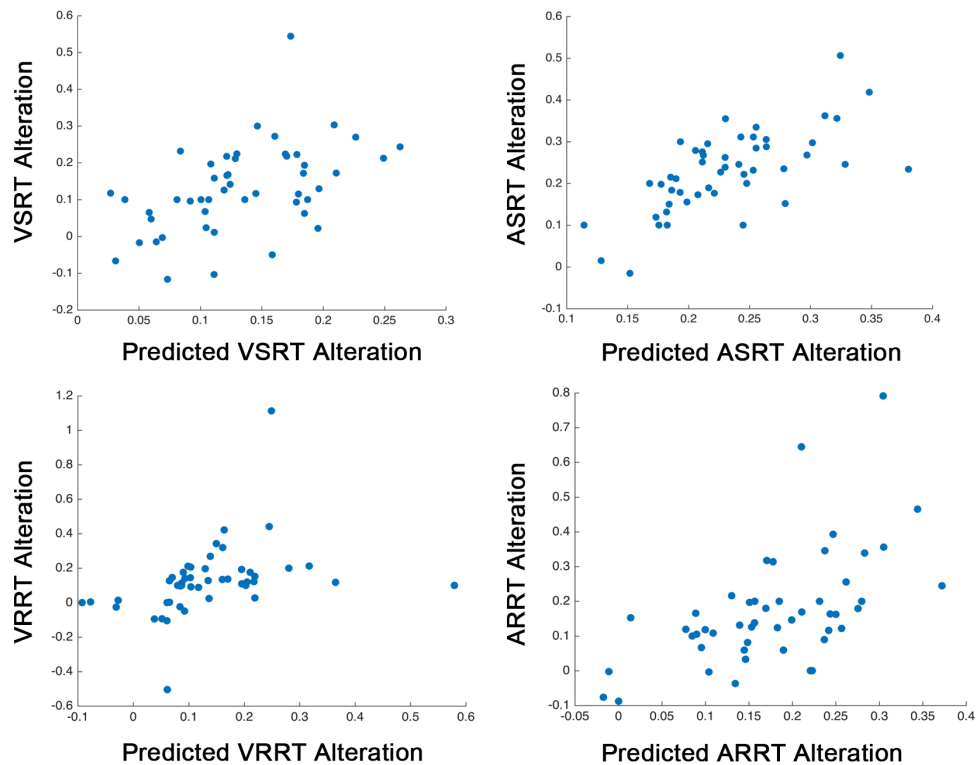


Figure 1. The scatter plots displaying the predicted neurobehavioral alterations (x-axis) against the actual values or targets (y-axis). VSRT, visual simple reaction time; ASRT, audial simple reaction time; VRRT, visual recognition reaction time; ARRT, audial simple reaction time.

concentrated in these regions.

The neurobehavioral and rs-fMRI data used in the current study have been analyzed and reported in our previous study (2). Previously, we aimed at identifying the brain regions related to high-altitude induced cognitive impairment. Similar to other conventional neuroimaging studies, we utilized univariate statistical analysis to compare the neuroimaging data before exposure with those after exposure. The results showed significant associations between ReHo changes in putamen and alterations of the neurobehavioral alterations. However, a major limitation of the univariate analysis we used is that it only describes differences at the group level and does not enable decisions at the individual level, which is of more limited use in practice. In the present study, instead of investigating association between neurobehavioral measures and brain activity at the group level, we applied pattern recognition approach, with the aim of determining whether the alteration of neurobehavioral measures at different time points could be decoded from patterns of whole-brain activity changes. To the best of our knowledge, this is the first study applying pattern recognition approach to predict individual's cognitive impairment under high-altitude exposure.

The strength of this study was guaranteed the two different cross-validation strategies, four-fold

cross-validation and leave-one-out cross-validation. Although it's common to leave one subject out and train the model with N-1 subjects (where N corresponds to the total number of subjects), demonstration of reproducibility between different cross-validation strategies is vital to display the stability of the results and for future clinical use of the predictive model. The R^2 and MSE between predicted and actual RT alterations were significant when the model was tested using the two different cross-validation strategies, suggesting the relationship between psychomotor function impairment and the brain activity alteration is reliable in the model establishment (9). Interestingly, we found the R^2 s between predicted and actual VRRT/ARRT alterations were lower than those in VSRT/ASRT alteration prediction (MSEs were higher). One possible explanation for these findings is the fact that recognition reaction tasks included more brain regions and neurophysiological processes in responding to signals of complex directions, thus it's more difficult for the learning algorithm to learn the relationship between the neurobehavioral measures and brain activity.

Some brain areas are probably more informative about regression targets than others. The weight map is therefore a spatial representation of the decision function, *i.e.* every voxel within the mask contributes with a certain weight to the decision function. Since the prediction is based on the whole brain pattern,

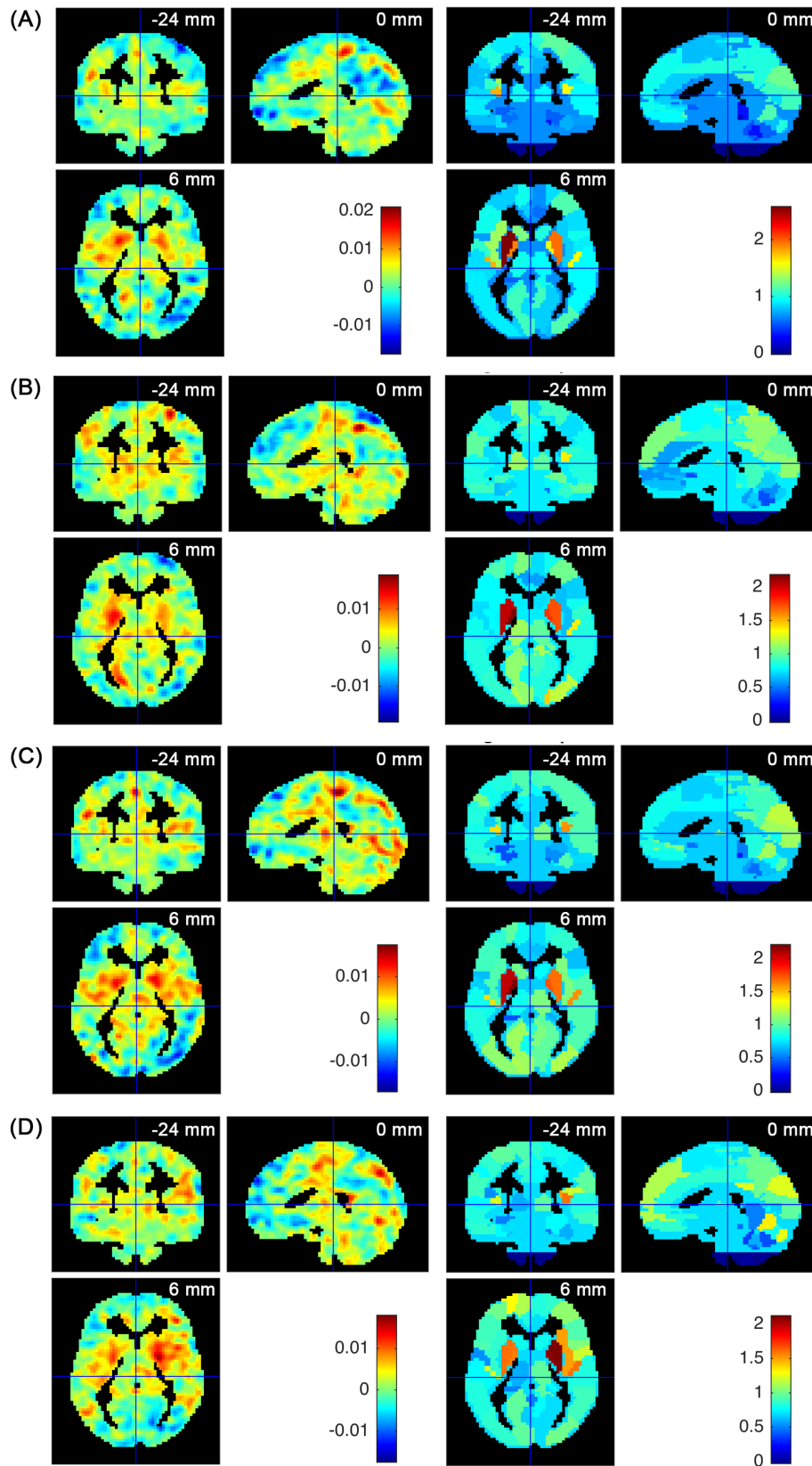


Figure 2. The weight map of patterns in the prediction of neurobehavioral alterations. (A) VSRT; (B) ASRT; (C) VRRT; (D) ARRT. The voxel-based weight maps were located on the left, and the color bar indicated the relative importance of the voxel in the decision function. The region-based pattern localization maps were located on the right, and the color bar indicated the normalized contribution of the region.

Table 1. The top ten ranked regions contributed to the prediction of VSRT/ASRT/VRRT/ARRT alterations

Regions	Weight (%)	Size (voxels)
Prediction of VSRT Alterations		
L Putamen	2.53	284
R Putamen	1.87	318
L Pallidum	1.82	79
L Heschl's Gyrus	1.76	72
R Heschl's Gyrus	1.51	60
R Pallidum	1.47	68
L Insula	1.27	560
R Gyrus Rectus	1.24	185
L Angular Gyrus	1.24	340
L Cuneus Gyrus	1.22	460
Prediction of ASRT Alterations		
L Pallidum	2.18	79
L Putamen	1.98	284
R Pallidum	1.72	68
R Putamen	1.63	318
R Superior Occipital Gyrus	1.48	391
R Inferior Occipital Gyrus	1.48	313
R Superior Frontal Gyrus, Orbital Part	1.40	166
R Heschl's Gyrus	1.31	60
R Middle Occipital Gyrus	1.24	565
R Precuneus	1.20	898
Prediction of VRRT Alterations		
L Pallidum	2.12	79
L Putamen	1.98	284
R Pallidum	1.68	68
R Heschl's Gyrus	1.57	60
R Putamen	1.57	318
L Heschl's Gyrus	1.39	72
L Cuneus Gyrus	1.21	460
L Angular Gyrus	1.20	340
R Middle Frontal Gyrus, Orbital Part	1.16	213
L Superior Occipital Gyrus	1.15	353
Prediction of ARRT Alterations		
R Putamen	2.07	318
R Pallidum	2.03	68
R Heschl's Gyrus	1.60	60
L Putamen	1.54	284
L Pallidum	1.46	79
R Insula	1.41	508
L Cerebellum Crus II	1.33	518
L Superior Frontal Gyrus	1.30	1,013
Vermis 6	1.29	87
L Cuneus Gyrus	1.27	460

The third column (weights) displayed the normalized contribution of each region. The rows of the table are sorted in descending order according to this value. The fourth column displayed the size of the patterns (voxels) in each region, indicating the overlap between the atlas and the data. VSRT, visual simple reaction time; ASRT, aural simple reaction time; VRRT, visual recognition reaction time; ARRT, aural simple reaction time.

rather than on individual regions or voxels, all voxels contribute to the regression and no conclusions should be drawn about a particular subset of voxels in isolation (4). The brain regions with the highest contribution to decoding the striatum, including the putamen and pallidum. This result is consistent with the results at group level in our previous study. The striatum is a critical component of the motor and reward systems, which receives glutamatergic and dopaminergic inputs from different sources and serves as the primary input to the rest of the basal ganglia. It is well established

that movement disorders such as dyskinesias, chorea and choreoathetosis are associated with abnormal functioning within these regions (11-13). As a result, our findings suggest that neural functionality loss in these motor regulating regions may contribute to psychomotor impairment in high-altitude immigrants. Our investigation therefore indicates that these brain regions may provide critical information for successfully estimating vulnerability to high-altitude stress at the individual level.

There were some limitations in the present study. To be most important, although we applied two different cross-validation strategies to demonstrate generalizability of the predicative models, ideally the models should be tested with truly independent samples. Further studies with larger sample sizes are necessary to assess the generalizability of the proposed modelling approach by completely independent training and testing sets.

4. Conclusion

This study was designed to examine whether pattern recognition approach could be applied to neuroimaging data to predict individual-level psychomotor impairment under high-altitude exposure. Future studies, using a combination of pattern recognition and neuroimaging approaches, can build on the present findings to determine the individual's vulnerability to other cognitive impairments under long-term high-altitude exposure. Furthermore, as the follow-up of our STI cohort continues, we are trying to decode the cognitive impairment under long time high-altitude exposure (4-year or more) from the existing neuroimaging data acquired in relatively short time (2-year), whose findings may be more persuasive in advising the voluntary high-altitude immigrants in the clinical practice.

Acknowledgement

This study was financially supported by the National Science Foundation of China (No. 81330045, 81730053, 81803194, 81502770) and the Military Logistics Research Project (No. AWS14L008, AWS16J022).

References

1. Yan X. Cognitive impairments at high altitudes and adaptation. *High Alt Med Biol.* 2014; 15:141-145.
2. Chen X, Zhang Q, Wang J, *et al.* Cognitive and neuroimaging changes in healthy immigrants upon relocation to a high altitude: A panel study. *Hum Brain Mapp.* 2017; 38:3865-3877.
3. Jiang L, Zuo XN. Regional homogeneity: A multimodal, multiscale neuroimaging marker of the human connectome. *Neuroscientist.* 2016; 22:486-505.
4. Schrouff J, Rosa MJ, Rondina JM, Marquand AF, Chu C,

- Ashburner J, Phillips C, Richiardi J, Mourão-Miranda J. PRoNTO: Pattern recognition for neuroimaging toolbox. *Neuroinformatics*. 2013; 11:319-337.
5. Taylor JA, Matthews N, Michie PT, Rosa MJ, Garrido MI. Auditory prediction errors as individual biomarkers of schizophrenia. *Neuroimage Clin*. 2017; 15:264-273.
 6. Mateos-Perez JM, Dadar M, Lacalle-Aurioles M, Iturria-Medina Y, Zeighami Y, Evans AC. Structural neuroimaging as clinical predictor: A review of machine learning applications. *Neuroimage Clin*. 2018; 20:506-522.
 7. Yan CG, Zang YF. DPARSF: A MATLAB toolbox for "Pipeline" data analysis of resting-state fMRI. *Front Syst Neurosci*. 2010; 4:13.
 8. Gualtieri CT, Johnson LG. Reliability and validity of a computerized neurocognitive test battery, CNS Vital Signs. *Arch Clin Neuropsychol*. 2006; 21:623-643.
 9. Portugal LC, Rosa MJ, Rao A, *et al*. Can Emotional and Behavioral Dysregulation in Youth Be Decoded from Functional Neuroimaging? *PloS One*. 2016; 11:e0117603.
 10. Ranlund S, Rosa MJ, de Jong S, Cole JH, Kyriakopoulos M, Fu CHY, Mehta MA, Dima D. Associations between polygenic risk scores for four psychiatric illnesses and brain structure using multivariate pattern recognition. *Neuroimage Clin*. 2018; 20:1026-1036.
 11. Kandiah N, Tan K, Lim CC, Venketasubramanian N. Hyperglycemic choreoathetosis: role of the putamen in pathogenesis. *Mov Disord*. 2009; 24:915-919.
 12. Singh-Bains MK, Waldvogel HJ, Faull RL. The role of the human globus pallidus in Huntington's disease. The role of the human globus pallidus in Huntington's disease. 2016; 26:741-751.
 13. Nakawah MO, Lai EC. Post-stroke dyskinesias. *Neuropsychiatr Dis Treat*. 2016; 12:2885-2893.

(Received January 10, 2019; Revised February 3, 2019; Accepted February 9, 2019)

"History, Tradition, and Progress": The ceremony of 150th Anniversary of the National Center for Global Health and Medicine held in Tokyo, Japan

Norihiro Kokudo*, Tetsuo Hara

National Center for Global Health and Medicine, Tokyo, Japan.

Summary "History, Tradition, and Progress", a grand ceremony in celebration of the 150th Anniversary of the National Center for Global Health and Medicine (NCGM) was held in Tokyo, Japan on December 3, 2018. Hundreds of distinguished guests from home and abroad attended the grand ceremony. The NCGM is a national research and development agency, which is a type of independent administrative entity. The NCGM originated from a temporary army hospital that was established in Tokyo in October 1868. After several rounds of restructuring and reorganization, the facility became the NCGM in April 2015. The NCGM has various departments, including the Center Hospital, Kohnodai Hospital, the Research Institute, the Center for Clinical Sciences, the Bureau of International Health Cooperation, and the National College of Nursing. The NCGM conducts research in various fields such as infectious diseases, immune disorders, diabetes, and metabolic disorders and it provides advanced and comprehensive medical care. The NCGM also comprehensively provides training for personnel in international cooperation and medicine. "As a research and development entity, the NCGM will continue to fulfil those tasks in accordance with Japan's national policies", Dr. Norihiro Kokudo, the president of NCGM, said in his speech of anniversary opening greeting.

Keywords: National Center for Global Health and Medicine (NCGM), hospital, international health, medical care

A grand ceremony in celebration of the 150th Anniversary of the National Center for Global Health and Medicine (NCGM) (1) was held in Tokyo, Japan on December 3, 2018 (Figure 1A). Hundreds of distinguished guests from home and abroad attended the grand ceremony.

Dr. Norihiro Kokudo, the president of NCGM, addressed the anniversary opening greeting, extending warm welcome to all the distinguished guests present (Figure 1B). Their Imperial Highnesses Prince and Princess Akishino attended the celebration, and their Imperial Highness Prince Akishinonomiya expressed the congratulation on opening of the 150th anniversary ceremony (Figure 1C). Dr. Takumi Nemoto (Figure

1D), the Minister of Health, Labour and Welfare of Japan, and Dr. Yoshitake Yokokura (Figure 1E), the president of Japan Medical Association, delivered their congratulatory speech at the ceremony, respectively. Furthermore, addressing the ceremony, Dr. Nguyen Quoc Trieu, Chairman of Central Office of Health Protection Care, Vietnam, sincerely expressed their wished to promote the cooperation with NCGM to a new operative development stage. A special keynote lecture was given by Dr. Kazuhide Yamazaki (Figure 1F) and Dr. Satoshi Omura (a Nobel Laureate) (Figure 1G), amid warm applause throughout the venue.

"History, Tradition, and Progress, the NCGM is celebrating its 150th anniversary this year", Dr. Kokudo, the president of NCGM said in his speech. The NCGM originated from a temporary army hospital that was established inside the Yamashita gate of the Imperial Palace in Hibiya, Tokyo in October 1868. In 1873, the army hospital moved to what is now Hayabusa-cho, Chiyoda and its name was changed to the army's Central Hospital. Over time, the hospital's name

Released online in J-STAGE as advance publication January 25, 2019.

*Address correspondence to:

Dr. Norihiro Kokudo, National Center for Global Health and Medicine, 1-21-1 Toyama Shinjuku-ku, Tokyo 162-8655, Japan.

E-mail: nkokudo@hosp.ncgm.go.jp



Figure 1. Event photos. The ceremony of 150th Anniversary of the National Center for Global Health and Medicine (NCGM) (A); the opening greeting addressed by Dr. Norihiro Kokudo, the president of NCGM (B); the congratulatory speech delivered by their Imperial Highness Prince Akishinonomiya (C), Dr. Takumi Nemoto, the Minister of Health, Labour and Welfare of Japan (D), and Dr. Yoshitake Yokokura, the president of Japan Medical Association (E); a special keynote lecture given by Dr. Kazuhide Yamazaki (F) and Dr. Satochi Omura (G); and a welcome reception held after the ceremony (H).

changed to the Tokyo Army Hospital, the 1st Garrison Hospital of Tokyo, and the First Army Hospital in Tokyo. In 1929, it moved again to what is now the Toyama area. After World War II, the hospital was placed under the auspices of the Ministry of Health and Welfare and it was relaunched as the First National Hospital of Tokyo. "To" is short for "Tokyo" and "ichi" means "one" or "first" in Japanese, which is why the hospital has long been known as "To-ichi." The hospital became the National Hospital Medical Center in 1974. In October 1993, the Medical Center was combined with another hospital to create the International Medical Center of Japan. After several rounds of restructuring and reorganization, the facility became the NCGM in April 2015. The NCGM is a national research and development agency, which is a type of independent administrative entity.

The NCGM has various departments, including the Center Hospital, Kohnodai Hospital, the Research Institute, the Center for Clinical Sciences, the Bureau of International Health Cooperation, and the National College of Nursing (2). The NCGM conducts research in various fields such as infectious diseases, immune disorders, diabetes, and metabolic disorders and it provides advanced and comprehensive medical care. The NCGM also comprehensively provides training for personnel in international cooperation and medicine. As a research and development entity, the NCGM will continue to fulfil those tasks in accordance with Japan's national policies.

Dr. Kokudo said that this year is memorable because it marks 150 years since the Meiji Restoration. The NCGM has changed in many ways over as times have changed, but it continues to provide needed medical care. "We pledge that will strive to make people even more aware of the NCGM in the future, we thank you for your continued advice and support", he said.

After the ceremony, a welcome reception was held for everyone in attendance (Figure 1H).

References

1. 150th Anniversary of the National Center for Global Health and Medicine (NCGM) <http://150th.nv.ncgm.go.jp/index.html> (accessed December 4, 2018). (in Japanese)
2. National Center for Global Health and Medicine (NCGM). <https://www.ncgm.go.jp/> (accessed December 4, 2018). (in Japanese)

(Received December 4, 2018; Accepted December 26, 2018)

Prevention of mother-to-child transmission (PMTCT) continues to play a vital role in the response to HIV/AIDS: Current status and future perspectives

Qi Tang^{1,2,§}, Min Liu^{3,§}, Hongzhou Lu^{1,2,4,*}

¹ Scientific Research Center, Shanghai Public Health Clinical Center, Fudan University, Shanghai, China;

² Department of Infectious Diseases, Shanghai Public Health Clinical Center, Fudan University, Shanghai, China;

³ Department of Gynecology and Obstetrics, Shanghai Public Health Clinical Center, Fudan University, Shanghai, China;

⁴ Department of Infectious Diseases, Huashan Hospital Affiliated to Fudan University, Shanghai, China.

Summary

Prevention of mother-to-child transmission (PMTCT) program offer a range of services for women of reproductive age living with or at risk of contracting the human immunodeficiency virus (HIV) in order to maintain their health and to protect their infants from acquiring HIV. The program has made significant progress in eliminating HIV. Thanks to the provision of PMTCT services, around 1.4 million HIV infections among children were prevented between 2010 and 2018. PMTCT program in China has developed substantially over the past few years, highlighting the national response to HIV/AIDS. Although huge strides have been made in PMTCT, a number of important issues, such as prevention at each step, monitoring of PMTCT services, and early infant diagnosis, need to be addressed in the future.

Keywords: Mother-to-child transmission, pregnant women with HIV, HIV infections among children, HIV/AIDS response

In September 2015, the World Health Organization (WHO) released guidelines recommending that all pregnant women living with human immunodeficiency virus (HIV) be immediately provided with lifelong treatment, regardless of their CD4 count; this resulted in 91% of 1.1 million women starting lifelong antiretroviral therapy (ART) (1-2). A year later, the WHO released guidelines recommending a "treat all" approach that increased the number of women of reproductive age who are receiving ART, regardless of whether they are pregnant or not (3). Prevention of mother-to-child transmission (PMTCT) program offers a range of services for women of reproductive age living with or at risk of HIV in order to maintain their health and

protect their infants from acquiring HIV. The program has made significant in eliminating HIV.

1. Definition of PMTCT

HIV can be transmitted from an HIV-positive woman to her child during pregnancy, childbirth, or breastfeeding. MTCT, which is also known as "vertical transmission", accounts for the vast majority of infections in children (0-14 years of age). A pregnant woman with untreated HIV infection has a 15% to 45% chance of transmitting the virus to a newborn. However, ART in combination with other interventions can reduce this risk to less than 5% (4).

PMTCT program provides a range of services to both women and infants. These include preventing HIV infections among women of reproductive age (15-49 years), preventing unwanted pregnancies among women living with HIV, and providing women living with HIV with lifelong ART to maintain their health and prevent transmission during pregnancy, labor, or breastfeeding. In addition, PMTCT services should also include early infant diagnosis at 4 to 6 weeks after birth, testing at

Released online in J-STAGE as advance publication January 25, 2019.

[§]These authors contributed equally to this work.

*Address correspondence to:

Dr. Hongzhou Lu, Shanghai Public Health Clinical Center, Fudan University, No.2901 Caolang Road, Jinshan District, Shanghai 201508, China.

E-mail: luhongzhou@fudan.edu.cn

18 months and/or when breastfeeding ends, and ART initiation as soon as possible for HIV-exposed infants to prevent HIV acquisition.

2. Current status of PMTCT

The Joint United Nations Programme on HIV/AIDS (UNAIDS) launched Start Free Stay Free AIDS Free in 2017; this initiative is committed to the dual elimination of mother-to-child transmission of both HIV and congenital syphilis (5). Targets for 2020 include reducing the number of new HIV infections among children to fewer than 20,000, reducing the number of new HIV infections among adolescent girls and young women (aged 10-24) to fewer than 100,000 by 2020, as well as providing 1.4 million children and 1 million 15-19-year-old adolescents with ART (6). Although meeting these targets may be difficult, such initiatives have led to substantial progress in tackling the HIV epidemic.

2.1. Global PMTCT response

Around 1.4 million HIV infections among children were prevented between 2010 and 2018 thanks to the provision of PMTCT services (7).

In 2017, 80% of pregnant women living with HIV were receiving ART, indicating a significant increase from 51% in 2010 (7). However, just over half (52%) of the 1.8 million children living with HIV were receiving ART. Among those without access to effective treatment, 110,000 died due to AIDS-related illnesses (8). Moreover, 180,000 children were newly infected with HIV that year, half of whom were infected during breastfeeding (5).

2.2. PMTCT response in China and especially in East China

PMTCT program in China has substantially developed over the past few years, highlighting the national response to HIV/AIDS. This has resulted in a reduction in the rate of MTCT from 7.4% in 2001 to 6.1% in 2014 (9).

Extensive records have been kept in Shanghai, which is one of China's largest municipalities. The Shanghai Public Health Clinical Center (SPHCC) is the only designated hospital providing comprehensive care including PMTCT for people living with HIV/AIDS in Shanghai. HIV-seropositive women receive comprehensive services at the Center, and viral suppression is achieved with ART before, during, and after pregnancy. Pregnant women who are diagnosed with HIV at a hospital before giving birth are referred to the Center and start ART as soon as possible. Some of the HIV-infected pregnant woman with a relatively high viral load (> 1,000) are encouraged to undergo a

cesarean section, while others are given the opportunity of a vaginal delivery. In fact, most women ultimately undergo a caesarean section because they worry too much about the possibility of mother-to-child transmission. Children born to HIV-infected mothers are given standardized prophylaxis and artificial feeding. Since 2006, no case of HIV infection among children born to pregnant women with HIV registered in Shanghai have been reported (10).

3. Perspectives on PMTCT

Although great progress has been achieved in PMTCT, a number of important issues still need to be addressed.

Prevention at each step Over the past few years, half of HIV-infected infants were infected during breastfeeding (11). Breastfeeding should be avoided regardless of whether or not viral suppression has been achieved in the mother. However, in some areas where resources are extremely limited, artificial feeding presents specific difficulties. Inappropriate artificial feeding may cause many problems and even increase perinatal mortality. In the case of exclusive breastfeeding, the sustained suppression of the virus is crucial to avoid mother-to-child transmission of HIV. Of course, guidance on proper breastfeeding is also essential. Breastfed infants should be monitored during the entire course of exposure for potential acquisition of HIV.

Monitoring of PMTCT services Healthcare providers should pay attention to the importance of viral testing, and particularly early infant diagnosis. Mothers and their infants should be followed up in pairs rather than separately. Some mothers living with HIV are lost to follow-up when they change healthcare providers, so better data systems are needed to enable the provision of appropriate services after transfer (5).

Early infant diagnosis The rapid expansion of point-of-care early infant diagnosis should become a key focus of PMTCT (8). Intensified efforts to identify infants and children living with HIV by incorporating testing in other healthcare services, such as immunization and nutrition, are also needed (5).

Acknowledgements

This research was funded by the 13th Five-Year National Science and Technology Major Project from Ministry of Science and Technology of the People's Republic of China (Grant No.: 2017ZX09304027).

References

1. World Health Organization. Guideline on when to start antiretroviral therapy and on pre-exposure prophylaxis for HIV. 2015. http://apps.who.int/iris/bitstream/handle/10665/186275/9789241509565_eng.pdf;sequence=1 (accessed October 21, 2018)

2. Joint United Nations Programme on HIV/AIDS. Prevention Gap Report. 2016. http://www.unaids.org/sites/default/files/media_asset/2016-prevention-gap-report_en.pdf (accessed November 11, 2018)
3. World Health Organization. Consolidated guidelines on the use of antiretroviral drugs for treating and preventing HIV infection: Recommendations for a public health approach. Second edition. 2016. http://apps.who.int/iris/bitstream/handle/10665/208825/9789241549684_eng.pdf;jsessionid=4881A8551DDD670012F9D06A4C585C2B?sequence=1 (accessed November 13, 2018)
4. World Health Organization. 2015 Progress Report on the Global Plan towards the elimination of new HIV infections among children and keeping their mothers alive. http://www.unaids.org/sites/default/files/media_asset/JC2774_2015ProgressReport_GlobalPlan_en.pdf (accessed November 3, 2018)
5. Joint United Nations Programme on HIV/AIDS. Start Free Stay Free AIDS Free: 2017 progress report. 2017. http://www.unaids.org/sites/default/files/media_asset/JC2923_SFSFAF_2017progressreport_en.pdf (accessed November 13, 2018)
6. Joint United Nations Programme on HIV/AIDS. President's Emergency Plan for AIDS Relief (PEPFAR) and Partners. Start Free, Stay Free, AIDS Free: A super fast-track framework for ending AIDS among children, adolescents and young women by 2020. 2016. <https://free.unaids.org/> (accessed November 23, 2018)
7. Joint United Nations Programme on HIV/AIDS. Miles to go: Global AIDS update 2018. http://www.unaids.org/sites/default/files/media_asset/miles-to-go_en.pdf (accessed November 15, 2018)
8. Joint United Nations Programme on HIV/AIDS. Global AIDS Monitoring 2018. Indicators for monitoring the 2016 United Nations Political Declaration on Ending AIDS. https://www.aidsdatahub.org/sites/default/files/highlight-reference/document/UNAIDS_Global_AIDS_Monitoring_2018.pdf (accessed November 29, 2018)
9. National Health and Family Planning Commission of the People's Republic of China. 2015 China AIDS Response Progress Report. http://www.unaids.org/sites/default/files/country/documents/CHN_narrative_report_2015.pdf (accessed November 12, 2018)
10. People's Daily Online. AIDS mothers can also have healthy babies. 2018. <http://sh.people.com.cn/n2/2018/1128/c134768-32339999.html> (accessed December 12, 2018)
11. Penazzato M, Lule F, Essajee S. Paediatric HIV: The unfinished business. *Lancet HIV*. 2017;4:e425-e427.

(Received January 15, 2019; Revised January 17, 2019; Accepted January 20, 2019)

Guide for Authors

1. Scope of Articles

BioScience Trends is an international peer-reviewed journal. BioScience Trends devotes to publishing the latest and most exciting advances in scientific research. Articles cover fields of life science such as biochemistry, molecular biology, clinical research, public health, medical care system, and social science in order to encourage cooperation and exchange among scientists and clinical researchers.

2. Submission Types

Original Articles should be well-documented, novel, and significant to the field as a whole. An Original Article should be arranged into the following sections: Title page, Abstract, Introduction, Materials and Methods, Results, Discussion, Acknowledgments, and References. Original articles should not exceed 5,000 words in length (excluding references) and should be limited to a maximum of 50 references. Articles may contain a maximum of 10 figures and/or tables.

Brief Reports definitively documenting either experimental results or informative clinical observations will be considered for publication in this category. Brief Reports are not intended for publication of incomplete or preliminary findings. Brief Reports should not exceed 3,000 words in length (excluding references) and should be limited to a maximum of 4 figures and/or tables and 30 references. A Brief Report contains the same sections as an Original Article, but the Results and Discussion sections should be combined.

Reviews should present a full and up-to-date account of recent developments within an area of research. Normally, reviews should not exceed 8,000 words in length (excluding references) and should be limited to a maximum of 100 references. Mini reviews are also accepted.

Policy Forum articles discuss research and policy issues in areas related to life science such as public health, the medical care system, and social science and may address governmental issues at district, national, and international levels of discourse. Policy Forum articles should not exceed 2,000 words in length (excluding references).

Case Reports should be detailed reports of the symptoms, signs, diagnosis, treatment, and follow-up of an individual patient. Case reports may contain a demographic profile of the patient but usually describe an unusual or novel occurrence. Unreported or unusual

side effects or adverse interactions involving medications will also be considered. Case Reports should not exceed 3,000 words in length (excluding references).

News articles should report the latest events in health sciences and medical research from around the world. News should not exceed 500 words in length.

Letters should present considered opinions in response to articles published in BioScience Trends in the last 6 months or issues of general interest. Letters should not exceed 800 words in length and may contain a maximum of 10 references.

3. Editorial Policies

Ethics: BioScience Trends requires that authors of reports of investigations in humans or animals indicate that those studies were formally approved by a relevant ethics committee or review board.

Conflict of Interest: All authors are required to disclose any actual or potential conflict of interest including financial interests or relationships with other people or organizations that might raise questions of bias in the work reported. If no conflict of interest exists for each author, please state "There is no conflict of interest to disclose".

Submission Declaration: When a manuscript is considered for submission to BioScience Trends, the authors should confirm that 1) no part of this manuscript is currently under consideration for publication elsewhere; 2) this manuscript does not contain the same information in whole or in part as manuscripts that have been published, accepted, or are under review elsewhere, except in the form of an abstract, a letter to the editor, or part of a published lecture or academic thesis; 3) authorization for publication has been obtained from the authors' employer or institution; and 4) all contributing authors have agreed to submit this manuscript.

Cover Letter: The manuscript must be accompanied by a cover letter signed by the corresponding author on behalf of all authors. The letter should indicate the basic findings of the work and their significance. The letter should also include a statement affirming that all authors concur with the submission and that the material submitted for publication has not been published previously or is not under consideration for publication elsewhere. The cover letter should be submitted in PDF format. For example of Cover Letter, please visit <http://www.biosciencetrends.com/downcentre.php> (Download Centre).

Copyright: A signed JOURNAL PUBLISHING AGREEMENT (JPA) form must be provided by post, fax, or as a scanned file before acceptance of the article. Only forms with a hand-written signature are accepted. This copyright will ensure the widest possible dissemination of information. A form facilitating transfer of copyright can be downloaded by clicking the

appropriate link and can be returned to the e-mail address or fax number noted on the form (Please visit [Download Centre](#)). Please note that your manuscript will not proceed to the next step in publication until the JPA Form is received. In addition, if excerpts from other copyrighted works are included, the author(s) must obtain written permission from the copyright owners and credit the source(s) in the article.

Suggested Reviewers: A list of up to 3 reviewers who are qualified to assess the scientific merit of the study is welcomed. Reviewer information including names, affiliations, addresses, and e-mail should be provided at the same time the manuscript is submitted online. Please do not suggest reviewers with known conflicts of interest, including participants or anyone with a stake in the proposed research; anyone from the same institution; former students, advisors, or research collaborators (within the last three years); or close personal contacts. Please note that the Editor-in-Chief may accept one or more of the proposed reviewers or may request a review by other qualified persons.

Language Editing: Manuscripts prepared by authors whose native language is not English should have their work proofread by a native English speaker before submission. If not, this might delay the publication of your manuscript in BioScience Trends.

The Editing Support Organization can provide English proofreading, Japanese-English translation, and Chinese-English translation services to authors who want to publish in BioScience Trends and need assistance before submitting a manuscript. Authors can visit this organization directly at <http://www.iacmhr.com/iac-eso/support.php?lang=en>. IAC-ESO was established to facilitate manuscript preparation by researchers whose native language is not English and to help edit works intended for international academic journals.

4. Manuscript Preparation

Manuscripts should be written in clear, grammatically correct English and submitted as a Microsoft Word file in a single-column format. Manuscripts must be paginated and typed in 12-point Times New Roman font with 24-point line spacing. Please do not embed figures in the text. Abbreviations should be used as little as possible and should be explained at first mention unless the term is a well-known abbreviation (e.g. DNA). Single words should not be abbreviated.

Title Page: The title page must include 1) the title of the paper (Please note the title should be short, informative, and contain the major key words); 2) full name(s) and affiliation(s) of the author(s), 3) abbreviated names of the author(s), 4) full name, mailing address, telephone/fax numbers, and e-mail address of the corresponding author; and 5) conflicts of interest (if you have an actual or potential conflict of interest to disclose, it must be included as a footnote on the title page of the manuscript; if no conflict of

interest exists for each author, please state "There is no conflict of interest to disclose"). Please visit [Download Centre](#) and refer to the title page of the manuscript sample.

Abstract: The abstract should briefly state the purpose of the study, methods, main findings, and conclusions. For article types including Original Article, Brief Report, Review, Policy Forum, and Case Report, a one-paragraph abstract consisting of no more than 250 words must be included in the manuscript. For News and Letters, a brief summary of main content in 150 words or fewer should be included in the manuscript. Abbreviations must be kept to a minimum and non-standard abbreviations explained in brackets at first mention. References should be avoided in the abstract. Key words or phrases that do not occur in the title should be included in the Abstract page.

Introduction: The introduction should be a concise statement of the basis for the study and its scientific context.

Materials and Methods: The description should be brief but with sufficient detail to enable others to reproduce the experiments. Procedures that have been published previously should not be described in detail but appropriate references should simply be cited. Only new and significant modifications of previously published procedures require complete description. Names of products and manufacturers with their locations (city and state/country) should be given and sources of animals and cell lines should always be indicated. All clinical investigations must have been conducted in accordance with Declaration of Helsinki principles. All human and animal studies must have been approved by the appropriate institutional review board(s) and a specific declaration of approval must be made within this section.

Results: The description of the experimental results should be succinct but in sufficient detail to allow the experiments to be analyzed and interpreted by an independent reader. If necessary, subheadings may be used for an orderly presentation. All figures and tables must be referred to in the text.

Discussion: The data should be interpreted concisely without repeating material already presented in the Results section. Speculation is permissible, but it must be well-founded, and discussion of the wider implications of the findings is encouraged. Conclusions derived from the study should be included in this section.

Acknowledgments: All funding sources should be credited in the Acknowledgments section. In addition, people who contributed to the work but who do not meet the criteria for authors should be listed along with their contributions.

References: References should be numbered in the order in which they appear in the text. Citing of unpublished results, personal communications, conference abstracts, and theses in the reference list is not recommended but these sources may be mentioned in the text. In the reference list,

cite the names of all authors when there are fifteen or fewer authors; if there are sixteen or more authors, list the first three followed by *et al.* Names of journals should be abbreviated in the style used in PubMed. Authors are responsible for the accuracy of the references. Examples are given below:

Example 1 (Sample journal reference): Inagaki Y, Tang W, Zhang L, Du GH, Xu WF, Kokudo N. Novel aminopeptidase N (APN/CD13) inhibitor 24F can suppress invasion of hepatocellular carcinoma cells as well as angiogenesis. *Biosci Trends*. 2010; 4:56-60.

Example 2 (Sample journal reference with more than 15 authors): Darby S, Hill D, Auvinen A, *et al.* Radon in homes and risk of lung cancer: Collaborative analysis of individual data from 13 European case-control studies. *BMJ*. 2005; 330:223.

Example 3 (Sample book reference): Shalev AY. Post-traumatic stress disorder: diagnosis, history and life course. In: Post-traumatic Stress Disorder, Diagnosis, Management and Treatment (Nutt DJ, Davidson JR, Zohar J, eds.). Martin Dunitz, London, UK, 2000; pp. 1-15.

Example 4 (Sample web page reference): Ministry of Health, Labour and Welfare of Japan. Dietary reference intakes for Japanese. <http://www.mhlw.go.jp/houdou/2004/11/h1122-2a.html> (accessed June 14, 2010).

Tables: All tables should be prepared in Microsoft Word or Excel and should be arranged at the end of the manuscript after the References section. Please note that tables should not be image format. All tables should have a concise title and should be numbered consecutively with Arabic numerals. If necessary, additional information should be given below the table.

Figure Legend: The figure legend should be typed on a separate page of the main manuscript and should include a short title and explanation. The legend should be concise but comprehensive and should be understood without referring to the text. Symbols used in figures must be explained.

Figure Preparation: All figures should be clear and cited in numerical order in the text. Figures must fit a one- or two-column format on the journal page: 8.3 cm (3.3 in.) wide for a single column, 17.3 cm (6.8 in.) wide for a double column; maximum height: 24.0 cm (9.5 in.). Please make sure that the symbols and numbers appeared in the figures should be clear. Please make sure that artwork files are in an acceptable format (TIFF or JPEG) at minimum resolution (600 dpi for illustrations, graphs, and annotated artwork, and 300 dpi for micrographs and photographs). Please provide all figures as separate files. Please note that low-resolution images are one of the leading causes of article resubmission and schedule delays. All color figures will be reproduced in full color in the online edition of the journal at no cost to authors.

Units and Symbols: Units and symbols

conforming to the International System of Units (SI) should be used for physicochemical quantities. Solidus notation (*e.g.* mg/kg, mg/mL, mol/mm²/min) should be used. Please refer to the SI Guide www.bipm.org/en/si/ for standard units.

Supplemental data: Supplemental data might be useful for supporting and enhancing your scientific research and BioScience Trends accepts the submission of these materials which will be only published online alongside the electronic version of your article. Supplemental files (figures, tables, and other text materials) should be prepared according to the above guidelines, numbered in Arabic numerals (*e.g.*, Figure S1, Figure S2, and Table S1, Table S2) and referred to in the text. All figures and tables should have titles and legends. All figure legends, tables and supplemental text materials should be placed at the end of the paper. Please note all of these supplemental data should be provided at the time of initial submission and note that the editors reserve the right to limit the size and length of Supplemental Data.

5. Submission Checklist

The Submission Checklist will be useful during the final checking of a manuscript prior to sending it to BioScience Trends for review. Please visit [Download Centre](#) and download the Submission Checklist file.

6. Online Submission

Manuscripts should be submitted to BioScience Trends online at <http://www.biosciencetrends.com>. The manuscript file should be smaller than 5 MB in size. If for any reason you are unable to submit a file online, please contact the Editorial Office by e-mail at office@biosciencetrends.com.

7. Accepted Manuscripts

Proofs: Galley proofs in PDF format will be sent to the corresponding author via e-mail. Corrections must be returned to the editor (proof-editing@biosciencetrends.com) within 3 working days.

Offprints: Authors will be provided with electronic offprints of their article. Paper offprints can be ordered at prices quoted on the order form that accompanies the proofs.

Page Charge: Page charges will be levied on all manuscripts accepted for publication in BioScience Trends (\$140 per page for black white pages; \$340 per page for color pages). Under exceptional circumstances, the author(s) may apply to the editorial office for a waiver of the publication charges at the time of submission.

(Revised February 2013)

Editorial and Head Office:

Pearl City Koishikawa 603
2-4-5 Kasuga, Bunkyo-ku
Tokyo 112-0003 Japan
Tel: +81-3-5840-8764
Fax: +81-3-5840-8765
E-mail: office@biosciencetrends.com

JOURNAL PUBLISHING AGREEMENT (JPA)

Manuscript No.:

Title:

Corresponding Author:

The International Advancement Center for Medicine & Health Research Co., Ltd. (IACMHR Co., Ltd.) is pleased to accept the above article for publication in BioScience Trends. The International Research and Cooperation Association for Bio & Socio-Sciences Advancement (IRCA-BSSA) reserves all rights to the published article. Your written acceptance of this JOURNAL PUBLISHING AGREEMENT is required before the article can be published. Please read this form carefully and sign it if you agree to its terms. The signed JOURNAL PUBLISHING AGREEMENT should be sent to the BioScience Trends office (Pearl City Koishikawa 603, 2-4-5 Kasuga, Bunkyo-ku, Tokyo 112-0003, Japan; E-mail: office@biosciencetrends.com; Tel: +81-3-5840-8764; Fax: +81-3-5840-8765).

1. Authorship Criteria

As the corresponding author, I certify on behalf of all of the authors that:

- 1) The article is an original work and does not involve fraud, fabrication, or plagiarism.
- 2) The article has not been published previously and is not currently under consideration for publication elsewhere. If accepted by BioScience Trends, the article will not be submitted for publication to any other journal.
- 3) The article contains no libelous or other unlawful statements and does not contain any materials that infringes upon individual privacy or proprietary rights or any statutory copyright.
- 4) I have obtained written permission from copyright owners for any excerpts from copyrighted works that are included and have credited the sources in my article.
- 5) All authors have made significant contributions to the study including the conception and design of this work, the analysis of the data, and the writing of the manuscript.
- 6) All authors have reviewed this manuscript and take responsibility for its content and approve its publication.
- 7) I have informed all of the authors of the terms of this publishing agreement and I am signing on their behalf as their agent.

2. Copyright Transfer Agreement

I hereby assign and transfer to IACMHR Co., Ltd. all exclusive rights of copyright ownership to the above work in the journal BioScience Trends, including but not limited to the right 1) to publish, republish, derivate, distribute, transmit, sell, and otherwise use the work and other related material worldwide, in whole or in part, in all languages, in electronic, printed, or any other forms of media now known or hereafter developed and the right 2) to authorize or license third parties to do any of the above.

I understand that these exclusive rights will become the property of IACMHR Co., Ltd., from the date the article is accepted for publication in the journal BioScience Trends. I also understand that IACMHR Co., Ltd. as a copyright owner has sole authority to license and permit reproductions of the article.

I understand that except for copyright, other proprietary rights related to the Work (e.g. patent or other rights to any process or procedure) shall be retained by the authors. To reproduce any text, figures, tables, or illustrations from this Work in future works of their own, the authors must obtain written permission from IACMHR Co., Ltd.; such permission cannot be unreasonably withheld by IACMHR Co., Ltd.

3. Conflict of Interest Disclosure

I confirm that all funding sources supporting the work and all institutions or people who contributed to the work but who do not meet the criteria for authors are acknowledged. I also confirm that all commercial affiliations, stock ownership, equity interests, or patent-licensing arrangements that could be considered to pose a financial conflict of interest in connection with the article have been disclosed.

Corresponding Author's Name (Signature):

Date:

